Investigations into the Inhibition of 3-Deoxy-D-*manno*-Octulosonate 8-Phosphate Synthase

---

A thesis submitted in partial fulfilment

of the requirements for the degree of

Doctor of Philosophy of Chemistry

at the

University of Canterbury

by

Aidan Nicholas Harrison

November 2010

Acknowledgements

Thank you to Emily Parker, perhaps the most patient supervisor in the world, who has supported me through the ups and downs of my PhD. I would not have got through much of it without you pushing me along, either with encouragement, or telling me the hard truths, when I needed to hear them. Thank you for your unwavering belief that I could finish my PhD, even when I wasn't entirely sure I could.

To Ted Baker and the Maurice Wilkins Centre of Molecular Biodiscovery, thank you for your support, both academic and financial, throughout my PhD. Without your assistance I would not be writing these acknowledgements, as I never would have started my doctoral studies. Thank you also to the NZIC who have provided me financial help with travel to a number of conferences within NZ over the years.

To many of the staff of the Chemistry Departments at Massey University and the University of Canterbury, thank you for your advice and insight whenever I required it. A great deal of thanks also goes to Andy Pratt who has been a fantastic help during the editing of my thesis. Thank you to the technical staff in the Massey University and University of Canterbury Chemistry Departments, and special thanks to Marie Fitchett, whose NMR, mass spectroscopy, and proof reading skills have proven invaluable during my PhD.

Thank you to the Parker group, past and present, who have all been fantastic to work beside, especially Hemi, Leonardo, David, Sebastian, Tim, Penel and most of all Scott, who is an absolute wealth of synthetic chemistry knowledge. I cannot think of a better person to have learnt the ropes from (except perhaps our habits regarding lab tidiness). Also thanks to the students of the University of Canterbury Chemistry Department who I have shared many a curry, beer, laugh and gossip with. You've all helped to keep me relatively sane, and I am grateful for it.

Finally I would like to thank my friends outside the Chemistry Department, and family for their support through my entire university career, especially my wonderful Mother, who has loved and supported me throughout the entire process and is probably more pleased that this is all over than even I am. Thank you for everything, I hope you know just how much it has meant to me.

Abstract

The enzyme 3-deoxy-D-*manno*-octulosonate 8-phosphate (KDO8P) synthase catalyses the aldol condensation of the five-carbon sugar phosphate, arabinose 5-phosphate (A5P), and phosphoenol pyruvate (PEP) to give the eight-carbon phosphorylated sugar, KDO8P. It is the second committed step in the synthesis of KDO, a necessary component of the cell wall of Gram-negative bacteria.

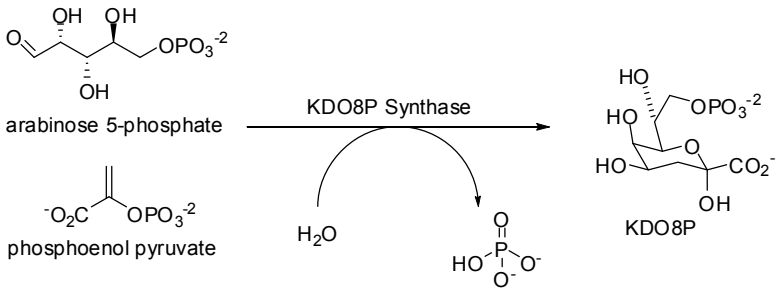

This thesis describes the design, synthesis and evaluation of a number of inhibitors of KDO8P synthase that utilise the functionality of one or both substrates.

The KDO8P synthase family can be divided based on the requirement of a divalent metal ion. Chapter 2 describes the growth, purification and characterisation of an example from both the metal-independent KDO8P synthases (*Neisseria meningitidis*, *Nme*) and metal-dependent KDO8P synthases (*Acidithiobacillus ferrooxidans*, *Afe*) in order to utilise these enzymes for the inhibition studies described in this thesis.

In Chapter 3, a number of small molecule PEP analogues were selected as mimics of KDO8P synthase reaction intermediates and tested as inhibitors of KDO8P synthase from *N. meningitidis* and *A. ferrooxidans*. Glyphosate, (*E*)-vinyl phosphonate and the fluorinated analogue of (*E*)-vinyl phosphonate were selected as mimics of the high-energy oxocarbenium intermediate through which the KDO8P synthase reaction is thought to occur. The two enantiomers of phospholactate were selected in order to investigate the chirality of the tetrahedral intermediate and determine the importance of this chirality for inhibition of KDO8P synthase. All five inhibitors were found to be moderate to poor inhibitors of both the KDO8P synthase from *N. meningitidis* and *A. ferrooxidans*.

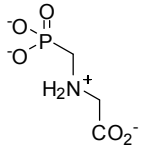

glyphosate
K_i (*Nme*): 260 ± 40 μM
K_i (*Afe*): 330 ± 40 μM

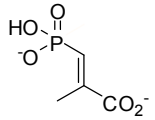

(*E*)-vinyl phosphonate
K_i (*Nme*): 320 ± 30 μM
K_i (*Afe*): 260 ± 10 μM

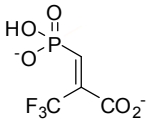

fluorinated (*E*)-vinyl phosphonate
K_i (*Nme*): 270 ± 30 μM
K_i (*Afe*): 280 ± 20 μM

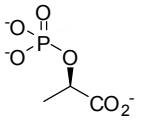

(2*R*)-phospholactate
K_i (*Nme*): 870 ± 90 μM
K_i (*Afe*): 390 ± 70 μM

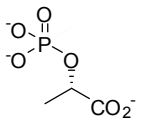

(2*S*)-phospholactate
K_i (*Nme*): 1200 ± 50 μM
K_i (*Afe*): 1000 ± 220 μM

Chapter 4 describes the design and synthesis of inhibitors that incorporated structural features of the second substrate, A5P, in order to improve inhibition from that observed for the PEP analogues investigated in Chapter 3. A bisphosphate inhibitor was designed that incorporated a terminal phosphate moiety, representative of the phosphate of A5P. A large increase in inhibition was found, compared to the phospholactates from which it was derived. A structure-activity-relationship study was undertaken on this compound by design of compounds that lacked one of the two phosphate moieties of the bisphosphate inhibitor, in order to determine their relative importance. The inhibition results indicate that the primary terminal phosphate, thought to bind in the A5P phosphate binding site, is more important for inhibition of KDO8P synthase than the secondary phosphate.

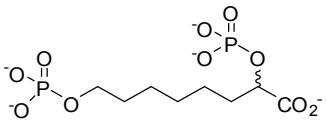

K_i (*Nme*): 7.9 ± 1.6 μM
K_i (*Afe*): 20 ± 3 μM

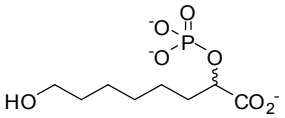

K_i (*Nme*): 1000 ± 80 μM
K_i (*Afe*): 540 ± 50 μM

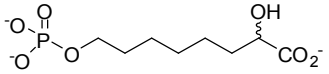

K_i (*Nme*): 270 ± 40 μM
K_i (*Afe*): 190 ± 40 μM

In Chapter 5 these investigations into the inhibition of KDO8P synthase are discussed in detail, and interpreted using the aid of computational studies. In addition several approaches are described for the completion and advancement of the studies presented here in this thesis.

Table of Contents

Abbreviations

A5P:	arabinose 5-phosphate
Ac:	acetyl
AEC:	anion exchange chromatography
aq:	aqueous
Bn:	benzyl
BSA:	bovine serum albumin
BTP:	1,3-bis(tris(hydroxymethyl)methylamino)propane
Bz:	benzoyl
COSY:	correlation spectroscopy
CV:	column volume
DAH7P:	3-deoxy D-*arabino* heptulosonate 7-phosphate
DMF:	dimethylformamide
DMP:	Dess-Martin periodinane
DMSO:	dimethylsulfoxide
E4P:	erythrose 4-phosphate
EDTA:	ethylenediaminetetraacetic acid
EPSP:	5-enolpyruvylshikimate 3-phosphate
ESI-TOF:	electrospray time-of-flight
Et:	ethyl
FPLC:	fast protein liquid chromatography
HIC:	hydrophobic interaction chromatography
HRMS:	high resolution mass spectroscopy
IBX:	2-iodoxybenzoic acid
IDF:	induced fit
Im	imidazole
*i*Pr:	isopropyl
IPTG:	isopropyl β-D-1-thiogalactopyranoside
k_{cat}:	turnover number
K_d:	dissociation constant
KDO:	3-deoxy D-*manno* 2-octulosonate
KDO8P:	3-deoxy D-*manno* 2-octulosonate 8-phosphate

K_i:	inhibition constant
K_m:	Michealis constant
L5P:	lyxose 5-phosphate
LPS:	lipopolysaccharide
m-CPBA:	*meta*-chloroperbenzoic acid
Me:	methyl
MOM:	methoxymethyl
Ms:	methanesulfonyl
MurZ:	UDP-GlcNAc enolpyruvyl transferase
NADPH:	Nicotinamide adenine dinucleotide phosphate
NeuNAc:	*N*-acetylneuraminic acid
NMR:	nuclear magnetic resonance
NOESY:	nuclear Overhauser effect spectroscopy
PEP:	phosphoenol pyruvate
Pg:	protecting group
Ph:	phenyl
Pi:	inorganic phosphate
R5P:	ribose 5-phosphate
R_f:	retention factor
RMSD:	root mean square deviation
RT:	room temperature
SDS-PAGE:	sodium dodecyl sulfate polyacrylamide gel electrophoresis
SEC:	size exclusion chromatography
S_NAr:	nucleophilic aromatic substitution (addition-elimination)
TBAF:	*tert*-butylammoniumfluoride
TBDMS:	*tert*-butyldimethylsilyl
TBDPS:	*tert*-butyldiphenylsilyl
Tf:	triflate
THF:	tetrahydrofuran
TLC:	thin layer chromatography
TMS:	trimethylsilyl
Ts:	tosyl
X5P:	xylose 5-phosphate
Δ:	at reflux

A. aeolicus (*Aae*)	*Aquifex aeolicus*
A. ferrooxidans (*Afe*)	*Acidithiobacillus ferrooxidans*
C. psittaci (*Cps*)	*Chlamydia psittaci*
E. coli (*Eco*)	*Escherichia coli*
H. influenza (Hin)	*Haemophilus influenza*
H. pylori (*Hpy*)	*Helicobacter pylori*
M. tuberculosis (*Mtu*)	*Mycobacterium tuberculosis*
N. meningitidis (*Nme*)	*Neisseria meningitidis*
S. typhimurium (*Sty*)	*Salmonella typhimurium*

Amino acid one-letter codes

A	alanine	E	glutamate	L	leucine	S	serine
R	arginine	Q	glutamine	K	lysine	T	threonine
N	asparagine	G	glycine	M	methionine	W	tryptophan
D	aspartate	H	histidine	F	phenylalanine	Y	tyrosine
C	cysteine	I	isoleucine	P	proline	V	valine

Chapter 1: Introduction

a wealth of knowledge
enzymatic synthesis
KDO8P

1.1. Lipopolysaccharide biosynthesis as a target for anti-microbial drugs

Gram-negative bacteria have both an inner and outer membrane, the former being the site of the electron transport chain, and the latter being a unique, asymmetric layer used in the protection of a fragile peptidoglycan layer. The outer membrane is asymmetric as the inner face is mainly phospholipids, whereas the outer face contains lipid A bound to a lipopolysaccharide (LPS) which extends out from the surface (Figure 1.1).[1]

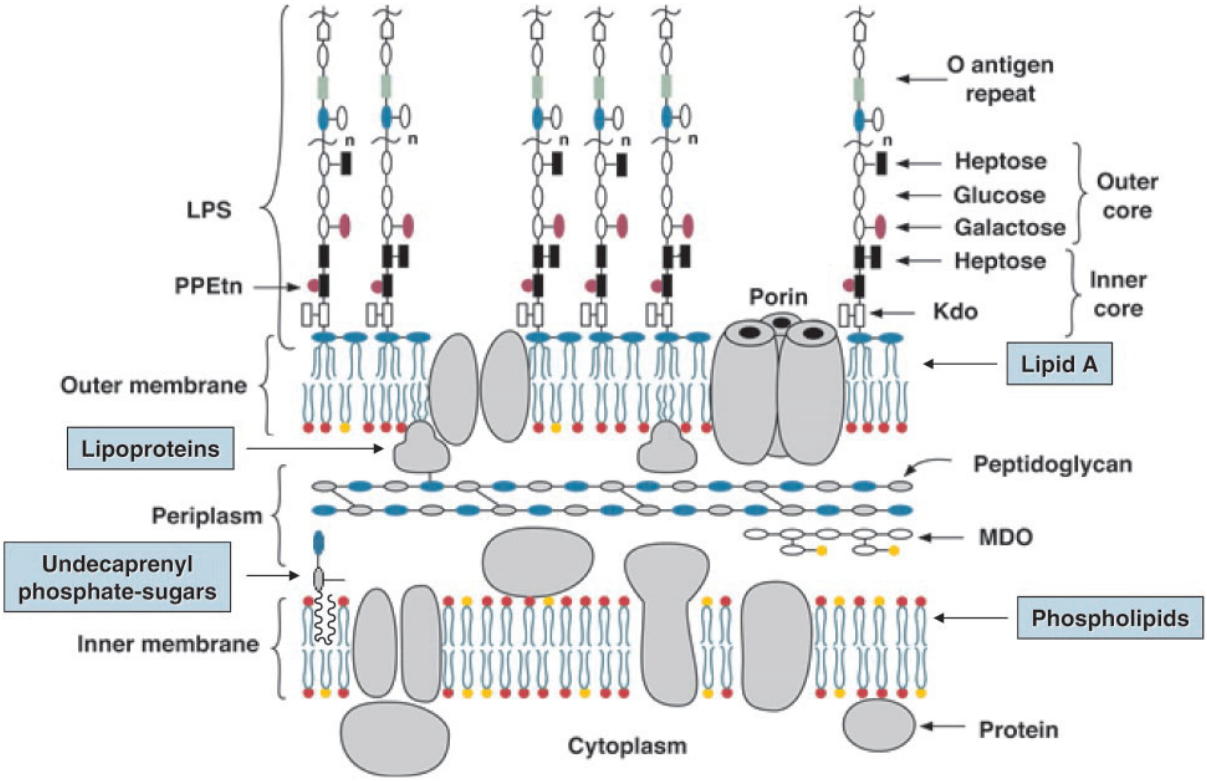

Figure 1.1: Model of the inner and outer membranes of *Escherichia coli* K-12. Taken from Raetz *et al.*[1]

This LPS is composed of four main regions;[1]

1. **Lipid A** is the hydrophobic component, composed of six fatty acids that anchor LPS to the outer surface of the bacterial cell.

2. The **inner core** region is composed of two to three molecules of 3-deoxy-D-*manno*-octulosonate (KDO) and two to three heptose residues. This region is usually conserved within bacterial families.

3. The **outer core** region is a pentasaccharide whose covalent structure is more variable than that of the inner core and is usually made up of sugars such as glucose, galactose and heptose. It provides an attachment site for the *O*-antigen polysaccharide.
4. The ***O*-antigen repeat** extends into the extracellular environment and can differ in the monomer glycoses, the position and stereochemistry of the *O*-glycosidic linkages, and the presence or absence of non-carbohydrate substituents. It provides the antigenic specificity of the bacterial species.

KDO has been shown to be the only conserved saccharide in nearly all LPS structures investigated thus far[2] and is synthesised from the five-carbon sugar ribulose 5-phosphate (Rib5P) (Figure 1.2). This pathway is only found in Gram-negative bacteria and certain plant species,[3] and is considered a potential target for the generation of anti-microbial drugs. Thus far work targeting this pathway has focussed on inhibition of the 3-deoxy-D-*manno*-2-octulosonic acid (KDO) pathway enzymes; arabinose 5-phosphate (A5P) isomerase, cytidine monophosphate (CMP)-KDO synthetase and 3-deoxy-D-*manno*-octulosonate 8-phosphate (KDO8P) synthase.[4]

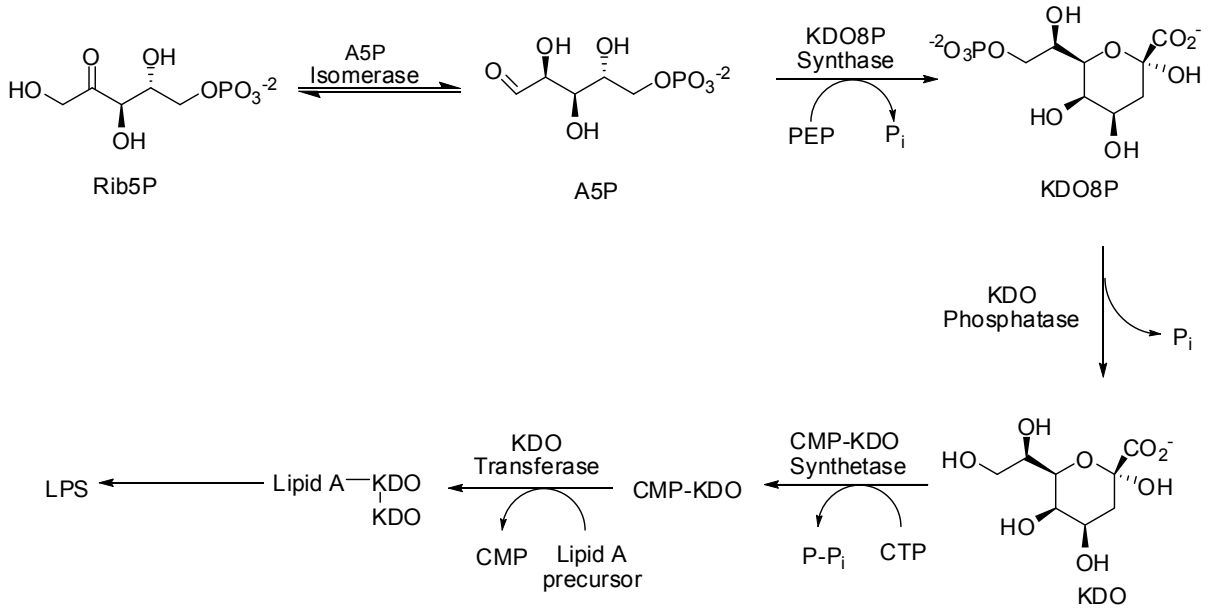

Figure 1.2: Biosynthesis of Lipid A from ribulose 5-phosphate

Investigation of A5P isomerase as an anti-microbial target is problematic as the enzyme has not been well characterised and the catalytic residues are still relatively unknown.[4] The pKa values of these catalytically important amino acids in *E. coli* have been estimated at 6.55 ±

0.04 and 10.34 ± 0.07 however,[5] and data suggests the presence of a histidine or possible carboxylate side chain, with an lysine or arginine in the active site.[6] These same amino acids are present in the active site and common to two other known isomerases, glucose 6-phosphate isomerase[7] and triose phosphate isomerase,[8,9] and this may reflect a common mechanism. The inhibition of A5P isomerase has thus far focussed on analogues of Rib5P and A5P and the most potent inhibitors have been found to have IC_{50} values ranging from 0.53–1.6 mM (Figure 1.3).[10]

The work to inhibit CMP-KDO synthetase has been far more successful, with initial studies into KDO analogues resulting in 2-deoxy-β-KDO (Figure 1.3) with a K_i of 3.9 μM *in vitro*.[9] This compound was found not to be active against Gram-negative bacteria *in vivo* however, and so a series of amino groups were derivitised at the C8 position, resulting in a series of dipeptide attached inhibitors that were found to have *in vivo* activity,[11-13] presumably due to their increased uptake *via* the oligopeptide permease system. Of these dipeptide prodrugs, the alanylalanyl, norvalylalanyl and arginylnorvalyl derivatives were also found to have good *in vitro* activity against CMP-KDO synthetase from *E. coli*[14] and *Salmonella typhimurium*[15] with IC_{50} values in the μM range.

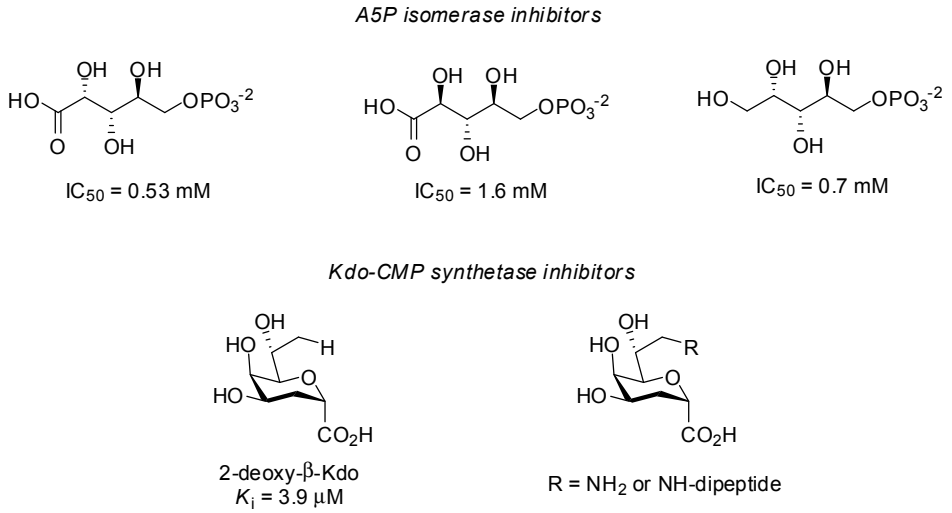

Figure 1.3: Known inhibitors of LPS pathway enzymes A5P isomerise and KDO-CMP synthetase

KDO8P synthase is the other enzyme in the KDO synthetic pathway that has been investigated in detail, and is the focus of this project.

1.2. KDO8P synthase

The second step in the synthesis of the sugar KDO from ribose 5-phosphate (R5P) is catalysed by KDO8P synthase, a key enzyme in the carbon flow of the LPS synthetic pathway. It catalyses the irreversible aldol-like condensation reaction between arabinose 5-phosphate (A5P) and phosphoenol pyruvate (PEP) to give the eight-carbon sugar KDO8P (Figure 1.4).

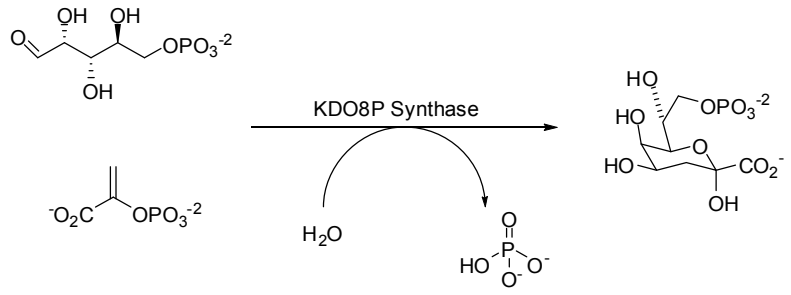

Figure 1.4: The reaction catalysed by KDO8P synthase

KDO8P synthase, when first characterised in 1959 from *Pseudomonas aeruginosa* was found to exclusively utilise A5P as a substrate, not accepting D-ribose 5-phosphate, D-xylose 6-phosphate,[16] D-glucose 6-phosphate, D-erythrose 4-phosphate and a number of other sugars and sugar phosphates.[17] A mutant of *S. typhimurium* that had a temperature sensitive KDO8P synthase was isolated by Rick and co-workers.[18] This mutant was shown to have a much decreased affinity to A5P at higher temperatures, with the K_m of A5P increasing 25-fold between 29 °C and 42 °C. Below 30 °C bacterial growth and synthesis of LPS was relatively normal, but as the temperature of incubation was increased to 37 °C the bacteria became increasingly dependent on exogenous A5P. At 42 °C exogenous A5P failed to halt the synthesis of protein, DNA, RNA and peptidoglycan, and the ultimate result was cell death. This lead to the conclusion that KDO8P synthase catalytic activity is required for cell growth, and as such is an attractive target for inhibitors acting as anti-bacterial compounds. Recently it has been shown that *E. coli* can survive without the KDO core in the LPS, but that depletion of KDO causes permeability of the cell wall to many large molecules not previously able to travel across the cell membrane, such as detergents and large hydrophobic antibiotics usually only effective against Gram-positive bacteria.[19] This permeability is responsible for cell death, at least in this bacterial species.

1.2.1. Mechanism of KDO8P synthase

The mechanism of KDO8P synthase has been the subject of in depth study and a number of observations have been made. In contrast with many other PEP utilising enzymes, the chemical mechanism of the reaction KDO8P synthase catalyses involves the cleavage of the C-O bond of PEP rather than the more common cleavage of the high energy P-O bond (ΔG^0 = -62.0 kJ/mol).[20] This was determined by studies using PEP labelled with ^{18}O in the bridging oxygen position, showing that the ^{18}O was recovered as inorganic phosphate.[21] The same study that determined the C-O bond cleavage also showed the reaction was irreversible by incubating KDO8P synthase and ^{32}P labelled inorganic phosphate with just PEP, PEP and R5P, and PEP and A5P. No exchange of ^{32}P into PEP was observed under any of these conditions.[21]

Analysis of the product formed from the KDO8P synthase catalysed reaction using stereospecifically deuterated PEP has shown the condensation proceeds in a stereospecific manner *via* the attack of the *si* face of PEP onto the *re* face of A5P[22] as shown in Figure 1.5.

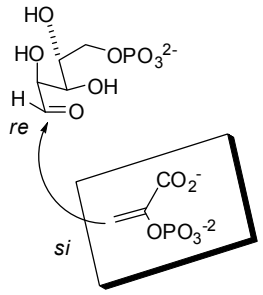

Figure 1.5: Stereospecificity of the KDO8P synthase reaction

This condensation was thought to occur *via* one of two mechanisms, involving either attack of the 3-hydroxy group or a water molecule on C2 of PEP to give cyclic (path b)[23] or acyclic (path a)[21] intermediates respectively (Figure 1.6).

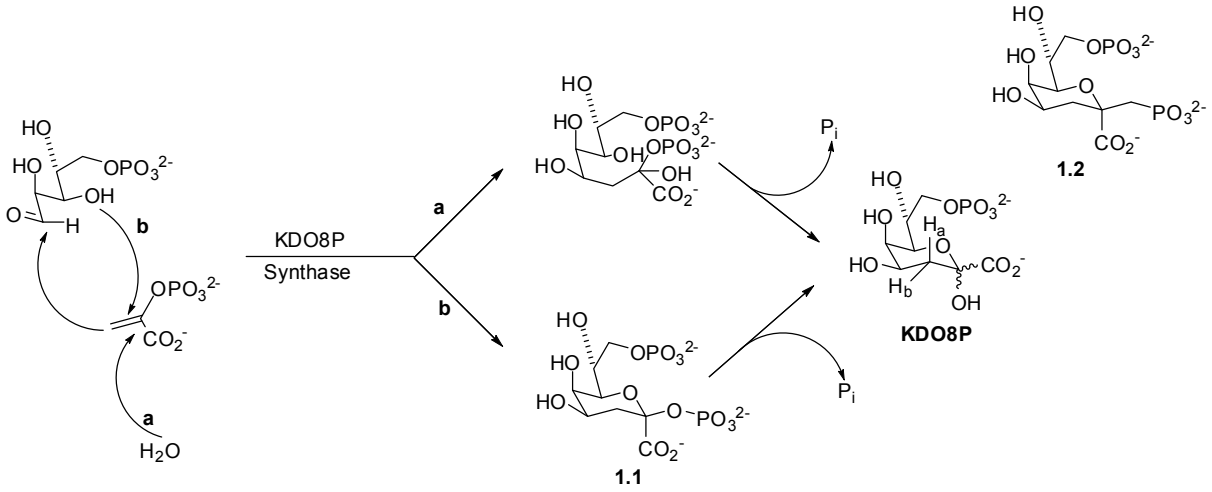

Figure 1.6: Two proposed mechanisms of KDO8P synthase and the isosteric cyclic phosphonate analogue 1.2.

The reaction through a cyclic intermediate (path b, Figure 1.6) has been largely discounted in a number of different studies. The proposed cyclic intermediate 1.1 has been synthesised and tested both as a substrate for, and inhibitor of KDO8P synthase.[24,25] It was found not to be a substrate for KDO8P synthase, broke down to KDO8P and inorganic phosphate at the same rate regardless of the presence of the enzyme, and was a competitive inhibitor with a moderate K_i value of 35 μM for *E. coli* KDO8P synthase (*Eco*KDO8PS). The best cyclic inhibitor to date, the isosteric phosphonate analogue 1.2, in which the bridged oxygen is replaced by a methylene group, had a K_i of only 4.9 μM for *Eco*KDO8PS,[23] which should be considered high for an inhibitor containing the topological and electrostatic properties of the reaction intermediate. Reaction *via* an acyclic intermediate (path a, Figure 1.6) was then thought to be the most likely reaction mechanism, with a linear transition state mimic showing the most potent inhibition to date with a K_i value of 0.42 μM against *Eco*KDO8PS.[26,27]

Shortly thereafter, the linear intermediate was identified by time-resolved ESI-TOF mass spectrophotometry, a technique that allows for the detection of enzyme-intermediate complexes with lifetimes of less than 10 ms. The technique can be considered a stopped-flow spectrophotometry equivalent of mass-spectrometry.[28] Using this technique the hemiketal phosphate intermediate bound to the enzyme was identified (Figure 1.7). This was the first direct evidence for the KDO8P synthase mechanism.

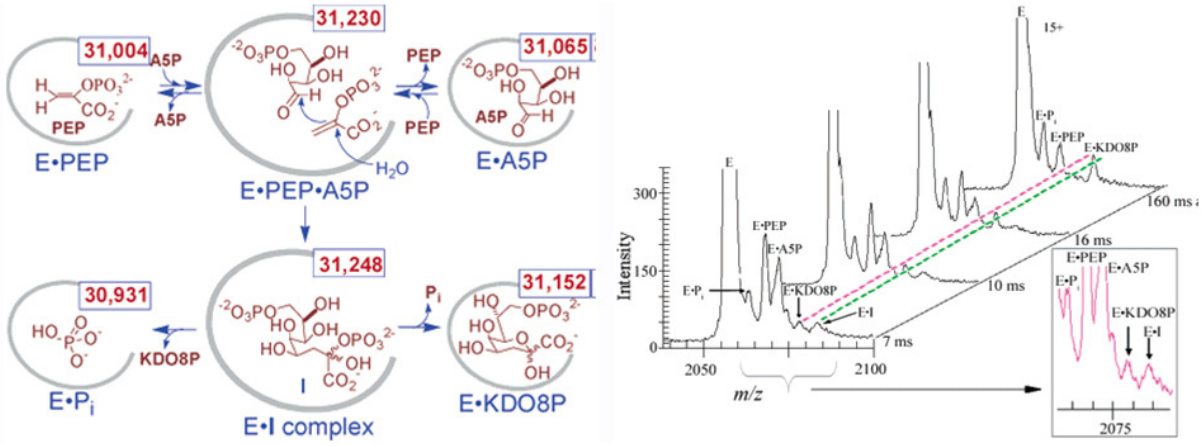

Figure 1.7: Time-resolved ESI-TOF mass spectra for the KDO8P synthase reaction showing the partial enzyme mechanism through analysis of the mass peaks. Taken from Li *et al.*[28]

Using the same technique, rate data were collected for the enzymic reaction (Figure 1.8).[29] The formation of the intermediate was found to be rate limiting (k = 95 s^{-1}) and the breakdown of this intermediate to KDO8P much faster (k = 500 s^{-1}). These values agree with the overall kinetic constant first determined for the KDO8P synthase reaction (k = 100 s^{-1}).

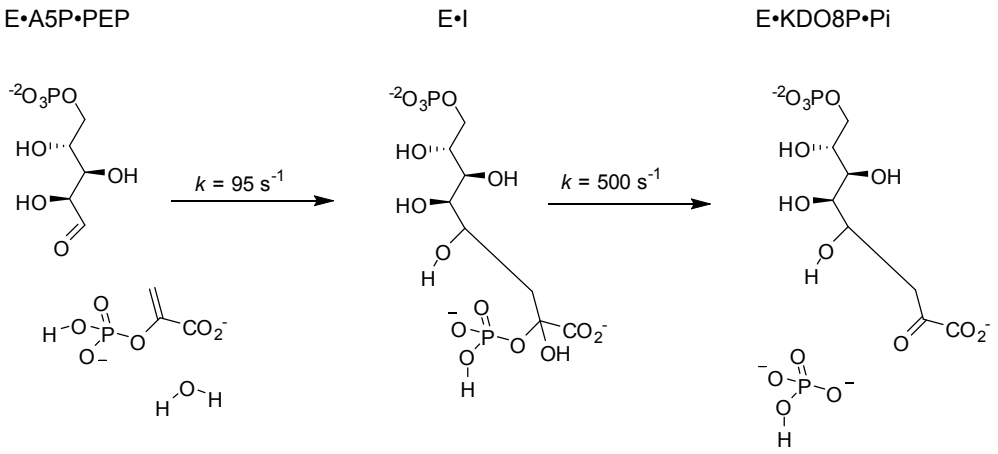

Figure 1.8: Rate constants for formation and breakdown of the tetrahedral intermediate in the KDO8P synthase reaction.

Two mechanisms have been proposed for the enzymic reaction through the known linear intermediate, and differ in how the water attacks the C2 carbon of PEP (Figure 1.9).

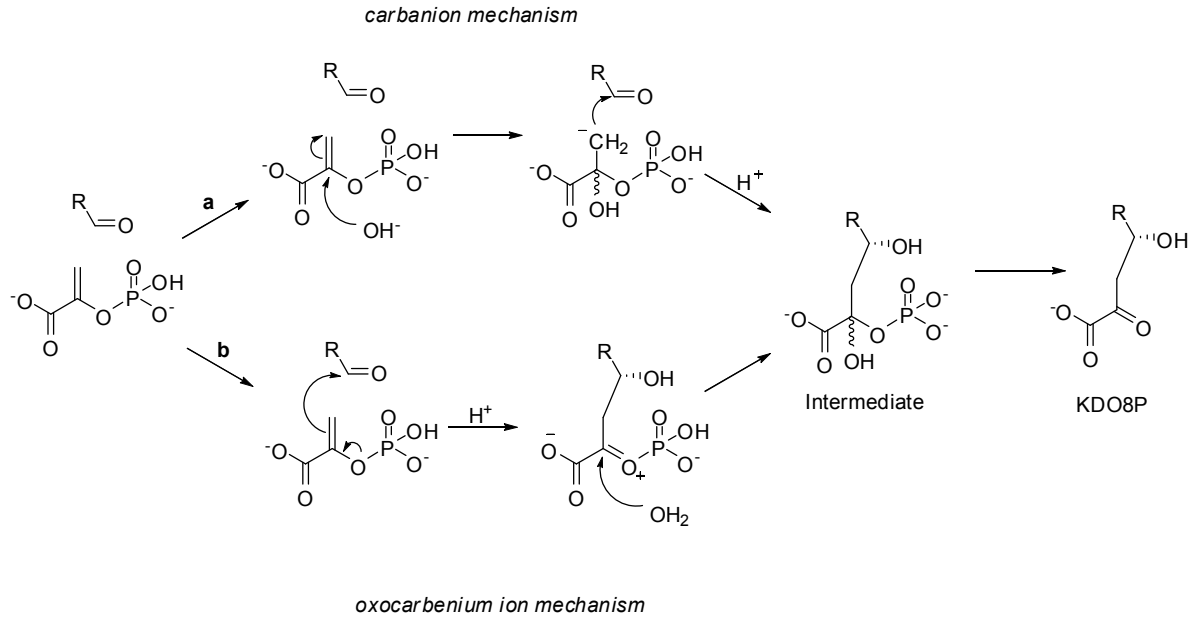

Figure 1.9: Two competing roles of the water molecule in the KDO8P synthase reaction.

The first (path a, Figure 1.9) involves deprotonation of a water molecule as the carbonyl moiety of A5P approaches. This hydroxide ion then attacks the C2 carbon of PEP either producing a transient carbanion molecule[30] producing a negatively charged C3 of PEP which reacts with the C1 atom of A5P, or through a concerted mechanism. The carbanion mechanism has many flaws associated with it. It requires that the C2 carbon of PEP have unprecedented electrophilic character in order for the hydroxide ion attack to occur, as well as requiring the existence of an unstabilised carbanion, with a pK_a likely to be > 30, inside the enzyme active site surrounded by protons of far greater acidity. It is highly likely that any carbanion, even one that only need exist for a short period of time, would immediately be quenched by one of these active site protons and therefore be unable to react to form the linear intermediate.

The second proposed mechanism (path b, Figure 1.9) is more plausible and involves the formation of an oxocarbenium ion, either a transition state with oxocarbenium character or a high energy intermediate *via* attack of the C3 atom of PEP with the C1 atom of A5P, and reaction of this ion with a water molecule on the C2 atom of this intermediate.[31] It has been proposed that both the related enolpyruvyl transferases, enolpyruvylshikimate-3-phosphate (EPSP) synthase and UDP-GlcNAc enolpyruvyl transferase (MurZ), catalyse a reaction that proceeds *via* a similar oxocarbenium ion, either as a reaction intermediate or highly unstable transition state molecule.[32,33] In the similar aldolase DAH7P synthase this is thought to be

aided by activation of the carbonyl *via* the divalent metal ion in the active site using Lewis acid catalysis. Not all KDO8P synthase enzymes require a metal ion however (*vide infra*), and in all crystal structures of the wild-type metal-dependent KDO8P synthase from *Aquifex aeolicus* (*Aae*KDO8PS) with A5P bound, the aldehyde moiety of the A5P is not close enough to the metal ion to interact with it.[34] Instead, it has been proposed that the bound PEP is in the monoanionic state, and the second weaker phosphate ionisation of PEP may be used to protonate the A5P carbonyl oxygen (Figure 1.10).[30] This theory is supported by the presence of a conserved phenylalanine residue in KDO8P synthases near the phosphate moiety of PEP that may promote this monoanionic binding. It should be noted that the opposite conformation, with the A5P aldehyde moiety within bonding distance of an asparagine residue, representative of the metal ion in metal-independent KDO8P synthase enzymes, has been observed in a mutant enzyme,[35] and will be discussed in more detail in Section 1.3.2.

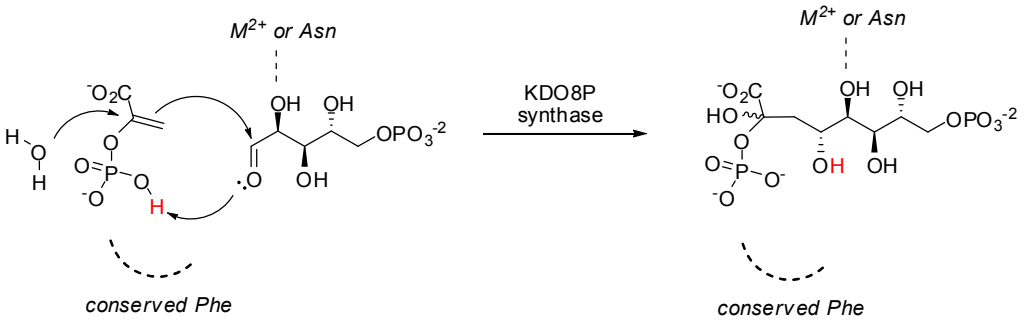

Figure 1.10: Proposed partial mechanism showing protonation of the aldehyde moiety by the monoanionic phosphate of PEP.

A 2009 study[36] used a crystal structure of a metal-independent C11N mutant of *Aae*KDO8PS[35] as the basis for computational studies in order to probe the two reaction pathways. They found that the most energetically favourable pathway to the formation of the intermediate (Figure 1.9) was a concerted mechanism between PEP, A5P and a water molecule in the enzyme active site.[36]

1.3. Two classes of KDO8P synthase

KDO8P synthases have been divided into two classes; those which require a divalent metal ion for catalytic activity (KDO8P synthases from *A. aeolicus*,[37] *Aquifex pyrophilus*,[38] *Helicobacter pylori*,[39] *Chlamydia psittaci*,[39] and those that do not (*E. coli*,[17] *Neisseria meningitidis*[40]). The similarity in sequence and structure between these two classes is high,

and a sequence alignment of annotated KDO8P synthase genes from different species reveals a number of conserved residues, as well as distinct differences between the two classes that can be putatively assigned as either a metal-dependent or metal-independent KDO8P synthase by the presence of either a conserved cysteine or arginine residue respectively in the metal binding site, or equivalent area of the metal-independent enzyme (Figure 1.13).

1.3.1. Evolutionary relationship to DAH7P synthases

The 3-deoxy-D-*arabino*-heptulosonate 7-phosphate (DAH7P) synthases, a related aldolase enzyme, that catalyses the condensation reaction between the four carbon aldehyde erythrose 4-phosphate and PEP (Figure 1.11), has been divided into two types based on sequence similarity, the type I and type II DAH7P synthases (Figure 1.12).[41] The sequence similarity between these two types is ~10 %, below the level of statistical significance for such a measurement. The type II enzymes are around 50 kDa. Until recently it was thought that type II DAH7P synthases were only found in plants, though they have now been found in some bacterial species such as *Mycobacterium tuberculosis, H. pylori* and *Campylobacter jejuni*. The type I DAH7P synthases are smaller at around 40 kDa, and can be further split into two classes, the Iα and Iβ DAH7P synthases (Figure 1.12). The Iα are considered the most ancestral of the aldolases, and contains species of comparatively ancient lineages such as *Pyrococcus furiosus* and *Thermotoga maritima*.[42] The Iβ class are thought to be related to the KDO8P synthases through divergent evolution, by sequence similarity and morphological studies and it is thought that the metal-independent KDO8P synthase enzymes diverged from the metal dependent enzymes.[39] All DAH7P synthase enzymes characterised thus far require a divalent metal ion for catalysis[43-48] and this is used as further evidence that the metal-independent KDO8P synthases are the newest branch of the aldolase evolutionary tree.[39]

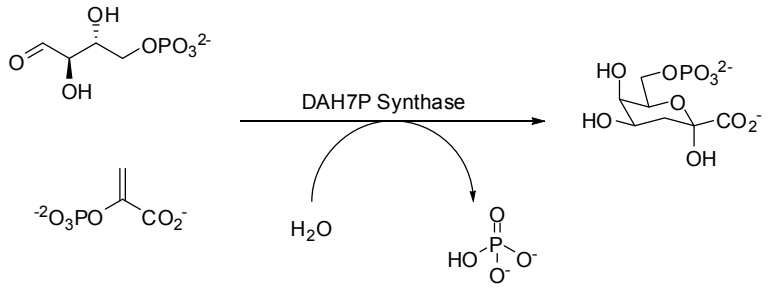

Figure 1.11: The reaction catalysed by DAH7P synthase.

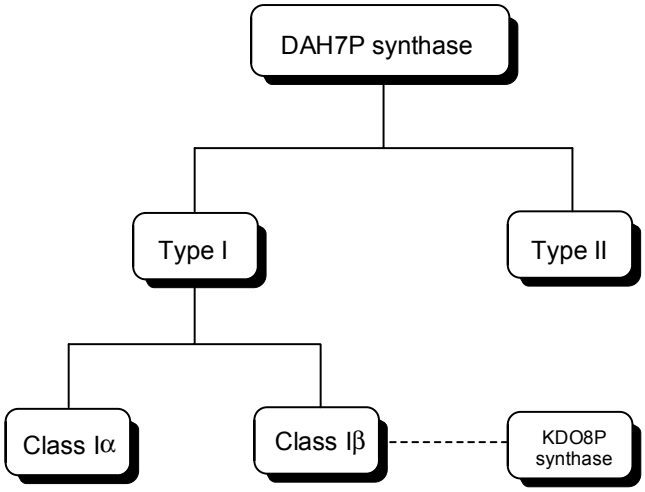

Figure 1.12: The types of DAH7P synthase and relationship to KDO8P synthase.

```
Eco             MKQKVVSIGDINVANDLPFVLFGGMNVLESRDLAMRICEHYVTVTQKL-GIPYVFKASFD
Nme             MDI---KINDITLGNNSPFVLFGGINVLESLDSTLQTCAHYVEVTRKL-GIPYIFKASFD
Hin             MQNKIVKIGNIDVANDKPFVLFGGMNVLESRDMAMQVCESYVKVTEKL-GVPYVFKASFD
Aae             ME---------------KFLVIAGPCAIESEELLLKVGEEIKRLSEKFKEVEFVFKSSFD
Afe             MRL-----CGFEAGLQHPFFLMAGPCAIESESLALRTAEDLRDICARL-GIPFIYKSSYD
Hpy             MKTS--------KTKPPKSVLIAGPCVIESLENLRSIAIKLQPLANNE-RLDFYFKASFD
Cps             MQKF--SVGTVSLPGPKGLFLIAGPCLIENRRMAMDVAAELDRIRKKE-DVRVIFKGSYR
                *                 .::.*   :*.            :  .   :   :*.*:

Eco             KANRSSIHSYRGPGLEEGMKIFQELKQTFGVKIITDVHEPSQAQPVADVVDVIQLPAFLA
Nme             KANRSSIHSYRGVGLEEGLKIFEKVKAEFGIPVITDVHEPHQCQPVAEVCDVIQLPAFLA
Hin             KANRSSIHSYRGPGMEEGLKIFQELKDTFGVKIITDVHEIYQCQPVADVVDIIQLPAFLA
Aae             KANRSSIHSFRGHGLEYGVKALRKVKEEFGLKITTDIHESWQAEPVAEVADIIQIPAFLC
Afe             KANRSSGQSFRGPGMDEGLRILEKVRREVGVPVVTDVHEKEDVSAVAEVVDVLQTPAFLC
Hpy             KANRTSLESYRGPGLEKGLEMLQIIKEEFGYKILTDVHESYQASVAAKVADILQIPAFLC
Cps             KANRSSASSYTGIGDRQALEILREIRDYFGMPVLTDVHETSEVELAASYVDVLQIPAFLC
                ****:*  *: * *   .:. :. ::  .*  : **:**  : . .*.  *::* ****.

Eco             RQTDLVEAMAKTGAVINVKKPQFVSPGQMGNIVDKFKEGG-------------NEKVILC
Nme             RQTDLVVAMAKTGNVVNIKKPQFLSPSQMKNIVEKFHEAG-------------NGKLILC
Hin             RQTDLVEAMAKTGAVINVKKPQFLSPSQMGNIVEKIEECG-------------NDKIILC
Aae             RQTDLLLAAAKTGRAVNVKKGQFLAPWDTKNVVEKLKFGG-------------AKEIYLT
Afe             RQTDFIQAVAAAGKPVNIKKGQFLAPWDMLHVASKAKATG-------------NEQIMVC
Hpy             RQTDLIVEVSQTNAIINIKKGQFMNPKDMQYSVLKALKTRDSSIQSPTYETALKNGVWLC
Cps             RQTDLIVAAASTGLAVNIKKGQFLAPEDMALAAAKAAATG-------------NKKIMLT
                ****::   : :.  :*:** **: * :    . *                    : :

Eco             DRGANFGYDNLVVDMLGFSIMKKVSGNSPVIFDVTHALQCRDPFGAASGGRRAQVAELAR
Nme             ERGSSFGYDNLVVDMLGFGVMKQTCGNLPVIFDVTHSLQTRDAGSAASGGRRAQALDLAL
Hin             DRGTNFGYDNLIVDMLGFSVMKKASKGSPVIFDVTHSLQCRDPFGAASSGRRAQVTELAR
Aae             ERGTTFGYNNLVVDFRSLPIMKQW---AKVIYDATHSVQLPGGLGDKSGGMREFIFPLIR
Afe             ERGASFGYNNLVSDMRSLAVMRQT--GCPVVFDATHSVQLPGGQGDRSGGQREFIPVLAR
Hpy             ERGSSFGYGNLVVDMRSLTIMREF---APVIFDATHSVQMPGGANGKSSGDSSFAPILAR
Cps             ERGTTFGYHNLVVDYRGLPIMAES--GWPVILDVTHSVQLPGAGAGVSGGDRRFLMPLAR
                :**:.*** **: *  .: :* :      *: *.**::*  .     *.*       *

Eco             AGMAVGLAGLFIEAHPDPEHAKCDGPSALPLAKLEPFLKQMKAIDDLVKG--FEEL--DT
Nme             AGMATRLAGLFLESHPDPKLAKCDGPSALPLHLLEDFLIRIKALDDLIKS--QP-I--LT
Hin             SGLAVGIAGLFLEAHPNPNQAKCDGPSALPLSALEGFVFQMKAIDDLVKS--FPEL--DT
Aae             AAVAVGCDGVFMETHPEPEKALSDASTQLPLSQLEGIIEAILEIREVASK--YYET--IP
Afe             AAVAAGVSGLFMETHPNPADALSDGPNAWPLGRMEDLLRILQHIDHVVKNQDFPENYPEE
Hpy             AAAAVGIDGLFAETHVDPKNALSDGANMLKPDELERLVTDMLKIQNL-------------
Cps             AAVAAGVDGLFFEVHPDPATAMSDASTQAPLAGFGEMVRELMQLQRCMQS--IREE--FH
                :. *.   *:* * * :*  * .*...      :  ::  :  :
```

Key: Metal a5p pep re-face H_2O *:. Well/moderately/partially conserved residues

Figure 1.13: Sequence alignment of KDO8P synthases from both classes. Including in the alignment are the sequences from the metal-independent class; *E. coli* (*Eco*), *N. meningitidis* (*Nme*), *Haemophilus influenza (Hin*), and the metal-dependent class; *A. aeolicus* (*Aae*), *Acidithiobacillus ferrooxidans* (*Afe*), *H. Pylori* (*Hpy*) and *C. psittaci* (*Cps*). Roles of key residues are indicated. Alignment generated with Expressio, www.tcoffee.org.

As shown in Figure 1.13, the active site residues are the same between the two classes of KDO8P synthase, except for those that contribute to the metal binding site (Figure 1.15).

In the metal-dependent KDO8P synthases, the metal binding site is in a distorted octahedral geometry, with the metal bound to four residues, C11, D233, E222 and H185 in *Aae*KDO8PS, and a conserved water molecule (Figure 1.14). In some crystal structures this water molecule is displaced when A5P is bound, with the C2 hydroxyl of A5P replacing it as a metal ligand.[34]

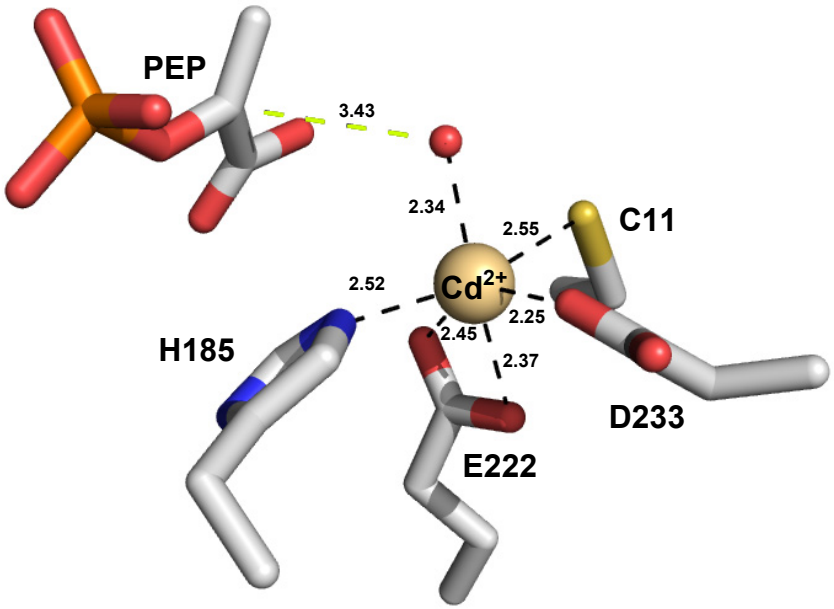

Figure 1.14: Metal coordination site of *Aae*KDO8PS (drawn from 1FWW[34]). The metal ion (cadmium, gold) is bound to absolutely conserved residues C11, D233, E222 and H185 with the fifth ligand normally being a conserved water molecule, shown to be bridging C2 of PEP (bonding between the cadmium ion and ligands is shown in black, bonding between the water molecule and C2 of PEP is shown in yellow). Substrates and amino acid side chains are shown in red/blue/yellow/grey/orange (O/N/S/C/P respectively). Distances are measured in angstroms.

In the metal-independent class of KDO8P synthase the cysteine residue that acts as a metal ligand is replaced with a conserved asparagine residue that probes further into the active site,[49] and displaces the aspartate residue that acts as a metal binding ligand in *Aae*KDO8PS.[34]

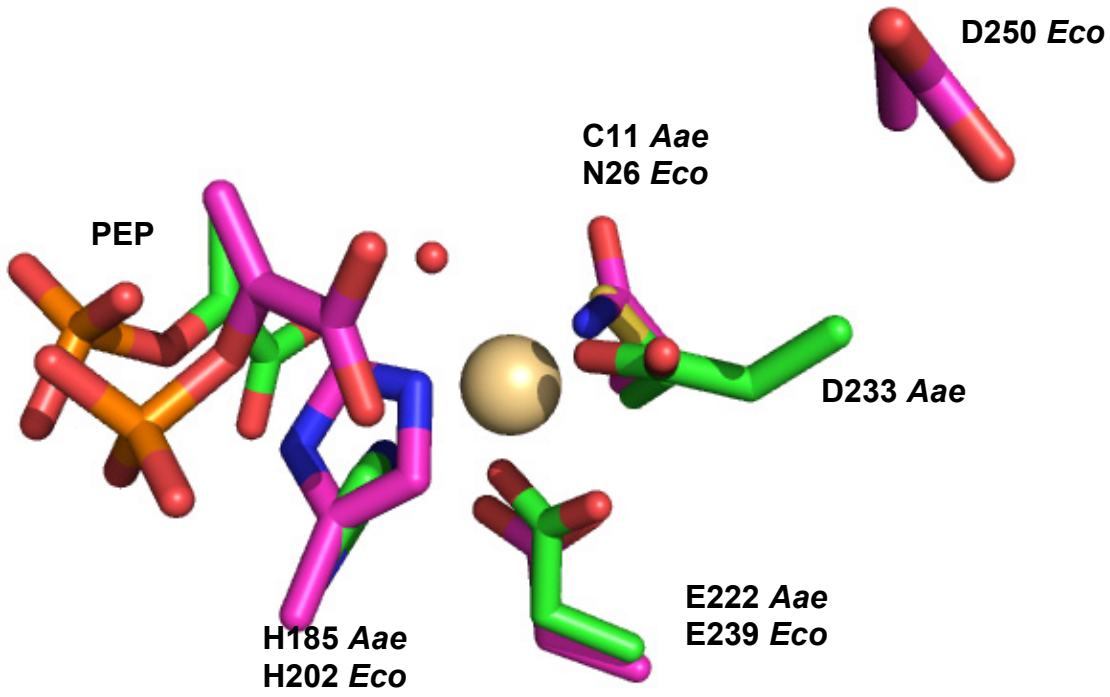

Figure 1.15: Overlay of the metal (cadmium, shown in gold) binding residues and active site bound PEP in *Aae*KDO8PS (shown in green, drawn from 1FWW[34]) and equivalent residues in the metal-independent *Eco*KDO8PS (shown in magenta, drawn from 1Q3N[50]). D250 from *Eco*KDO8PS (top right) is equivalent to D233 from *Aae*KDO8PS (middle left).

1.3.2. Conversion of metal-dependency by site-directed mutagenesis

Many of the conserved residues that differ between the two classes of KDO8P synthase have been mutated to determine whether it is possible to convert a KDO8P synthase from one class into the other. Conversion of the two classes by mutation of conserved residues may give insight into the evolutionary path the KDO8P synthase enzyme took from an ancestral DAH7P synthase-like enzyme, and show how it evolved to become metal-independent in some bacterial species.

As previously discussed, the most obvious difference in the active site between the two classes of enzyme is the replacement of a conserved, metal binding cysteine residue in the metal-dependent class of KDO8P synthase with a conserved asparagine residue in the metal-independent class. Initially this was attempted with *Aae*KDO8PS to remove metal-dependency and the C11 residue in *Aae*KDO8PS was mutated to an asparagine residue.[51] The result of this single C11N mutation was an enzyme that was no longer activated by the addition of divalent metal ions, and whose catalytic activity was unaffected by the presence of the metal chelating agent ethylenediaminetetraacetic acid (EDTA), which has been shown

to significantly reduce the wild-type *Aae*KDO8PS activity to 0.4 % of the maximum activity in the presence of divalent metal ions.[37] The specific activity of the C11N mutant was 75 % that of wild-type, but was catalytically more efficient; the k_{cat}/K_m for PEP increased from 0.0027 to 0.053 s^{-1} μM^{-1}, and PEP bound more tightly; K_m of PEP decreased from 155 µM for wild-type to 12 µM for the C11N mutant, at 60 °C. The K_m for A5P was largely unaffected, which is expected as the mutation is found in the PEP binding site, and not the A5P binding site. The crystal structure of the C11N mutant of *Aae*KDO8PS[34] shows that the N11 residue overlays with the equivalent residue (N26) in *Eco*KDO8PS.[50]

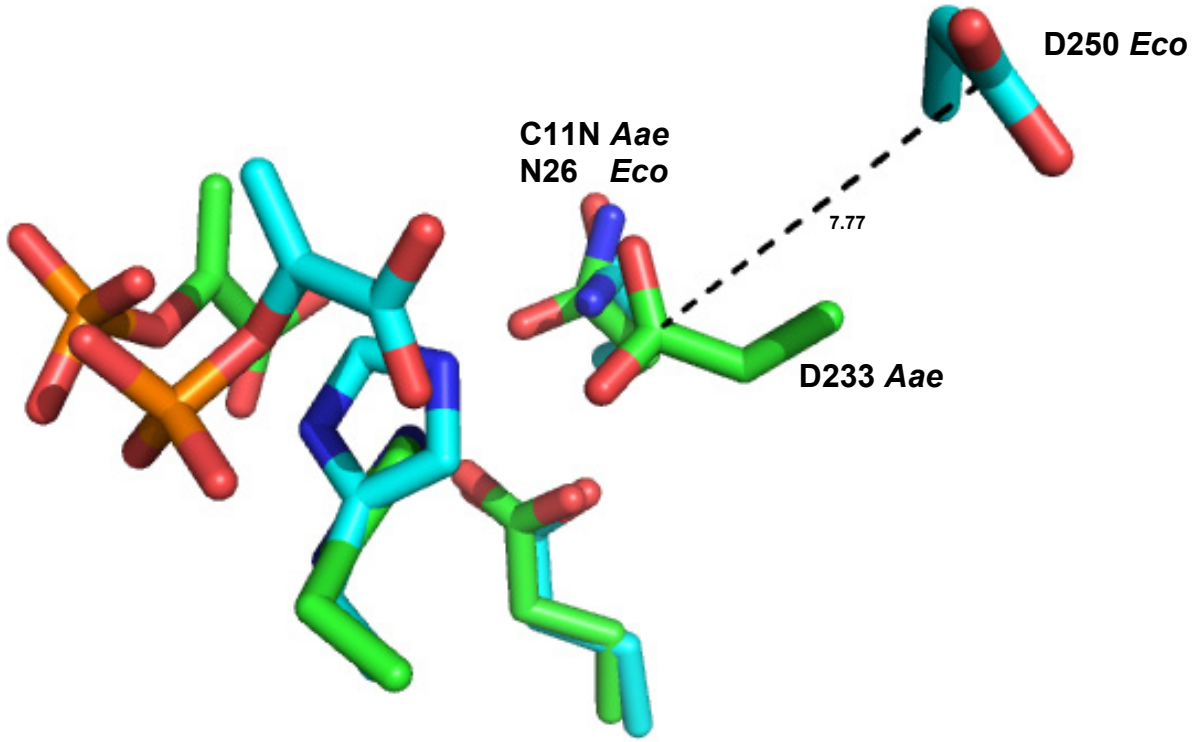

Figure 1.16: Overlay of the previously metal binding residues and active site bound PEP in the C11N mutant of *Aae*KDO8PS (shown in green, drawn from 2NWS[34]) and equivalent residues in the metal-independent *Eco*KDO8PS (shown in cyan, drawn from 1Q3N[50]). Important residues have been identified and distances are measured in angstroms.

The reverse mutation (N26C) was also attempted in *Eco*KDO8PS to determine whether a single mutation could convert a metal-independent enzyme into a metal-dependent enzyme. This was not as successful however, and produced mixed results over a number of different studies.[51,52] The same 2004 study that produced the metal-independent C11N mutant of *Aae*KDO8PS reported a virtually inactive enzyme when the N26C mutation was performed in *Eco*KDO8PS.[51,52] A second 2004 study by Shulami *et al.* produced an N26C mutant of *Eco*KDO8PS that had a specific activity of 0.14 U mg^{-1} that increased to 0.73 U mg^{-1} in the

presence of EDTA, but that had a more than five-fold increase in k_{cat} when assayed in the presence of Mn^{2+} or Cd^{2+} metal ions.[52] In the presence of Cd^{2+} the K_m of PEP for the N26C mutant was comparable to the value for wild-type *Eco*KDO8PS (5.8 and 6.0 μM respectively). The increase in specific activity may have been due to the presence of inhibitory metal ions such as Pb^{2+} that were removed upon addition of EDTA. The results from the study of *Eco*KDO8PS N26C demonstrated that the conversion of metal-dependency may not be achieved solely by single point mutations, and changes to other correlated residues may be required.

It had been shown that a single point mutation was not sufficient in creating a bonafide metal-dependent KDO8P synthase from a metal-independent KDO8P synthase, and so a study was undertaken in 2004 that implemented a double mutation in *Eco*KDO8PS adjacent to the N26 residue.[53] Metal-dependent KDO8P synthases have a conserved proline before the conserved cysteine that contributes to the metal binding site. In *Eco*KDO8PS and some other metal-independent KDO8P synthases this residue is instead a methionine. Thus a double M25P/N26C mutation was created in *Eco*KDO8PS. The k_{cat} for the M25P/N26C mutant enzyme doubled when Mn^{2+} was added, from 1.65 to 3.2 s^{-1} which is a small increase but one that is greater than for the single N26C mutation (0.8 to 1.23 s^{-1}). The M25P/N26C mutant enzyme can still not be considered a bonafide obligate metal-dependent enzyme however, as in the absence of divalent metal ions 52 % of wild-type activity was retained.

As shown in Figure 1.15 and Figure 1.16, a conserved aspartate (D233) that is a metal binding ligand in metal-dependent KDO8P synthases such as that from *A. aeolicus* (Figure 1.14) is not found in the same position for the metal-independent *Eco*KDO8PS. Instead the aspartate (D250 in *Eco*KDO8PS) adopts an opposing orientation close to 7.7 Å away from the position it adopts in the *Aae*KDO8PS active site and has its side chain projected away from the metal binding site in *Aae*KDO8PS.[50] However in some crystal structures of the metal-independent KDO8P synthase from *E. coli*[54] and *N. meningitidis*[55] this area of the protein is poorly defined, indicating increased mobility. Two separate studies mutated amino acids around this conserved aspartate in order to probe their importance in the orientation of this residue.

A 2009 study by Cochrane *et al.* attempted to create a metal-dependent KDO8P synthase from the metal-independent *N. meningitidis* KDO8P synthase (*Nme*KDO8PS) by a combination of four mutations.[55] The N23C mutation is identical to that which was created

in *Eco*KDO8PS in order to re-establish the metal binding scaffold.[51,52] The other three residues targeted, C246, D247 and P249 are part of a conserved CDGP sequence in metal-independent KDO8P synthase enzymes, that is only sometimes present amongst metal-dependent KDO8P synthases.[56] Instead, the cysteine residue is usually replaced with a serine residue, glycine is sometimes substituted for an alanine, and less commonly a serine, and the proline is often substituted for an alanine, serine or threonine. C246 was mutated to a serine, which is present in most putative metal-dependent KDO8P synthase sequences. P249 was mutated to a conformationally less restrictive alanine residue, as it was thought that in metal-independent KDO8P synthases, this residue may be involved in the orientation of the conserved aspartate residue. Finally, the conserved aspartate, D249, was mutated to glutamate, as the extended side chain would provide additional flexibility and potentially give improved metal binding. All of the combinations of mutated residues that were created showed an increase in specific activity when treated with Mn^{2+} instead of the metal chelating agent EDTA, with three of the mutants showing activity only in the presence divalent metal ions; N23C/C246S/D247E, showing an increase in specific activity from 0.01 to 8.4 U mg^{-1} and k_{cat} of 3.9 s^{-1}; N23C/C246S/P249A showing an increase in specific activity from 0.06 to 9.8 U mg^{-1} and k_{cat} of 4.79 s^{-1}; N23C/C246S/D247E/P249A showing an increase in specific activity from 0.01 to 5.64 U mg^{-1} and k_{cat} of 4.4 s^{-1}. The N23C/D247E/P249A triple mutant still showed some activity (0.35 U mg^{-1}) in the presence of EDTA, which demonstrates the importance of the C246S mutation in the creation of the metal-dependent enzyme. In crystal structures of mutant *Nme*KDO8PSs C246 forms a disulphide bond with N23C when the C246S mutation is not present (Figure 1.17), and this may negatively affect metal binding. The crystal structure of the quadruple mutant (3FYP)[55] has a poorly defined L8 loop, on which the C246S/D247E/P249A mutations are found, and this may indicate a large amount of disorder in this region. It has been proposed that the conserved cysteine in the CDGP sequence found in metal-independent KDO8P synthases plays a role in positioning the L8 loop by hydrogen bonding to an asparagine residue found on the L2 loop.[55] The difference in this sequence for metal-dependent KDO8P synthases may be be due to the conserved aspartate on the L8 loop acting as a metal ligand, thereby locking the L8 loop in place, making the cysteine-asparagine interaction unnecessary.

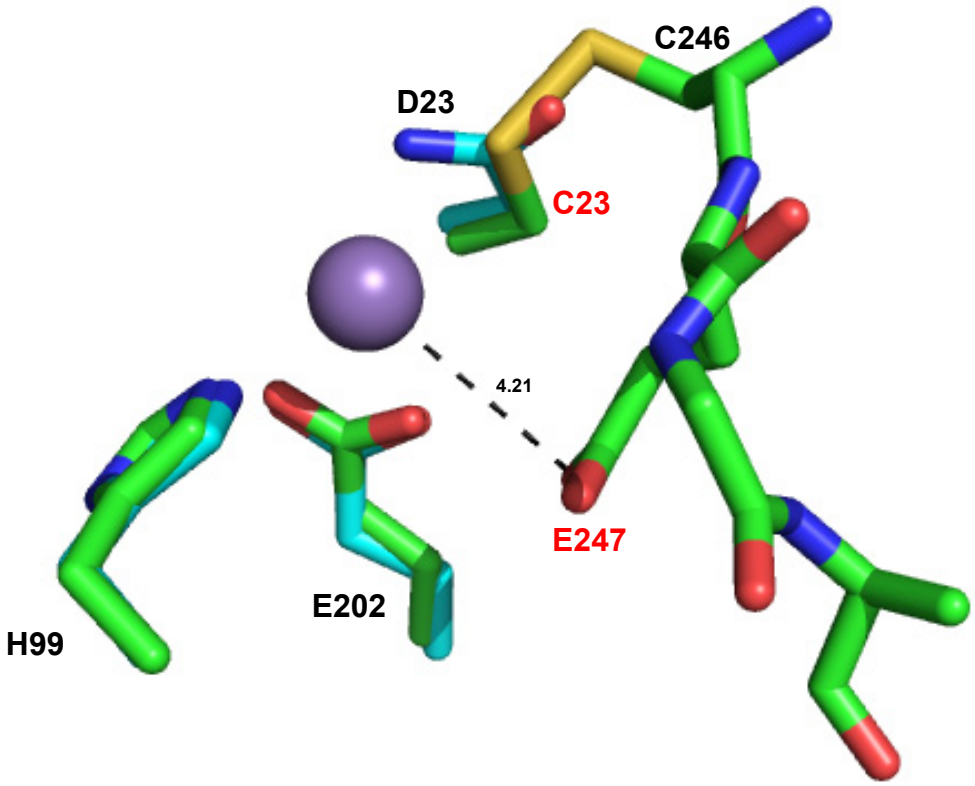

Figure 1.17: Overlay of the metal binding site of *Nme*KDO8PS N23C/D247E/P249A triple mutant (3FYO, green),[55] and wild-type *Nme*KDO8PS residues (2QKF, cyan).[55] Manganese ion in the triple mutant structure is coloured purple. The new disulphide linkage between C246 and the new C26 residue in the triple mutant is shown. Residues distinct to the *Nme*KDO8PS N23C/D247E/P249A triple mutant are labelled in red. Distance from the bound manganese ion to E247 is measured in angstroms.

Similar mutations have been created in the metal-dependent *Aae*KDO8PS, with a series of multiple point mutations; C11N, P10M/C11N, C11N/S235P/Q237A and P10M/C11N/S235P/Q237A.[35] S235 and Q237 are found on the L8 loop and S235 is analogous to the proline in the CDGP sequence of metal-independent KDO8P synthases. The importance of the proline to methionine mutation between the two classes of KDO8P synthases has previously been discussed with regard to the 2004 mutagenesis study on *Eco*KDO8PS. The single and double mutations produced enzyme active sites that did not differ significantly from crystal structures of previous C11N mutants of *Aae*KDO8PS but crystals of the quadruple mutant diffracted very poorly. However, in the crystal structure of the C11N/S235P/Q237A mutant (2NX3) co-crystallised with A5P and PEP, the A5P bound in such a way that the C2 hydroxyl was not positioned towards the N11 residue (or metal ion in metal-dependent KDO8P synthase enzymes) as seen in all previous crystal structures of *Aae*KDO8PS. Instead the aldehyde moiety occupied this position, being within hydrogen

bonding distance of not only the N11 residue but also H185 and D233 that normally contribute to the metal binding site in *Aae*KDO8PS (Figure 1.18). Interestingly, a second crystal structure of the same mutant (2NXG) had the A5P bound in a configuration that resembled the A5P bound in the wild-type *Aae*KDO8PS. Thus, it cannot be concluded that either binding mode in the crystal structures is representative of the native binding mode in solution.

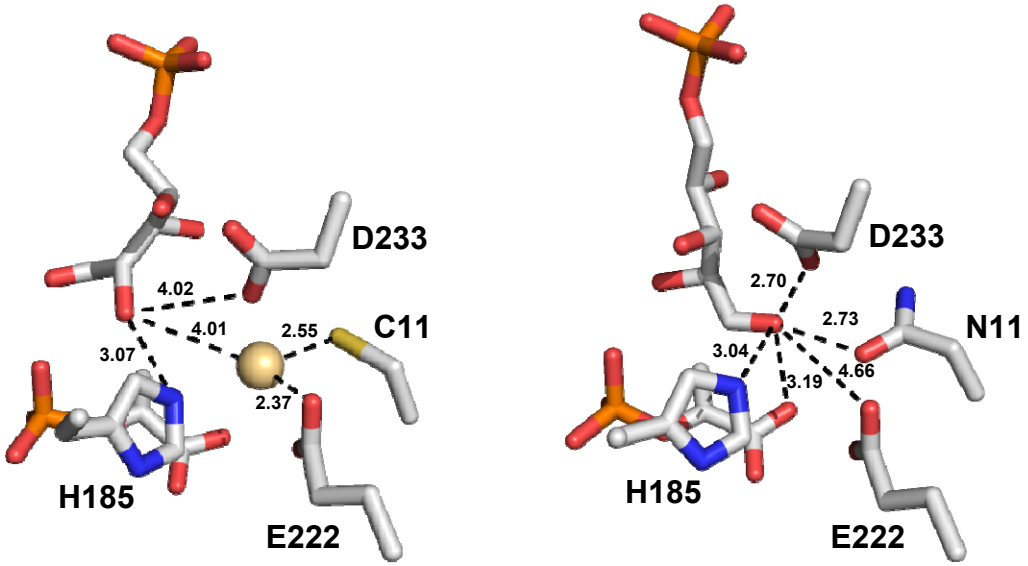

Figure 1.18: Comparison of A5P binding sites of wild-type *Aae*KDO8PS (left, 1FWW[34]) and the C11N/S235P/Q237A triple mutant (right, 2NX3[35]). A5P, PEP and surrounding residues are coloured orange/red/grey and blue (P, O, C and N respectively) and in the wild-type structure, the metal ion (cadmium) is coloured gold. Distances to neighbouring atoms are measured in angstroms.

1.3.3. Reactive water molecule

As previously discussed, the KDO8P synthase reaction occurs through the attack of a water molecule onto the C2 atom of PEP. Two possible candidates exist, conserved water molecules on the *re* and *si* face of PEP.[34] The *si* face water molecule, in metal-dependent KDO8P synthases, is a metal ligand,[30,34] though has shown to be displaced by the C2 hydroxyl of A5P in some crystal structures,[34] including the C11N mutant of *A. aeolicus*.[35] The *re* face water molecule may hydrogen bond with an aspartate and glutamate residue, and is also within bonding distance of the phosphate moiety of PEP (Figure 1.19).

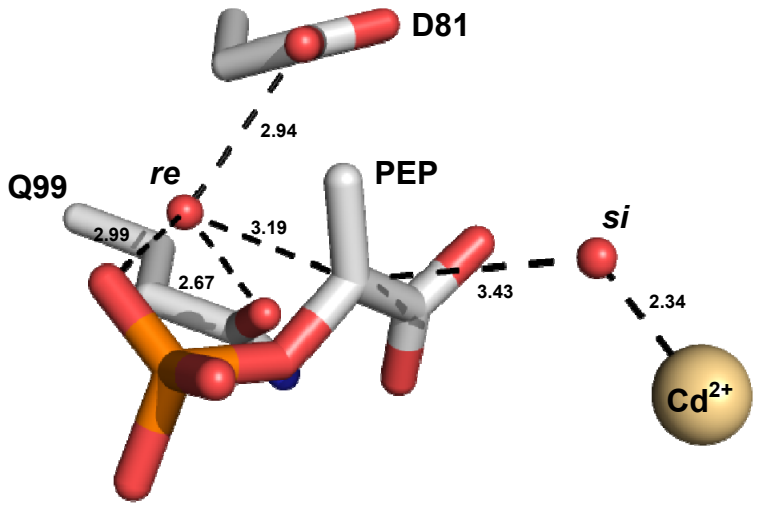

Figure 1.19: Conserved water molecules in the active site of *Aae*KDO8PS (1FWW[34]), found on the *re* and *si* faces of PEP that may be involved in enzyme catalysis. Also indicated are cadmium ion (gold) and surrounding residues D81 and Q99 (grey/red/blue) that may be involved in their activation and deprotonation. Distances to neighbouring atoms are measured in angstroms.

1.3.4. Observation of tetrahedral reaction intermediate

The asymmetric unit in the two crystal structures of the C11N/S235P/Q237A *Aae*KDO8PS triple mutant in the aforementioned 2007 paper by Kona *et al.* contain 12 (2NX3) and 2 (2NXG) subunits. In one of the subunits from each crystal structure a hemiketal tetrahedral intermediate of the KDO8P synthase reaction was modelled into the active site.[35] The authors claim that the modelled intermediate has the (*R*) configuration at the ketal carbon, implying PEP has reacted with the *si* face water molecule, *via* a carbanion mechanism or quenching of the oxocarbenium ion.

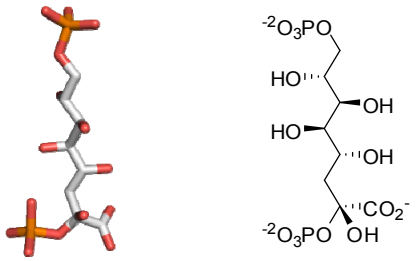

Figure 1.20: Hemiketal phosphate intermediate as reported by Kona *et al.* for the C11N/S235P/Q237A triple mutant of *Aae*KDO8PS; crystallographic and skeletal representations.[35]

The conclusion that the tetrahedral intermediate can be modelled over the electron density found in the KDO8P synthase active site is disputed. It has previously been reported that the hemiketal tetrahedral intermediate is highly unstable and the rate constants for formation and

breakdown of it were determined to be 95 s^{-1} and 500 s^{-1} respectively, for *Eco*KDO8PS,[29] so it seems unlikely it would be observable by crystallographic methods As already mentioned, the proposed intermediate is observed in only one active site of a large unit cell of twelve distinct monomers of the 2NX3 crystal structure, and only one of the two subunits in the 2NXG structure. In the other subunits for both crystal structures, a ternary enzyme-PEP-A5P complex is modelled and the trigonal planarity of the PEP molecule is still evident in most active sites. The PEP molecules have some bent character at C2, which has been assigned as degradation of PEP due to Michael addition of water at C3. This bent character is also seen in other KDO8P synthase crystal structures[34] and in some DAH7P synthase structures.{Shumilin, 2003 #130;Shumilin I., 2004 #131;Konig, 2004 #62} Additionally, as previously discussed in Section 1.3.2, the A5P orientation is rotated 180° between the two crystal structures of the C11N/S235P/Q237A *Aae*KDO8PS triple mutant, being in an orientation similar to that of the wild-type *Aae*KDO8PS structures with A5P bound for the 2NXG structures, where as in the 11 subunits not containing the intermediate from the 2NX3 structure it is bound with the aldehyde moiety orientated towards the N11 residue as discussed.

The authors show in their paper a $|F_o\text{-}F_c|$ σA map of the modelled enzyme without the intermediate included, overlaid with the proposed model of said intermediate (Figure 1.21). The amplitudes of the experimentally observed factors (F_o) are compared after subtraction of the structure factors that would be observed for the proposed model (F_c); the mean structure factor amplitude is denoted as σ. Usually, in such a diagram, one would expect to see a large unexplained area of electron density due to the difference between the observed data F_o (containing the ligand) and the calculated data F_c (not containing the ligand). The heavy atoms of the ligand (atomic weights > 12) should all appear inside this area. This should occur at a level of high electron density, that is much greater than σ. This is a simple method for assessing the viability of a ligand inside the enzyme active site. As seen in Figure 1.21, the new oxygen atom, being the only heavy atom to distinguish the proposed intermediate from the substrates, lies outside the density map contoured at 3σ, casting doubt onto the existence of the ligand in the crystal structure at all. As seen in both A and B of Figure 1.21, the C4 and C5 atoms of the intermediate are also deformed away from the electron density, giving additional weight to the theory that the intermediate may be incorrectly modelled inside the active site. C4 and C5 of the intermediate correspond to C1 and C2 of A5P and

this kind of deformation in the model could occur if the intermediate had been modelled over the electron density derived from two separate molecules.

These lines of evidence lead to the conclusion that the partial tetrahedral character could arise from the breakdown of PEP by Michael addition. It is possible that the proposed intermediate is simply an artefact, and more work is required in order to substantiate the observation of the proposed intermediate and its stereochemistry, bound in the KDO8P synthase active site.

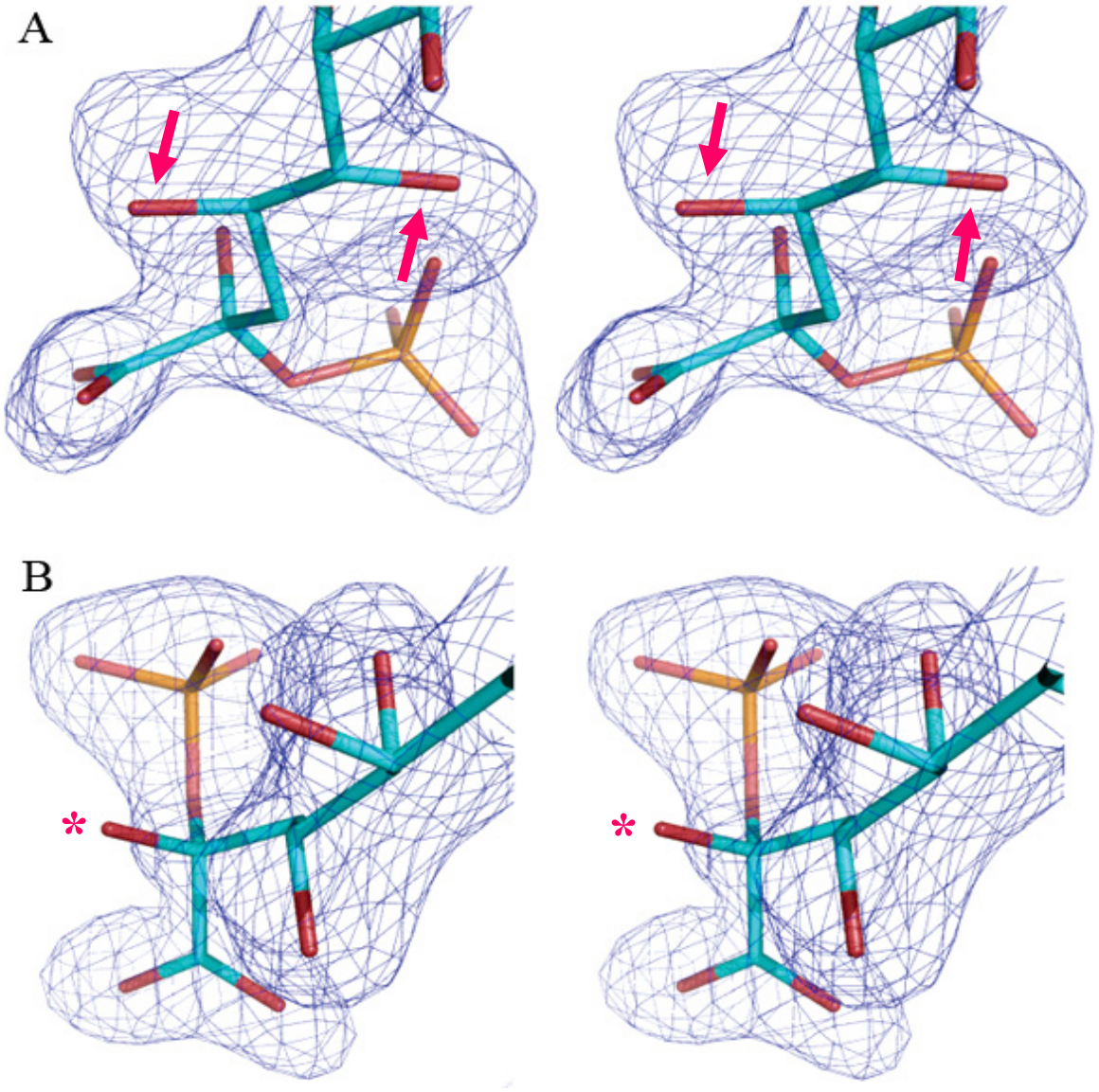

Figure 1.21: |*Fo* – *Fc*| σA (omit) map of the C11N/S235P/Q237A KDO8P synthase from *A. aeolicus* contoured at 3σ, with the tetrahedral intermediate overlaid. A and B are in different orientations designed to show that the C2 centre is no longer planar, the C2 hydroxyl residue protrudes outside the modelled electron density (pink *) and the C4 and C5 hydroxyls are deformed away from electron density (pink arrows). Diagram is taken from Kona *et al.*[35] and pink elements have been added.

As previously discussed, a 2009 study[36] used the crystal structure of the engineered metal-independent C11N mutant of *Aae*KDO8PS (which has both PEP and A5P bound)[35] as a basis for modelling potential energy surfaces for possible reaction pathways. This study showed that the lowest energy pathway was *syn* addition of the water molecule, that is, attack of the *si* face water molecule, and subsequent attack of the C3 of PEP onto the C1 of A5P, with an energy barrier of 19 kcal mol^{-1} for the formation of the tetrahedral intermediate. The *anti* addition involving attack of the *re* face water onto the C2 of PEP had a much higher energy barrier of 44 kcal mol^{-1}, and the authors concluded that the *syn* addition was much more likely. However, this study did not take into account the entire effect of the surrounding residues, and it is likely that these would have a large effect on the energy barrier of the KDO8P synthase reaction, nor did it test all possible and relevant reaction pathways, such as water attacking the *re* side of C2 of PEP and C3 of PEP attacking the *re* side of C1A5P; with the PEP phosphate partially protonated. At this stage it is unclear which water molecule is involved in the reaction mechanism of KDO8P synthase, and additional work will have to be undertaken in order to resolve this, some of which will be discussed further in chapters three and four.

1.4. KDO8P synthase structure

1.4.1. Tertiary and quaternary structure

A metal-dependent (*A. aeolicus*[34]) and two metal-independent (*E. coli*,[54] *N. meningitidis*[55]) KDO8P synthase have been thoroughly investigated by X-ray crystallography. Comparison of the structures indicates nearly identical tertiary structure. Each monomer is folded into a $(\beta/\alpha)_8$ TIM barrel (Figure 1.22**)**, with the active site located near the C-terminus end, which is typical for proteins of this fold.[60] Each monomer contains a β-hairpin which seals off the N-terminus end of the TIM barrel.

The first crystal structures of *Eco*KDO8PS showed the enzyme to be a homotetramer with a mass of around 120 kDa, calculated from the M_R of the monomeric product containing 284 amino acids (30833 Da).[54] Crystal structures of *Aae*KDO8PS show homodimers, but in solution it had a similar elution profile in size exclusion chromatography to KDO8P synthases from *E. coli* and *S. typhimurium*, suggesting *in vivo* it is tetrameric.[34] Additionally three other KDO8P synthases have been shown to be tetrameric; The metal-dependent *H.*

pylori KDO8P synthase[61] was shown to exist as both a dimer and tetramer in solution, with the tetramer breaking down to the dimer in the gas phase; KDO8P synthase from *A. ferrooxidans* (*Afe*KDO8PS) was shown to be a tetramer of 123 kDa by size exclusion chromatography;[62] the metal-independent *Nme*KDO8PS was shown to be a tetramer of 130 kDa in solution by gel filtration chromatography.[55]

The KDO8P synthase contact surface between subunits A and B (or C and D) are characterised by hydrophobic and polar interactions between the H6, H7 and H8 helices of one subunit and the same helices on the other subunit with two loops (L2 and L6) completing the tetrameric arrangement.[54] L2 on subunit A binds to the H4 and H5 helices on the C subunit, and the L6 loop of subunit A binds to the same loop of subunit C in the centre of the tetramer (Figure 1.23).

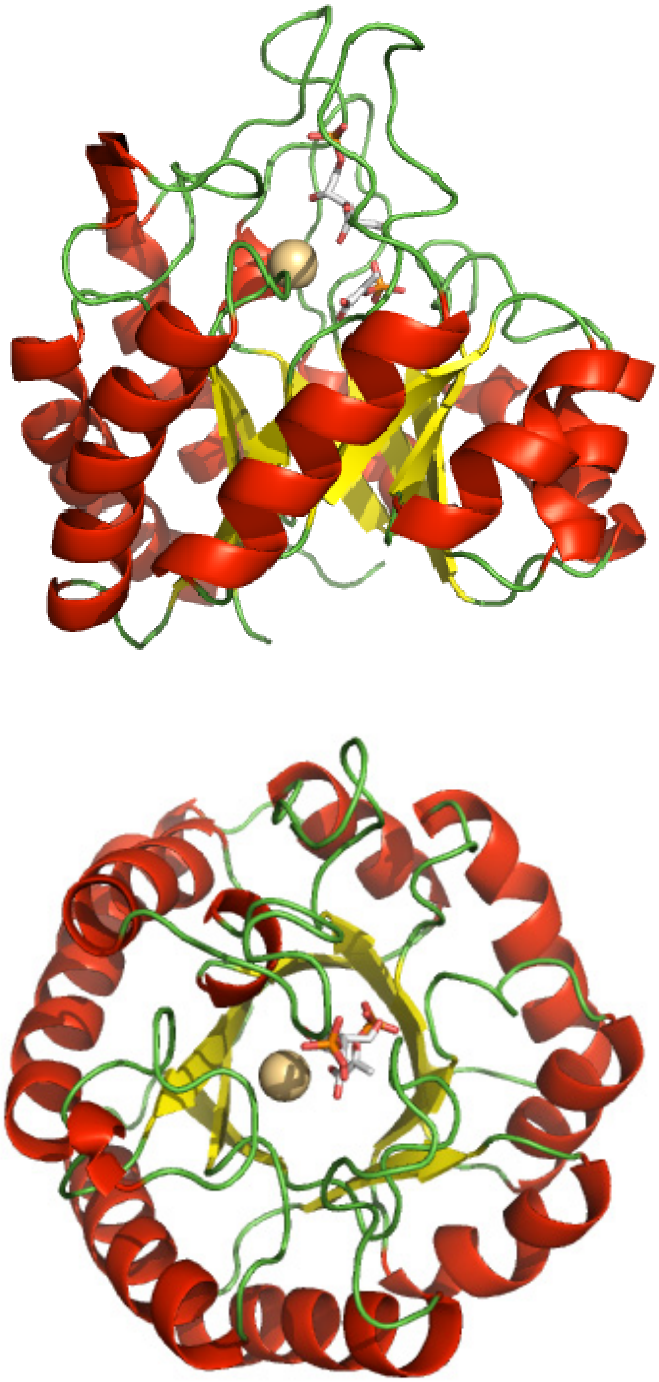

Figure 1.22: Side (top) and top (bottom) views of a monomeric enzyme unit from *Aae*KDO8PS (1FWW[34], chain A) with α-helix (red), β-sheet (yellow) and loop (green) regions indicated. A5P and PEP (orange/red/grey) and the cadmium ion (brown) are also shown.

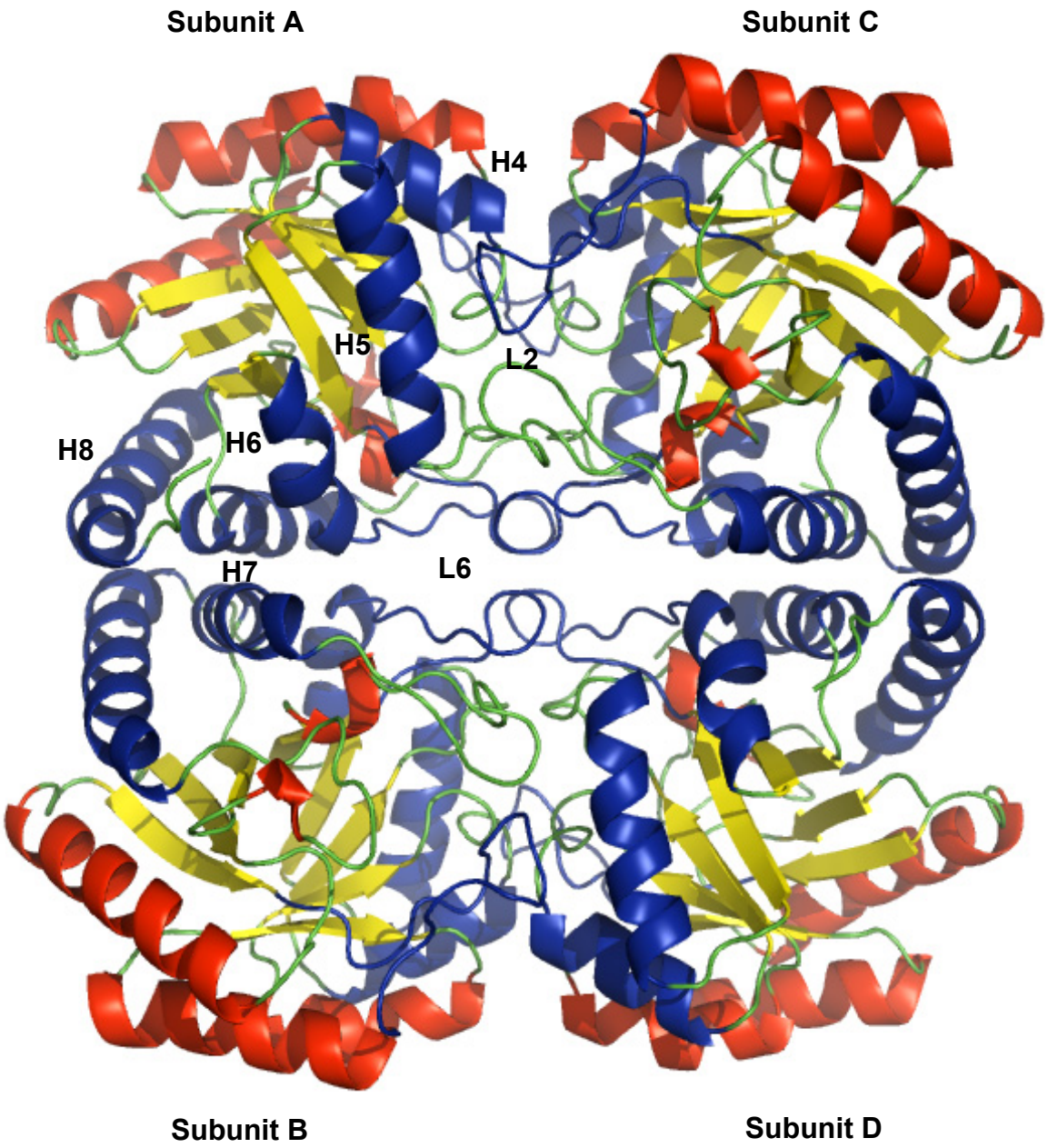

Figure 1.23: *Eco*KDO8PS tetramer (drawn from 1D9E[54]) showing the arrangement of the four subunit monomers (A-D). Regions involved in intersubunit contacts are highlighted in blue and labelled on subunit A. Secondary structures are also indicated as α-helices (red), β-sheets (yellow) and loops (green).

KDO8P synthase is able to control access to the active site *via* the L7, L8 and L2 loops (Figure 1.24), with the L7 loop becoming ordered and hence observable crystallographically only upon binding of both substrates. This was first observed in crystal structures of *Aae*KDO8PS, where the L7 loop which was disordered in previous structures of *Eco*KDO8PS (where only one or neither of the substrates were bound), was fully ordered, but only in subunits with both A5P and PEP bound in the active site.[30,34]

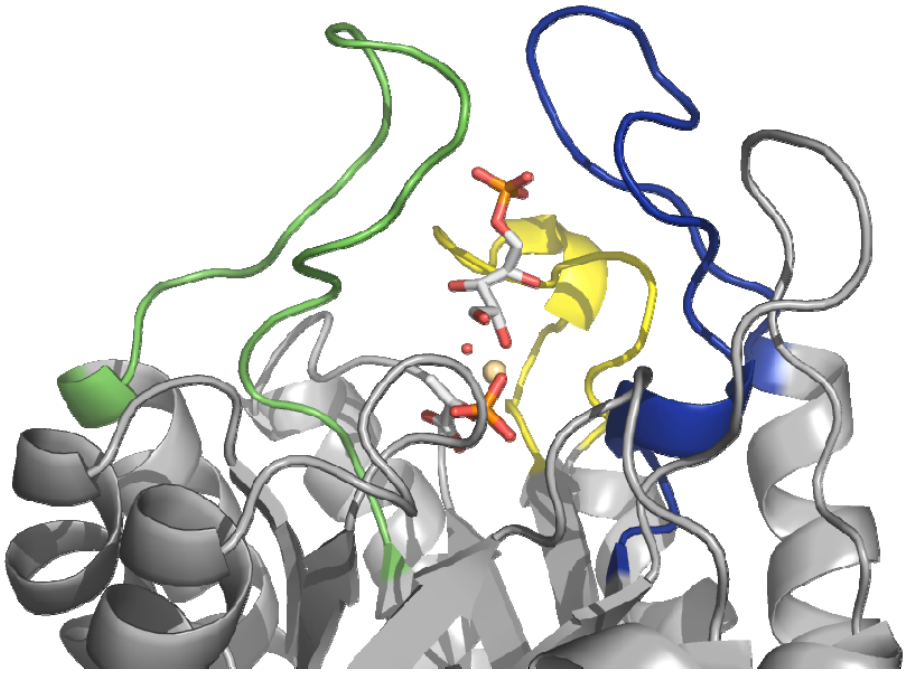

Figure 1.24: Interaction of active site loops L2 (green), L7 (blue) and L8 (yellow) to close off the active site in *Aae*KDO8PS. A5P, PEP and a conserved water molecule are coloured orange/red/grey (P/O/C respectively) and a metal ion (cadmium) is coloured brown. Taken from Gatti *et al.*,[63] drawn from 1FWW.[34]

The importance of these loops in closing off the active site was demonstrated in mutagenesis studies of a conserved arginine which is present on the L4 loop, R106 in *Aae*KDO8PS.[63] This residue is interesting because it reaches across from one enzyme subunit to interact with a serine (S50) and asparagine (N48) on the L2 loop of the adjacent subunit (all residues are numbered from *Aae*KDO8PS unless specified), allowing the L2 loop to act as a "latch" to the "lid" that is the L7 loop, as well as R106 binding the phosphate moiety of A5P, which will be discussed later. With the L7 loop disordered, the active site of the enzyme is open to the bulk solvent and a number of changes can occur; the A5P and PEP phosphate distance increases from 10.32–11.14 Å; C2-OH and C3-OH positions of A5P change from those found in crystal structures of the wild-type enzyme; PEP binds more tightly, but A5P is less effective as a substrate and both products of the enzymic reaction, KDO8P and Pi, bind more tightly, and are more effective as inhibitors. The end result of this mutation was that higher substrate concentrations were needed for the enzyme reaction and lower product concentrations were required to ensure the reaction occurred with normal catalytic efficiency. Without the mutation it appears as though the active site upon catalysis undergoes a conformational change that leads to expulsion of the Pi molecule, but this conformational change is removed with the mutation of the R106 residue.

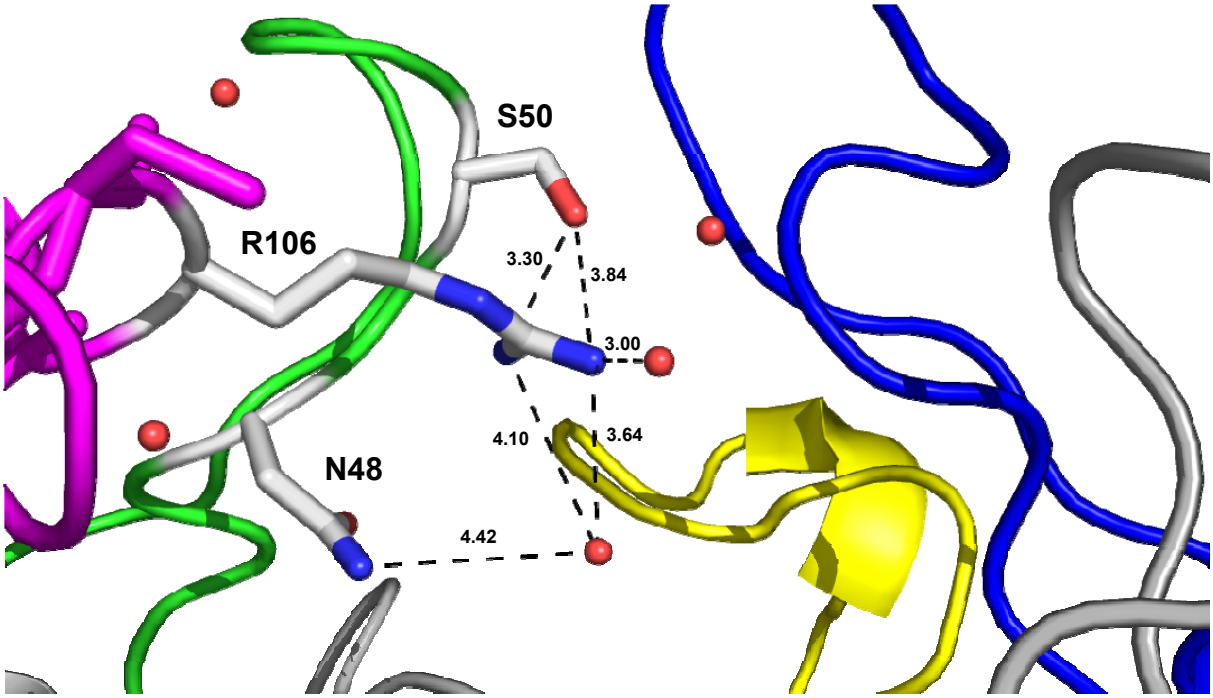

Figure 1.25: R106 residue from L2 loop on subunit A (magenta) interacting with S50, N48 on L2 loop of subunit A (green) and conserved water molecules (red) from subunit C. Distances to neighbouring atoms are measured in angstroms. Drawn from 1FWW.[34]

Sequence alignment identified this R106 residue as a conserved residue across all identified or annotated KDO8P synthases. As shown in Figure 1.13, a number of other conserved residues make up the PEP and A5P binding sites, which is the focus of the next section.

1.4.2. Substrate binding sites

PEP is bound at the bottom of the active site funnel (Figure 1.24) and forms non-covalent bonds with a number of conserved residues (Figure 1.26). In *Aae*KDO8PS the phosphate moiety of PEP interacts with the positively charged side chains of a lysine and arginine (K124 and R154) and the nitrogen atom of an alanine main chain amide (A102). The amine side chain of K124 also interacts with the bridging oxygen of the PEP phosphate. This lysine is also within bonding distance of one of the carboxylate oxygen atoms. A number of other conserved residues bind the other oxygen atom, namely K41, K46 and S43 in the *Aae*KDO8PS structure (1FWW).[34] It should be noted here that the effect of these residues binding the carboxylate moiety of PEP is to pull it slightly out of planarity with the PEP alkene, increasing the carboxylate/alkene dihedral angle. This has been observed in a number of other KDO8P synthase structures as well as in PEP-bound structures of the related aldolase

DAH7P synthase. It has been calculated that this bent character lowers the delocalisation across the α-β carboxylate system, localising the electrons in the alkene bond and increasing the nucleophilicity of the C3 carbon of PEP.[64] As previously discussed in Section 1.2, the conserved hydrophobic residue F103 is found not far from the phosphate moiety of PEP, and is thought to promote monoanionic binding of PEP, in order to protonate the A5P aldehyde residue during the reaction (Figure 1.10).[30]

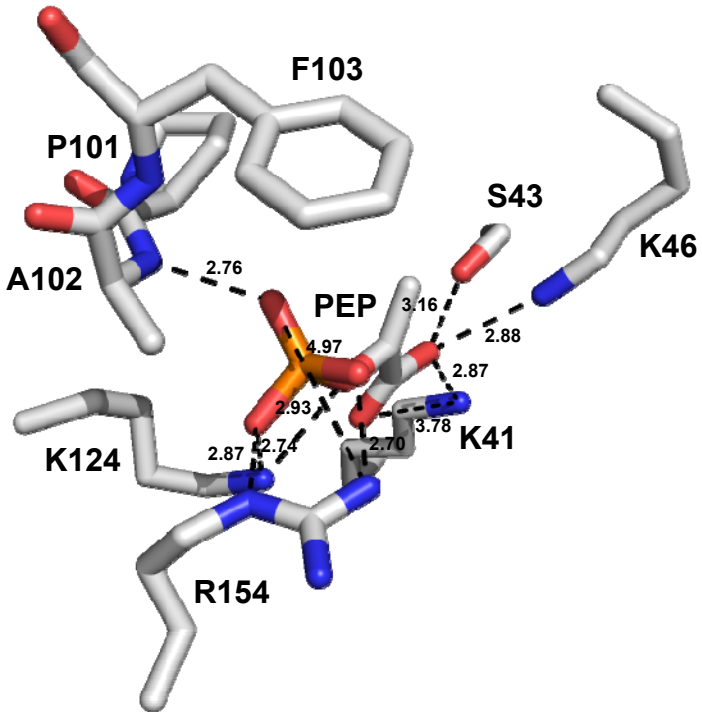

Figure 1.26: PEP (orange/red/grey) bound in the active site of *Aae*KDO8PS (1FWW[34]) showing hydrogen and electrostatic bonding with surrounding conserved active site residues (distances measured in angstroms). A conserved phenylalanine side chain (F103) is shown close to the phosphate moiety of PEP.

A conserved active site histidine residue (H185, a metal binding ligand in *Aae*KDO8PS) has been shown to be important in the orientation of the PEP substrate[65] and a mutation of this residue to glycine in *Aae*KDO8PS causes activity of the mutant to drop to 8 % that of wild-type. The mutation also causes PEP to be orientated incorrectly, binding the metal ion *via* its carboxylate moiety and the *si* face water molecule to be displaced. This gives more weight to the theory that this water molecule is not involved in catalysis, due to the remaining 8 % activity even when PEP is orientated in such an unusual fashion. It was originally thought that this histidine residue may be involved in signal transduction to the L7 loop but the mutation does not interfere with L7 ordering upon substrate binding.[65] It has been shown that this residue has conformational flexibility in the metal-independent *Eco*KDO8PS and it has

been proposed that this gives the residue the ability to block the bottom of the active site off from non-PEP substrates, as seen in its ability to change orientation from the major conformation seen in the ligand-free enzyme and stop KDO8P rebinding to the bottom of the active site.[66]

As previously discussed, the C2 hydroxyl of A5P binds the active site metal ion either directly or through the conserved *re* face water molecule. The A5P substrate also forms contacts with a number of absolutely conserved residues (Figure 1.27). Of note is the conserved asparagine (R106), found on the L6 loop of the adjacent subunit, interacting with the phosphate moiety along with the conserved serine S197 found on the now ordered L7 loop. A conserved glutamate, Q188, also found on the L7 loop, interacts with the C4 hydroxyl of A5P along with an aspartate residue, D233. Of additional importance are three residues, N48, R49 and S50 which interact with the C3 and C4 hydroxyl groups as well as the phosphate moiety of A5P. These residues make up part of a conserved KANRS(T) sequence motif found only in KDO8P synthases and not the related aldolase DAH7P synthase, which instead possesses an equivalent KPRT(S) motif.

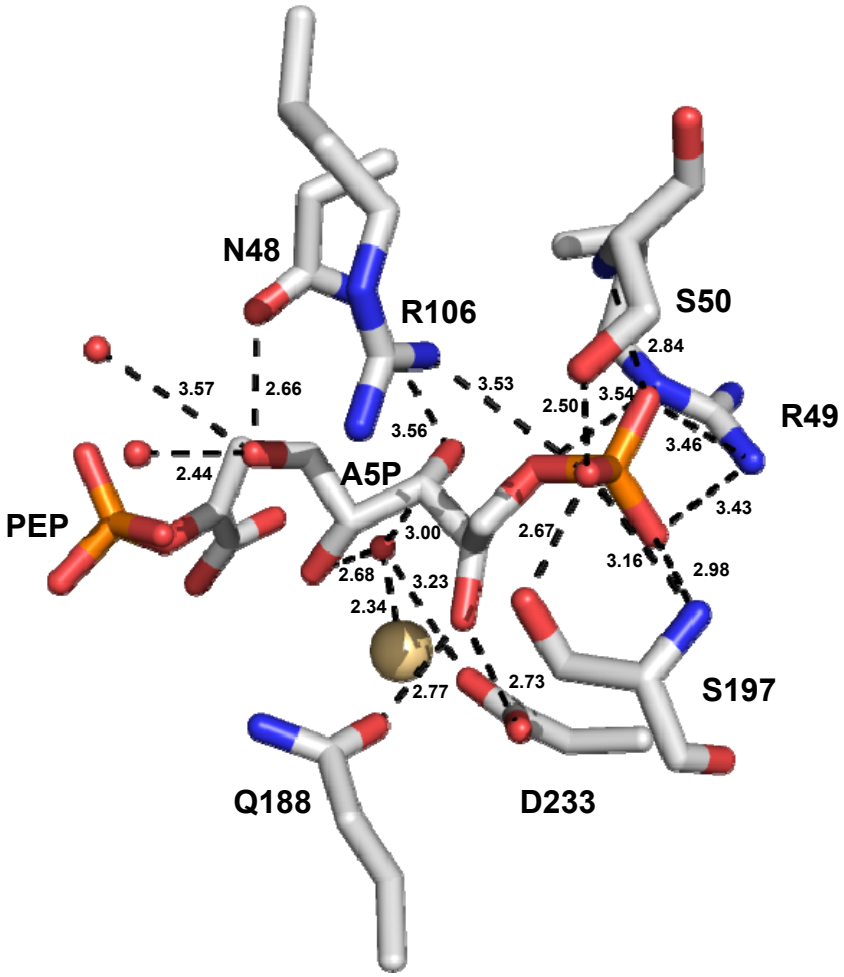

Figure 1.27: Binding of A5P in *Aae*KDO8PS (drawn from 1FWW[34]). Residues within 4 Å of A5P are shown, as are PEP (orange/grey/red) and a cadmium ion (brown). Of note is part of the conserved KANRS(T) motif (N48/R49/S50) that binds the aldehyde and phosphate moieties. Distances to neighbouring atoms are measured in angstroms.

1.4.3. Alternative aldolase substrates

The importance of the C2 and C3 hydroxyl active site contacts is reinforced by alternative substrate studies with KDO8P synthase from *N. meningitidis* that show that D-ribose 5-phosphate (R5P),[17,67] D-lyxose 5-phosphate (L5P), D-xylose 5-phosphate (X5P),[40] all containing an inversion of stereochemistry at the C2 or C3 position, are not substrates for the enzyme but L-xylose 5-phosphate which has a stereochemical inversion at C4 is a substrate with a moderate K_m of 57 μM for the monosaccharide, around 5-fold greater than A5P, and a slightly reduced k_{cat} of 1.1 s^{-1}, around two-fold lower than the natural substrate (Figure 1.28).[40] D-Ribose 5-phosphate has also been tested as a substrate with *Afe*KDO8PS where it was not a substrate,[62] and *Eco*KDO8PS where it was a poor substrate with a K_m approximately 40-fold greater than A5P.[68] Interestingly, removal of the C2 hydroxyl in 2-

deoxy ribose 5-phosphate does not destroy its ability to act as a substrate in *Nme*KDO8PS but does result in it being processed far less efficiently by the enzyme, with an almost 400-fold reduction in k_{cat}/K_m,[67] and a 1500-fold reduction in k_{cat}/K_m for *Afe*KDO8PS.[62] It may be that these active site contacts are vital in orientating the aldehyde moiety into a reactive conformation.

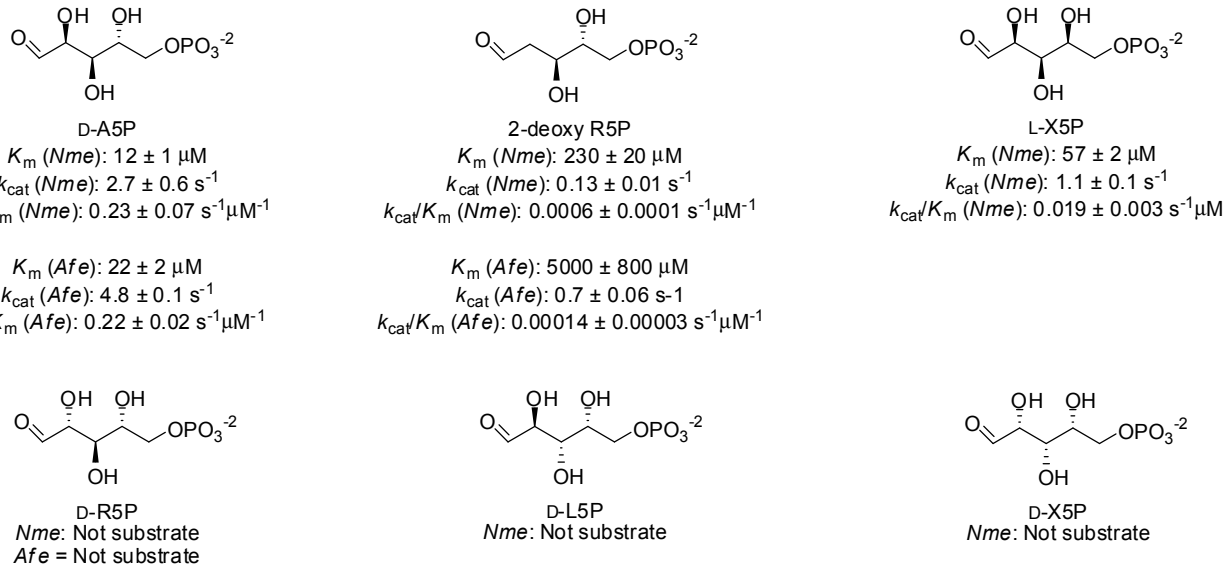

Figure 1.28: Five carbon monosaccharides that have been tested as substrates for *Nme*KDO8PS[40,67] and *Afe*KDO8PS[62].

DAH7P synthase differs in that it contains an absolutely conserved KPRT(S) sequence for binding the shorter four-carbon sugar E4P[67] instead of the KANRS(T) sequence found in KDO8P synthase that binds to A5P. It should be noted whilst the conserved alanine and asparagine in the KDO8P synthase KANRS(T) sequence is a proline in DAH7P synthases, the hydrophobic recognition of the C3 carbon of PEP and hydrogen bonding to the monosaccharide's main chain hydroxyl groups has been preserved. Also, the side chain hydroxyl groups of E4P do not seem to be as important to the overall enzymic reaction as they are in A5P, as shown by the ability to change their position or remove them completely and still obtain relatively normal catalytic activity (Figure 1.29).[67,69] This is not entirely surprising given the C2 hydroxyl of E4P in DAH7P synthase is thought to not bind to the metal ion as the C2 hydroxyl of A5P is shown to in most crystal structures of KDO8P

synthase, and therefore may not be as important in orientating the aldehyde moiety for enzyme catalysis.

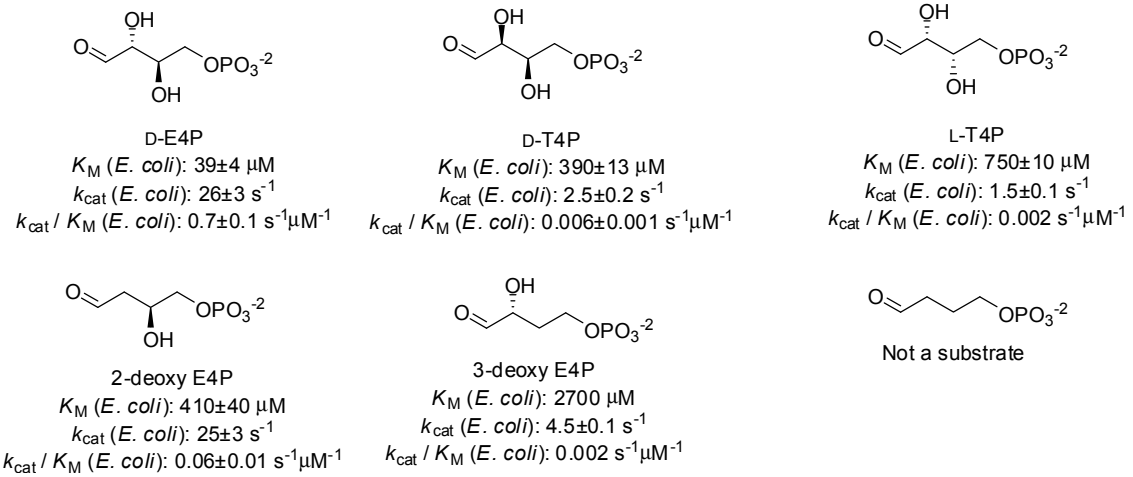

Figure 1.29: Four carbon monosaccharides that have been tested against DAH7P synthase from *E. coli* as alternative substrates.[67,69,70]

1.5. Related Enzymes

There are four other identified enzymes that share the unusual C-O bond cleavage of the PEP phosphate moiety; DAH7P synthase,[71] *N*-acetylneuraminic acid (NeuNAc) synthase,[72] 5-enolpyruvoylshikimate 3-phosphate (EPSP) synthase[73] and UDP-GlcNAc enolpyruvyl transferase (MurZ).[74] These can be divided into two subclasses of enzymes, the enolpyruvyl transferases which include EPSP synthase and MurZ, catalysing the transfer of an enolpyruvyl moiety from PEP to an acceptor alcohol, and the aldolases, including KDO8P synthase, DAH7P synthase and NeuNAc(P) synthase, which catalyse the aldol-like addition of PEP to an aldehyde (Figure 1.30).

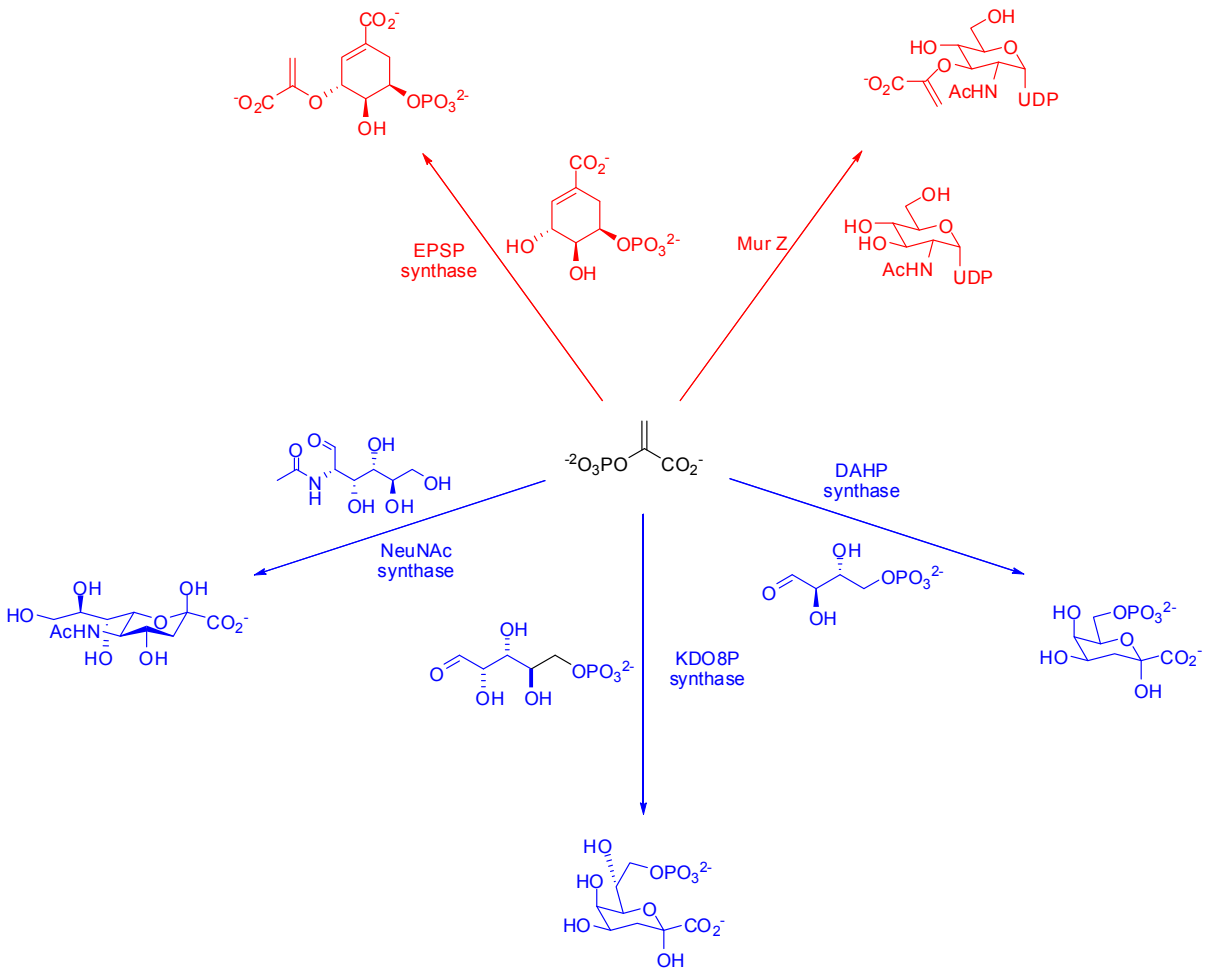

Figure 1.30: Enzymes that catalyse the C-O bond cleavage of PEP. The enolpyruvyl transferases (EPSP synthase, MurZ) are highlighted in red and the PEP aldolases (NeuNAc synthase, KDO8P synthase and DAH7P synthase) are highlighted in blue.

These aldolases, originally thought to be unrelated due to low overall sequence similarity, are now thought to be closely related, and are believed to share both a common mechanism and ancestor. DAH7P synthase has the four-carbon sugar E4P as a substrate and catalyses the reaction with PEP to give the seven-carbon sugar DAH7P. NeuNAc(P) synthase reacts either *N*-acetyl mannosamine or *N*-acetyl mannosamine-6-phosphate with PEP to give N-acetyl neuraminic acid and N-acetyl neuraminic acid-9-phosphate respectively. The relationship between these three enzymes is summarised in the phylogenetic tree in Figure 1.31.[75] The tree shows the differences in sequence similarity between the three enzymes from a variety of bacterial organisms with line junctions indicating a common ancestor sequence, and the length of lines from branch points being indicative of the degree of similarity between the sequences.

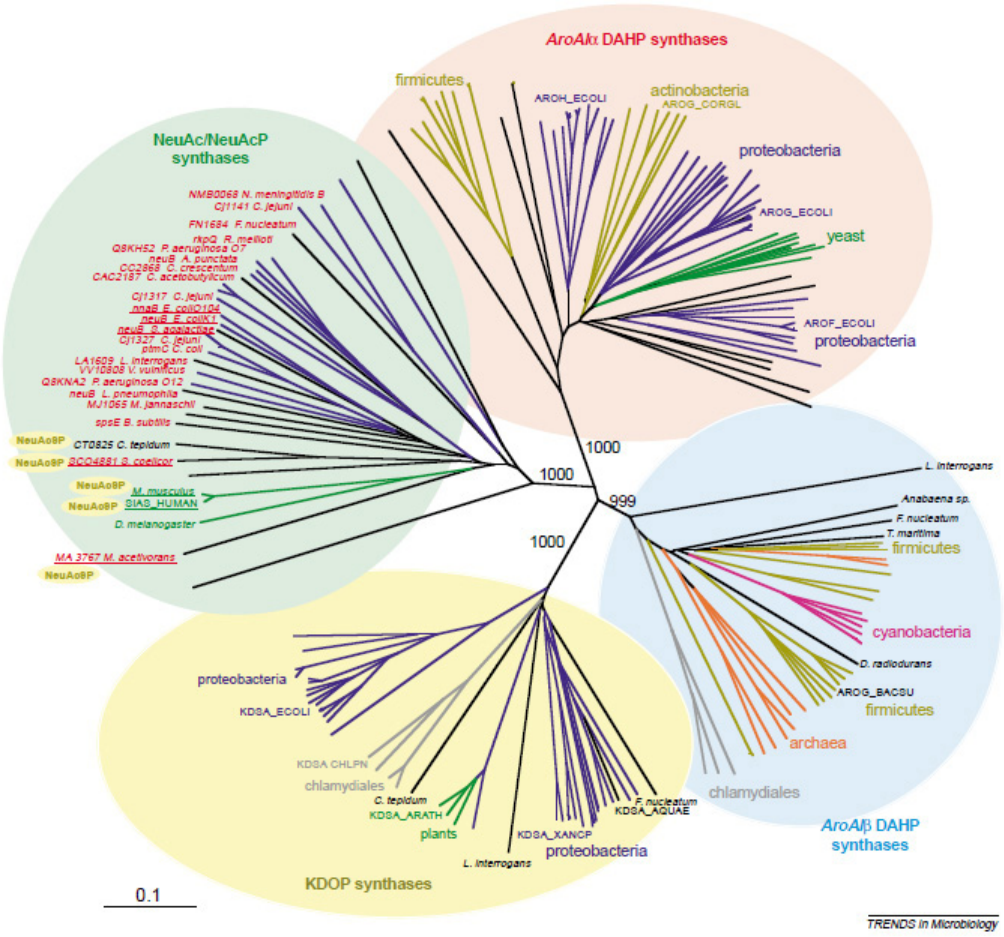

Figure 1.31: Phylogenetic tree showing genetic relationship between the aldolases, DAH7P synthase, KDO8P synthase and NeuNAc synthase. Taken from Bravo *et al.*[75]

1.5.1. NeuNAc(P) synthase

The NeuNAc(P) synthases are involved in the synthesis of the most common sialic acid in nature, N-acetyl neuraminic acid. Though sialic acids are mainly found in mammalian systems, where they are involved in cellular recognition and cell adhesion processes,[76,77] many neuroinvasive bacterial species also incorporate the nine-carbon sugars into their own cell walls in order to conceal them from the host's immune system.[78] Thus far only NeuNAc(P) synthases that take *N*-acetyl mannosamine 6-phosphate have been found in mammalian systems, and thus in order to synthesise *N*-acetyl neuraminic acid they must also utilise *N*-acetyl mannosamine kinase and *N*-acetyl mannosamine 9-phosphate phosphatase in a three step reaction scheme. Many bacterial species are able to bypass this step, and take *N*-acetyl mannosamine directly as a substrate (Figure 1.32).[79]

NeuNAc(P) synthase shows a requirement for a divalent metal ion, with most having maximum catalytic activity in the presence of Mn^{2+}. Crystal structures have shown that the aldehyde moiety is a metal ligand, and the metal ion may be involved in activation of the aldehyde in catalysis.[72] The active site is quite different from KDO8P synthases however, with two histidines and a glutamate residue composing the metal binding site, and a number of different residues involved in binding the substrate (Figure 1.33). It also appears that an antifreeze domain is present at the C terminus (Figure 1.34), and this is involved in sealing off the active site by forming non-covalent bonds with the substrate and surrounding residues in order to orientate the *N*-acetyl mannosamine substrate effectively.[80] Studies utilising stereospecifically deuterated PEP with NeuNAc synthase from *Campylobacter jejuni* isozyme 1 have shown that the stereochemistry of the reaction involves attack of the *si* face of the aldehyde by the *si* face of PEP.[81] This differs from KDO8P and DAH7P synthases as previously described, which involve attack of the *re* face of the aldehyde.

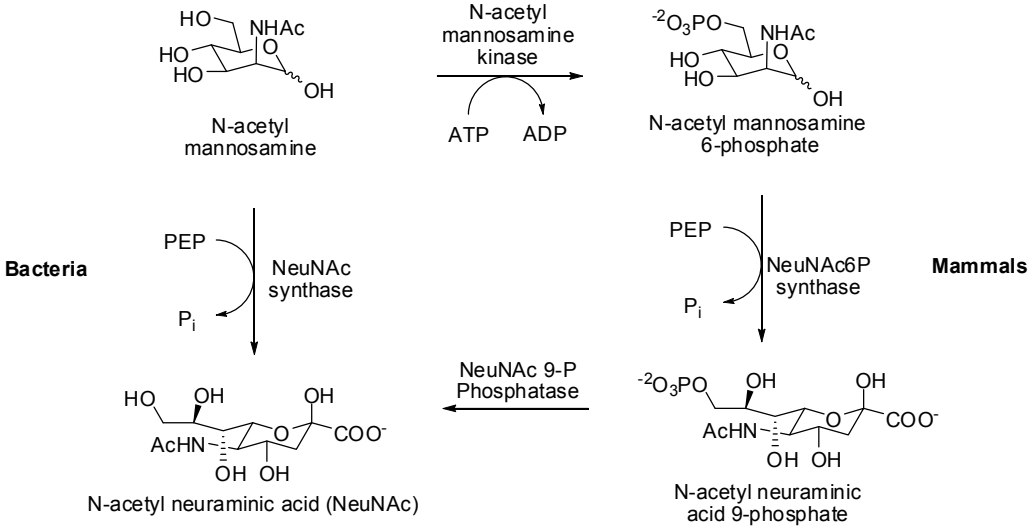

Figure 1.32: Biosynthesis of *N*-acetyl neuraminic acid (NeuNAc) in mammalian and bacterial systems.

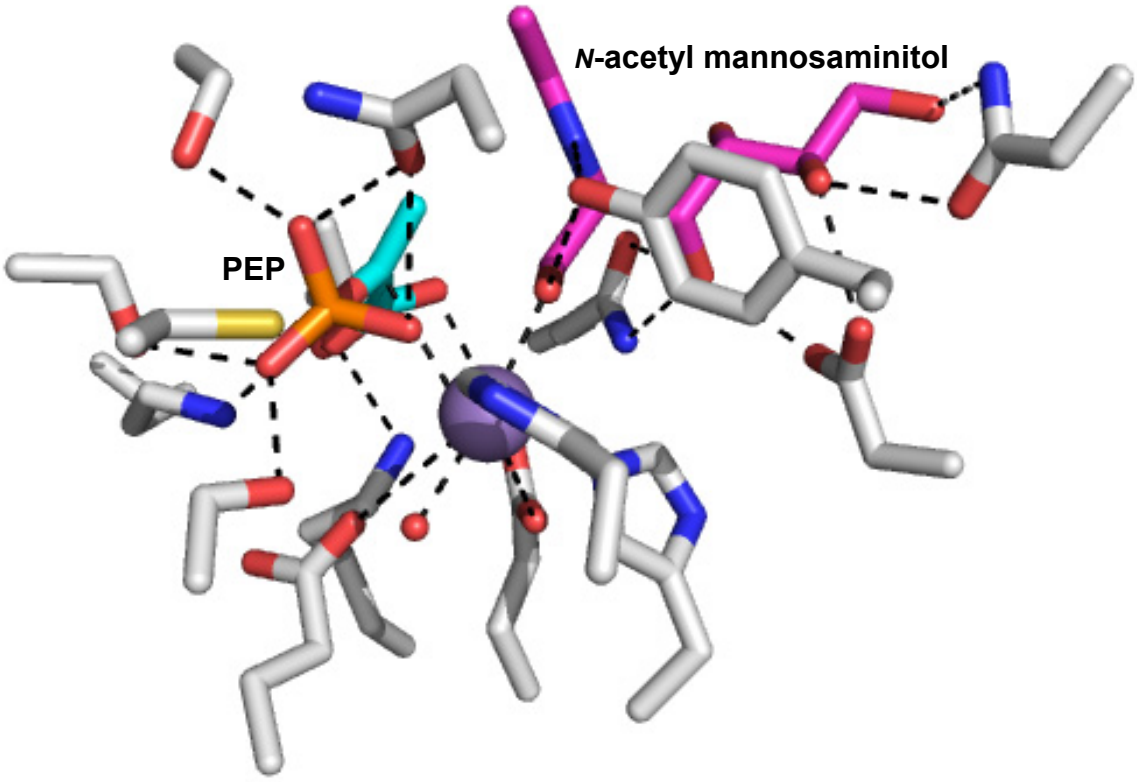

Figure 1.33: Active site of *N. meningitidis* NeuNAc synthase from 1XUZ[72] showing binding of PEP (cyan), N-acetyl mannosaminitol (magenta) and a manganese ion (purple). Residues (grey) within 4 Å of substrates and the metal ion are shown and potential bonding indicated with dashed lines.

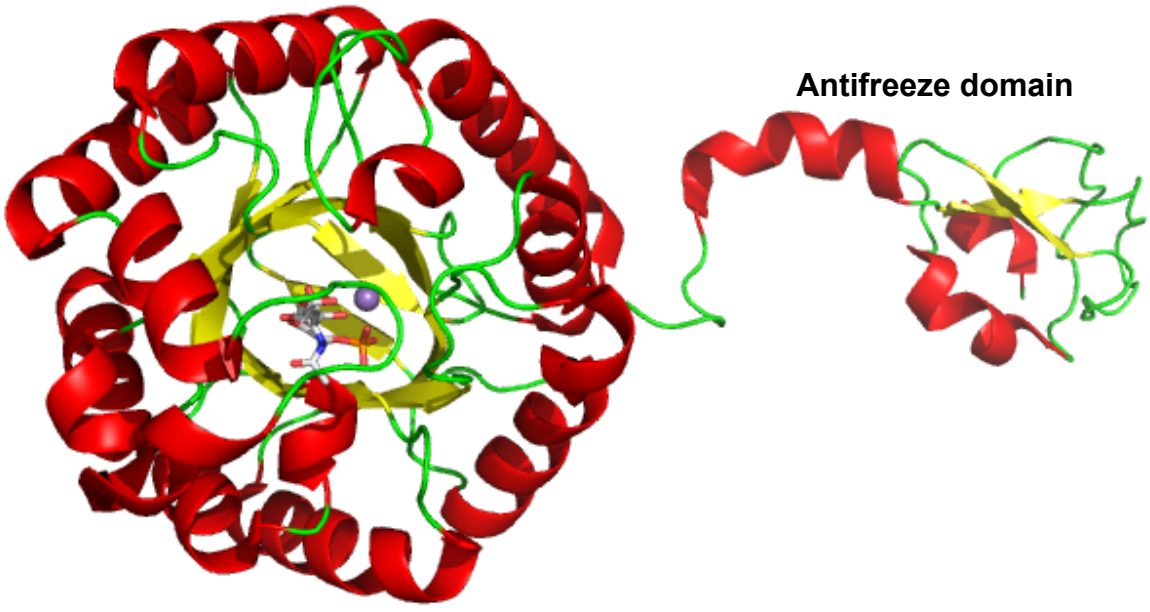

Figure 1.34: Top view of a monomeric enzyme unit from NeuNAc synthase from *N. meningitidis* (1XUZ)[72] showing the TIM barrel structure and C-terminal antifreeze domain, with α-helices (red), β-sheets (yellow) and loop (green) regions indicated. *N*-acetyl mannosaminitol and PEP (orange/red/grey/blue) and the manganese ion (purple) are also shown.

1.5.2. DAH7P synthase

The DAH7P synthases, as previously discussed in Section 1.3, catalyse the same aldol-like condensation but between E4P and PEP to give the seven-carbon phosphorylated sugar DAH7P (Figure 1.11).

DAH7P synthases have the same stereospecificity as KDO8P synthases in that the *si* face of PEP attacks the *re* face of the aldehyde moiety.[82] Unlike KDO8P synthases however, all DAH7P synthases are metal-dependent[43-48] and mutations to change this dependency such as those performed on KDO8P synthase have been unsuccessful,[67] leading to the assumption that the divalent metal ion is involved in the reaction mechanism.

The metal binding site is similar to that found in metal-dependent KDO8P synthases as seen in Figure 1.35, and is conserved with the metal ion binding four ligands; a histidine, cysteine, aspartate and glutamate residue.

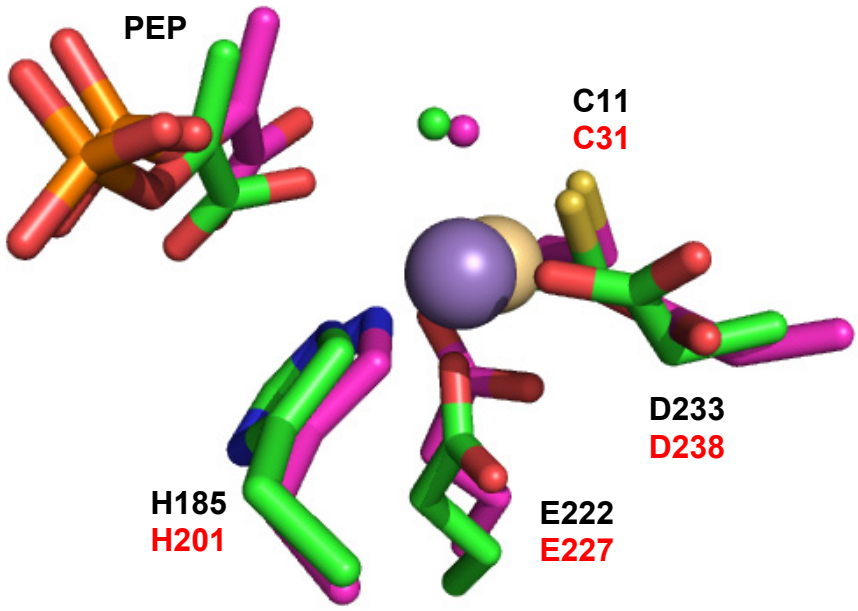

Figure 1.35: Overlay of the metal binding site of *Aae*KDO8PS (1FWW[34], magenta, residues labelled in black) and *Eco*DAH7PS (1N8F{Shumilin, 2003 #130}, green, residues labelled in red) with PEP bound (orange/red and green or magenta). The cadmium ion in the *Aae*KDO8PS structure is coloured brown and the manganese ion from *E. coli* structure is coloured purple.

As in KDO8P synthase, the PEP and E4P binding sites also contain residues that are conserved across the greater DAH7P synthase family.

Three residues, two arginines and a lysine, bind the phosphate moiety of PEP. In type I DAH7P synthases the phosphate moiety also makes close contact with a main chain amide between a conserved glycine and alanine residue, while in type II *M. tuberculosis* and *H. pylori* DAH7P synthases the alanine is replaced by a glutamate residue.[43,44] The conserved phenylalanine found in KDO8P synthase is replaced with a conserved arginine residue. This may be because DAH7P synthase may not require a monoprotonated phosphate moiety in order to activate the aldehyde moiety of E4P, as modelling of E4P into the active site shows the aldehyde moiety likely binds as a metal ligand,[67] and can subsequently be activated through Lewis-acid catalysis (Figure 1.36).

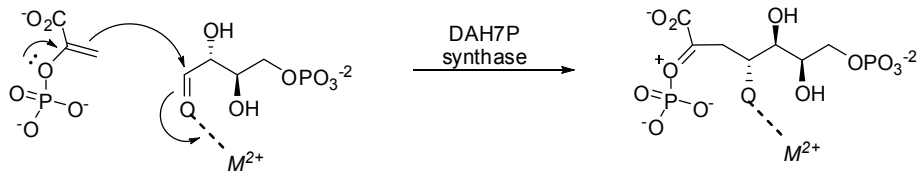

Figure 1.36: Proposed partial mechanism of DAH7P synthase utilising Lewis-acid catalysis.

The carboxyl moiety of PEP is also within bonding distance of two conserved residues, an arginine and lysine, the latter being part of the absolutely conserved KPRT(S) sequence in DAH7P synthases that binds the E4P substrate, as previously discussed.[67] In addition, a conserved aspartate D342 (numbering from *Saccharomyces cerevisiae* DAH7PS) is thought to bind the C3 hydroxyl moiety, as seen in crystal structures with D-glycerol 3-phosphate (GO3P) bound.[59] In this same crystal structure a number of water molecules are found that are thought to mediate the binding of residues to E4P.

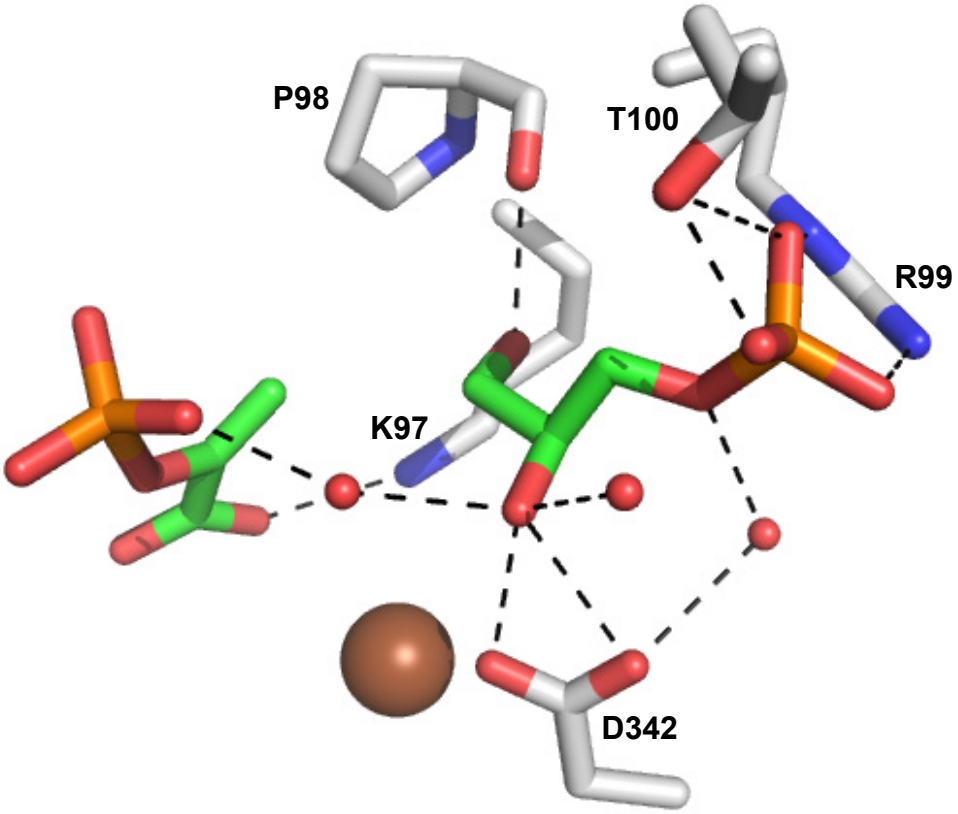

Figure 1.37: The binding of GO3P in the *S. cerevisiae* DAH7P synthase active site (1OF8)[59] with PEP and GO3P (green/red/orange), surrounding residues, including the conserved KPRT sequence and conserved aspartate D342 (grey/red/blue), water molecules thought to mediate binding (red) and cobalt ion (brown). Potential bonding (residues and water molecules within 4 Å) is shown by dashed lines.

1.6. The project

This project involves the synthesis and testing of a number of mono- and bi-substrate inhibitors of KDO8P synthase. It is hoped that the results from this study will help to determine the importance of certain substrate moieties as well as provide an understanding of the enzyme mechanism for future inhibitor design.

Four previously designed bi-substrate inhibitors of KDO8P synthase have been characterised kinetically and are shown below (Figure 1.38).

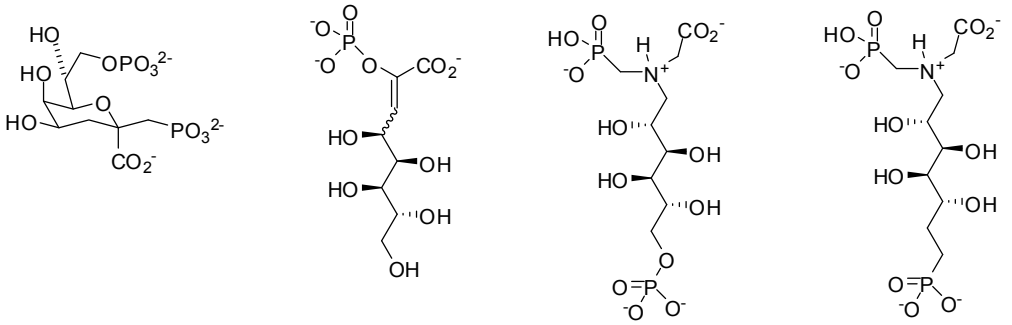

1.2
K_i (*Eco*): 4.9 μM

1.3
IC_{50} (*Hpy*): 132 μM

1.4
K_i (*Eco*): 0.37 μM

1.5
K_i (*Eco*) 50 μM

Figure 1.38: Previous bi-substrate inhibitors of KDO8P synthase.[27,83-85]

The first inhibitor 1.2, a pyran molecule (Figure 1.38, left) was designed to resemble the proposed cyclic intermediate of the KDO8P synthase reaction (1.1,

Figure 1.6).[83] The K_i is surprising when consideration is given to the fact that the reaction through the cyclic intermediate has been largely discounted, as discussed in Section 1.2.

The enol phosphate inhibitor 1.3 (Figure 1.38) was designed to mimic the planar nature of the PEP molecule. Even though it has the *gluco* configuration of hydroxyl groups and lacks a terminal phosphate group, it inhibited the KDO8P synthase enzyme from *H. pylori* with a modest K_i of 132 μM, though could not be incorporated into the active site of *A. aeolicus* KDO8P synthase in crystallographic studies, even at concentrations up to 4.4 mM.[84] The crystallisation was only achieved at pH 5.0, and this inability of the inhibitor to be found in the enzyme active site may be a result of this.

The two amino phosphonate inhibitors were designed in order to mimic the proposed high energy oxocarbenium intermediate, with the phosphonate 1.5 (Figure 1.38)[85] being created in an attempt to improve the anti-bacterial properties due to a possible dephosphorylation of the original inhibitor (1.4).[27] However, this led to a 100-fold increase in K_i which gives evidence of the importance of the phosphate enol oxygen in binding to the active site residues.

The structures of the most potent of these two inhibitors in complex with KDO8P synthase from *E. coli*[31] and *A. aeolicus*[30] have been determined by X-ray crystallography. The *Aae*KDO8PS crystal structures show that the inhibitor binds to the enzymes in a similar fashion to the two substrates, using the same carboxylate and phosphate binding pockets (Figure 1.39).

The main difference seems to be the position of the main chain hydroxyl groups that are bound differently between A5P and the inhibitor. The inhibitor hydroxyl, representative of the aldehyde moiety of A5P, acts as a metal ligand, and thus the other hydroxyl groups are also bound in different positions within the active site. These hydroxyls are well defined in the crystal structure. A σA omit map of the inhibitor bound however has shown that the carboxyl group is not well defined, leading to the conclusion that it may not be as tightly bound as the phosphate and phosphonate moieties. Further evidence of this was observed when the carboxyl group was removed from the bi-substrate inhibitor without much loss of inhibitory activity, but removal of the phosphonate group led to a complete loss of inhibition (Figure 1.40).[84]

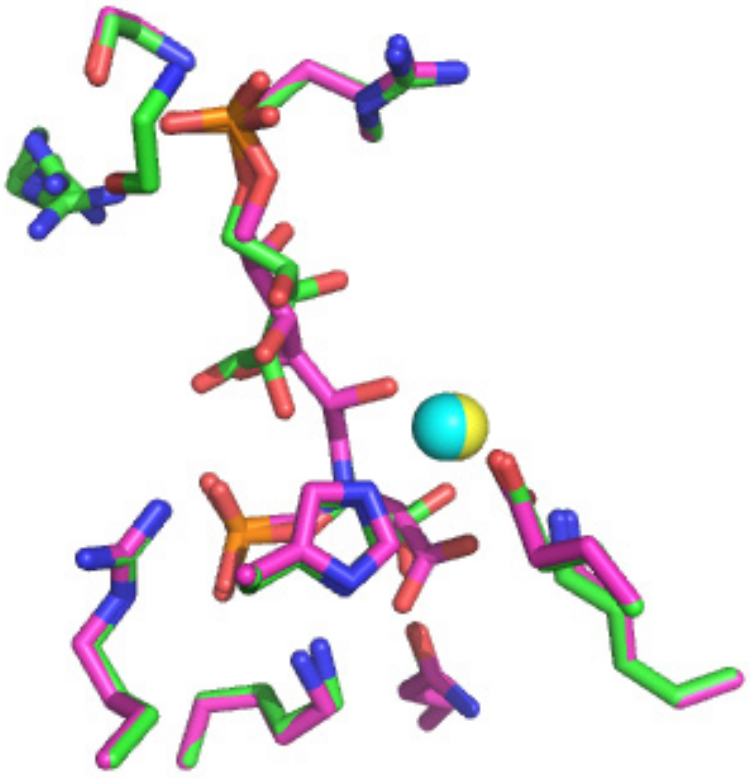

Figure 1.39: Overlay of aminophosphonate inhibitor 1.4 (1JCX[30] magenta/red/orange) and enzyme substrates A5P and PEP (1FWW[34], green/red/orange) bound in the *Aae*KDO8PS active site showing differences in hydroxyl binding. Phosphate and carboxylate binding residues are shown in magenta/blue/red (1FWW) and green/blue/red (1JCX). Cadmium ions for 1FWW and 1JCX are shown in cyan and yellow respectively.

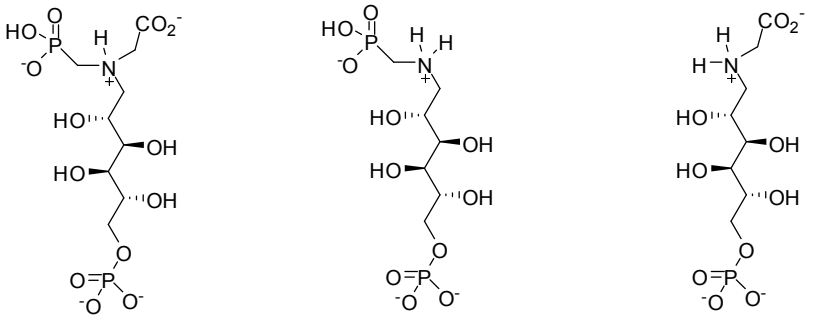

Figure 1.40: Limited structure-activity relationships of amino phosphonate bi-substrate inhibitors towards *Eco*KDO8PS.[84]

The most potent amino phosphonate inhibitor was made using a one pot synthesis, involving the reaction of mannose 6-phosphate with glyphosate (1.6) (Figure 1.41),[27] a previously identified inhibitor of EPSP synthase.

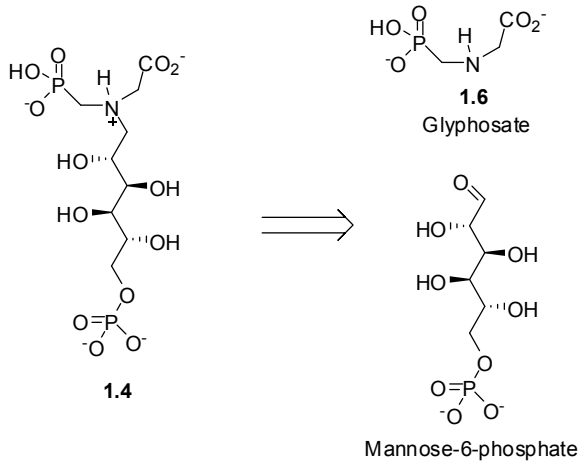

Figure 1.41: Retrosynthetic analysis of the amino bi-substrate inhibitor (1.1).[27]

This is an example of an inhibitor whereby a known PEP mimic (glyphosate, 1.6) was extended to resemble the bi-substrate complex, and in this case, the high energy transition state, in order to more strongly bind to the enzyme active site through increased active site interactions. Studies such as these, investigating the inhibitory changes when small molecule PEP mimics are extended have been investigated in our laboratory for the related enzyme DAH7P synthase with some promising results.[86]

As such, a number of small molecule PEP mimics have been synthesised and tested against DAH7P synthase, but not KDO8P synthase, or only against a member of the metal-

independent class of KDO8P synthase. Given the success of these compounds in inhibiting DAH7P synthase, we decided to test a number of small molecules on a metal-dependent (*Afe*KDO8PS) and metal-independent (*Nme*KDO8PS) enzyme, and then subsequently extend some of these molecules to incorporate an A5P-like binding motif in order to determine the effect on inhibition these additional motifs will have.

Chapter 2: Purification and characterisation of KDO8P synthase

pure protein sample
simply fantastic result
not for E. coli

2.1. Introduction

As part of the proposed studies into the inhibition of KDO8P synthase, enzyme examples of both the metal-independent and metal-dependent type were required. In our laboratory, the two examples available were the metal-independent KDO8P synthase from *N. meningitidis* and the metal-dependent KDO8P synthase from *A. ferrooxidans*. Both these enzymes have been previously purified but enzyme samples was not available for the current work. A known procedure for the purification of each enzyme[40,62] was modified in order to obtain pure protein for inhibition studies.

N. meningitidis is a mesophilic Gram-negative bacterium, first isolated in 1887.[87] It is most well known as the causative pathogen in meningococcal disease and septicaemia. The disease usually develops rapidly, and can cause brain damage, hearing loss and in 4-10 % of cases, death.[88-90] Those people that survive the effects of meningococcal disease often suffer from permanent tissue damage, and neurological sequelae.[88] *N. meningitidis*, being a Gram-negative bacterium, contains LPS as part of the cell wall that is important for the structural integrity of the cell. As KDO8P synthase is one of the first committed steps in the synthesis of LPS, it is a novel target for drug design.

A. ferrooxidans is not pathogenic, but is a mesophilic Gram-negative bacterium that lives in pyrite deposits and metabolises iron and sulfur producing sulfuric acid.[91,92] The KDO8P synthase enzyme from *A. ferrooxidans* has recently been identified as a putative metal-dependent enzyme by sequence analysis.[62]

2.2. Purification of KDO8P synthase from *N. meningitidis*

Previously, the KDO8P synthase gene from *N. meningitidis* (*kdsA*) was successfully cloned into the pT7-7 plasmid.[40] This plasmid also contained a gene for ampicillin resistance to enable selection for competent cells, and also allowed for overexpression of the *Nme*KDO8PS gene by induction with isopropyl-1-thio-β-D-galactopyranoside (IPTG). The pT7-7 *Nme*KDO8PS plasmid was then transformed into *E. coli* BL21(DE3) cells for expression, which were subsequently stored in glycerol stock at -80 °C until use.

The glycerol stock was used to inoculate a preculture of *Nme*KDO8PS wild-type containing ampicillin, and was grown overnight and used to inoculate a large culture. The large culture

was grown and cells harvested by centrifugation four hours after IPTG induction. The cell pellet was not used immediately but instead stored at -80 °C. The cell pellet was resuspended in lysis buffer and sonicated in order to lyse the cells to obtain access to the soluble protein. The cellular material suspended in lysis buffer was then subjected to centrifugation to remove the insoluble cell debris.

2.2.1. Purification by anion exchange chromatography

The first purification step in the established protocol for the purification of KDO8P synthase from *N. meningitidis* utilised Anion Exchange Chromatography (AEC).[40] AEC involves passing a mixture of proteins down a column of positively charged resin, and separating the proteins based on their overall ionic charge at a given pH. KDO8PS from *N. meningitidis* has a theoretical pI of 6.25[93] and so at pH 7.5 has an overall negative charge. The overall negative charge means the KDO8P synthase enzyme binds to the AEC resin, and by increasing the concentration of an ionic solution the protein can be eluted by countering the charges on the surface amino acids.

The supernatant at pH 7.5 was loaded onto the anion exchange (SOURCE™ 15Q) column with protein eluted from the column using a gradient between 0.1 and 0.2 M sodium chloride at 4 °C (Figure 2.1). These fractions were analysed by sodium dodecyl sulfate polyacrylamide gel electrophoresis (SDS-PAGE) (Figure 2.2) and those fractions containing the KDO8P synthase protein, shown as a protein with an approximate molecular weight of 31 kDa, were pooled. Both the overall shape of the traces in Figure 2.1 (showing a variety of peaks within the shaded region) and the SDS-PAGE analysis shown in Figure 2.2 indicates that a number of impurities remained in the protein sample. The protocol for the purification of the KDO8P synthase enzyme called for further purification steps to remove these impurities.

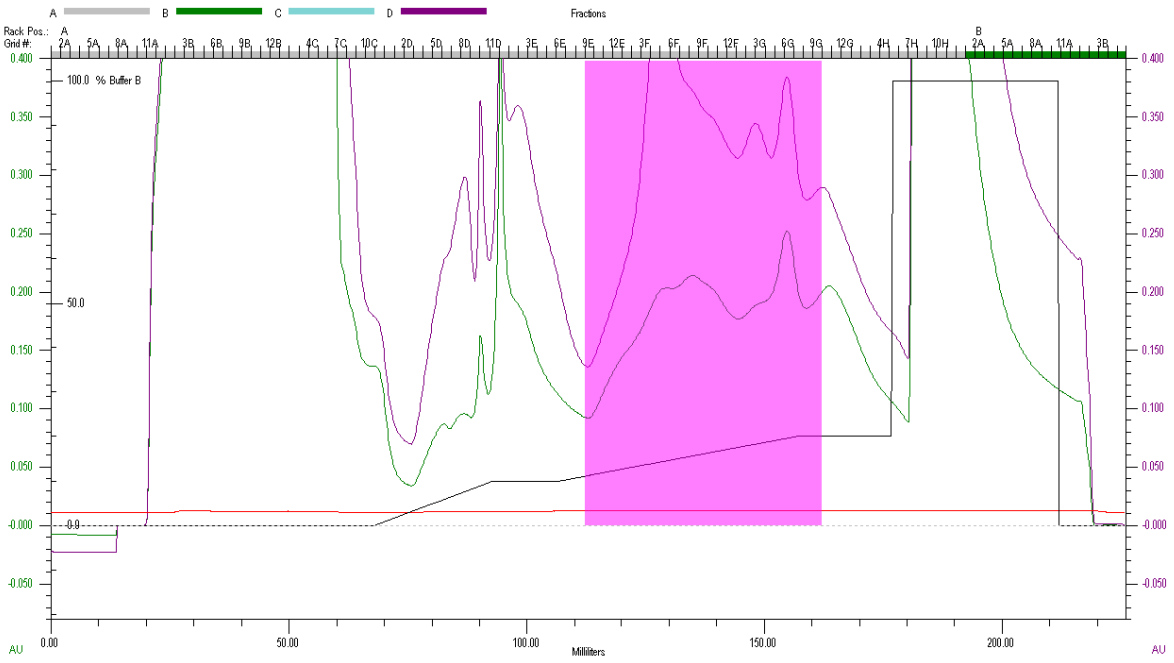

Figure 2.1: Chromatogram trace of AEC purification of *Nme*KDO8PS. Fractions containing KDO8P synthase that were pool for further purification are highlighted in magenta. Purple and green traces are 280 nm and 260 nm detectors respectively. Black trace shows the sodium chloride gradient (0-1 M). Red trace is conductivity detector.

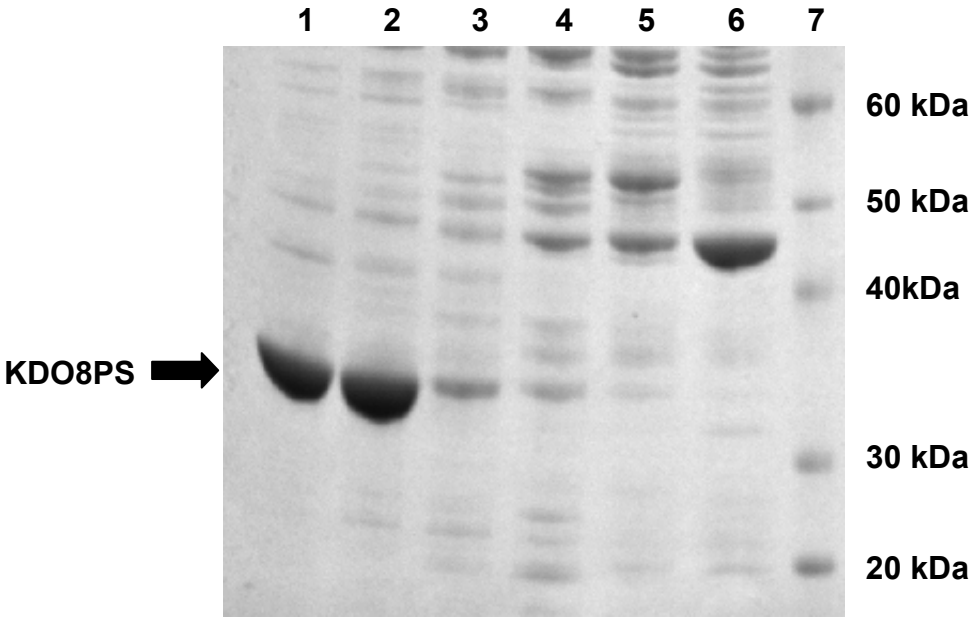

Figure 2.2: SDS-PAGE analysis of AEC purification of *Nme*KDO8PS. SDSPAGE analysis was performed on a 12 % polyacrylamide gel and visualised with Coomassie Brilliant Blue R 250. Lane 1-6: fractions as they were eluted from the AEC column (0.11-0.2 M NaCl, fractions from lanes 1-5 were pooled); Lane 7: Molecular markers.

2.2.2. Purification by hydrophobic interaction chromatography (HIC)

As discussed, a number of contaminants remained in the *Nme*KDO8PS protein sample after AEC, and so further purification by another method was necessary. Proteins differ with regards to their overall surface hydrophobicity, and Hydrophobic Interaction Chromatography (HIC) separates proteins based on their interactions with hydrophobic ligands attached to an uncharged matrix. HIC requires a large surface area on the protein, and therefore can be affected by temperature. It has previously been found for the established purification protocol that the elution profile gave sharper signals when the chromatography is performed at room temperature rather than at 4 °C.[94]

The pooled fractions from AEC purification were exchanged into buffer containing 1 M ammonium sulfate and loaded onto a hydrophobic interaction (SOURCE™ 15Phe) column. Bound protein was eluted from the column with a decreasing concentration gradient of ammonium sulfate. Fractions that contained *Nme*KDO8PS, as determined by SDS-PAGE analysis (Figure 2.3), were subsequently pooled for further purification. Comparisons with a previous purification of the *N. meningitidis* KDO8P synthase enzyme using the established protocol,[40] showed less contaminants present, as judged by SDS-PAGE.[94] A third purification step was employed in this modified purification protocol in order to remove the final contaminants and desalt the protein sample obtained from HIC.

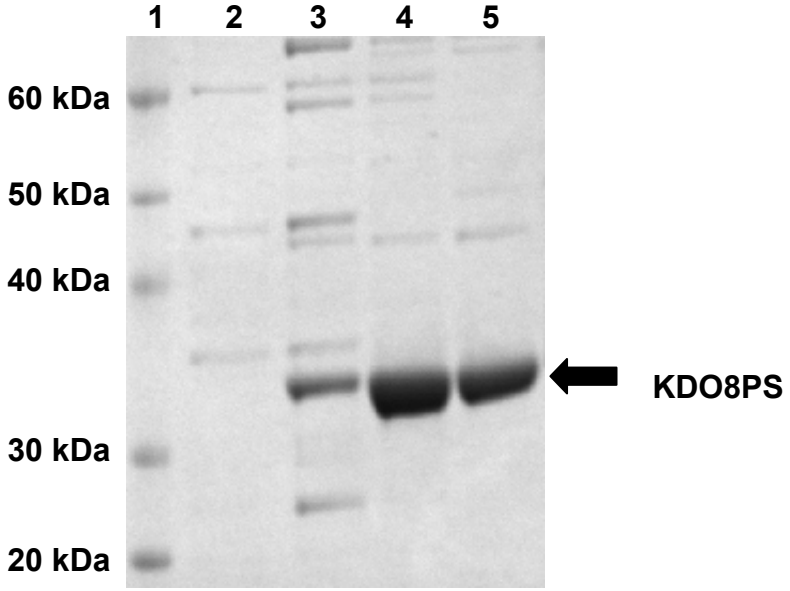

Figure 2.3: SDS-PAGE analysis of HIC purification of *Nme*KDO8PS. SDS-PAGE analysis was performed on a 12 % polyacrylamide gel and visualised with Coomassie Brilliant Blue R 250. Lane 1: Molecular marker; Lane2-5: fractions 11H-B12 (0.6 and 0.45 M ammonium sulfate) as they were eluted from the HIC column (Fractions from lanes 3-5 were pooled for further purification).

2.2.3. Purification by size exclusion chromatography (SEC)

Size Exclusion Chromatography (SEC) is often used as a polishing step in purification protocols. It separates proteins based on hydrodynamic radius, and is often used as a desalting step, making it useful as a final step in protein purification protocols.

The pooled fractions of *Nme*KDO8PS from HIC were loaded onto a Superdex™ S200 26/60 GL column in two aliquots and fractions containing KDO8P synthase were pooled, concentrated, exchanged into a low salt buffer, snap frozen with liquid nitrogen and stored at -80 °C. The eluted protein was very pure as seen by the isolated KDO8P synthase peak on the chromatograph in Figure 2.4, and final SDS-PAGE gel showing the entire purification, as given in Figure 2.5.

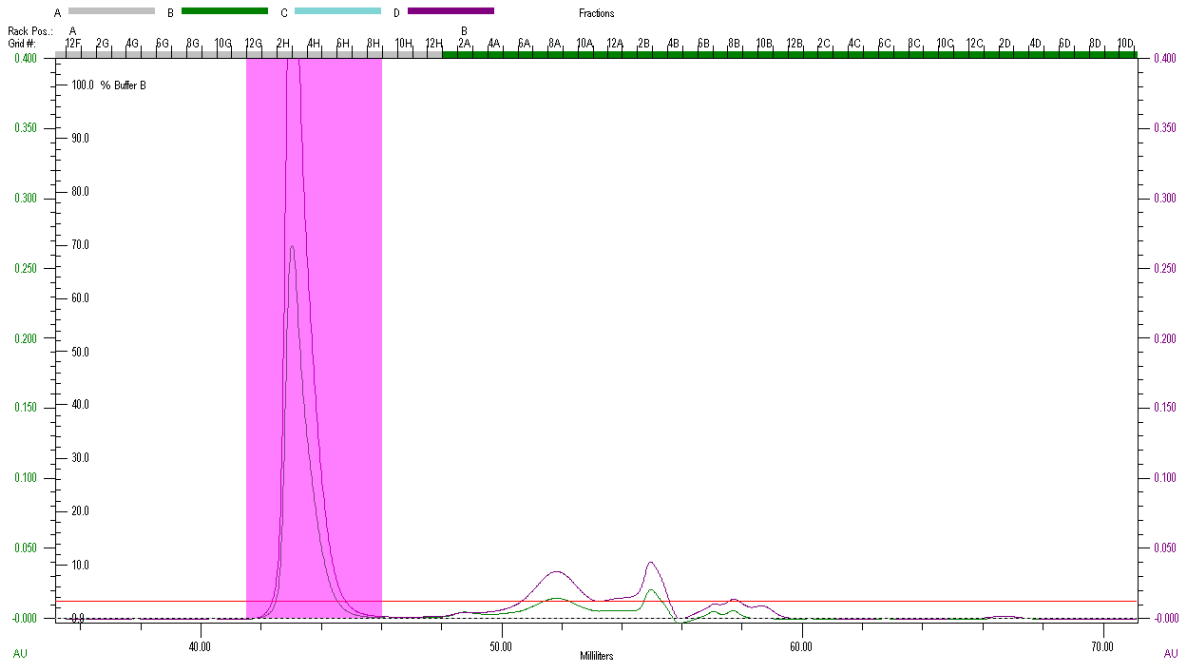

Figure 2.4: Chromatogram trace of SEC purification of NmeKDO8PS. Fractions containing KDO8P synthase that were pooled are highlighted in magenta. Purple and green traces are 280 nm and 260 nm detectors respectively. Red trace is conductivity detector.

2.2.4. Purification summary

The three-step purification of KDO8P synthase from *N. meningitidis* was successful, giving a more than six-fold increase in purity over the three steps from the crude lysate.

Step	Total protein (mg)	Total enzyme activity (U)	Specific activity (U/mg)	% Yield	Relative purity
Crude lysate	170	320	1.9	100	1.0
Anion exchange	38	78	2.1	24	1.1
Hydrophobic interaction	19	72	3.8	22	2.0
Size-exclusion	5.4	66	12	21	6.3

Table 2.1: Summary of three-step purification of wild-type *Nme*KDO8P synthase. % Yield is calculated from crude lysate total enzyme activity and relative purity from crude lysate specific activity.

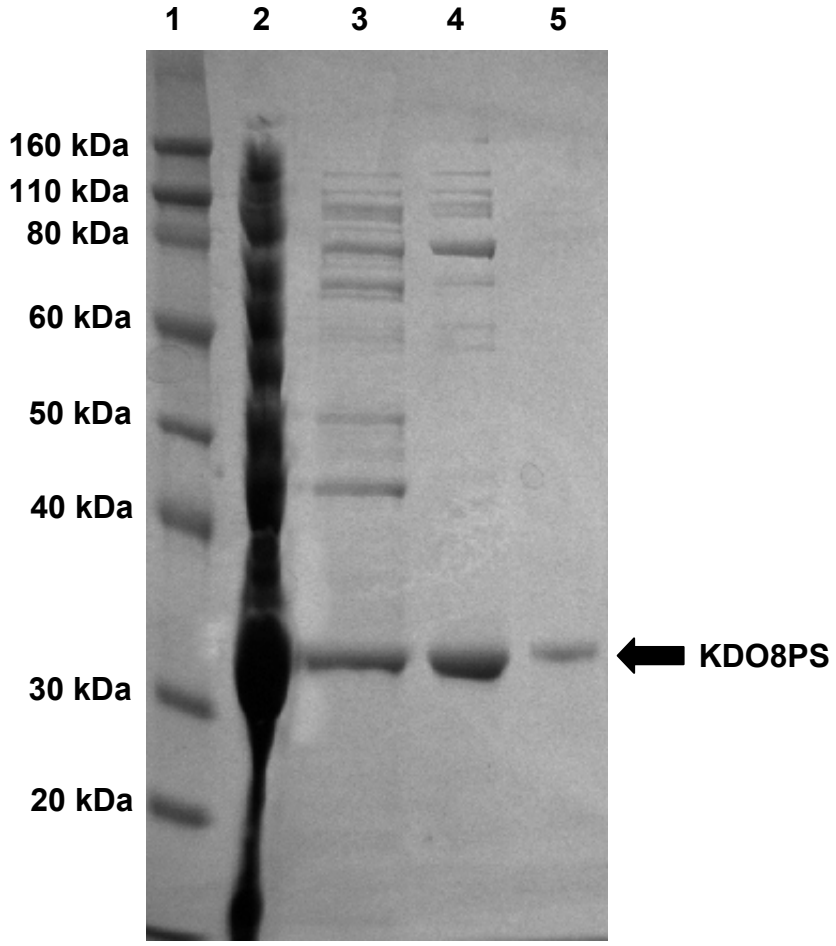

Figure 2.5: SDS-PAGE analysis of three-step purification of *Nme*KDO8PS. SDSPAGE analysis was performed on a 12 % polyacrylamide gel and visualised with Coomassie Brilliant Blue R 250. Lane 1: Molecular marker; Lane 2: cell lysate; Lane 3: AEC pooled fractions; Lane 4: HIC pooled fractions; Lane 5: SEC pooled fractions.

During the AEC purification step a large amount of protein was lost, including some of the protein of interest, KDO8P synthase from *N. meningitidis*. This is reflected in the four-fold

decrease in % yield, but only 10 % increase in relative purity. Previous purifications of *N. meningitidis* KDO8P synthase show a similar loss of total protein but a much smaller loss of total enzyme activity.[94] This step could be further optimised by altering the gradient at which the KDO8P synthase protein is eluted and by further analysis of the fractions to incorporate all the KDO8P synthase protein, as some may be eluting earlier into the waste fractions, which were not analysed by SDS-PAGE. The increase in relative purity for the HIC purification step was more in line with previous purifications.[40,94] Purification with SEC produced a protein of high purity, relative to these previous purifications using the established protocol, and was characterised accordingly.

2.2.5. Enzyme characterisation

The steady-state kinetic parameters of the wild-type *Nme*KDO8PS were determined by following the consumption of PEP ($\varepsilon = 2.8 \times 10^3$ $M^{-1}cm^{-1}$) by measuring the absorbance at 232 nm at pH 7.2 and 25 °C.[94] The concentration of one substrate was fixed while the other was varied in order to collect initial rate data that could be fitted to the Michaelis-Menten equation. This gave the apparent Michaelis constant (K_m) and turnover number (k_{cat}) for each substrate (Figure 2.6).

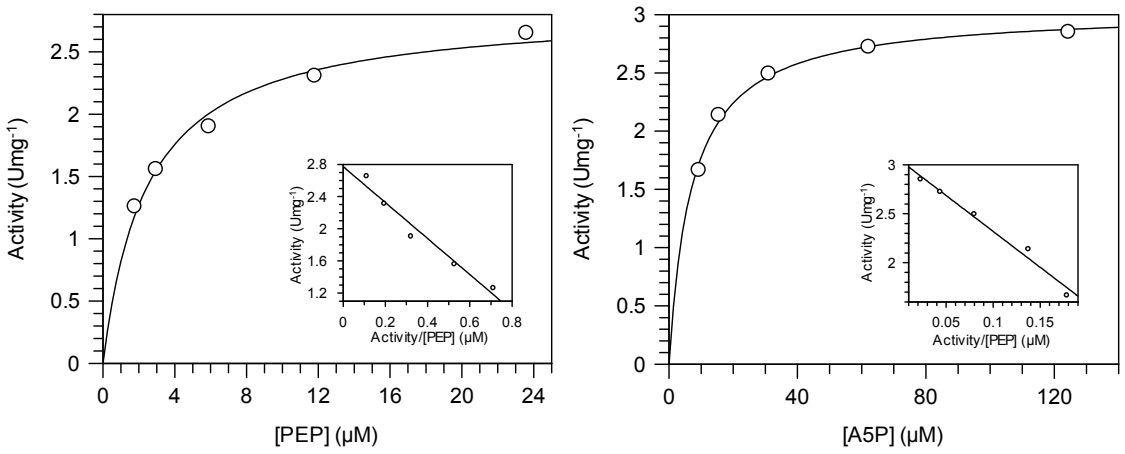

Figure 2.6: Michaelis-Menten plots for determination of K_m for PEP (left) and A5P (right) for KDO8P synthase from *N. meningitidis* with Eadie-Hofstee plot inlay. PEP and A5P concentrations were fixed at 30 μM and 50 μM, for the determination of K_m^{A5P} and K_m^{PEP} respectively.

The values of the kinetic parameters for wild-type NmeKDO8PS (K_m^{A5P} = 7.1 ± 0.5 μM, K_m^{PEP} = 2.5 ± 0.3 μM and k_{cat} = 1.54 ± 0.02 s^{-1}) are comparable to values found in three

previous studies, and to those found for other metal-independent KDO8P synthases from *S. typhimurium*, *E. coli* and *Neisseria gonorrhoea* (Table 2.2).

Source of KDO8P synthase	Assay temp. (°C)	K_m^{PEP} (μM)	K_m^{A5P} (μM)	k_{cat} (s^{-1})	Reference
N. meningitidis	30	2.5 ± 0.3	7.1 ± 0.5	1.5 ± 0.02	This study
N. meningitidis	30	2.1 ± 0.2	4.2 ± 0.5	1.2 ± 0.03	[94]
N. meningitidis	30	< 1	12±1	2.7 ± 0.6	[67]
N. meningitidis	37	2.5 ± 0.2	5.7 ± 0.5	8.0 ± 0.1	[55]
S. typhimurium	37	4.2 ± 0.2	9.3 ± 0.6	6.7 ± 0.5	[95]
E. coli	37	5.9	20	2.5	[17]
N. gonorrhoeae	37	3.1 ± 0.2	8.5 ± 0.1	1.0 ± 0.1	[96]

Table 2.2: Comparison of kinetic parameters of microbial metal-dependent KDO8P synthase.

2.3. Purification of KDO8P synthase from *A. ferrooxidans*

Growth and purification of *Afe*KDO8PS were undertaken using a modification of an established purification protocol.[62] The gene for *Afe*KDO8PS was previously cloned into a pT7-7 plasmid which was transformed into *E. coli* BL21(DE3) cells for expression, and stored in glycerol stock at -80 °C.[62] A small preculture was inoculated with this glycerol stock and grown overnight before being used to inoculate a large culture. The large culture was grown and the cells harvested by centrifugation four hours after IPTG induction. The cell pellet was stored at -80 °C before being resuspended in lysis buffer and sonicated to obtain access to the soluble protein. This solution was then subjected to centrifugation to remove the cell debris.

2.3.1. Purification by anion exchange chromatography (AEX)

KDO8P synthase from *A. ferrooxidans* has a theoretical pI of 5.54.[93] The supernatant, at pH 7.5, was loaded onto a (SOURCE™ 15Q) column with protein eluted from the column using a linear gradient between 0.15 and 0.3 M sodium chloride at 4 °C (Figure 2.7). The UV trace in the anion exchange chromatogram shown in Figure 2.7 indicates that *Afe*KDO8PS was eluted as a single peak with slight contamination from other protein components at the

beginning and end of *Afe*KDO8P synthase elution. This is consistent with subsequent analysis by SDS-PAGE (Figure 2.8) which shows only one major unknown contaminant at ~45 kDa.

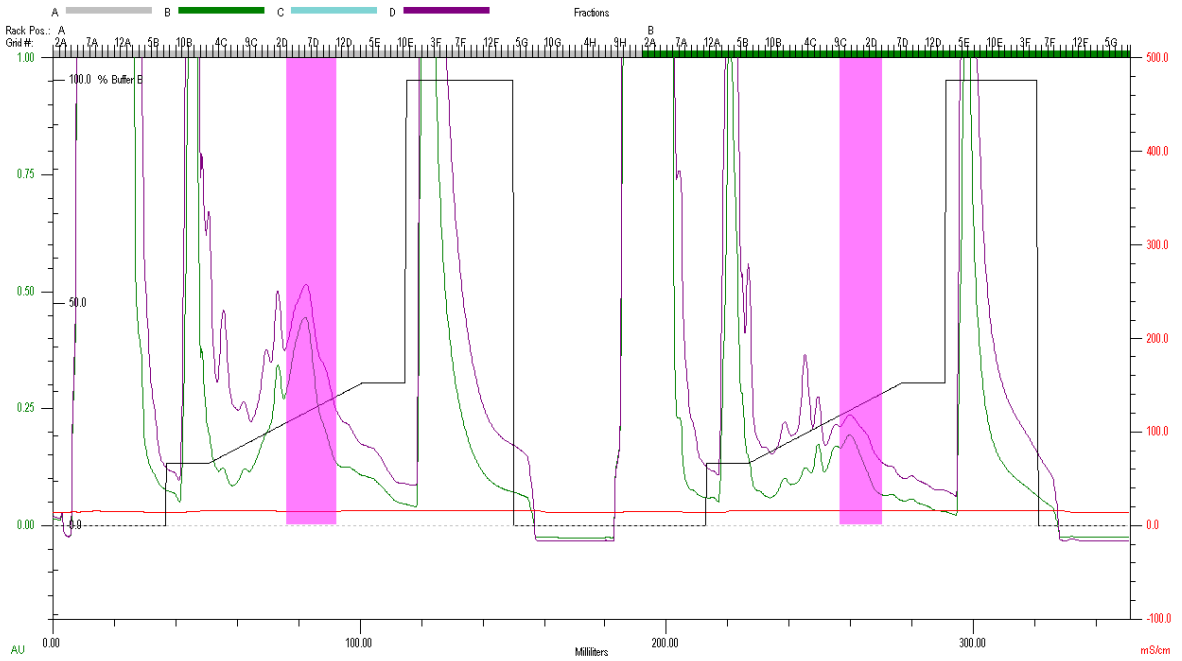

Figure 2.7: Chromatogram trace of AEC purification of *Afe*KDO8PS showing two injections of lysis supernatant. Fractions containing KDO8P synthase are highlighted in magenta. Purple and green traces are 280 nm and 260 nm detectors respectively. Black trace shows sodium chloride gradient (0-1 M). Red trace is conductivity detector.

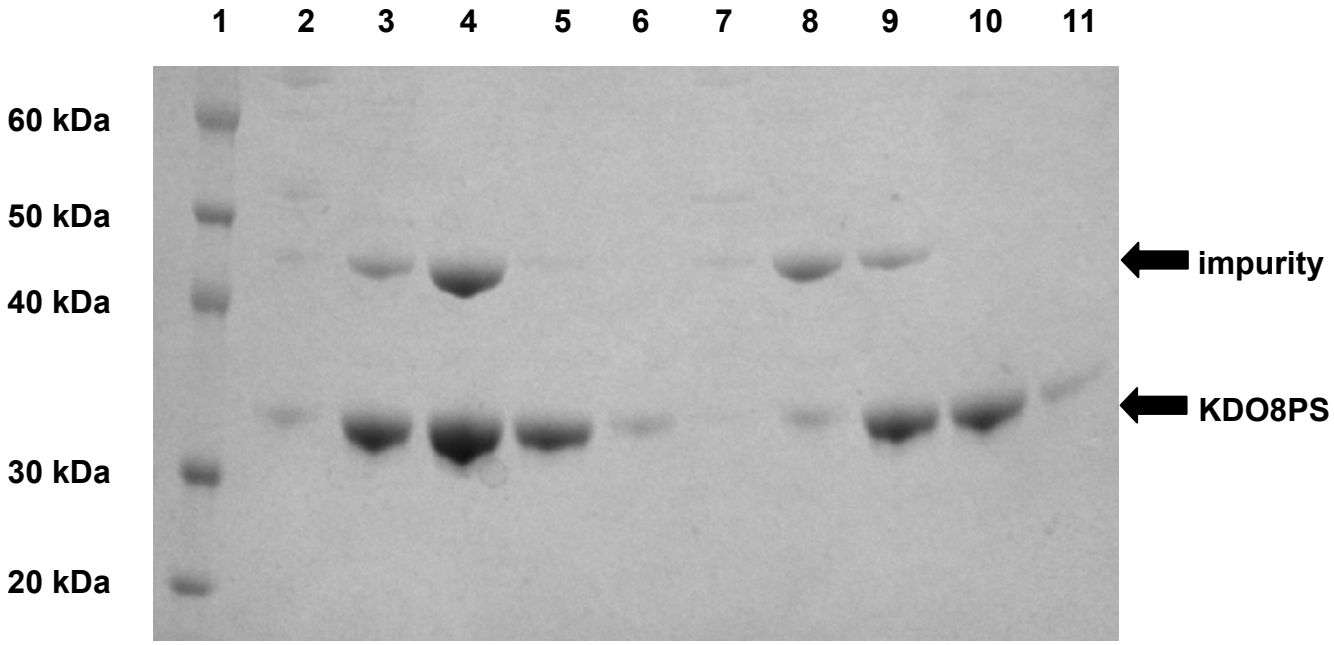

Figure 2.8: SDS-PAGE analysis of AEC purification of *Afe*KDO8PS. SDSPAGE analysis was performed on a 12 % polyacrylamide gel and visualised with Coomassie Brilliant Blue R 250. Lane 1: Molecular marker; Lane 2-6: Fractions as they eluted off the AEC column for first injection; Lane 7-11: Fractions as they eluted off the AEC column for second injection. KDO8P synthase at 31 kDa and an impurity at ~45 kDa are both labelled.

2.3.2. Purification by hydrophobic interaction chromatography (HIC)

The fractions pooled from AEC were exchanged into 1 M ammonium sulfate buffer and loaded onto the hydrophobic interaction column as outlined in the established purification protocol for KDO8P synthase from *A. ferrooxidans*.[62] Bound protein was eluted from the HIC column by a decreasing ammonium sulfate gradient (Figure 2.9), and the fractions thought to contain *Afe*KDO8PS were analysed by SDS-PAGE (Figure 2.10); those fractions that contained the desired protein, as indicated by a component at approximately 31 kDa (eluted between 0.15 and 0.3 M ammonium sulfate) were pooled. The increased purity of the protein sample is reflected in both the chromatogram, as a single peak with small impurities at the end of the elution profile for the protein (Figure 2.9), and the SDS-PAGE analysis showing only small amounts of impurities, found above 40 kDa (Figure 2.10). The protein was exchanged into low salt buffer and concentrated at this point in the purification, as per the established purification protocol for *A. ferrooxidans* KDO8P synthase.[62]

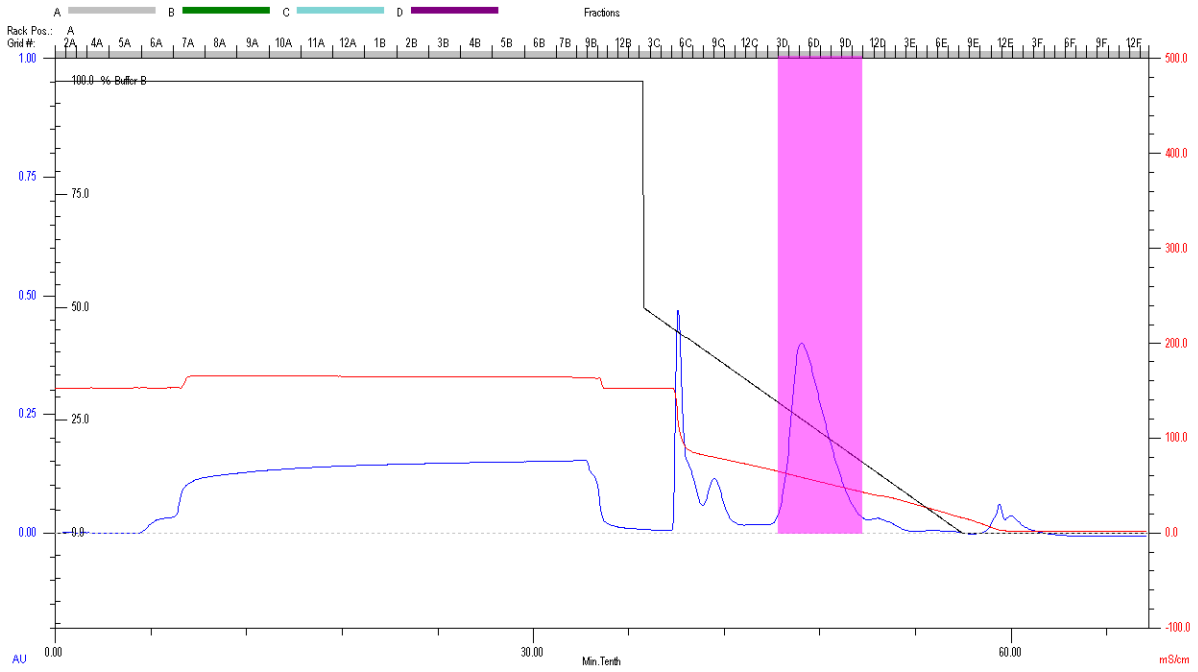

Figure 2.9: Chromatogram trace of HIC purification of *Afe*KDO8PS. Fractions containing KDO8P synthase are highlighted in magenta. Blue and red traces are 280 nm and conductivity measurements respectively. Black trace shows ammonium sulfate gradient (1-0 M). Red trace is conductivity detector.

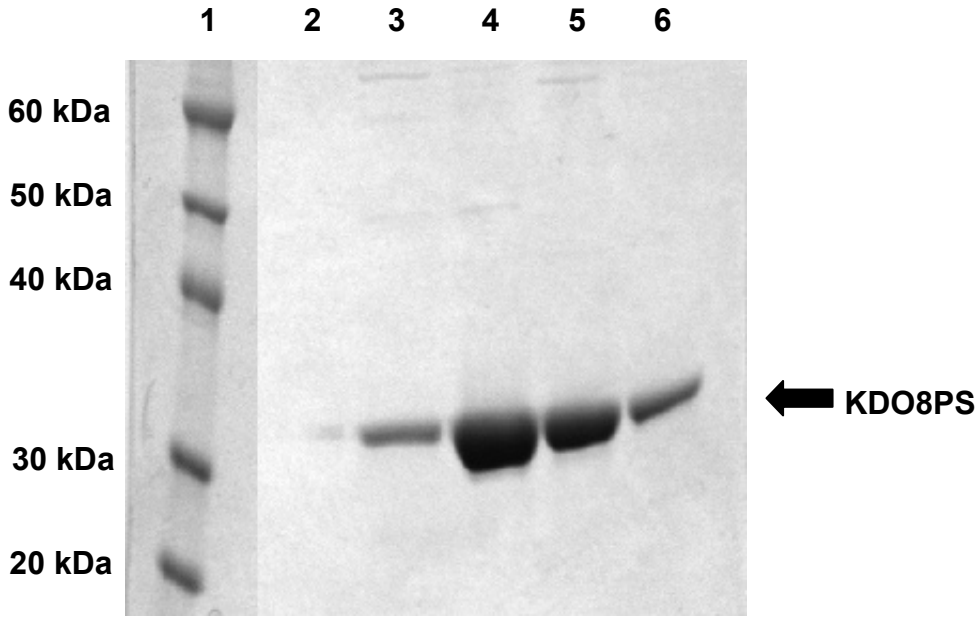

Figure 2.10: SDS-PAGE analysis of HIC purification of *Afe*KDO8PS. SDSPAGE analysis was performed on a 12 % polyacrylamide gel and visualised with Coomassie Brilliant Blue R 250. Lane 1: Molecular marker; Lane 2-6: Fractions as they eluted from the HIC column.

2.3.3. *Purification by size exclusion chromatography (SEC)*

The purification thus far had provided a large increase in purity, as discussed. However a small number of components above 40 kDa remained, as determined by SDS-PAGE analysis (Figure 2.10). The relative purity of the *N. meningitidis* KDO8P synthase sample had been increased more than three-fold by the addition of a third SEC purification step to the existing purification protocol.[40] It was thought that by employing a SEC step into the existing purification protocol for KDO8P synthase from *A. ferrooxidans* the relative purity of the HIC sample could be similarly increased. The concentrated HIC sample was loaded onto the Superdex™ S200 10/300 column for SEC purification and fractions containing KDO8P synthase as determined by SDS-PAGE analysis (not shown) were pooled, concentrated and stored at -80 °C. The chromatogram of the SEC purification showed a single peak (Figure 2.11) indicating a pure protein with very little contamination. This result was also seen on the final SDS-PAGE analysis of the purification procedure (Figure 2.12), as a single band with no contaminating proteins visible on the SDS-PAGE gel.

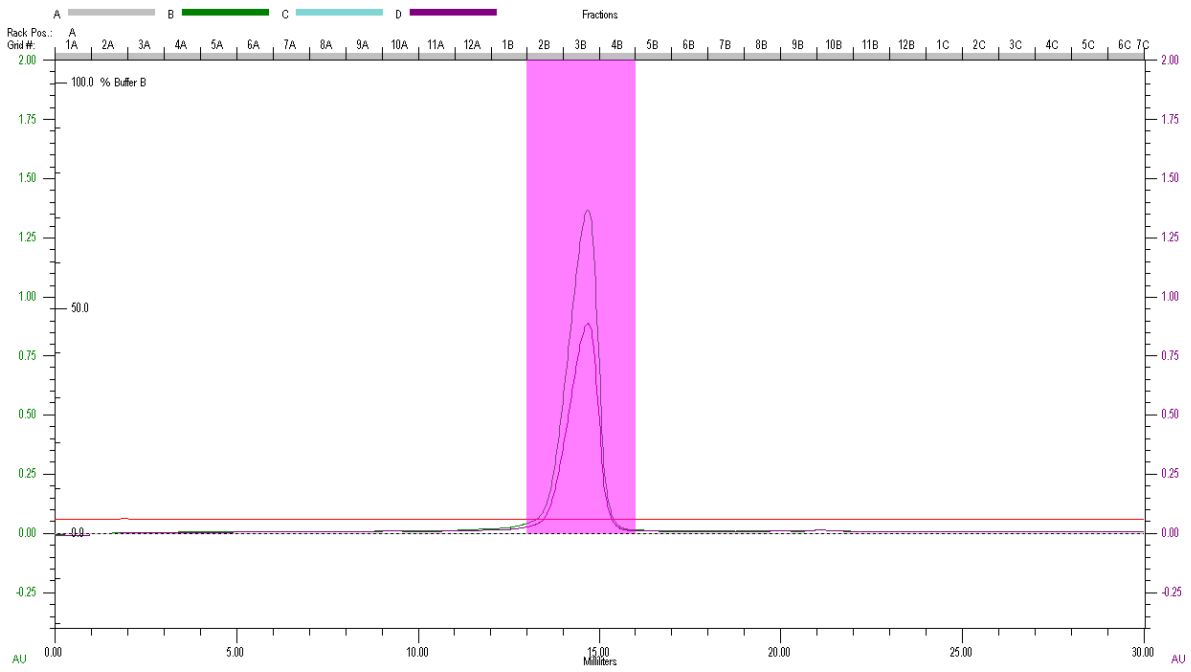

Figure 2.11: Chromatogram trace of SEC purification of *Afe*KDO8PS. Fractions containing KDO8P synthase are highlighted in magenta. Purple and green traces are 280 nm and 260 nm detectors respectively. Red trace is conductivity detector.

2.3.4. Purification summary

The three step purification achieved an almost five-fold purification of the *Afe*KDO8PS enzyme. The purification table below (Table 2.3) shows some anomalous values which will be discussed below.

Step	Total protein (mg)	Total enzyme activity (U)	Specific activity (U/mg)	% Yield	Relative purity
Crude lysate	150	290	1.9	100	1.0
Anion exchange	22	140	6.4	48	3.4
Hydrophobic interaction	15	190	13	66	6.8
Size-exclusion	9.8	85	8.7	29	4.6

Table 2.3: Summary of three-step purification of wild-type *Afe*KDO8PS. % Yield is calculated from crude lysate total enzyme activity and relative purity from crude lysate specific activity.

The SDS-PAGE analysis of the purification (Figure 2.12) shows a substantial decrease in protein contaminants over the three purification steps, with the most visible difference between the crude lysate and AEC fractions. This is reflected in the almost seven-fold loss of total protein between the two samples. SEC purification removed all visible contaminants from the enzyme sample, including the rest of the major contaminant at ~45 kDa as discussed in Section 2.3.1.

However, the purification table reveals inconsistencies in the results for enzyme activity as the total enzyme activity increases after HIC purification (Table 2.3). This may be a result of incorrect estimations of either the total protein or total enzyme activity in the samples obtained after the three purification steps. A repeat of the purification of *Afe*KDO8PS that was modified for this study, reports the specific activity after AEC purification to be 4.3, and following HIC, 5.6.[94] Though the specific activity was slightly higher following AEC in this study, the result following HIC is more than double the previously obtained value. We can conclude from this result that the specific activity following HIC shown for the inhibition of *Afe*KDO8PS in this study is likely to be incorrect. For the purpose of this study, enzyme samples that exhibit correct kinetic parameters, and are shown to be pure by SDS-PAGE analysis should be sufficient for use in the inhibition studies discussed in Chapters 3 and 4. Kinetic characterisation, shown below in Figure 2.13, in comparison with previously obtained

values for the *A. ferrooxidans* KDO8P synthase enzyme, given in Table 2.4 showed this to be the case.

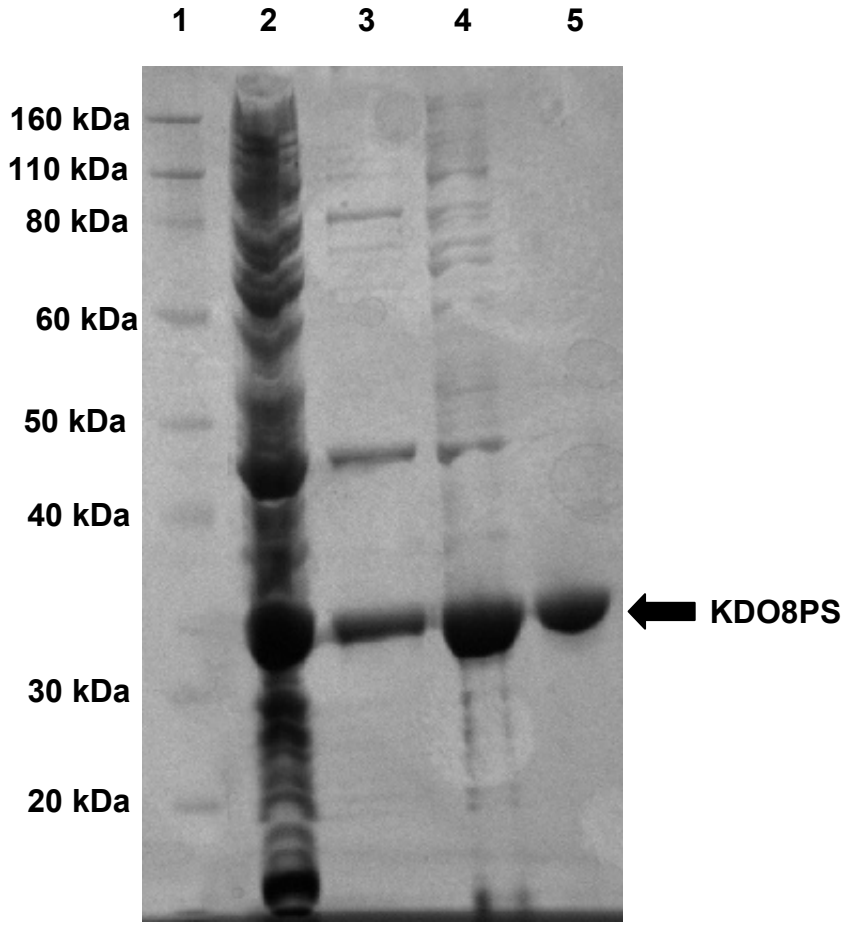

Figure 2.12: SDS-PAGE analysis of three-step purification of *Afe*KDO8PS. SDSPAGE analysis was performed on a 12 % polyacrylamide gel and visualised with Coomassie Brilliant Blue R 250. Lane 1: Molecular marker; Lane 2: cell lysate; Lane 3: AEC pooled fractions; Lane 4: HIC pooled fractions; Lane 5: SEC pooled fractions.

2.3.5. Enzyme characterisation

The steady-state kinetic parameters of the wild-type *Afe*KDO8PS were measured as per *Nme*KDO8PS, following the consumption of PEP ($\varepsilon = 2.8 \times 10^3$ $M^{-1}cm^{-1}$) by measuring the absorbance at 232 nm with modified conditions from a previous study,[94] pH 7.2 and 30 °C. This gave the apparent Michaelis constant (K_m) and turnover number (k_{cat}) for the two enzyme substrates (Figure 2.13).

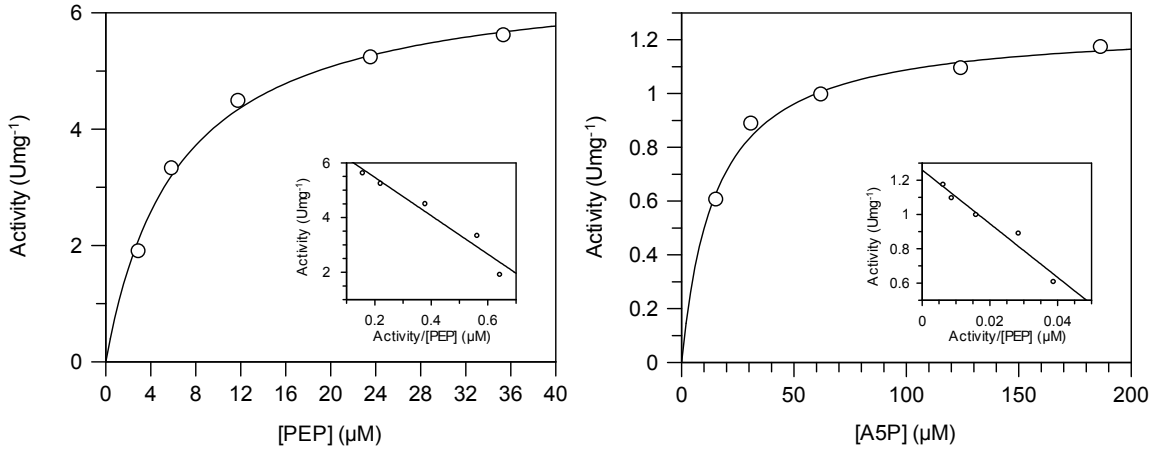

Figure 2.13: Michaelis-Menten plots for determination of K_m for PEP (left) and A5P (right) for KDO8P synthase from *A. ferrooxidans* with Eadie-Hofstee plot inlay. PEP and A5P concentrations were fixed at 50 μM and 100 μM, for the determination of K_m^{A5P} and K_m^{PEP} respectively.

The values of the kinetic parameters for wild-type *Afe*KDO8PS (K_m^{A5P} = 15 ± 2 μM and K_m^{PEP} = 6.4 ± 0.7 μM) are comparable to values found in three previous studies, and to those found for other metal-independent KDO8P synthases from *H. pylori*, *A. aeolicus* and *Aquifex pyrophilus* (Table 2.4).

Source of KDO8P synthase	Assay temp. (°C)	K_m^{PEP} (μM)	K_m^{A5P} (μM)	k_{cat} (s^{-1})	Reference
A. ferrooxidans	37	6.4 ± 0.7	15 ± 2	3.4 ± 0.1	This study
A. ferrooxidans	37	4.8 ± 0.8	49 ± 3.9	5.1 ± 0.15	[94]
A. ferrooxidans	37	22 ± 2	12 ± 1	4.8 ± 0.1	[62]
H. pylori J99	37	1.8 ± 0.5	4.8 ± 0.3	1.2 ± 0.03	[97]
A. aeolicus	90	28 ± 4	74 ± 8	2.00 ± 0.11	[37]
A. pyrophilus	60	290 ± 40	70 ± 8	4	[38]

Table 2.4: Comparison of kinetic parameters of microbial metal-independent KDO8P synthase.

2.4. Summary

The three-step purification using modified existing protein purification protocols for KDO8P synthase from *N. meningitidis*[40] and *A. ferrooxidans*[62] were successful, producing milligram samples of pure enzyme for use in the inhibition studies of Chapters 3 and 4. The characterisation of both classes of KDO8P synthase gave results for K_m^{PEP}, K_m^{A5P} and k_{cat} that were similar to those previously found for the respective enzymes (Table 2.2 and Table 2.4).

Chapter 3: Single site inhibitors of KDO8P synthase

five small molecules
mimics as inhibitors
intermediate

3.1. Introduction

The ability of enzymes to stabilise the high energy transition states and intermediates of a reaction is believed to be one of the factors leading to their catalytic efficiency. This selective binding will lead to the reduction of the energy barrier associated with the formation of transient species, increasing the overall rate of reaction.[98-100] This 'Transition State Theory' is the basis for the design of many modern transition state analogues as enzyme inhibitors. Dissociation constants more than 90 million times higher than the K_m for the substrate of an enzyme have been observed for inhibitors resembling the transition state.[101]

The KDO8P synthase reaction, as previously discussed in Chapter 1, is thought to occur *via* an oxocarbenium ion transition state or high energy intermediate, which is attacked by a water molecule on either the *re* or *si* face of the PEP fragment to give a tetrahedral intermediate. This tetrahedral intermediate then undergoes C-O bond breakage in a dephosphorylation reaction to give the eight-carbon sugar KDO8P. Small PEP mimics that resemble the possible transition state or intermediate in this proposed reaction mechanism should show inhibition against KDO8P synthase. Three sets of inhibitors, previously synthesised in our laboratory,[102] were chosen for inhibitory studies against KDO8P synthase (Figure 3.1).

Two sets of molecules were chosen to mimic the two potential charge distributions of the oxocarbenium species (3.1 and 3.2). Glyphosate, 1.6, contains a positive charge on the nitrogen atom, representative of the carbocation on the C2 trigonal centre from PEP (oxocarbenium ion 3.1). However, there is some charge distribution on the oxygen in the intermediate, with trigonal planar geometry on the C2 carbon of PEP (oxocarbenium ion 3.2). Vinyl phosphonate 3.3 and the fluorinated analogue 3.4 have this trigonal planar geometry at the C2 carbon, and so may better represent the geometric features of the transition state. Finally, the two stereoisomers of phospholactate ((2*R*)-phospholactate 3.5 and (2*S*)-phospholactate 3.6) were utilised as inhibitors, as they contain a tetrahedral centre at C2, representative of the two possible stereoisomers of the tetrahedral hemiketal phosphate intermediate arising from attack of a water molecule on the *re* or *si* face of PEP.

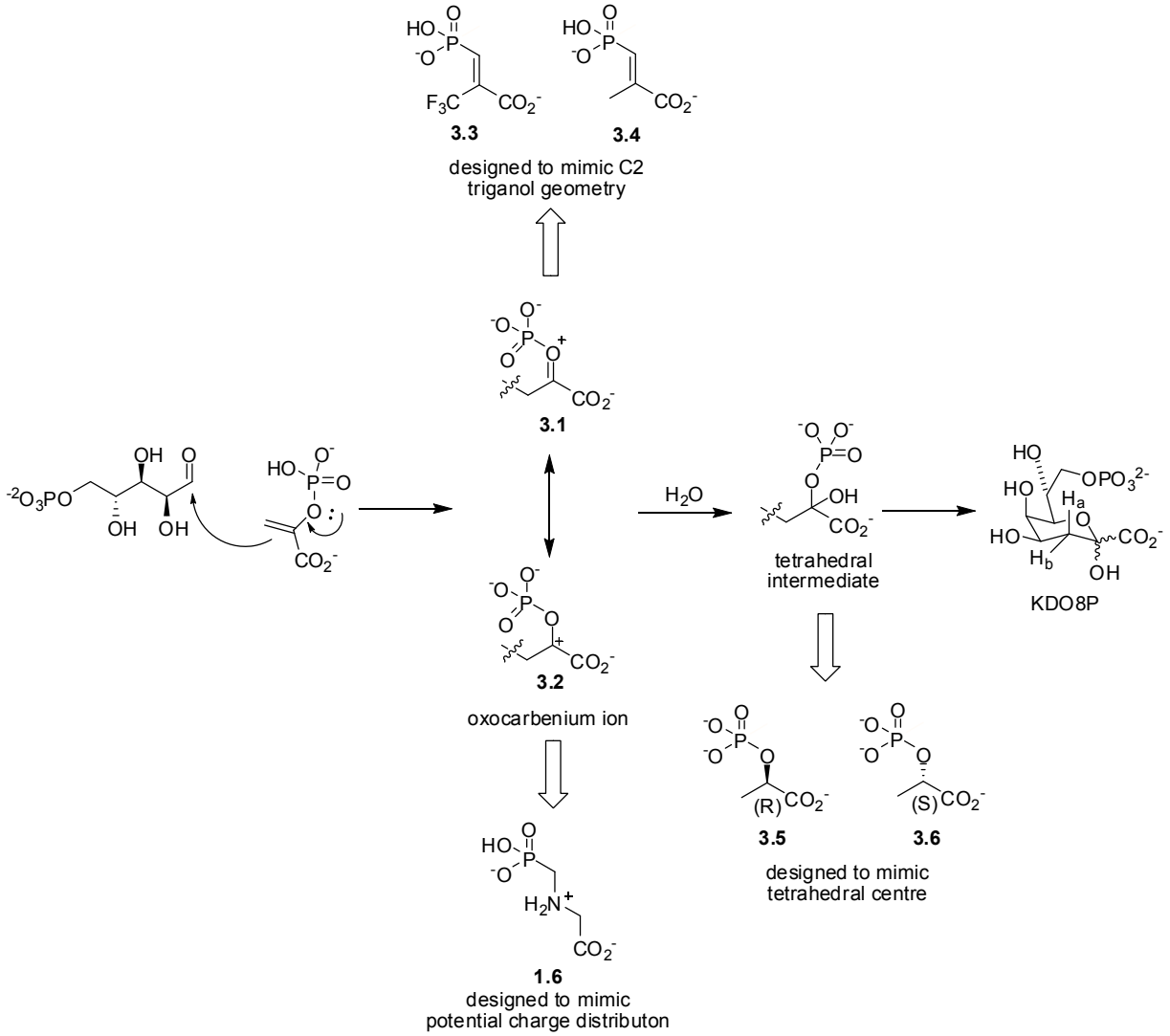

Figure 3.1: Small molecule inhibitors chosen as mimics of oxocarbenium ion species and tetrahedral intermediate of the proposed KDO8P synthase reaction mechanism.

These five molecules will be tested as potential inhibitors of the metal-independent KDO8P synthase from *N. meningitidis* and the metal-dependent KDO8P synthase from *A. ferrooxidans*. The information gathered from these inhibition studies can then be used to infer details about the proposed mechanism, and any difference in mechanism between the two classes of enzyme. The relative inhibition for each molecule can also be used in the design of more sophisticated inhibitors for the two classes of KDO8P synthase

3.2. Aminophosphonates as carbocation analogues

Glyphosate, 1.6, was tested as the first small molecule inhibitor of KDO8P synthase in this study. As discussed, it is representative of the carbocation as a potential charge distribution of the oxocarbenium ion species (oxocarbenium ion 3.1, Figure 3.2).

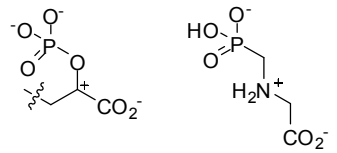

Figure 3.2: Comparison of potential charge distribution of the oxocarbenium ion 3.1 with glyphosate, 1.6.

Glyphosate, 1.6, is a known inhibitor of the shikimate pathway in bacteria and plants. It acts upon 5-enolpyruvylshikimate-3-phosphate (EPSP) synthase and has been shown to inhibit the *E. coli* enzyme with a K_i value of 1.0 μM.[103] The reaction mechanism for EPSP synthase is also thought to occur *via* an oxocarbenium ion species derived from PEP.[104] Glyphosate, 1.6, has previously been tested as an inhibitor of the related aldolase DAH7P synthase from *E. coli* where it was found to be a very poor inhibitor, only showing slight inhibition at concentrations of 1 mM, but has not been tested against KDO8P synthase

3.2.1. Inhibition of KDO8P synthase by glyphosate, 1.6

Glyphosate, 1.6, obtained from commercial sources, was tested against the metal-independent KDO8P synthase from *N. meningitidis* and the metal-dependent KDO8P synthase from *A. ferrooxidans via* kinetic assay, following the loss of PEP at 232 nm. The initial rate data for each enzyme was then fitted to a Michaelis-Menten equation, modified for competitive inhibition and plotted as a graph of substrate concentration vs rate. A visual inspection of the fit of the data was also displayed as a double-reciprocal Lineweaver-Burke plot. These results showed that glyphosate was a competitive inhibitor with respect to PEP, and bound to both enzymes with inhibition constants (K_i) of 260 ± 40 μM (Figure 3.3) and 330 ± 40 μM for the KDO8P synthase from *N. meningitidis* (Figure 3.3) and *A. ferrooxidans* (Figure 3.4) respectively (Figure 3.4).

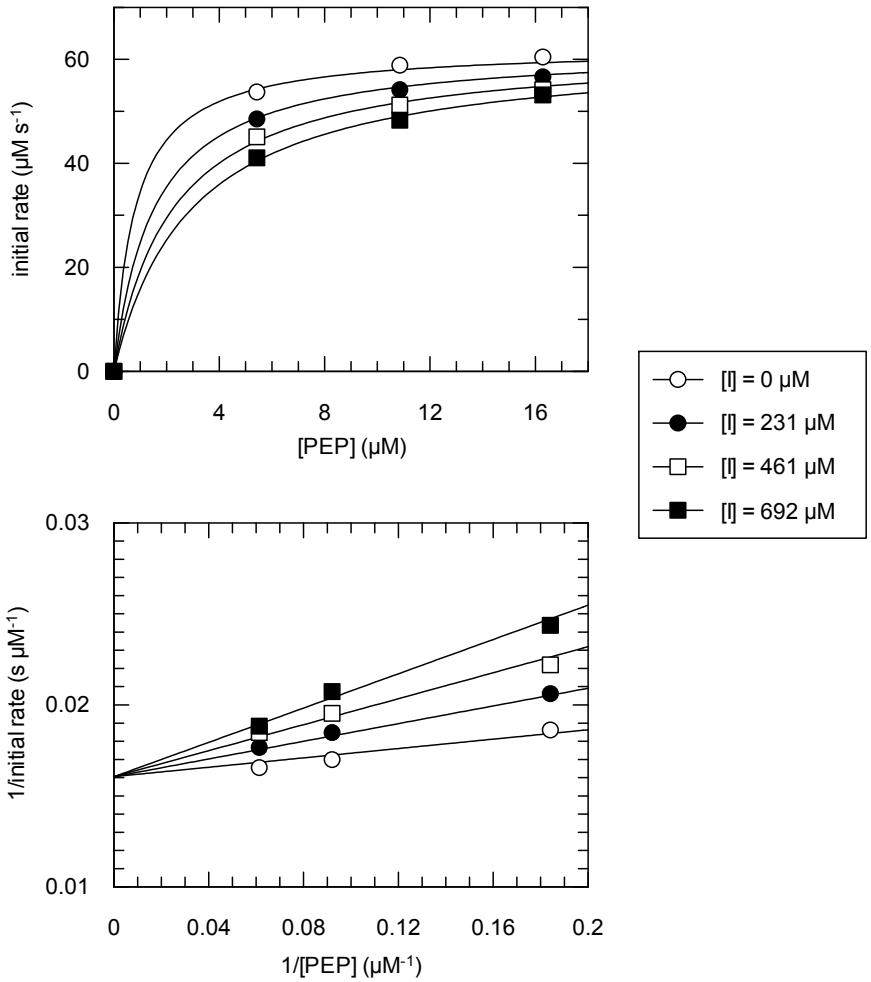

Figure 3.3: Inhibition of KDO8P synthase from *N. meningitidis* by glyphosate, 1.6, as Michaelis-Menten (top) and Lineweaver-Burke (bottom) plots. Solutions of PEP (5-15 μM), A5P (50 μM), and glyphosate, 1.6 (0-692 μM), in 1 mL BTP buffer (50 mM, pH 7.2) were initiated by addition of *N. meningitidis* KDO8P synthase (2 μg) and the loss of PEP followed spectrophotometrically at 232 nm. Initial rates were obtained by linear least squares regression and converted to progress rates (μM s^{-1}).

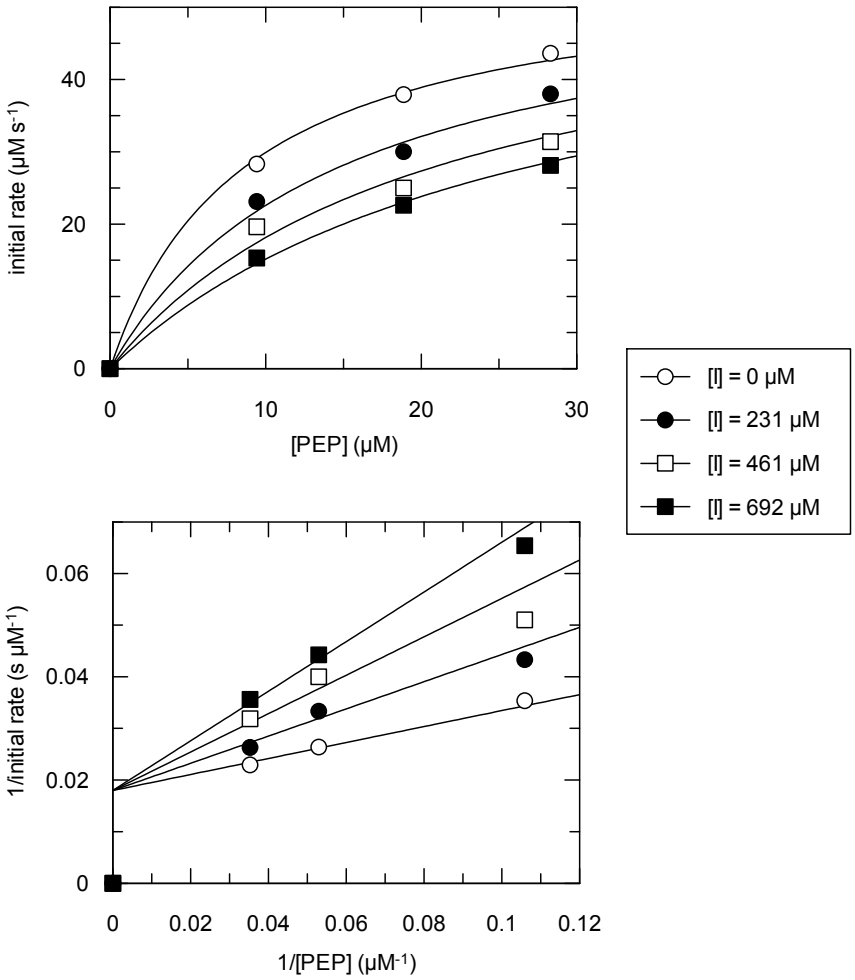

Figure 3.4: Inhibition of KDO8P synthase from *A. ferrooxidans* by glyphosate, 1.6, as Michaelis-Menten (top) and Lineweaver-Burke (bottom) plots. Solutions of PEP (10-30 μM), A5P (100 μM), manganese chloride (10 μM) and glyphosate, 1.6 (0-790 μM), in 1 mL BTP buffer (50 mM, pH 7.2) were initiated by addition of *A. ferrooxidans* KDO8P synthase (2 μg) and the loss of PEP followed spectrophotometrically at 232 nm. Initial rates were obtained by linear least squares regression and converted to progress rates (μM s^{-1}).

3.3. Vinyl phosphonates as oxocarbenium analogues

(*E*)-Vinyl phosphonate 3.3 was chosen as a molecule with potential inhibitory properties against KDO8P synthase due to the trigonal planar geometry at the C2 carbon, representative of the C2 trigonal centre of PEP in the oxocarbenium intermediate 3.2 (Figure 3.5). The vinyl phosphonate 3.3 has been shown to be an inhibitor of the related aldolase DAH7P synthase from *E. coli* with a K_i value of 4.7 ± 0.7 μM.[102]

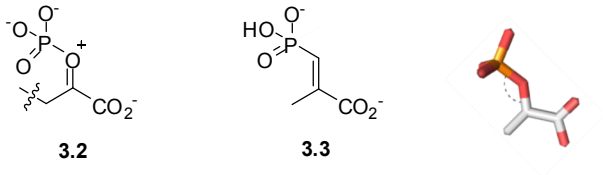

Figure 3.5: Comparison of potential trigonal planar oxocarbenium ion 3.2 and PEP active site geometry (right) (PEP structure from *A. aeolicus* KDO8P synthase, 1FWW)[34] with (*E*)-vinyl phosphonate 3.3.

The (*E*)-vinyl phosphonate 3.3 also retains the observed geometry of enzyme bound PEP, seen in a variety of enzyme crystal structures to have the *syn* relationship between the phosphorous atom and C3 of PEP (Figure 3.5).[31,34,105] Phosphonate 3.3 is locked in this *syn* configuration and as such might be expected to have an entropic advantage over potential inhibitors that did not have this *syn* relationship; any entropic cost of forming the correct conformation of the phosphonate within the active site has already been paid during formation of the vinyl phosphonate alkene, rather than during association of the inhibitor with the enzyme active site.

Phosphonates such as 3.3 however, have decreased acidity with respect to the analogous phosphate moieties, due to decreased electronegativity of the methylene group compared to the enol oxygen. This decreased acidity leads to the requirement for an increased pH for the second ionisation of the phosphate moiety (pK_{a^2}). As discussed in Chapter One, the second ionisation of the phosphate group may be important for the enzyme reaction mechanism and so inhibitors that contain a monoanionic phosphate or phosphonate moiety within the enzyme active site may bind more strongly than the dianionic equivalent.

It has been shown that the pK_{a^2} value can be influenced by the addition of electron withdrawing groups adjacent to the phosphorous atom.[106] Some representative data is given in Figure 3.6.

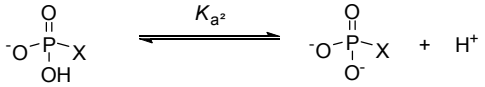

X	O	CH_2	CHF	CF_2
pK_{a^2}	6.4	7.6	6.5	5.4

Figure 3.6: Acidities of phosphates, phosphonates and fluorophosphonates from Romanenko *et al.*[106]

The use of fluorophosphonates as an alternative to phosphonates, in order to improve inhibition, has been shown for a number of different enzymes including phosphoglycerate kinase (PGK)[107,108] and purine nucleoside phosphorylase (PNP).[109] In each of these cases it is thought that this is a result of the increased acidity of the phosphonate group, with PGK showing a mild correlation between the IC_{50} values and pK_a values for the third and fourth ionisations for the twenty two diphosphonates tested, and the inhibitory differences for the difluorophosphonate over phosphonate inhibitors for PNP from four different sources became far more pronounced (5-26 fold lower for the fluorophosphonates) when assayed at pH 6.2 over 7.4.

A version of phosphonate 3.3 that is fluorinated at the C3 position was previously designed within our laboratory (Figure 3.7).[102] Though the fluorine atoms are not on the carbon atom adjacent to the phosphonate moiety, they are vinylogous to it, and so should have some of the desired effect in increasing the overall acidity of the phosphonate group. Fluorinated phosphonate 3.4 has been tested against the DAH7P synthase from *E. coli* where it was found to have a K_i value of 8.8 ± 2.5 μM.[102] This is not significantly different than the results obtained for vinyl phosphonate 3.3. This is not surprising however when the difference in the proposed mechanisms for these two aldolases are considered, as discussed in Chapter 1, where a monoanionic PEP molecule is not thought to be required for the DAH7P synthase mechanism but is possibly required for KDO8P synthase.

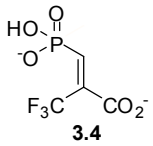

3.4

Figure 3.7: Trifluorinated (E)-vinyl phosphonate

3.3.1. Inhibition of KDO8P synthase by (E)-vinyl phosphonate 3.3

(*E*)-Vinyl phosphonate 3.3, obtained from Scott Walker, was tested as an inhibitor of both the metal-independent and metal-dependent KDO8P synthase from *N. meningitidis* and *A. ferrooxidans*, using the same kinetic assay as previously described. The initial rate data was analysed as before, and it was determined that (*E*)-vinyl phosphonate 3.3 inhibits KDO8P synthase competitively with respect to PEP. The K_i values for vinyl phosphonate 3.3 were found to be 320 ± 30 μM and 260 ± 10 μM for KDO8P synthase from *N. meningitidis* (Figure 3.8) and *A. ferrooxidans* (Figure 3.9) respectively.

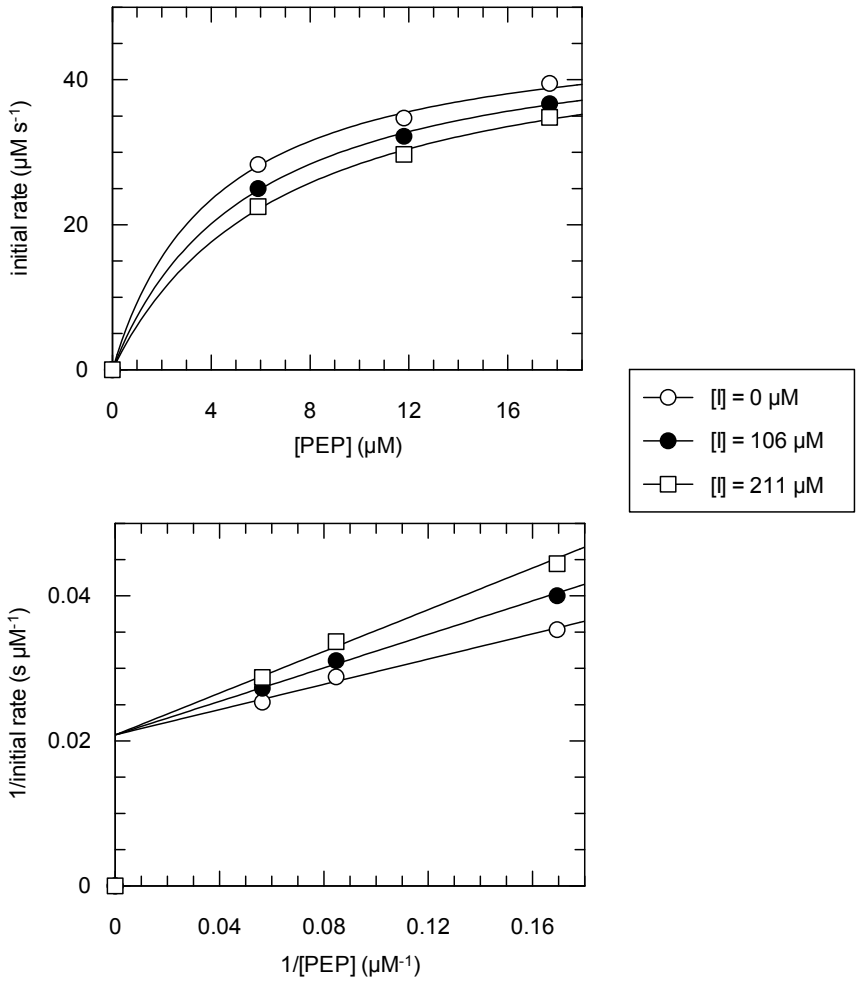

Figure 3.8: Inhibition of KDO8P synthase from *N. meningitidis* by phosphonate 3.3 as Michaelis (top) and Lineweaver-Burke (bottom) plots. Solutions of PEP (5-20 μM), A5P (50 μM), and phosphonate 3.3 (0-211 μM) in 1 mL BTP buffer (50 mM, pH 7.2) were initiated by addition of *N. meningitidis* KDO8P synthase (2 μg) and the loss of PEP followed spectrophotometrically at 232 nm. Initial rates were obtained by linear least squares regression and converted to progress rates (μM s^{-1}).

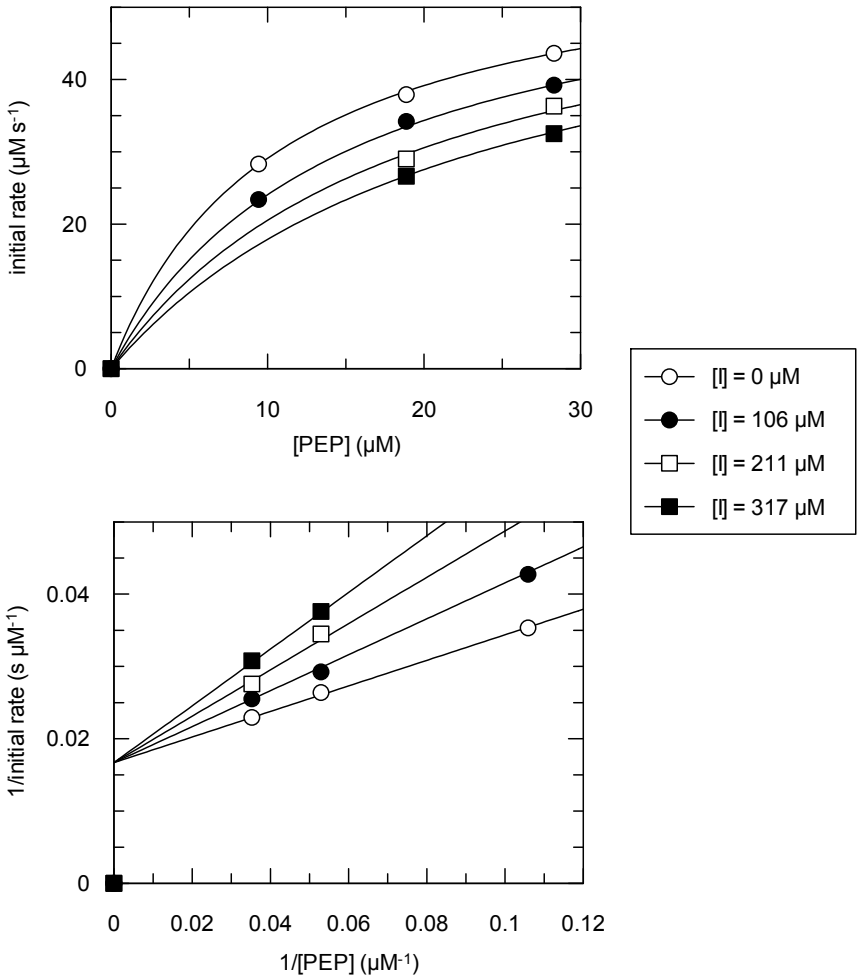

Figure 3.9: Inhibition of KDO8P synthase from *A. ferrooxidans* by phosphonate 3.3 as Michaelis (top) and Lineweaver-Burke (bottom) plots. Solutions of PEP (10-30 μM), A5P (100 μM), manganese chloride (10 μM) and phosphonate 3.3 (0-317 μM) 1 mL BTP buffer (50 mM, pH 7.2) were initiated by addition of *A. ferrooxidans* KDO8P synthase (2 μg) and the loss of PEP followed spectrophotometrically at 232 nm. Initial rates were obtained by linear least squares regression and converted to progress rates (μM s^{-1}).

3.3.2. Inhibition of KDO8P synthase by (E)-vinyl phosphonate 3.4

Trifluorinated (*E*)-vinyl phosphonate 3.4, obtained from Scott Walker, was tested against the KDO8P synthase from *N. meningitidis* and *A. ferrooxidans via* kinetic assay and analysed as described for glyphosate, 1.6. Vinyl phosphonate 3.4 was a competitive inhibitor with respect to PEP, and gave K_i values of 270 ± 30 μM for KDO8P synthase from *N. meningitidis* (Figure 3.10) and 280 ± 20 μM for KDO8P synthase from *A. ferrooxidans* (Figure 3.11).

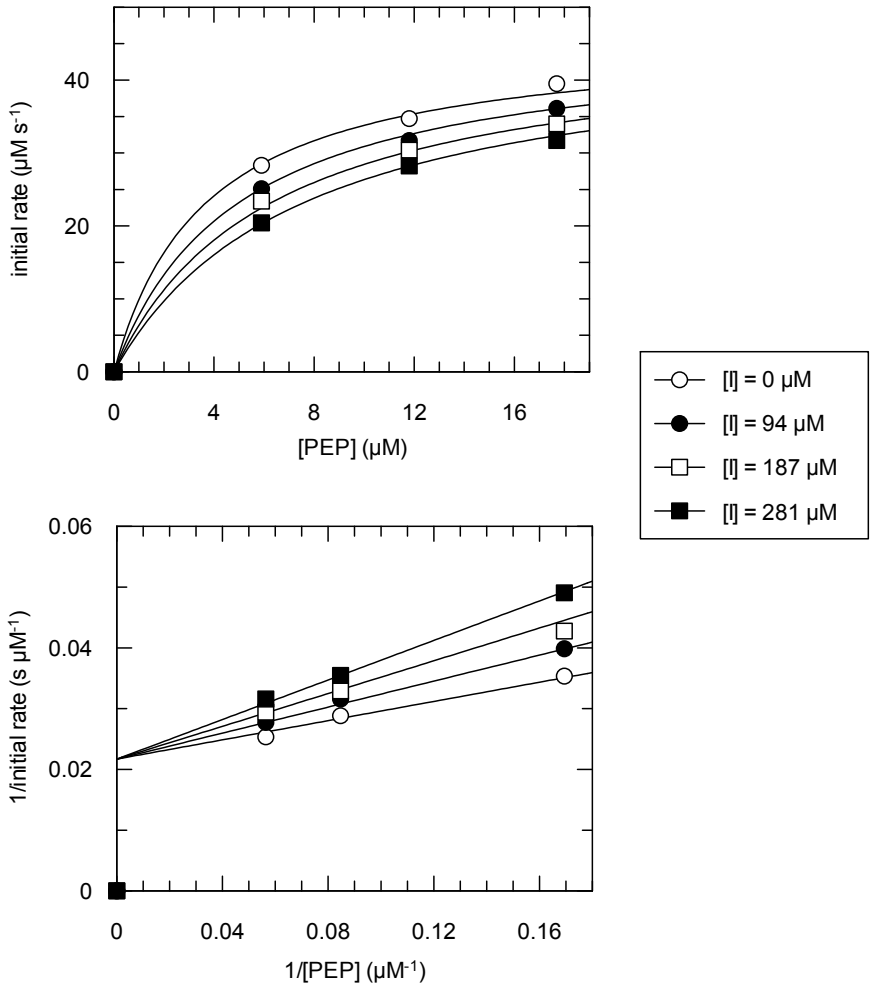

Figure 3.10: Inhibition of KDO8P synthase from *N. meningitidis* by fluorinated phosphonate 3.4 as Michaelis (top) and Lineweaver-Burke (bottom) plots. Solutions of PEP (5-20 μM), A5P (50 μM), and fluorinated phosphonate 3.4 (0-281 μM) in 1 mL BTP buffer (50 mM, pH 7.2) were initiated by addition of *N. meningitidis* KDO8P synthase (2 μg) and the loss of PEP followed spectrophotometrically at 232 nm. Initial rates were obtained by linear least squares regression and converted to progress rates (μM s^{-1}).

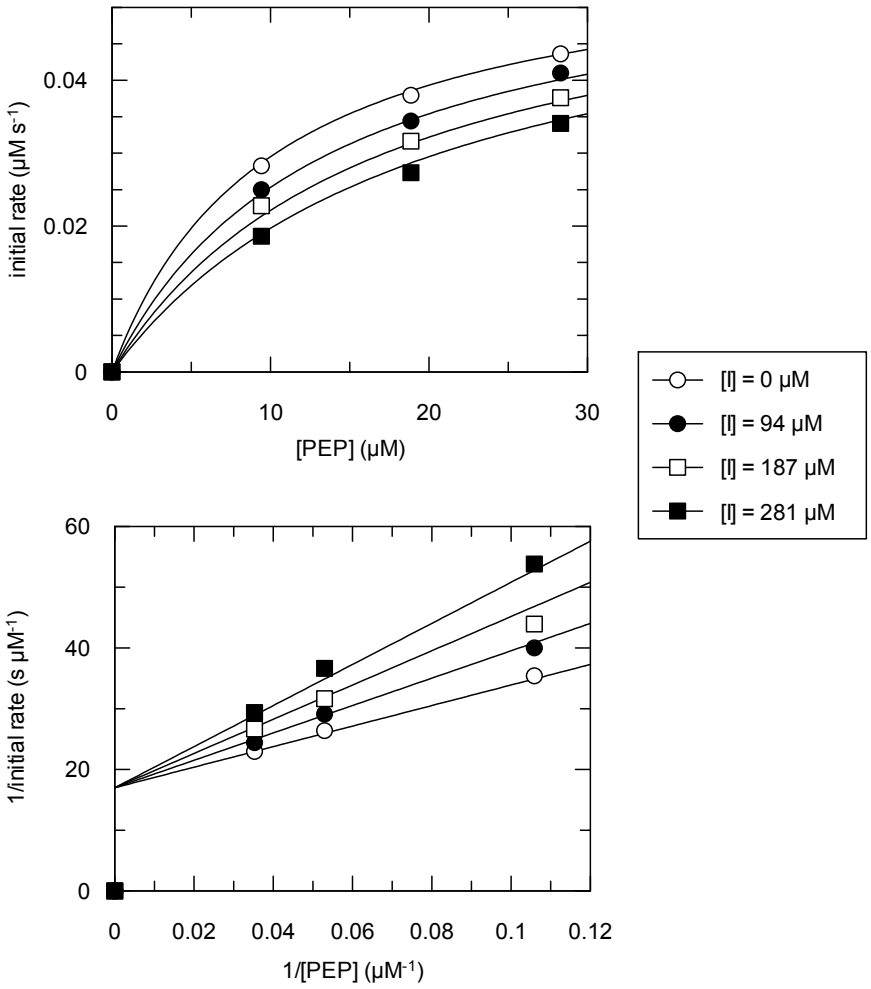

Figure 3.11: Inhibition of KDO8P synthase from *A. ferrooxidans* by fluorinated phosphonate 3.4 as Michaelis (top) and Lineweaver-Burke (bottom) plots. Solutions of PEP (10-30 μM), A5P (100 μM), manganese chloride (10 μM) and fluorinated phosphonate 3.4 (0-280 μM) 1 mL BTP buffer (50 mM, pH 7.2) were initiated by addition of *A. ferrooxidans* KDO8P synthase (2 μg) and the loss of PEP followed spectrophotometrically at 232 nm. Initial rates were obtained by linear least squares regression and converted to progress rates (μM s^{-1}).

3.4. Phospholactates as tetrahedral intermediate analogues

The two stereoisomers of phospholactate were utilised as inhibitors of KDO8P synthase as they contain a tetrahedral centre at the C2 carbon (Figure 3.12), representative of the tetrahedral intermediate, as described in Section 1.3.4.

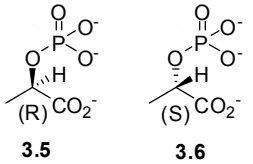

3.5 **3.6**

Figure 3.12: (2*R*)- (3.5) and (2*S*)-phospholactate (3.6) molecules as inhibitors of KDO8P synthase.

These phospholactates have been tested as possible inhibitors of other PEP utilising enzymes such as pyruvate kinase and enolase from rabbit muscle.[110] Pyruvate kinase was inhibited ten-fold greater by the phospholactate 3.5 due to the methyl group on the phospholactate 3.6 being sterically hindered by a proton donor group, normally found near the C3 carbon of PEP.[111] Enolase did not discriminate between the two stereoisomers due to the proton donor group in the active site being located near the C2 rather than C3 carbon of PEP, though inhibition was poor for both isomers, thought to be due to the incapacity of the enzyme to tolerate steric bulk at the C3 position.[112] In the related aldolase DAH7P synthase, phospholactate 3.5 was shown to inhibit the enzyme ten-fold greater than phospholactate 3.6. This was rationalised as the *re* face water attacking PEP at the C2 position, with the methyl group of phospholactate 3.5 binding in the *re*-face water pocket in the enzyme active site.[86] The enantiomeric preference shown by KDO8P synthase will be analysed in the same way as these three enzymes, and used to determine aspects of the mechanism and tetrahedral intermediate.

The two stereoisomers of phospholactate have been tested as inhibitors of the metal-independent KDO8P synthase from *N. meningitidis* where they were found to have K_i values of 870 ± 90 μM and 1200 ± 50 μM for phospholactate 3.5 and 3.6 respectively.[113] The testing of these molecules on a metal-dependent KDO8P synthase has not been previously undertaken however, and so the two molecules were tested on the KDO8P synthase enzyme from *A. ferrooxidans* to determine whether there are any differences between the two classes of enzyme, and between the two stereoisomers of phospholactate.

3.4.1. Inhibition of KDO8P synthase from A. ferrooxidans by phospholactates 3.5 and 3.6

The (2*R*)- (3.5) and (2*S*)-phospholactates (3.6), obtained from Hemi Cumming and Sebastian Reichau respectively, were tested as inhibitors of the metal-dependent KDO8P synthase from *A. ferrooxidans via* kinetic assay and fitted to the Michaelis-Menten equation as previously described. They were found to have K_i values of 390 ± 70 μM (Figure 3.13) and 1000 ± 220 μM (Figure 3.14) respectively.

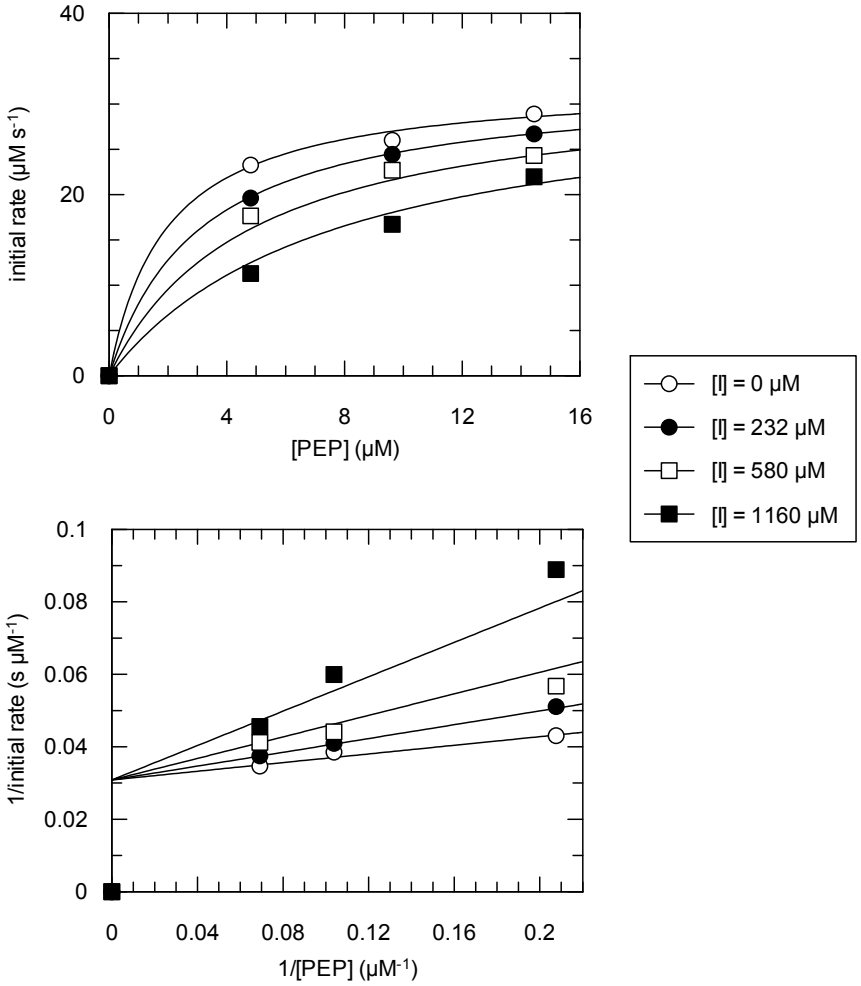

Figure 3.13: Inhibition of KDO8P synthase from *A. ferrooxidans* by (2*R*)-phospholactate, 3.5, as Michaelis (top) and Lineweaver-Burke (bottom) plots. Solutions of PEP (5-15 μM), A5P (100 μM), manganese chloride (10 μM) and (2*R*)-phospholactate, 3.5, (0-1160 μM) in 1 mL BTP buffer (50 mM, pH 7.2) were initiated by addition of *A. ferrooxidans* KDO8P synthase (2 μg) and the loss of PEP followed spectrophotometrically at 232 nm. Initial rates were obtained by linear least squares regression and converted to progress rates (μM s^{-1}).

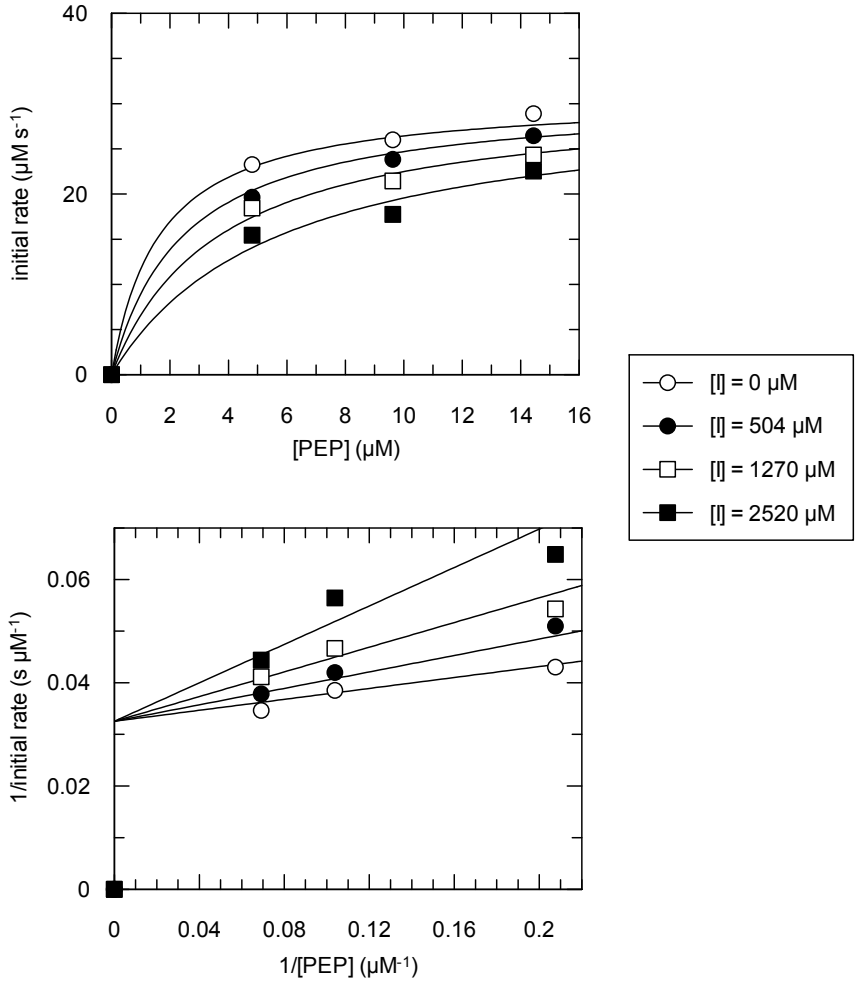

Figure 3.14: Inhibition of KDO8P synthase from *A. ferrooxidans* by (2*S*)-phospholactate, 3.6, as Michaelis (top) and Lineweaver-Burke (bottom) plots. Solutions of PEP (5-15 μM), A5P (100 μM), manganese chloride (10 μM) and (2*S*)-phospholactate, 3.6, (0-2520 μM) in 1 mL BTP buffer (50 mM, pH 7.2) were initiated by addition of *A. ferrooxidans* KDO8P synthase (2 μg) and the loss of PEP followed spectrophotometrically at 232 nm. Initial rates were obtained by linear least squares regression and converted to progress rates (μM s^{-1}).

3.5. Discussion and summary

A number of small molecule PEP-mimics were tested as inhibitors on both the metal-independent KDO8P synthase from *N. meningitidis* and the metal-dependent KDO8P synthase from *A. ferrooxidans*. These inhibitors either mimicked the two possible charge distributions of the trigonal planar oxocarbenium ion species (glyphosate 1.6, and vinyl phosphonates 3.3 and 3.4), or the tetrahedral intermediate (phospholactates 3.5 and 3.6).

Glyphosate, 1.6, chosen to mimic the potential oxocarbenium ion charge distribution 3.1, showed moderate to poor inhibition of KDO8P synthase from both the metal-independent and metal-dependent class of enzyme (Figure 3.15).

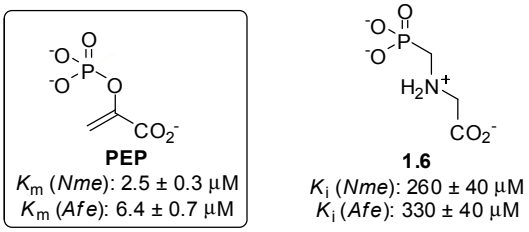

Figure 3.15: Inhibitory properties of glyphosate 1.6 with PEP for KDO8P synthase from *N. meningitidis* and *A. ferrooxidans*.

The vinyl phosphonates 3.3 and 3.4 were designed to mimic the oxocarbenium ion with a trigonal planar centre at the C2 carbon of the PEP fragment (3.2). Both the (*E*)-vinyl phosphonate 3.3 and the fluorinated analogue 3.4 had similar K_i values to the other oxocarbenium ion mimic tested, glyphosate, 1.6 (Figure 3.16).

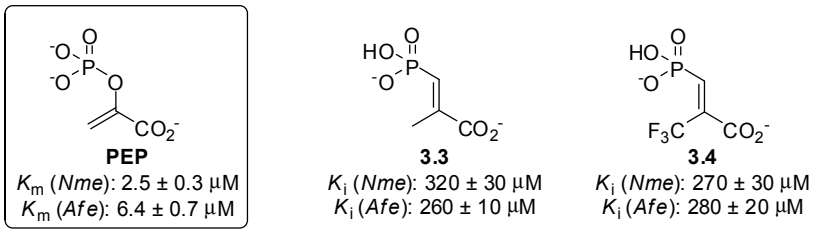

Figure 3.16: Inhibitory properties of (*E*)-vinyl phosphonate 3.3 and fluorinated (*E*)-vinyl phosphonate 3.4 with PEP for KDO8P synthase from *N. meningitidis* and *A. ferrooxidans*.

The (2*R*)- (3.5) and (2*S*)-phospholactate (3.6) molecules were chosen as mimics of the two possible stereoisomers of the tetrahedral intermediate of the KDO8P synthase reaction. They had previously been tested as inhibitors of the metal-independent KDO8P synthase from *N. meningitidis* were also tested here as inhibitors of the metal-dependent KDO8P synthase from *A. ferrooxidans*. The (2*R*)-phospholactate 3.5 inhibited the KDO8P synthase enzyme more than the (2*S*)-phospholactate 3.6 for both the metal-independent and metal-dependent class, though the difference was far more pronounced for the metal-dependent enzyme (Figure 3.17). The K_i values were generally two to three-fold higher for the phospholactates than for the transition state inhibitors 1.6, 3.3 and 3.4, except in the case of phospholactate 3.5 with the *Afe*KDO8PS enzyme.

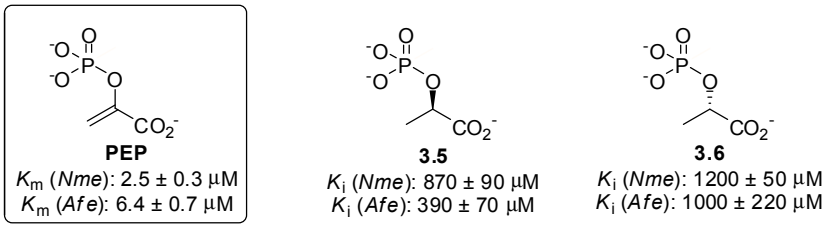

Figure 3.17: Inhibitory properties of (2*R*)-phospholactate 3.5 and (2*S*)-phospholactate 3.6 with PEP for KDO8P synthase from *N. meningitidis* and *A. ferrooxidans*.

The results from the inhibition of these five inhibitors against KDO8P synthase from *N. meningitidis* and *A. ferrooxidans* reveal some interesting insights into the mechanism of KDO8P synthase and reveal trends that can be used in the synthesis of future inhibitors.

Glyphosate, 1.6, and vinyl phosphonate 3.3 had similar inhibition against KDO8P synthase from both the metal-independent and metal-dependent class of enzyme. This result is in some ways surprising as they are quite different in structure. This is good evidence to suggest that they are both mimicking the same oxocarbenium ion species, as per their original purpose. The fluorinated analogue of vinyl phosphonate 3.3 (3.4) did not show significantly different inhibition towards the KDO8P synthase from either class of enzyme. It may be that the KDO8P synthase mechanism does not require a monoanionic phosphate as discussed in Chapter 1.

The (2*R*)- (3.5) and (2*S*)-phospholactate (3.6) molecules showed differing results for the KDO8P synthase enzyme from the metal-independent and metal-dependent class. Both enzymes showed binding preference for the (*R*)-stereoisomer over the (*S*)-stereoisomer but this was far greater for the metal-dependent enzyme from *A. ferrooxidans*. At first glance it would appear that this preference infers that the C2 of PEP is attacked by the water molecule *si* face of PEP (Chapter 1). Recent crystallographic studies of a tetrahedral intermediate analogue bound in the active site of the related aldolase DAH7P synthase show that the stereoisomer bound in the active site is the (*R*) stereoisomer which best accommodates the *re* face water molecule. This isomer showed greater inhibition than the (*S*) isomer, which does not accommodate this *re* face water as well when bound in the active site (unpublished data).[114] It may be that the phospholactate inhibitors behave the same way. This will be explored further in Chapter 5 with modelling studies.

Overall, the inhibitors that resembled the trigonal planar oxocarbenium ion species were more effective than the phospholactates that mimicked the tetrahedral intermediate. The

inhibition constants were similar for the metal-independent KDO8P synthase from *N. meningitidis* and the metal-dependent KDO8P synthase from *A. ferrooxidans* even though the K_m value for PEP is more than twice as large for the metal-dependent enzyme as it is for the metal-independent analogue. This effectively makes the inhibitors twice as effective against the metal-dependent KDO8P synthase enzyme from *A. ferrooxidans*. This may be the result of inhibitors binding more tightly to the active site of metal-dependent KDO8P synthases, possibly by bonding to the metal ion itself. The significance of this is future inhibitors may be designed to be more effective against bacterial species with metal-dependent KDO8P synthase enzymes.

Chapter 4: Dual site inhibitors of KDO8P synthase

a slow start becomes
recipe for success
dual inhibition

4.1. Introduction

The insights into the inhibition of KDO8P synthase gained by the studies presented in Chapter 3 were used as the basis for development of new inhibitors with increased binding affinity. The approach utilised the concept of polyvalency; altering a previously designed inhibitor to include additional binding motifs, allowing the inhibitor to interact with multiple regions of the target enzyme. This creates a more stable enzyme-ligand complex by utilising the energy associated with these additional binding events (Figure 4.1).[115]

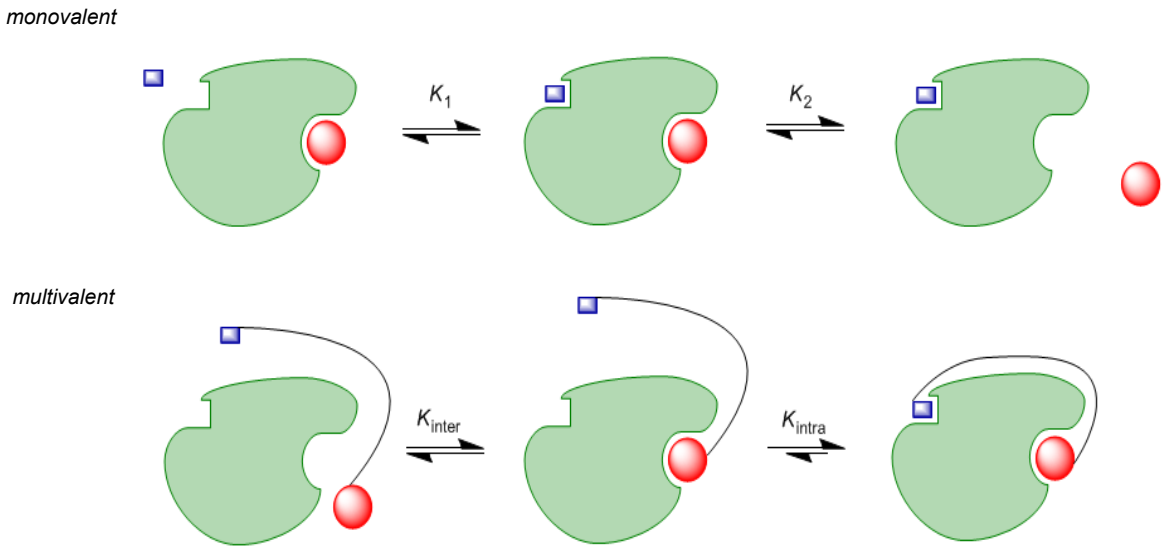

Figure 4.1: Comparison between mono and multivalent binding in an enzyme with two substrate binding sites.

Utilising a polyvalent ligand makes the second binding event intramolecular. The first binding event is influenced by the dissociation constant K_d (K_{inter}) and the concentration of both the enzyme and ligand, but the second binding event is only dependent on the effective concentration, a function of the probability of the two binding motifs being located at a distance that allows the second binding event to occur.[115] The intramolecular binding interaction is stronger than for the equivalent intermolecular interaction, in part because of a decrease in the entropic cost of binding a polyvalent ligand over two monovalent ligands. This theory has been utilised in the synthesis of bisubstrate inhibitors for type 1 17β-hydroxysteroid dehydrogenase (17β-HSD1), an enzyme which controls the formation and inactivation of the most potent endogenous estrogen, estradiol and NADPH/$NADP^+$ as the

proton donor/acceptor. Bisubstrate inhibitor EM-1745 was designed to mimic both the substrate estradiol and $NADP^+$ molecule, and was shown to have an apparent K_i of 3 nM for the oxidation of estradiol to estrone.

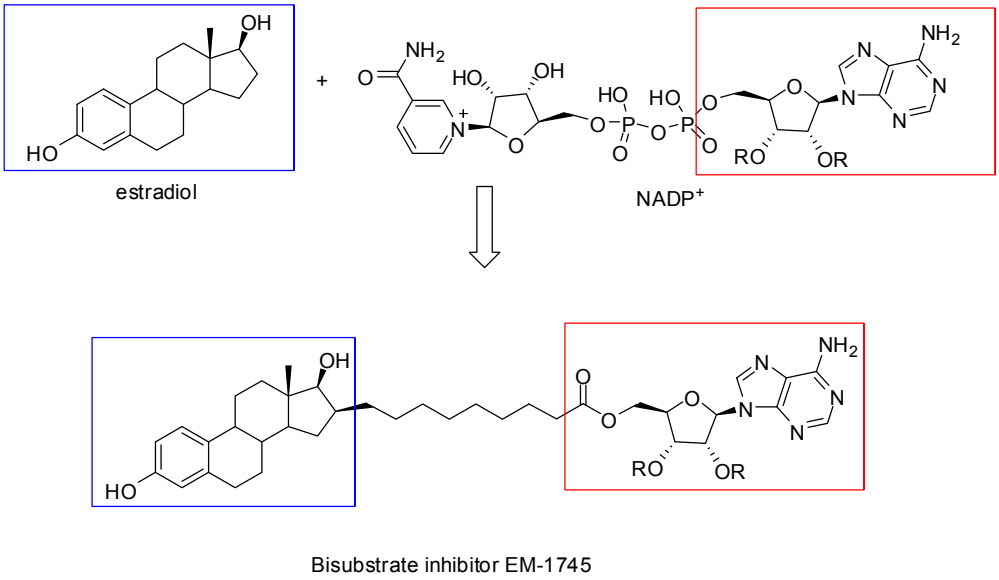

Figure 4.2: Design of 17β-HSD1 bisubstrate inhibitor EM-1745 from substrates estradiol (shown in blue box) and $NADP^+$ (shown in red box).

This concept has been previously applied in the design of a bisubstrate inhibitor for KDO8P synthase.[26] Aminophosphonate 1.4, retains a glyphosate head group to mimic the oxocarbenium ion species, with A5P hydroxyl stereochemistry and terminal phosphate to provide additional contact points with the KDO8P synthase sugar phosphate binding site (Figure 4.3). It is these additional contacts with the active site provide a large increase in binding and subsequent inhibition of the KDO8P synthase enzyme.

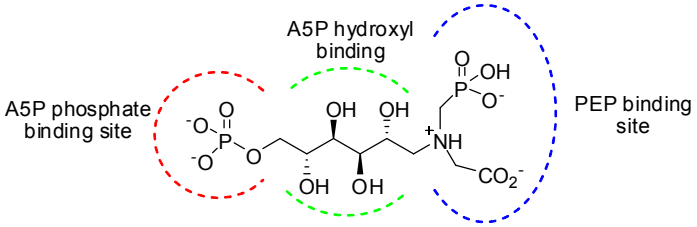

Figure 4.3: Aminophosphonate inhibitor 1.4 with binding motifs labelled; A5P phosphate binding site motif, in red; A5P hydroxyl stereochemistry binding motif, in green; PEP binding site motif, in blue.

Chapter 3 described the inhibition of KDO8P synthase by a number of PEP analogues that are assumed to inhibit the enzyme by binding to the PEP binding site. The research presented in Chapter 4 examines the effect of the various binding motifs in KDO8P synthase inhibition

by the design of five additional inhibitors based on a selection of these PEP analogues (Figure 4.4). Glyphosate was selected as an oxocarbenium mimic and the phospholactates 3.5 and 3.6 were selected as a mimics of the tetrahedral intermediate. Extended phospholactate 4.1 was designed to contain the A5P hydroxyl stereochemistry functionality and terminal phosphate in order to take advantage of all the A5P contacts made with the KDO8P synthase active site to determine the effect on inhibition of the KDO8P synthase enzyme. Extended phospholactate 4.33, and aminophosphonate 4.19 were designed as potential inhibitors with a simpler structure, retaining the A5P-like terminal phosphate, but lacking the hydroxyl stereochemistry of the main chain, in order to determine the effect these hydroxyls have on inhibition of KDO8P synthase.

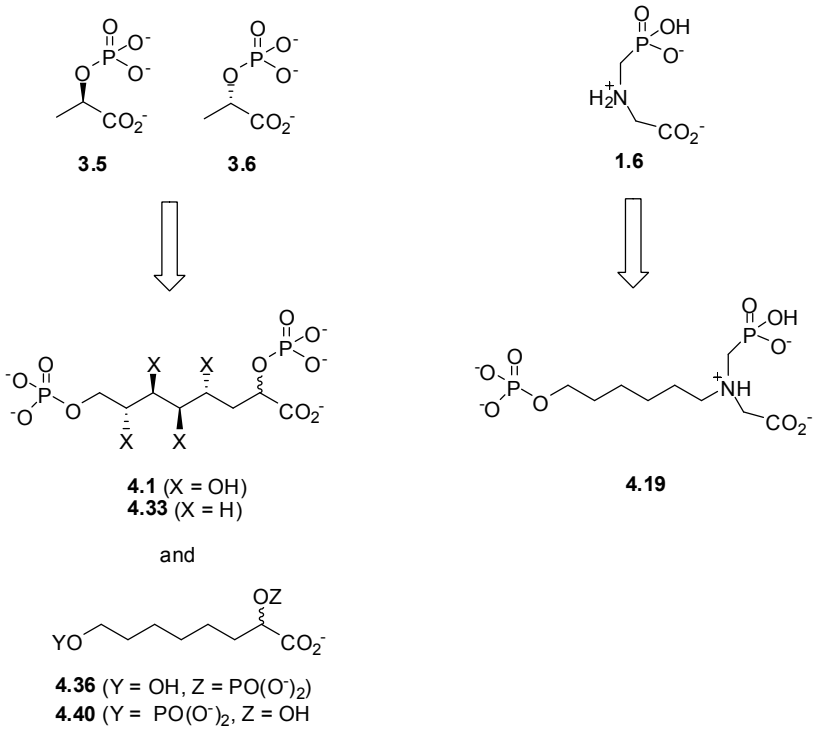

Figure 4.4: Multivalent inhibitors to be investigated in Chapter 4.

4.2. Extended inhibitors retaining the A5P hydroxyl stereochemistry functionality

The extended phospholactate 4.1 contains both the terminal phosphate and hydroxyl stereochemistry functionality of the A5P substrate, joined to the previous KDO8P synthase inhibitors investigated in Chapter 3, phospholactate 3.5 and 3.6. The proposed route to extended phospholactate 4.1 is outlined in Figure 4.5. The α-hydroxy ester 4.2 required for synthesis of phospholactate 4.1 can be synthesised in two steps with a two carbon elongation

of the six carbon aldehyde 4.4, *via* a Darzens condensation reaction between the aldehyde and isopropyl dichloroacetate, 4.5,[116] of which the product, 4.3, is reduced to give α-hydroxyester 4.2.[117]

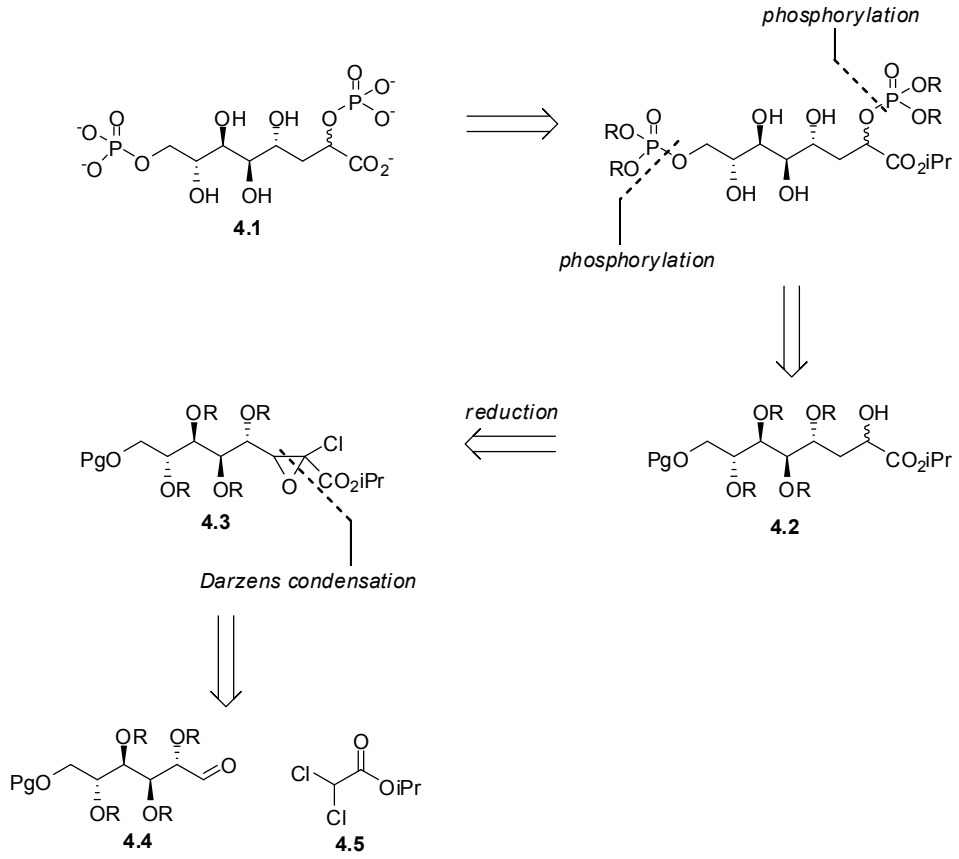

Figure 4.5: Retrosynthetic scheme showing synthesis of the extended phospholactate 4.1 from the aldehyde 4.4.

The chirality of aldehyde 4.4 was derived from the relatively cheap and abundant six carbon carbohydrate D-mannose (Figure 4.6).

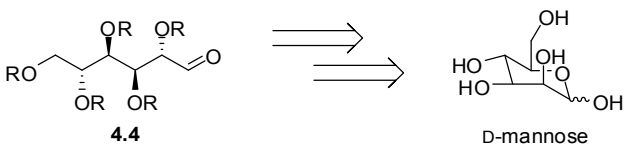

Figure 4.6: The source of chirality for aldehyde 4.4; the six carbon carbohydrate D-mannose.

The sugar 4.4 must be protected in such a way to allow selective access to the aldehyde moiety for the Darzens condensation reaction, followed by selective deprotection of the primary C6 hydroxyl group for diphosphorylation of the diol. Two methods were

investigated for this deprotection, differing in whether the hydroxyl groups or aldehyde moiety were protected first (Figure 4.7). In the first method, D-mannose was to be protected as either the diacetonide 4.6 or 4.7. The diacetonide 4.6 is an ideal target for the synthesis of aldehyde 4.4 as it has the free aldehyde functionality and 1,2:3,4 hydroxyl groups protected so that they do not interfere in subsequent reactions. The synthesis of diacetonide 4.6 is speculative however, resting on a single patent report.[118] Lactol 4.7 is widely reported as an initial starting material in many syntheses, including the first synthesis of aminophosphonate 1.4,[26] and extended PEP mimic 1.2.[84] However, this relies on lactol-aldehyde equilibration at the key carbon-carbon bond forming step, and Darzens condensations with lactols are not reported in the literature. The second method was based on initial protection of the aldehyde moiety as the dithiane 4.13, and the subsequent protection of the hydroxyl. The aldehyde moiety would then be unmasked in order to react in the Darzens condensation with isopropyl dichloroacetate, 4.5.

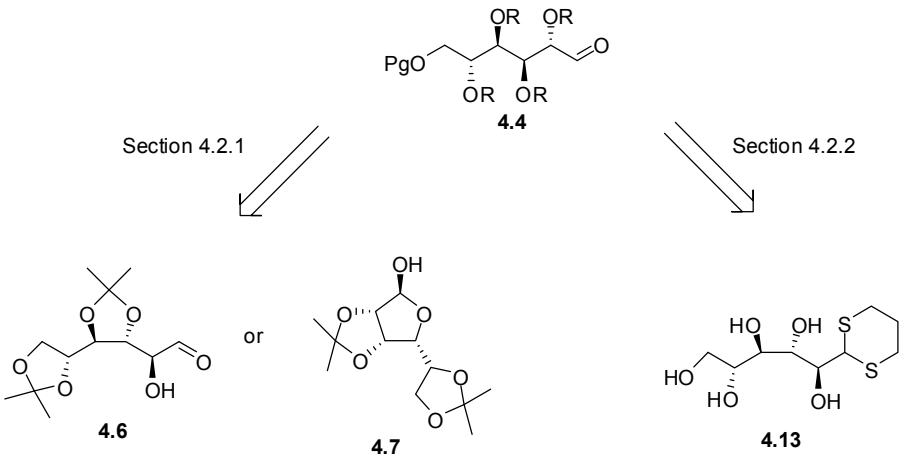

Figure 4.7: Retrosynthesis showing possible syntheses of the aldehyde 4.4 from the protected chiral carbohydrates 4.6, 4.7 and 4.13.

4.2.1. Initial protection as diacetonide

The initial protection scheme for D-mannose utilised acetonide protection of the secondary hydroxyl groups so that the aldehyde moiety would be free to react in the Darzens condensation reaction. A literature preparation utilising a boron-trifluoride catalysed protection of D-mannose offered a useful starting point, reportedly giving the 3,4:5,6 diacetonide, 4.6.[118] The diacetonide 4.6 was not formed in detectable amount as judged by ^{1}H NMR analysis of the reaction products, all of which failed to show any trace of an aldehyde moiety. However, the 2,3:5,6 diacetonide, 4.7, was found to be formed in 50 %

yield. The diacetonide 4.7 was identified by ^{13}C NMR spectra that showed the acetonide quaternary carbons at 110 and 114 ppm respectively, indicating they are found in five membered rings.[119] High resolution mass spectroscopy (HRMS) identified the lactol 4.7 as a compound with molecular mass 283.1146 (calculated mass for sodiated lactol 4.7: 283.1158).

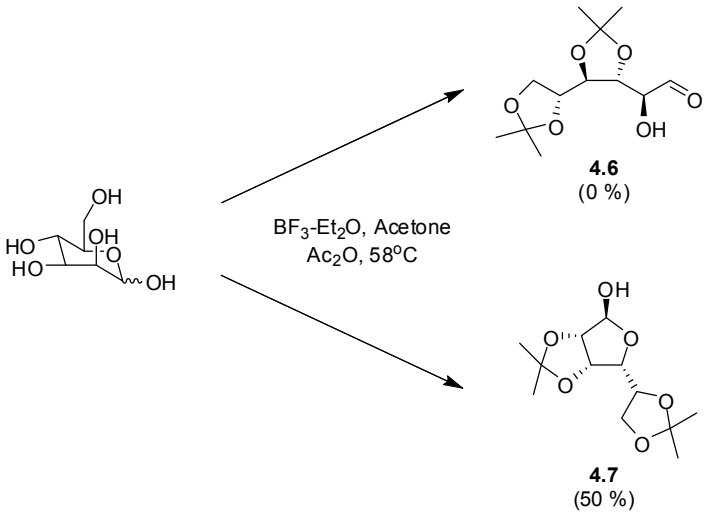

Figure 4.8: Attempted synthesis of diacetonide 4.7.

With the availability of diacetonide 4.7, and the unsuccessful preparation of diacetonide 4.6, it was decided to continue to develop synthetic routes based on the 2,3:5,6 diacetonide, 4.7. The diacetonide 4.7 can be prepared *via* a protic acid catalysed reaction in acetone, and so two different modified procedures were trialled using sulfuric acid[120] and *p*-toluenesulfonic acid monohydrate ($TsOH.H_2O$)[121] as the catalyst in order to improve the yield from the boron-trifluoride catalysed protection. Stirring D-mannose in acetone with catalytic amounts of $TsOH.H_2O$ gave diacetonide 4.7 in an improved yield of 63 %.

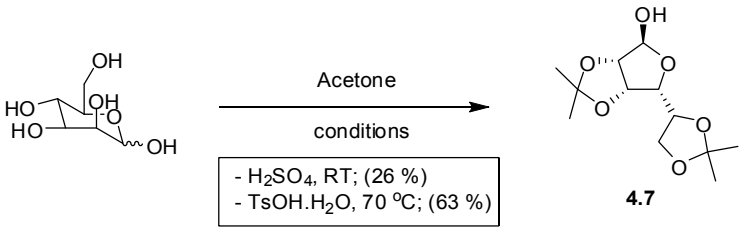

Figure 4.9: Acetonide protection of D-mannose.

As previously discussed, it was hoped that the lactol 4.7 could be directly reacted with isopropyl dichloroacetate, 4.5, to give the required α-chloroglycidic ester 4.8. No such

literature examples exist for Darzens reactions, although lactols have been used in reactions that also utilise an anionic nucleophile, such as Wittig[122] and Horner-Emmons[123,124] reactions.

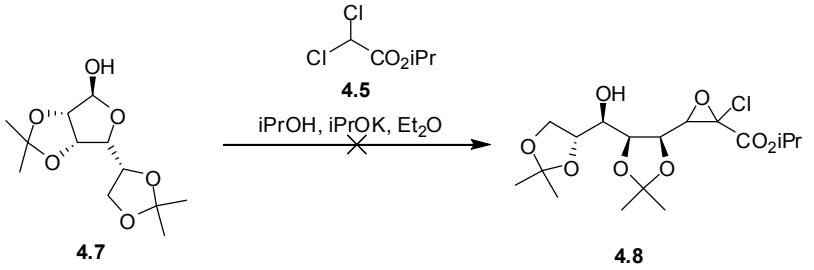

Figure 4.10: Unsuccessful synthesis of the α-chloroglycidic ester 4.8.

Unfortunately this reaction was unsuccessful. A number of new spots were seen by TLC analysis, but no product was able to be isolated by flash chromatography, and most of the starting material diacetonide 4.7 remained. A 2005 study by Coutrot *et al.*, formed an α-chloroglycidic ester from the C3-silane protected *gluco*-acetonide (Figure 4.11) and this result may reflect the need for the free aldehyde to be used in the Darzens condensation reaction, rather than the lactol.[125]

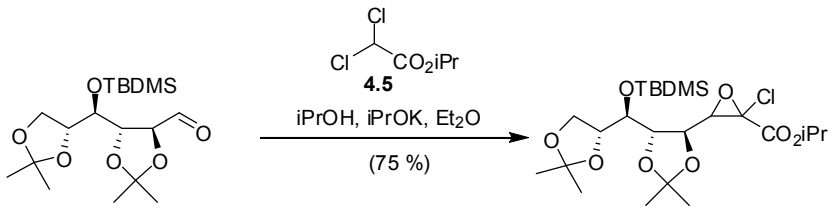

Figure 4.11: Darzens reaction of the *gluco*-diacetonide as reported by Coutrot *et al.*[125]

The result shown in Figure 4.10 suggests that the free aldehyde functionality of protected aldehyde 4.4 is required for the Darzens condensation reaction, rather than the lactol of diacetonide 4.6. In order to achieve this, lactol 4.6 was reduced with sodium borohydride[126] to give the diol 4.9, in 91 % yield. This was determined by ^{1}H NMR spectroscopic analysis showing the overall change in methylene and methine proton shifts from the lactol 4.7, and a broad two proton hydroxyl peak at 3.18 ppm.

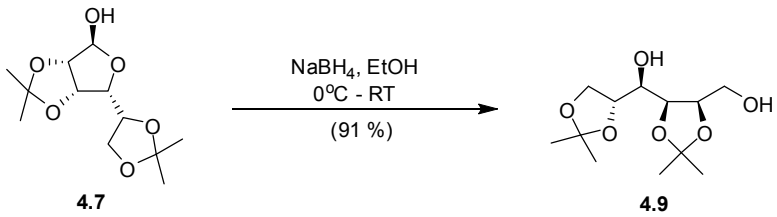

Figure 4.12: Reduction of the lactol 4.6.

The primary hydroxyl was protected by reaction with benzoyl chloride,[127] chosen as a protecting group for its selectivity of the primary hydroxyl due to its relative steric bulk, and its ability to be selectively deprotected in the presence of acetonide groups using basic conditions, such as 1 % sodium hydroxide in methanol at room temperature.[128] This ester linkage is also compatible with the use of the planned C6 hydroxyl protecting group, *tert*-butyldiphenylsilane (TBDPS).[129,130] Utilising pyridine as a base and, the primary hydroxyl group was protected as the benzoyl moiety in 52 % yield. The product was identified as protected diacetonide 4.10 by ^{1}H NMR showing the presence of the five aromatic protons at 7.44 – 8.12 ppm, and ^{13}C NMR showing the benzoyl quaternary carbon at 166.2 ppm. Additionally, HRMS detected diacetonide 4.10 as a compound with molecular mass 389.1567 (calculated mass for sodiated diacetonide 4.10: 389.1571). Nuclear Overhauser Effect Spectroscopy (NOESY), which shows correlation between atoms in space (distances of less than 5 Å), did not show correlation between any of the benzoyl group atoms and the main chain or acetonide groups. However, only one product was seen by TLC analysis and isolated, and previous literature examples would suggest the benzoylation reaction described is selective for the primary over the secondary hydroxyl group.[131]

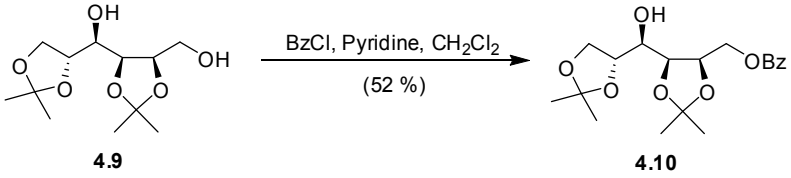

Figure 4.13: Primary benzoyl protection of the protected diacetonide 4.9.

As previously discussed, in order to synthesise the extended phospholactate 4.1, the sugar must be differently protected at both the C1 and C6 hydroxyl. This is to ensure that the C1 hydroxyl can be selectively deprotected and oxidised to generate the aldehyde for the Darzens condensation, followed by deprotection of the C6 hydroxyl moiety for phosphorylation. It was considered that the selective deprotection of the 1,2-acetonide and

protection of the C6 hydroxyl moiety may not be straight forward, and as such would best be performed early in the synthesis. As such the deprotection of the primary acetonide was attempted. Similar deprotections are well reported in the literature.[132] A range of conditions were tried for this reaction, utilising modified procedures from similar compounds (Figure 4.14).[132,133]

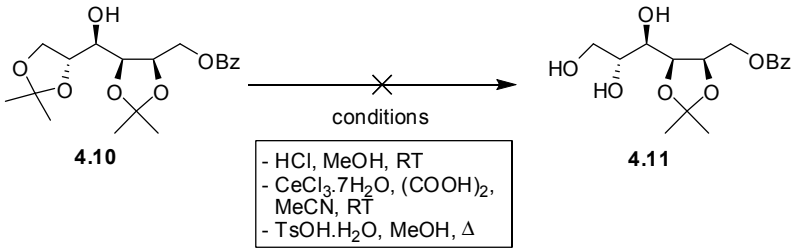

Figure 4.14: Failed primary acetonide deprotections.

The first two sets of conditions, utilising hydrochloric acid in methanol, and cerium trichloride and oxalic acid in acetonitrile both resulted in a new compound that could be detected by TLC. This new compound had a lower R_f than the diacetonide 4.10, indicating that it could potentially be the monoacetonide 4.11. The new product could not be isolated by flash chromatography however, and the diacetonide 4.10 could not be recovered, indicating destruction of this diacetonide starting material. After refluxing the starting material 4.10 in methanol with catalytic $TsOH.H_2O$, a product of the reaction, determined not to be the diacetonide 4.10 by ^1H NMR spectroscopy, was able to be partially isolated by flash chromatography, albeit in low yield (< 20 mg, from ~200 mg diacetonide 4.10). ^1H NMR analysis revealed that it was two monoacetonide compounds, in a 2:1 ratio. This was judged by the presence of two methyl peaks, at ~ 1.3 ppm, and four methine and two methylene peaks, at 3.5 – 5.0 ppm, for each compound. Due to the inability to see correlations for the acetonide methyl protons with the main chain or benzoyl protons using NOESY experiments, it could not be determined in what ratio the two monoacetonide compounds were. The two compounds could not be separated by flash chromatography as their R_f values were too similar under a wide variety of solvent mixtures, but high resolution mass spectroscopic analysis revealed the mixture to contain a compound with a molecular mass of 349.1255 (calculated mass: 349.1258 for both sodiated monoacetonide 4.11, and the 1:2 monoacetonide). The low yield and inability to separate the two monoacetonides by flash

chromatography led to this route being abandoned in favour of the dithiane route discussed below.

4.2.2. Initial protection as dithiane

The unsuccessful deprotection of diacetonide 4.10 to give the monoacetonide 4.11 was disappointing. It was now necessary to investigate a new synthetic scheme in order to synthesise the required aldehyde for the Darzens condensation. Previous reports have indicated that the dithiane 4.14 could be synthesised from D-mannose in three steps (Figure 4.15).[134] This compound is ideal as it has the aldehyde selectively protected as the dithiane moiety and the C6 primary hydroxyl moiety free, for selective protection.

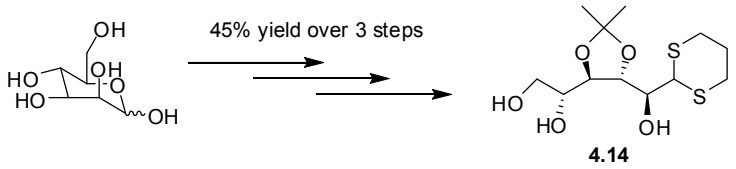

Figure 4.15: Synthesis of the partially protected D-mannose sugar.[134]

The initial step in the synthesis of protected sugar 4.14 was the protection of the aldehyde as the dithiane, with propandithiol stirring in a 2:1 mixture of chloroform and concentrated hydrochloric acid. Overnight, the reaction mixture had become too viscous to stir and D-mannose could no longer be detected by TLC analysis, and so the reaction mixture was neutralised with ammonia, and the solvents and water evaporated off to give a white solid. Recrystallisation from methanol as reported in the literature[134] was attempted, but the compound stayed in solution. However, treatment of the crude product containing dithiane 4.12 with acetone and hydrochloric acid gave 4.13 in 46 % yield after flash chromatography, over two steps, only slightly less than the literature yield of 56 %.[134] The diacetonide 4.13 was identified by ^{1}H NMR spectroscopic analysis and HRMS. The six dithiane proton resonances appeared 2.98, 2.81, 2.05 and 1.95 ppm, and acetonide methyl peaks at 1.39, 1.33 (two methyl groups) and 1.31 ppm. Additionally, the structure was confirmed by 2D proton Correlation Spectroscopy (COSY) showing the main chain C1-C5 methine and C6 methylene protons, correlated to each other with corresponding coupling constants. The dithiane was detected by HRMS as a compound with molecular mass of 373.1120 (calculated mass for sodiated dithiane 4.10: 373.1114).

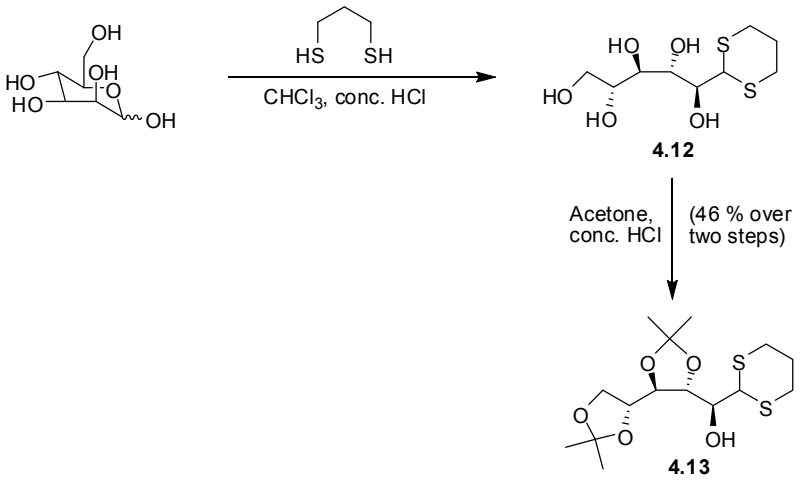

Figure 4.16: Two step protection of D-mannose to give the dithiane protected *manno*-diacetonide 4.13.

The selective deprotection of the primary acetonide was reported in the same paper, and involved stirring the protected sugar 4.13 in methanol with hydrochloric acid to give the partially deprotected sugar 4.14 in 77 % yield. This was comparable to the literature value of 82%.[134] The structure of monoacetonide 4.14 was characterised by the disappearance of two acetonide peaks in the ^{1}H NMR spectrum and HRMS, detecting the sodiated monoacetonide 4.14 as a compound with molecular mass of 311.0995 (calculated mass: 311.0981).

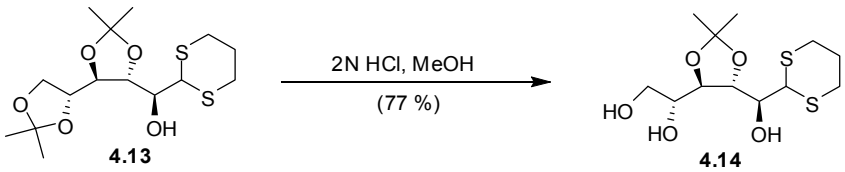

Figure 4.17: Primary acetonide deprotection of 4.13.

The bulky silyl protecting group TBDPS was chosen as the candidate to protect the primary C6 hydroxyl of the dithiane acetonide 4.14. This group has been used extensively for the selective protection of primary hydroxyl groups over secondary hydroxyl groups.[135-137] Flash chromatography revealed two compounds in 62 and 12 % yield respectively, that both contained aromatic resonances at 7 – 8 ppm, and a *tert*-butyl methyl resonance at ~ 1 ppm, along with the main chain methylene and methine peaks, and dithioacetal peaks as seen for previous compounds. Selective excitation NOESY experiments could not determine whether the primary or secondary hydroxyl group was silylated; however as mentioned, previous literature examples demonstrate that the TBDPS group is selective for primary hydroxyl

groups. Therefore, it was assumed that the silylated compound formed in greater yield was silyl ether 4.15.

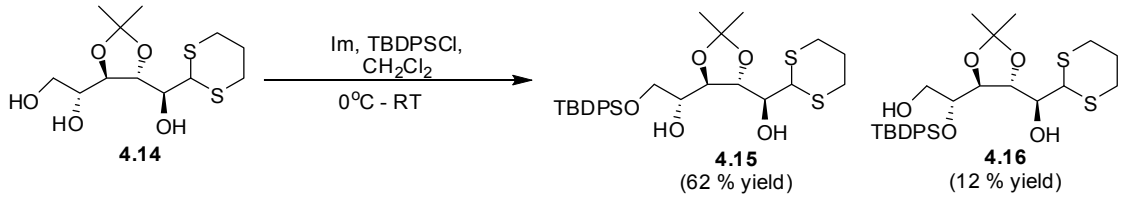

Figure 4.18: Selective primary silyl protection of acetonide 4.14.

The C2 and C5 hydroxyl groups remained unprotected in the monoacetonide 4.15. These two hydroxyl moieties are sterically hindered by the silyl, acetonide and dithioacetal groups and so a protecting group with little steric bulk was required. It was also considered that during the final deprotection step in the synthesis of the extended phospholactate 4.1, it would be advantageous if all the secondary hydroxyl groups could be deprotected in a single step. Acetyl protecting groups fulfilled both requirements, and are well reported in the literature as a general protecting group for both primary and secondary hydroxyl moieties.[132,138] Two sets of conditions were trialled, using either acetic anhydride or acetyl chloride as the acetyl group donors, with pyridine as a base, and dimethylaminopyridine (DMAP) as a nucleophilic catalyst.[139] The former yielded a mixture of products that were unable to be isolated and characterised. The reaction utilising acetyl chloride gave protected sugar 4.17, in 69 % yield. The product was determined by a ^{1}H NMR spectrum showing the acetyl group methyl resonances at 2.09 and 2.13 ppm, and a ^{13}C NMR spectrum showing the acetyl group quaternary carbon resonances at 170.0 and 170.2 ppm and HRMS detection of the sodiated protected sugar 4.17 as a compound with molecular mass of 655.2190 (calculated mass: 655.2199).

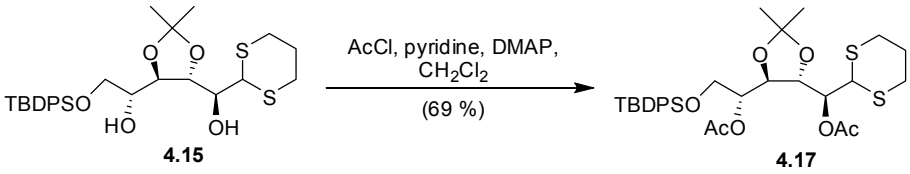

Figure 4.19: Diacetylation of 4.15 to give protected sugar 4.17.

With the hydroxyl groups selectively protected, the aldehyde functionality could be unmasked. A wide variety of conditions have been reported for the deprotection of

dithioacetals.[138] This is perhaps a reflection of the context-dependent nature of the deprotection step.

A wide variety of conditions were trialled for the removal of the dithioacetal group of 4.17.[138] However, the unmasking of the aldehyde functionality of protected sugar 4.18 proved very difficult. Mercuric compounds are often used for the deprotection of dithianes, exploiting the specificity of the interaction between sulfur and mercury. These methods have fallen out of favour in recent years however, as mercury is quite toxic, and more environmentally friendly methods are now preferred. A wide range of conditions were investigated. Methyl iodide, calcium carbonate in acetonitrile and water; *N*-bromosuccinimide (NBS), silver(I) nitrate, 2,6-lutidine in acetonitrile and water; bis(trifluoroacetyl) peroxide, iodobenzene in methanol and water; *N*-bromosuccinimide, collidine in methanol and acetonitrile; copper(II) oxide, copper(II) chloride in acetone and water were all trialled. All produced multiple compounds detectable by TLC. No identifiable compounds could be isolated by flash chromatography. ^{1}H NMR analysis of the fractions obtained from flash chromatography of all five reaction mixtures showed that they contained mixed compounds, in very low yields (~10 mg mixed compound from ~200 mg starting material 4.17), that contained *tert*-butyl (singlet at approximately 1 ppm) and aromatic proton resonances (multiplets at 7-8 ppm) from the TBDPS protecting group, and lacked the dithioacetal methylene group resonances found at approximately 3 ppm. All five reactions resulted in destruction of the starting material 4.17. Dithioacetal 4.17 was only able to be isolated from the unsuccessful deprotections with Dess-Martin periodinane (DMP) in acetonitrile and dichloromethane, and mercuric oxide, mercuric chloride in acetone and water, in 7 and 15 % yield respectively.

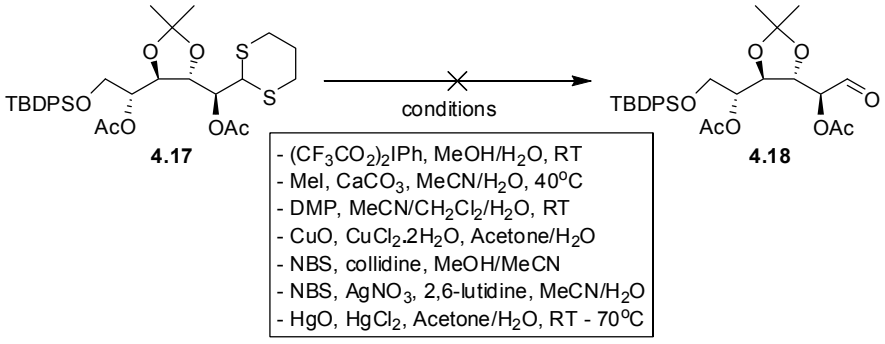

Figure 4.20: Attempted deprotection of dithioacetal group.

4.2.3. Summary

The inability to perform key deprotection steps resulted in the failure of two routes to the protected sugar 4.4. Diacetonide 4.6, the most promising candidate for the Darzens condensation, could not be synthesised from a literature procedure. The diacetonide 4.10, synthesised from the lactol 4.6, was unable to be selectively deprotected to give the monoacetonide 4.11. The dithiane group of protected sugar 4.17 could not be removed to generate aldehyde 4.18. It was also shown that the lactol 4.7 could not be reacted with isopropyl dichloroacetate, 4.5, in a Darzens condensation reaction to give the α-chloroglycidic ester 4.8. This route was abandoned in favour of the simplified inhibitors lacking the complicated A5P-like hydroxyl stereochemistry functionality.

4.3. Extended inhibitors lacking the A5P hydroxyl stereochemistry functionality

Recent studies have shown that for the related aldolase DAH7P synthase, extended dual-site inhibitors that lacked the E4P-like hydroxyl functionality associated stereochemistry still inhibited DAH7P synthase with K_i values in the low micromolar range.[86] These compounds provide a basis for simpler inhibitors. Two of the PEP analogues tested as inhibitors in Chapter 3 were selected as examples of an oxocarbenium mimic (glyphosate, 1.6) and tetrahedral intermediate (phospholactates 3.5 and 3.6) to be used as the structural basis for inhibitors of this type. The design of each includes a terminal phosphate, connected *via* pentamethylene spacer group in order to represent the terminal phosphate of the five-carbon sugar phosphate, A5P. These two inhibitors, aminophosphonate 4.19 and extended phospholactate 4.33 (Figure 4.21) were to be synthesised as part of the studies presented in Chapter 4. Additionally, two monophosphorylated analogues of extended phospholactate 4.33 were designed and synthesised that either lacked the primary (monophosphorylated compound 4.36) or secondary phosphate (monophosphorylated compound 4.40) (Figure 4.21). These four molecules, once synthesised, were to be tested as inhibitors of the metal independent KDO8P synthase from *N. meningitidis* and the metal dependent KDO8P synthase from *A. ferrooxidans*. The information gained from these studies was used to investigate the contribution of the various binding motifs to inhibition of KDO8P synthase.

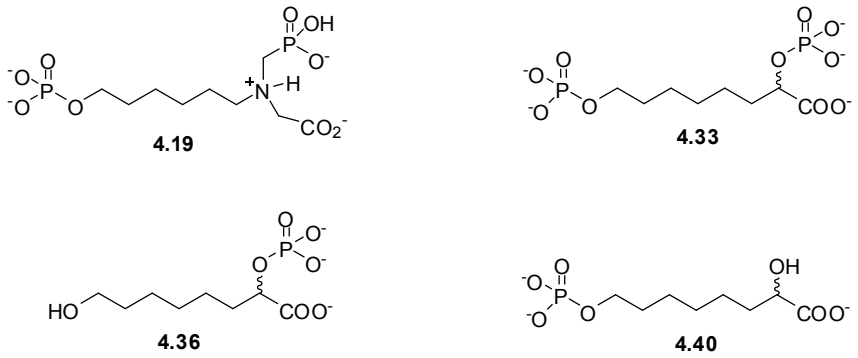

Figure 4.21: Inhibitors lacking the A5P-like stereochemistry associated functionality, to be synthesised and tested as inhibitors of KDO8P synthase.

4.3.1. Aminophosphonate 4.19

The proposed route for the synthesis of aminophosphonate inhibitor 4.19 is outlined in Figure 4.22. It was to be synthesised from 1,6-hexandiol, monoprotected and oxidised to the aldehyde 4.21 for reductive amination with glycine ethyl ester. This would be followed by phosphonomethylation of the secondary amine and phosphorylation of the deprotected hydroxyl group which, after final deprotection of the phosphate and carboxyl esters, gives the desired inhibitor, 4.19.

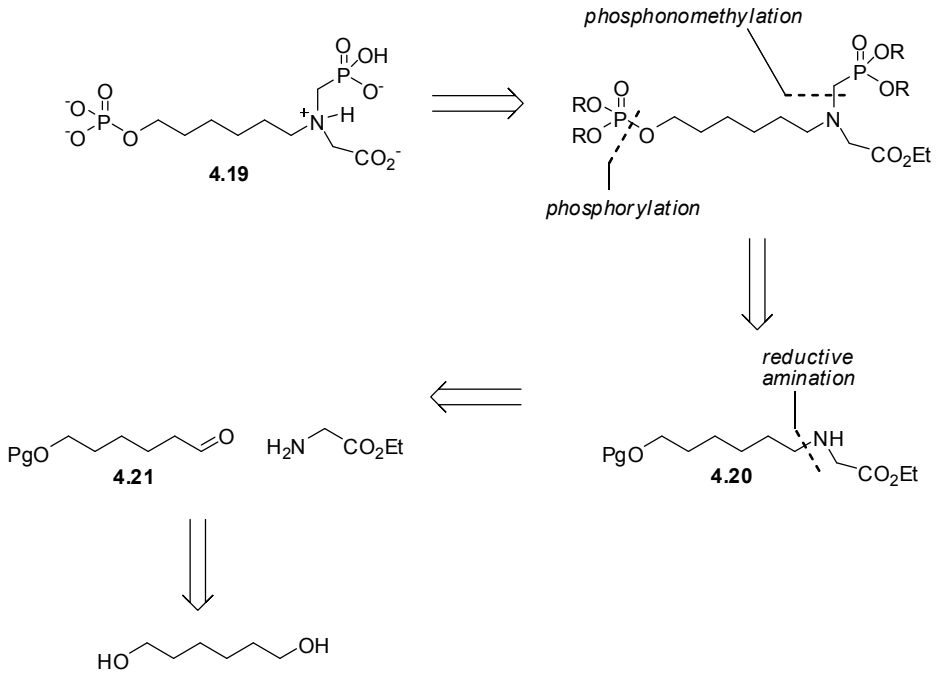

Figure 4.22: Retrosynthetic scheme showing synthesis of aminophosphonate 4.19.

This synthetic scheme began with monoprotection of 1,6-hexandiol with a benzyl bromide, to give the benzyl ether 4.22[140] in 50 % yield. The benzyl protecting group was chosen due to its robust nature under a wide variety of conditions, and relative ease in deprotection *via* hydrogenation utilising a palladium catalyst.[141,142] The dibenzyl ether, was also isolated in 32 % yield. The two compounds were distinguished by the presence of either three or six distinct methylene resonances as judged by ^{1}H NMR spectroscopic analysis, and comparison with the literature ^{1}H NMR spectroscopic data for benzyl ether 4.22.[140]

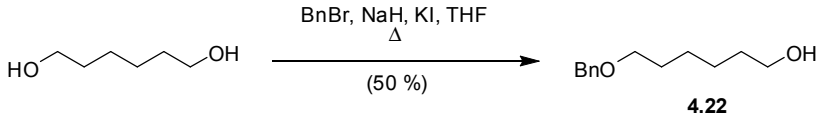

Figure 4.23: Initial monobenzylation of the1,6-hexandiol.

The oxidation method initially chosen utilised Dess-Martin periodinane (DMP),[143] which was prepared in the laboratory and stored at -20 °C until use. After flash chromatography, the aldehyde 4.23 was isolated in 57 % yield. The spectroscopic properties of aldehyde 4.23 were consistent with the reported data for this compound.[140] Additionally, the Swern oxidation[144] was investigated, and gave the aldehyde in 60 % yield following purification by flash chromatography. The Swern oxidation, due to the use of oxalyl chloride as a dehydrating agent, must be kept below -60 °C to avoid side reactions. In comparison, the Dess-Martin oxidation can be carried out at room temperature, and as the yield was not significantly different between the two methods, the Dess-Martin oxidation was preferred.

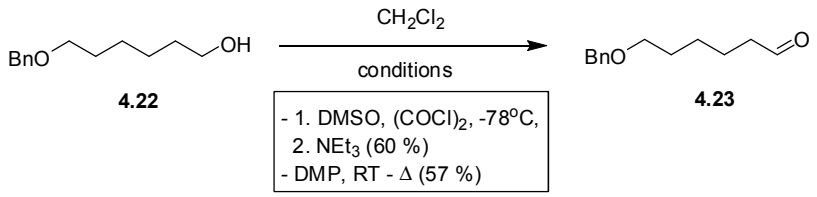

Figure 4.24: Oxidation of benzyl ether 4.22.

Secondary amines can be synthesised through reductive amination of an aldehyde by a primary amine (Figure 4.25). The aldehyde and primary amine first react to give a hydroxyamine species, which is dehydrated to give an iminium ion, which is subsequently reduced *in situ* to give the secondary amine.[145,146]

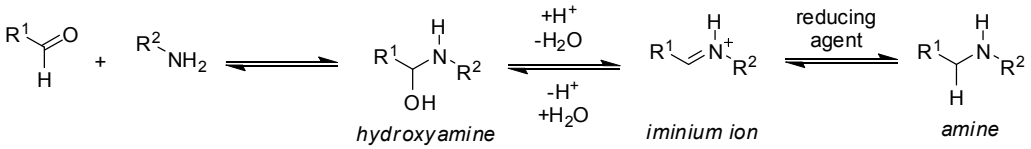

Figure 4.25: Mechanism through which aldehydes are reductively aminated with primary amines to give secondary amines.[146]

A range of reducing agents and reaction conditions were trialled for the reductive amination of aldehyde 4.23 by ethyl glycine (Figure 4.26). The initial conditions utilising sodium cyanoborohydride as the reducing agent, stirring in methanol, were similar to that used in the synthesis of known aminophosphonate inhibitor 1.4.[26] A ninhydrin stain, used in the detection of nitrogen containing compounds, showed two faint spots by TLC analysis with R_f values less than the aldehyde 4.23, and a strong baseline spot, potentially being the positively charged iminium ion or glycine ethyl ester starting material. However, upon aqueous workup and flash chromatography, no amine product was able to be isolated. The starting material, aldehyde 4.23, was recovered in 11 % yield, and the monobenzylated alcohol 4.22, formed *via* reduction of the aldehyde, in 5 % yield. Two other reducing agents (2-picoline borane[147] and triacetoxyborohydride[146]) were investigated because they had been shown to be successful in similar reactions. Triacetoxyborohydride especially has been shown to be successful with electron deficient amines such as *para* substituted nitro-, carbethoxy- and cyanoanilines,[146] as these, like glycine ethyl ester, have reduced nucleophilicity towards the aldehyde moiety. Both of these reducing agents failed to yield the desired secondary amine however. The starting material aldehyde 4.23 was not able to be recovered from reactions utilising either reducing agent, with the monobenzylated alcohol 4.23 isolated in 5 % or 6 % yield for 2-picoline borane and triacetoxyborohydride respectively.

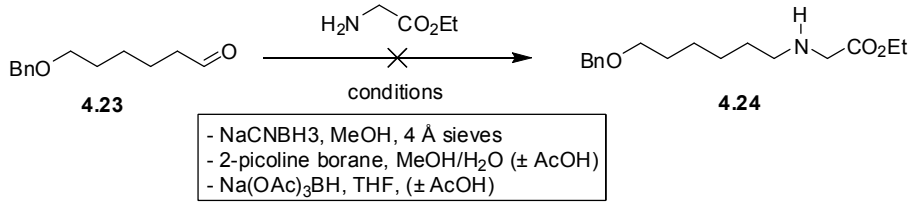

Figure 4.26: Unsuccessful reductive amination of aldehyde 4.23 and glycine ethyl ester.

The reductive amination of aldehyde 4.23 had been unsuccessful. Another possible synthetic route to the secondary amine 4.24 is the nucleophilic substitution reaction between glycine ethyl ester (nucleophile) and an alkylating agent (Figure 4.27).

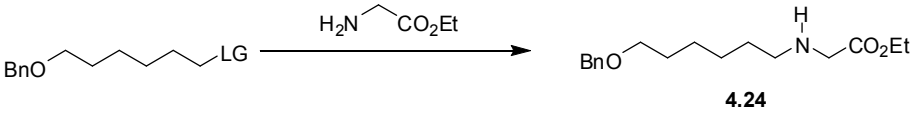

Figure 4.27: Nucleophilic substitution reaction between glycine ethyl ester and six carbon electrophile (leaving group represented by LG).

Two electrophiles were investigated as possible alternative routes to the secondary amine 4.24, the mesylate 4.25 and bromo ether 4.26.

Mesylates have proven to be good leaving groups in nucleophilic substitution reactions with primary amines such as glycine ethyl ester.[148] The preparation of mesyl ester 4.25 involved stirring the monoprotected diol with triethylamine, followed by addition of mesyl chloride (Figure 4.28).[149] After two hours the starting material 4.22 could no longer be detected by TLC analysis. The reaction was quenched and the product, mesylate 4.25, was isolated in a 54 % yield following purification by flash chromatography. The mesylate 4.25 was characterised by comparison with known spectroscopic data for the compound.[150] Though the mesylate 4.25 was synthesised successfully, it degraded quickly, as concluded by ^{1}H NMR spectroscopy, even when stored at -20 °C, so was not used as an alkylating reagent with ethyl glycine.

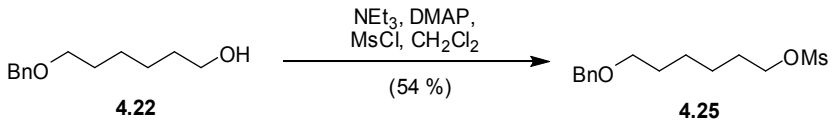

Figure 4.28: Mesylation of alcohol 4.22.

The second target electrophile for the nucleophilic substitution reaction with glycine ethyl ester was the bromo ether 4.26. Since the monobenzylated diol 4.22 was available from the previous attempted reductive aminations, it was decided that bromination of the alcohol would be an appropriate route. Various brominating agents were tried; hydrogen bromide[151] was unsuccessful; phosphorous tribromide[152] and triphenylphosphine dibromide[153] (synthesised from the reaction between bromine and triphenylphosphine)[154] gave the bromo ether 4.25 in yields of 19 % and 25 % respectively. The spectroscopic data for bromo ether 4.25 matched that found for the products of the reactions utilising phosphorous tribromide and triphenylphosphine dibromide.[155] (Figure 4.29). The starting material, monobenzylated alcohol 4.22, could not be recovered from any of the reaction mixtures by flash chromatography.

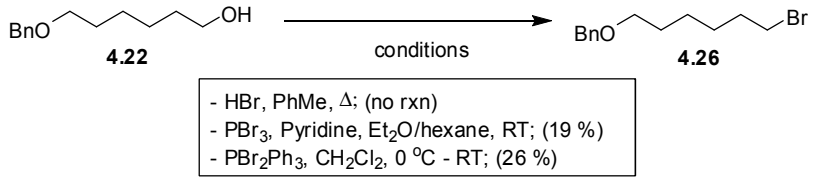

Figure 4.29: Bromination of alcohol 4.20.

These results can be interpreted in terms of the bromination mechanisms for the different reagents (Figure 4.30). Hydrogen bromide promoted bromination involves protonation of the hydroxyl group and elimination of a water molecule as a leaving group. In contrast, the two successful reactions involving use of phosphorous tribromide and triphenylphosphine dibromide occur *via* initial activation of the hydroxyl oxygen by the more electrophilic phosphorous atom to form a bromophosphate adduct and a bromine ion, followed by the substitution reaction. The bromophosphate leaving group is eliminated, much more readily than the less electrophilic water molecule.

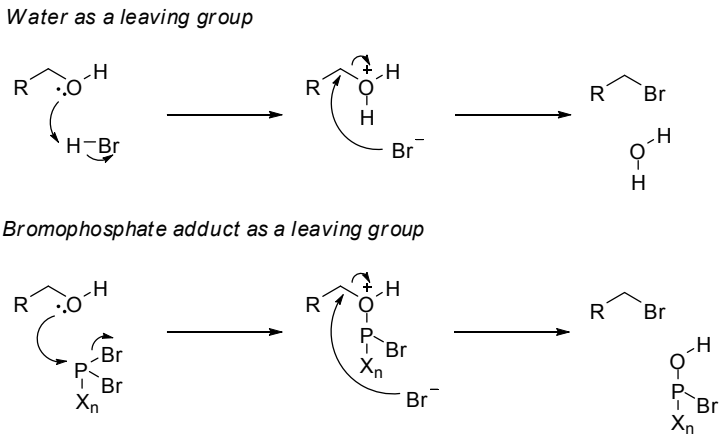

Figure 4.30: Bromination mechanisms for hydrogen bromide, phosphorous tribromide (X = Br, n = 1) and triphenylphosphine dibromide (X = Ph, n = 3).

The main issue with monoalkylations of amines is that the product, secondary amine 4.24, is potentially more nucleophilic than the primary amine, glycine ethyl ester.[156] This generally results in dialkylation, and in order to avoid this, a large excess of the amine must be used. New methods have been devised however where addition of cesium hydroxide is used to produce the monoalkylated product almost exclusively from the free amine and brominated electrophile, and these were investigated.[157]

The bromo ether 4.25 was reacted with glycine ethyl ester, in the presence of cesium hydroxide in order to prevent dialkylation (Figure 4.31). After twenty four hours stirring, the

starting material bromo ether was no longer detectable by TLC analysis. After aqueous workup and flash chromatography neither the product, secondary amine 4.24, or the starting material, bromo ether 4.25, could be isolated. A mixture of products in low yield (> 10 mg from ~ 200 mg bromo ether 4.25) were analysed by ^{1}H NMR spectroscopy and showed the presence of methylene and aromatic protons, detected as multiplets at 1.5 – 5.0 and 7 – 8 ppm respectively, but the structures could not be resolved by 1D or 2D NMR analysis.

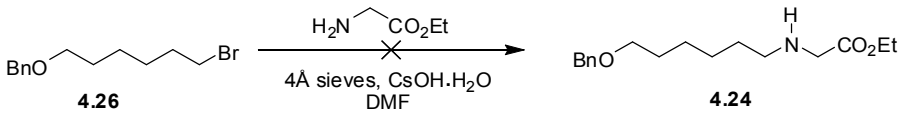

Figure 4.31: Attempted substitution reaction between glycine ethyl ester and alkyl bromide 4.25.

The secondary amine 4.24 was unable to be successfully synthesised *via* reductive amination of the aldehyde 4.23 or alkylation of ethyl glycine with bromo ether 4.26. At this stage the synthesis of the extended aminophosphonate 4.19 was abandoned in favour of the extended phospholactates. Their synthesis is described below.

4.3.2. Extended phospholactates 4.33, 4.36 and 4.40

The extended phospholactate 4.33 was proposed as an inhibitor that connected known KDO8P synthase inhibitors, (2*R*)- (3.5) and (2*S*)-phospholactate (3.6) with a terminal phosphate, *via* a pentamethylene chain, representative of the phosphate found in the second substrate, A5P. As well as this inhibitor, two other synthetic targets were designed that lacked either the primary (4.36) or secondary phosphate (4.40) of inhibitor 4.33. The inhibition of these two compounds relative to extended phospholactate 4.33 will determine the relative importance of the two phosphate functionalities to inhibition of KDO8P synthase.

The proposed route to all three extended phospholactate molecules is outlined in Figure 4.32. *Tert*-butyldimethylsilane (TBDMS) was chosen as the initial protecting group of 1,6-hexandiol. It is widely reported in the literature as a hydroxyl protecting group, stable to the conditions of the reactions that follow, and is readily cleaved under basic or acidic conditions.[132,138] Oxidation of the alcohol[143] and subsequent Darzens condensation reaction[116] with isopropyl dichloroacetate and reduction of the α-glycidic ester, as previously described, provides a route to the α-hydroxy ester[117] which is used as a precursor for all three phospholactate derived synthetic targets. The synthesis of phospholactates 4.33 and 4.36

were able to proceed by alternating TBDMS deprotection[158] and phosphorylation[159-161] to give the corresponding dibenzylphosphate ethers. Benzyl protecting groups were selected for the phosphate moieties as they can be readily cleaved under a hydrogen atmosphere by 10 % palladium over carbon.[162] The monophosphorylated compound 4.40 was synthesised *via* protection of the secondary hydroxyl of α-hydroxy ester with a benzyl moiety, selected as it can be deprotected in the same step as the phosphate benzyl ethers, and is stable to a wide range of conditions.[53] The compound could then be subjected to the TBDMS deprotection and phosphorylation as previously described. As a final deprotection step, the benzyl ethers on all three inhibitors would be hydrogenated and the isopropyl ester groups removed under basic conditions to give the target molecules, 4.33, 4.36 and 4.40.

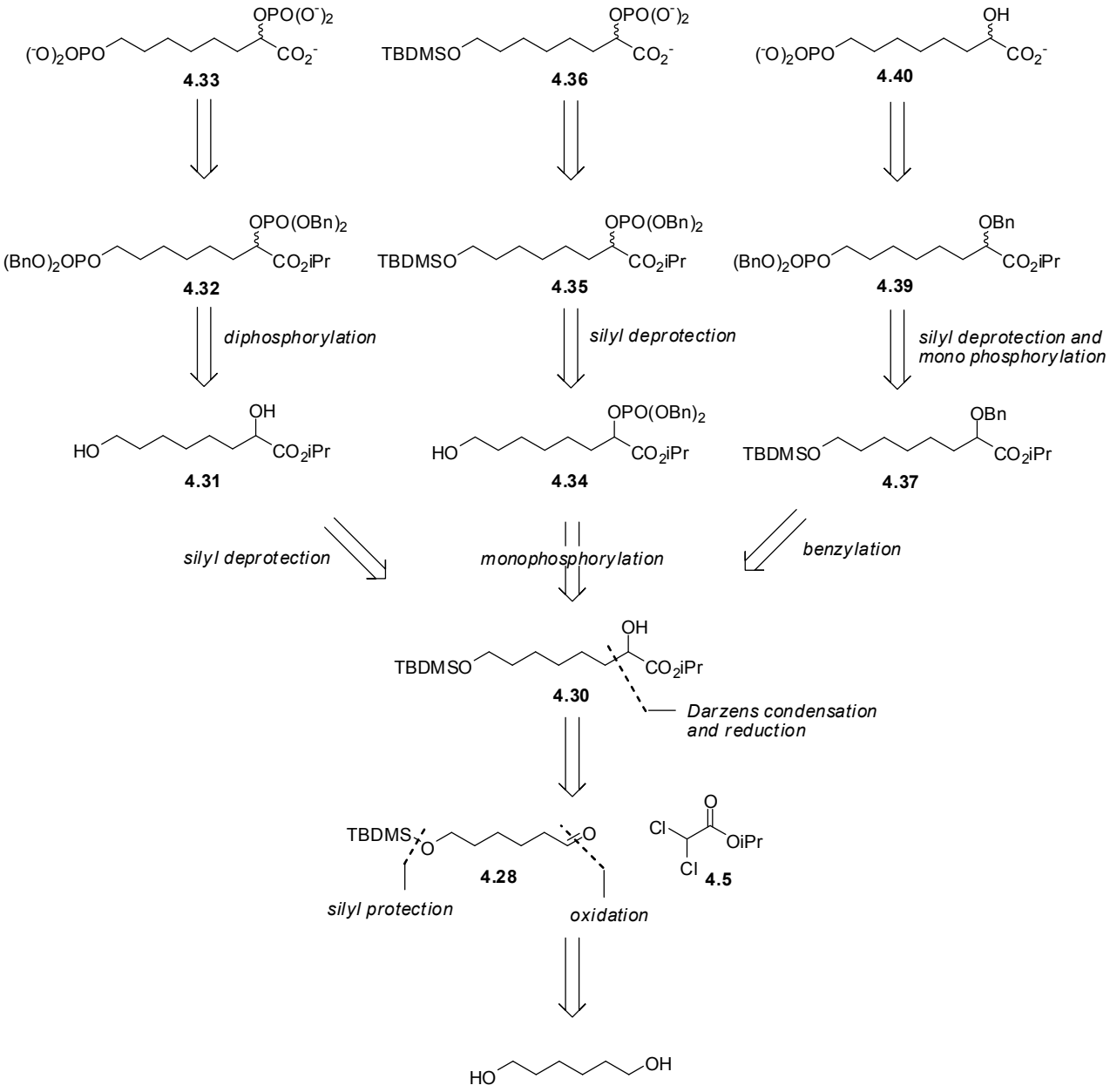

Figure 4.32: Retrosynthesis of extended phospholactates 4.33, 4.36 and 4.40.

When TBDMS chloride was reacted with three equivalents of 1,6-hexandiol in dichloromethane the monoprotected diol 4.27 was isolated in 61 % yield. This product was characterised by the ^{13}C NMR spectra showing nine distinct carbon resonances, and ^{1}H NMR spectra showing the methyl group resonances, from the silyl protecting group, at 0.01 and 0.85 ppm. Additionally, the silane 4.27 was detected by HRMS as the protonated compound, with molecular mass of 233.1938 (calculated mass: 233.1937). The yield increased to 72 % yield when tetrahydrofuran was used as the solvent. The disilylated compound was

synthesised in low yields for the reactions reported here, as determined by TLC analysis, and was not isolated.

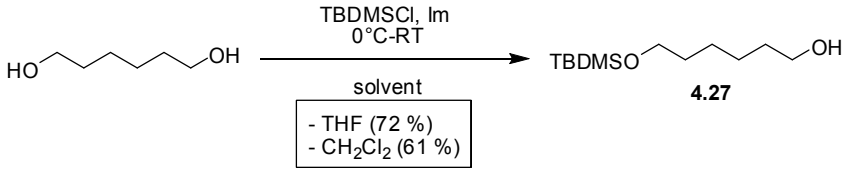

Figure 4.33: Silyl monoprotection of 1,6-hexandiol.

Dess-Martin periodinane was used as the oxidant[143] for the synthesis of the aldehyde 4.28 (Figure 4.34) as it had previously been successfully used for similar compounds. Analysis of the crude product after aqueous workup by ^{1}H NMR spectroscopy showed it to be solely aldehyde 4.28, as judged by the aldehyde proton resonance at 9.76 ppm (t, J = 1.7 Hz, 1H). The crude product was used directly in the Darzens condensation reaction with isopropyl dichloroacetate 4.5 (Figure 4.35).

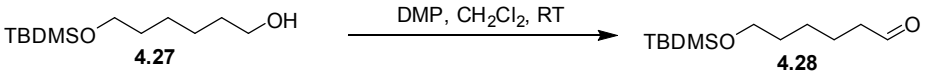

Figure 4.34: Oxidation of the silyl ether 4.27.

The synthesis of the α-chloroglycidic ester 4.29 was achieved *via* the reaction of the aldehyde 4.28 with isopropyl dichloroacetate 4.5. This ester precursor 4.5, was chosen due to its reported applications in the literature,[116,163] and availability in the laboratory from previous Darzens condensation reactions.[86] Treatment of the isopropyl dichloroacetate 4.5 with potassium isopropoxide in ether and addition of the aldehyde 4.28 gave the α-chloroglycidic ester 4.29[116] after aqueous workup, as judged by the disappearance of the aldehyde proton resonance at 9.76 ppm, and the appearance of two new peaks at 5.10 ppm (sept. J = 6.2 Hz, 1H) and 3.35 ppm (t, J = 6.0 Hz, 1H), indicative of the isopropyl group methine, and epoxide geminal proton resonances respectively. The crude α-chloroglycidic ester 4.29, shown to be pure by ^{1}H NMR spectroscopic analysis, was immediately dissolved in isopropyl alcohol and treated with sodium cyanoborohydride at 65 °C. Reduction of the α-chloroglycidic ester 4.29 to the α-hydroxy ester 4.30[117] was followed by TLC analysis. Once the α-chloroglycidic ester 4.29 could no longer be detected, the reaction was quenched. After aqueous workup and flash chromatography the α-hydroxy ester 4.30 was isolated in 26 % yield over three

steps from the silyl ether 4.27 (Figure 4.35). The product was characterised by 2D COSY NMR analysis showing the presence of a methine proton at 4.10 ppm (dd, J = 7.3, 4.2 Hz, 1H), vicinal to the methylene group at 1.37-1.46 ppm (m, 2H) formed from the aldehyde moiety, and coupled to both methylene protons separately. The α-chloroglycidic ester 4.29 does not contain this methine proton. Additionally, the ^{1}H NMR spectrum showed a broad singlet peak at 2.73 ppm, indicative of the free hydroxyl moiety. The α-hydroxy ester 4.30 was confirmed by HRMS detection of the protonated compound with a molecular mass of 333.2468 (calculated: 333.2461). The yield of α-hydroxy ester 4.30 was comparable to that for the seven-carbon analogue, also synthesised within our research group.[164] The α-hydroxy ester 4.30 was used as precursor for all three phospholactates, 4.30, 4.36 and 4.40.

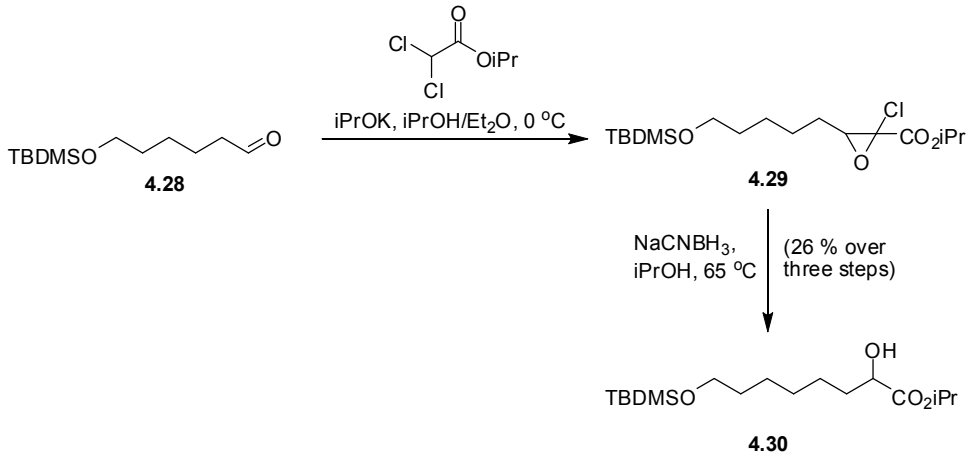

Figure 4.35: Synthesis of α-hydroxy ester 4.30 *via* a modified Darzens condensation.

The synthesis of diphosphorylated compound 4.33 involved initial desilyation of α-hydroxy ester 4.30 with the mild base, *tert*-butylammonium fluoride (TBAF) (Figure 4.36) to produce the requisite diol 4.31.[158] The reaction was followed by the depletion of silyl ether 4.30, detected by TLC analysis, and the organic solvents were removed under vacuum once the reaction was complete. After purification by flash chromatography the diol 4.31 was isolated in 83 % yield. ^{1}H NMR analysis confirmed the loss of the silyl ether, showing the disappearance of the silane *tert*-butyl and methyl resonances and a two proton resonance at 2.42 ppm for the two hydroxyl protons.

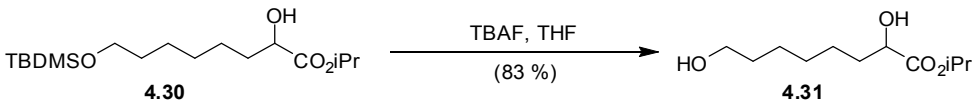

Figure 4.36: Silane deprotection of 4.30.

The diol 4.31 was then phosphorylated in a two-step procedure (Figure 4.37). *N*,*N*-Diisopropyl-dibenzyl phosphoramidite, and 1H-tetrazole as a proton donor, were used to synthesise the bisphosphite.[159] The reaction was followed to completion by consumption of the starting material 4.31, by TLC analysis. This bisphosphite was then oxidised to bisphosphate 4.32 with *meta*-chloroperbenzoic acid (Figure 4.38). [159-161] After aqueous workup and flash chromatography the bisphosphate 4.32 was isolated in 65 % yield. Structural characterisation by ^{1}H NMR analysis showed aromatic proton resonances from 7.29-7.37 ppm, and ^{31}P NMR analysis showed two phosphate resonances not previously seen at -0.38 (sext., J = 7.8 Hz) and -1.24 (sept., J = 7.3 Hz) for the secondary and primary phosphates respectively. These coupling constants corresponded to the α-hydroxy ester methine and C6 methylene proton couplings, J = 7.8 and 7.3 Hz respectively. This result was confirmed by HRMS detection of a compound with molecular mass 593.3063 (calculated mass for protonated bisphosphate 4.32: 593.3061).

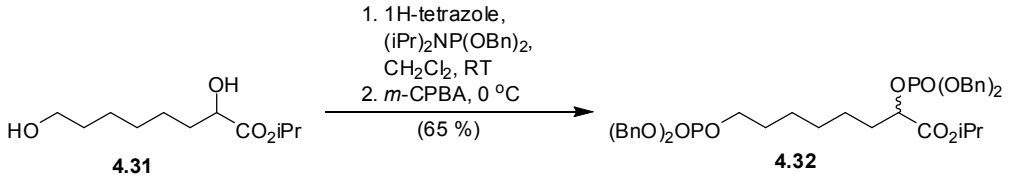

Figure 4.37: Diphosphorylation of diol 4.31.

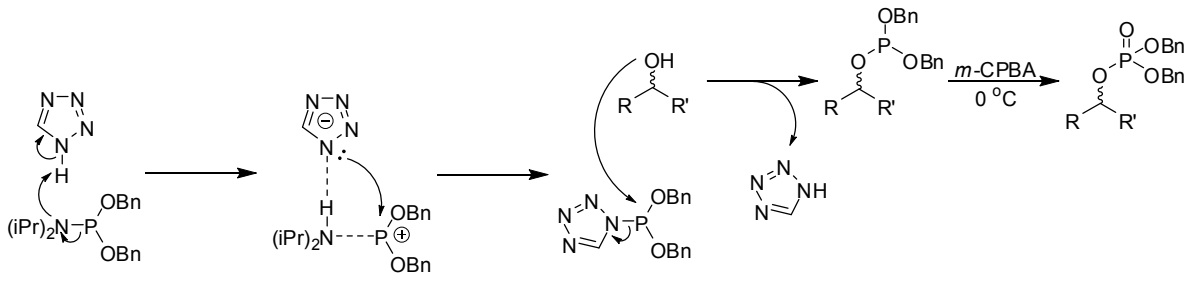

Figure 4.38: Phosphorylation mechanism using *N*,*N*-diisopropyl-dibenzyl phosphoramidite.[159]

Hydrogenation, with 10 % palladium over carbon, cleaved the benzyl groups from the phosphate moieties. After the dibenzyl phosphate 4.32 was no longer detectable by TLC analysis the reaction mixture was passed through celite and the organic solvents evaporated. Analysis by ^{1}H NMR spectroscopy confirmed the loss of both benzyl groups, as demonstrated by lack of aromatic proton resonances at 7-8 ppm. This was followed by treatment of the residue with aqueous potassium hydroxide which removed the carboxy

isopropyl ester protecting group (Figure 4.39). This ester hydrolysis was followed by ^{1}H NMR spectral analysis, following the shift of the isopropyl protecting group methyl proton resonances, seen as a doublet at 1.31 ppm following hydrogenolysis of the benzyl esters, and a doublet at 1.50 ppm following ester hydrolysis. This latter value matched the literature value for the isopropyl alcohol methyl proton resonances, in deuterated methanol.[165]

The resulting mixture of products was purified by anion exchange chromatography on SourceQ resin, eluted with aqueous ammonium bicarbonate with the bisphosphate 4.33 eluting at 130-170 mM ammonium bicarbonate. Detection of the desired compound 4.33 was achieved by utilising the Lanzetta assay, a colourimetric assay for inorganic phosphate.[166] The assay conditions, being highly acidic, cleave organic phosphates present to inorganic phosphate, allowing detection of the product. After lyophilisation of the fractions containing bisphosphate 4.33, the desired compound was isolated in 2 % yield from the bisphosphate 4.32 (Figure 4.39). ^{31}P NMR spectroscopic analysis revealed two distinct resonances at 1.1 ppm (d, J = 8.7 Hz) and 2.5 (t, J = 6.7 Hz). The coupling constants matched those found for the methine and C6 methylene peak respectively, determined by ^{1}H NMR characterization. Additionally the composition of the compound was confirmed by HRMS detection of the mono deprotonated bisphosphate 4.33 with a molecular mass of 335.0310 (calculated mass: 335.0297). The yield for this final deprotection is very low, but the reaction provided sufficient material for the inhibitory studies presented in this thesis. Additional fractions were isolated that contained the desired compound 4.33, but also contained impurities and so were discarded.

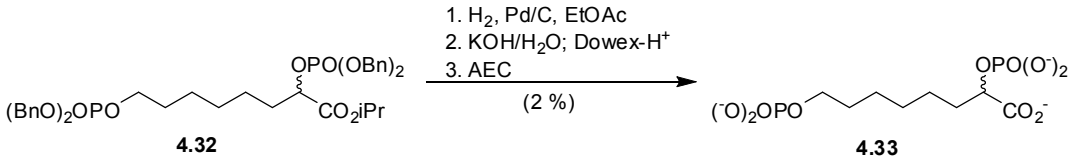

Figure 4.39: Deprotecton of precursor 4.32 to target 4.33.

To synthesise the secondary monophosphorylated extended phospholactate 4.36, the α-hydroxy ester 4.30 was phosphorylated *via* the procedure as described for the synthesis of 4.33.[160] This monophosphorylated ester was characterised by a ^{1}H NMR spectroscopic analysis showing the aromatic proton resonances at 7-8 ppm, and ^{31}P NMR showing a sextet phosphorous resonance at -1.39 ppm, coupled to the main chain methine and benzyl methylene protons, with a coupling constant of 7.6 Hz. This was followed by deprotection of

the silyl ether with TBAF[158] (Figure 4.40) as previously described, to give the alcohol 4.35, as judged by ^{1}H NMR spectroscopic analysis, the disappearance of the two singlets representative of the methyl protons of the TBDMS protecting group, and the appearance of the broad singlet at 2.13 ppm, representative of the deprotected C6 hydroxyl group. The composition of alcohol 4.35 was confirmed by HRMS detection of a compound with molecular mass of 479.2191, corresponding to the protonated molecule, of calculated mass 479.2199.

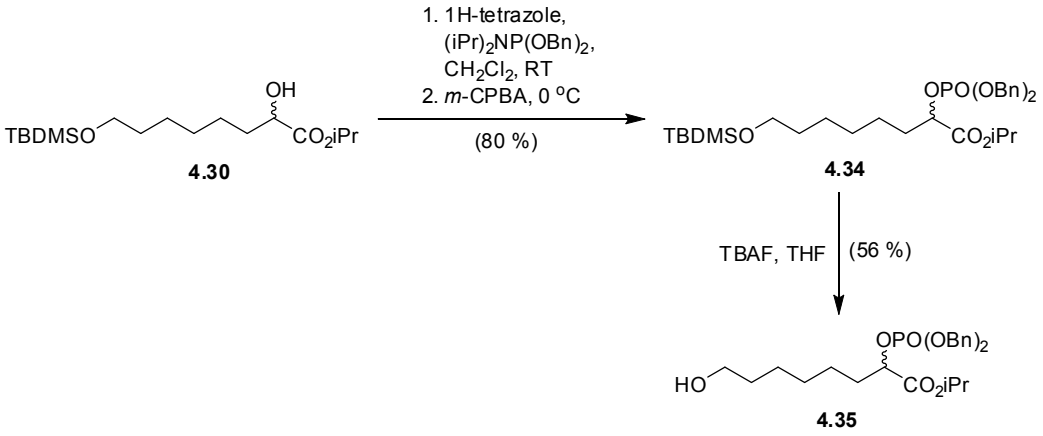

Figure 4.40: Phosphorylation and silyl deprotection of α-hydroxy ester 4.30.

The monophosphorylated ester 4.35 was then deprotected, as described for the synthesis of inhibitor 4.33 with hydrogenolysis of the benzyl esters,[162,167] as judged by ^{1}H NMR spectra showing a lack of aromatic proton peaks at 7-8 ppm. This was followed by isopropyl ester hydrolysis with aqueous potassium hydroxide. The hydrolysis of the isopropyl ester was followed by ^{1}H NMR spectral analysis as previously described, by the shift of the isopropyl protecting group methyl proton resonances from a doublet at 1.31 ppm to a doublet at 1.50 ppm, matching the literature value of the isopropyl alcohol methyl proton resonances in deuterated methanol.[165]

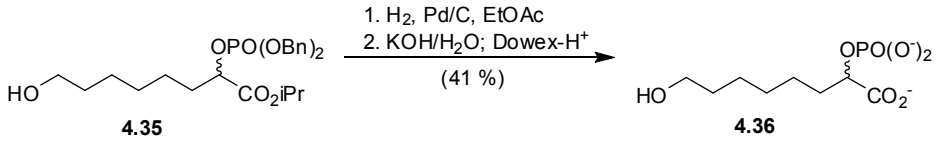

Figure 4.41: Final deprotection of phosphorylated ester 4.35.

Purification of monophosphate 4.36 by anion exchange chromatography with an ammonium bicarbonate gradient as per inhibitor 4.33 resulted in streaking of the compound across

multiple fractions, as detected by Lanzetta assay and ^{1}H NMR spectroscopy. It was not possible to isolate pure samples of monophosphate 4.36 during three separate anionic exchange chromatography purifications. Instead of purification by anion exchange chromatography the non-polar compounds were extracted with chloroform and the organic phase discarded, before the aqueous phase was passed down a DOWEX-H^{+} column. The aqueous DOWEX-H^{+} fractions were freeze dried and analysed by ^{1}H NMR spectroscopy and shown to be pure. Quantification by Lanzetta assay[166] showed that the monophosphorylated compound 4.36 was synthesised from benzylphosphate ester 4.35 in 41 % yield. The deprotected monophosphate 4.36 was characterised by ^{31}P NMR spectroscopic analysis showing a doublet resonance at 2.5 with a coupling constant, J = 5.5 Hz, corresponding to that for the methine resonance found in the ^{1}H NMR spectra. This structure was confirmed by HRMS detection of the mono deprotonated compound with a molecular mass of 255.0645 (calculated mass: 255.0634).

For the synthesis of the C6 primary monophosphorylated compound 4.40, the secondary hydroxyl of α-hydroxy ester 4.30 was protected as a benzyl ether so that the C6 hydroxyl moiety could be selectively phosphorylated. Initially the benzylation was performed on a small 100 mg scale utilising a combination of benzyl bromide, sodium hydride and a catalytic amount of potassium iodide, at reflux.[168,169] No product was seen however and the starting material remained after two days at reflux, detectable by TLC analysis. After aqueous workup less than 50 mg of crude material was isolated and this mixture was not subjected to any further purification. When a modified procedure using benzyl bromide, catalytic potassium iodide and freshly prepared silver(I) oxide in dichloromethane,[170] benzylated compound 4.37 was isolated in 66 % yield. The product was characterised by ^{1}H NMR spectroscopic analysis showing the disappearance of the broad singlet from the hydroxyl group proton and the appearance of peaks indicative of benzyl group methylene proton resonances at 4.70 and 4.40 ppm, and aromatic proton resonances at 7.25-7.40 ppm.

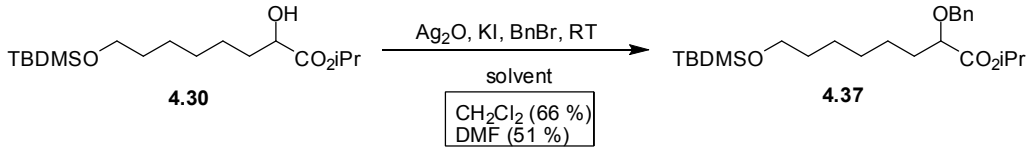

Figure 4.42: Benzylation of α-hydroxy ester 4.30.

The silyl ether 4.37 was treated with TBAF in order to free the primary hydroxyl moiety for phosphorylation, which was performed under similar conditions to that previously discussed in the synthesis of both bisphosphate 4.33 and monophosphate 4.36.[160] The alcohol 4.38 was characterised by ^{1}H NMR spectroscopic analysis showing the disappearance of the methyl and *tert*-butyl proton resonances of the silyl protecting group, and a broad singlet at 2.01 ppm, indicative of the free hydroxyl moiety. The presence of the monophosphate 4.39 was confirmed by HRMS detection of the sodiated compound 4.39 with a molecular mass of 591.2484 (calculated mass: 591.2482). ^{1}H NMR spectroscopic analysis showed the aromatic proton integral increased to fifteen, and ^{31}P NMR revealed a previously unseen septet peak at -0.8 ppm, coupled to the C6 methylene protons with a coupling constant of 7.0 Hz. A second compound was detected by ^{31}P NMR at 7.8 ppm (dp, J = 707.4, 9.5 Hz) and identified as the phosphonate molecule, a breakdown product of *N*,*N*-diisopropyl-dibenzyl phosphoramidite. It could not be removed from monophosphate 4.39 by flash chromatography and the mixture was used directly in the next step.

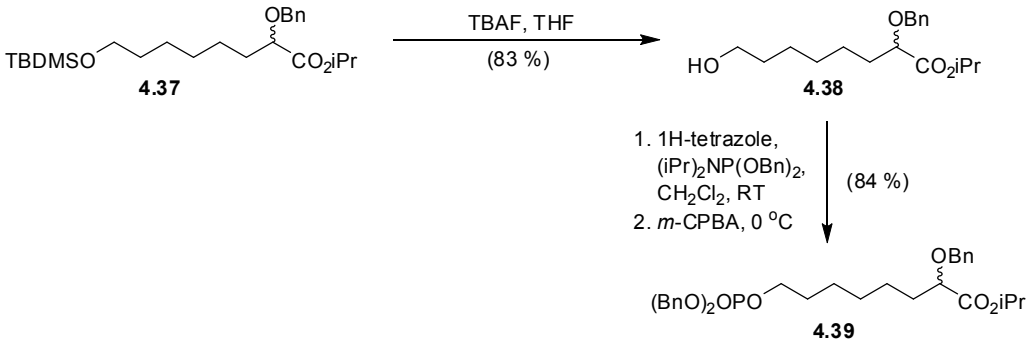

Figure 4.43: Silyl deprotection and monophosphorylation of the ester 4.40.

The phosphorylated ester 4.39 was then deprotected by hydrogenolysis of the benzyl groups protecting the secondary hydroxyl group, and the phosphate hydroxyl groups, [162,167] The reaction was followed as previously described by ^{1}H NMR spectroscopic analysis showing the removal of the benzyl ethers by the lack of aromatic proton resonances at 7-8 ppm. This was followed by ester hydrolysis in aqueous potassium hydroxide, the reaction followed by ^{1}H NMR spectroscopic analysis of the solution showing the shift of the isopropyl methyl proton resonance from a doublet at 1.26 ppm to a doublet at 1.17 ppm, matching the literature value for the isopropyl alcohol methine proton in deuterium.[165] The crude extracts were purified by anion exchange chromatography as described for the purification of inhibitor 4.33 where the compound of interest, 4.40, eluted at 80-95 mM ammonium bicarbonate. After

lyophilisation of these fractions, monophosphate 4.40 was obtained as a white powder in 12 % yield (Figure 4.44). The deprotected monophosphate 4.40 was characterised by HRMS detection of the mono deprotonated compound with a molecular mass of 255.0642 (calculated: 255.0634). Additionally ^{31}P NMR spectroscopy revealed a triplet peak with coupling constant J = 5.0 Hz, corresponding to that found for the H6 methylene proton resonance by ^{1}H NMR spectroscopy.

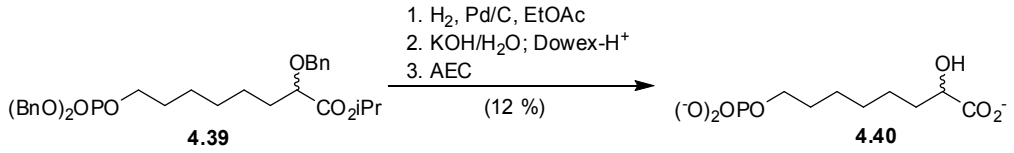

Figure 4.44: Deprotection of monophosphorylated ester 4.42.

4.3.3. Inhibition of KDO8P synthase by extended phospholactates 4.33, 4.36 and 4.40

The extended phospholactate 4.33, and its monophosphorylated analogues 4.36 and 4.40 were tested as inhibitors of the metal independent KDO8P synthase from *N. meningitidis* and the metal dependent KDO8P synthase from *A. ferrooxidans*. This was done *via* kinetic assay, following the loss of PEP at 232 nm. The initial rate data was fitted to the Michaelis-Menten equation, modified for competitive inhibition, and this data displayed for inspection as a Lineweaver-Burke plot. All three molecules were shown to be competitive inhibitors with respect to PEP. The inhibition results are shown in the table below.

Inhibitor	K_i *N. meningitidis*	K_i *A. ferrooxidans*
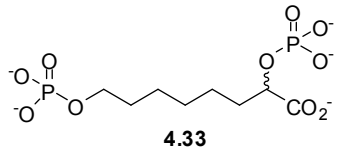 4.33	7.9 ± 1.6 μM (Figure 4.45)	20 ± 3 μM (Figure 4.46)
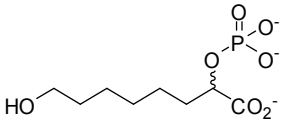 4.36	1000 ± 180 μM (Figure 4.47)	540 ± 50 μM (Figure 4.48)
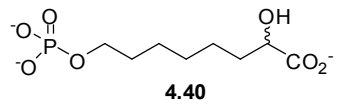 4.40	270 ± 40 μM (Figure 4.49)	190 ± 40 μM (Figure 4.50)

Table 4.1: Inhibition constants for extended phospholactates 4.33, 4.36 and 4.40 against KDO8P synthase from *N. meningitidis* and *A. ferrooxidans*.

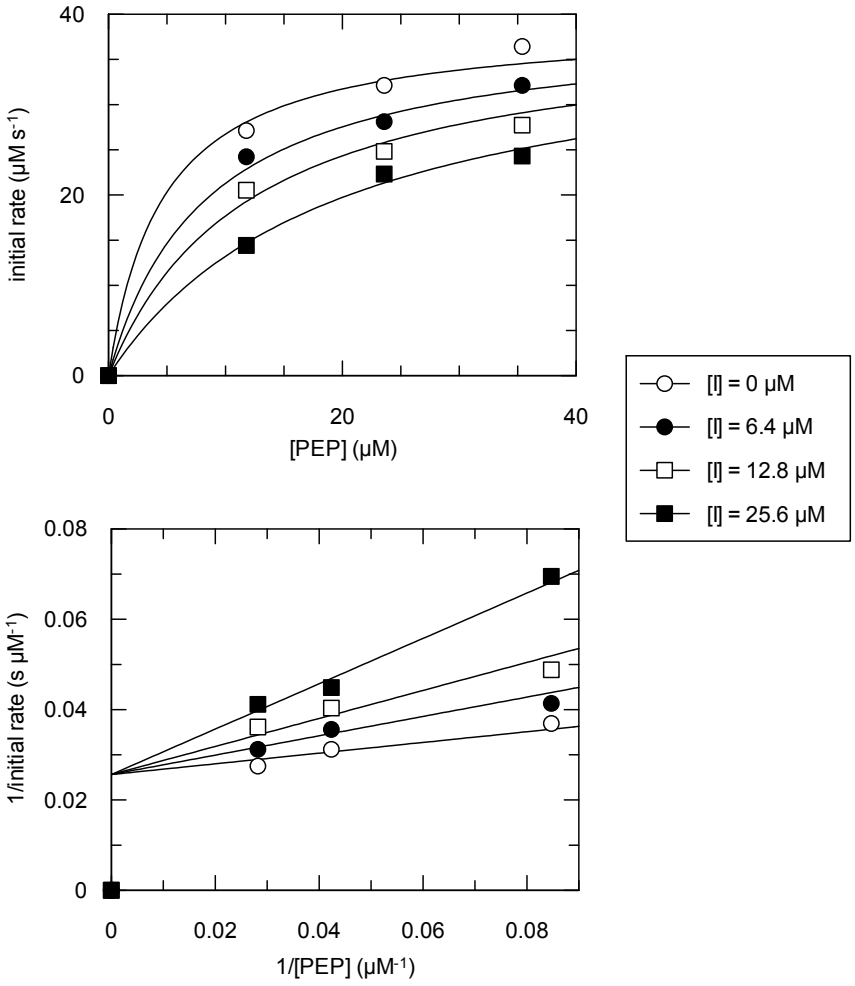

Figure 4.45: Inhibition of KDO8P synthase from *N. meningitidis* by diphosphorylated extended phospholactate 4.33 as Michaelis (top) and Lineweaver-Burke (bottom) plots. Solutions of PEP (12-35 μM), A5P (50 μM), and extended phospholactate 4.33 (0-25.6 μM) in 1 mL BTP buffer (50 mM, pH 7.2) were initiated by addition of *N. meningitidis* KDO8P synthase (2 μg) and the loss of PEP followed spectrophotometrically at 232 nm. Initial rates were obtained by linear least squares regression and converted to progress rates (μM s^{-1}).

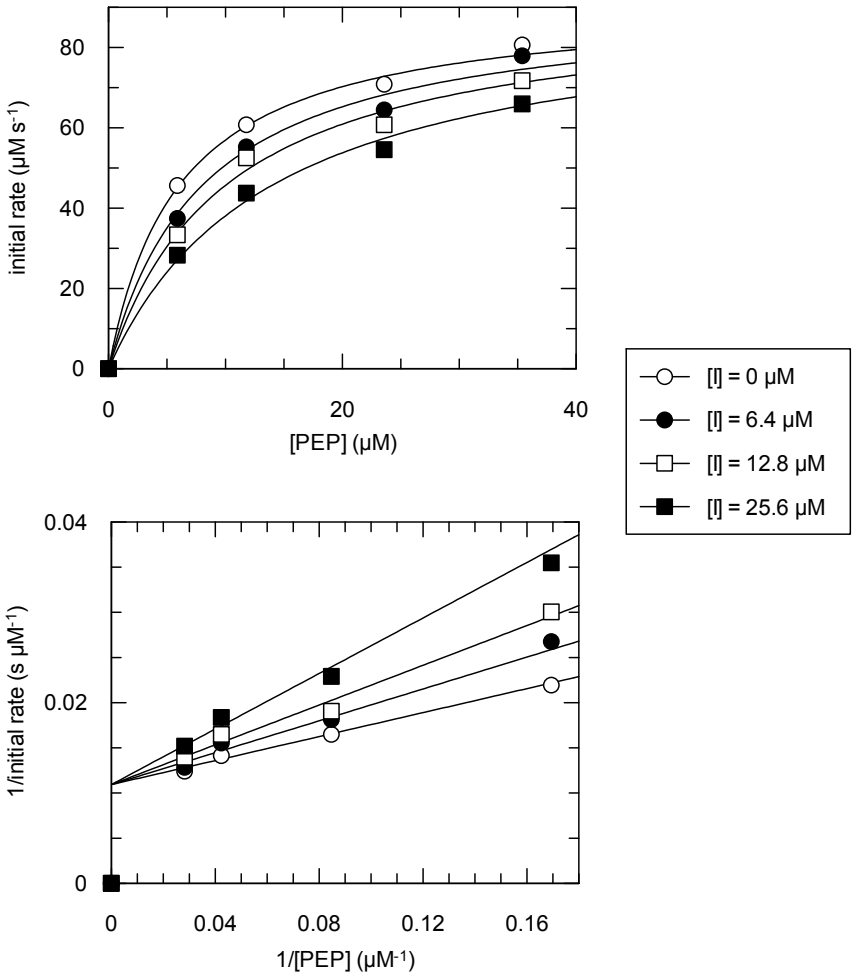

Figure 4.46: Inhibition of KDO8P synthase from *A. ferrooxidans* by diphosphorylated extended phospholactate 4.33 as Michaelis (top) and Lineweaver-Burke (bottom) plots. Solutions of PEP (6-35 μM), A5P (100 μM), manganese chloride (10 μM) and extended phospholactate 4.33 (0-25.6 μM) in 1 mL BTP buffer (50 mM, pH 7.2) were initiated by addition of *A. ferrooxidans* KDO8P synthase (2 μg) and the loss of PEP followed spectrophotometrically at 232 nm. Initial rates were obtained by linear least squares regression and converted to progress rates (μM s^{-1}).

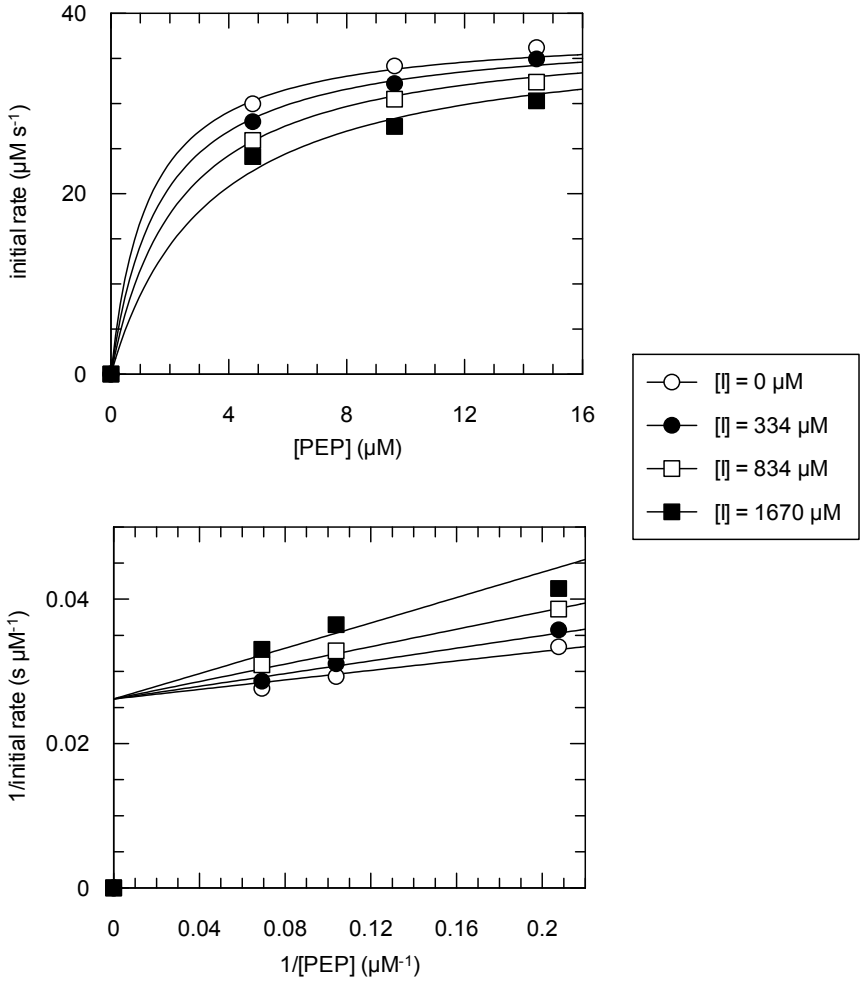

Figure 4.47: Inhibition of KDO8P synthase from *N. meningitidis* by monophosphorylated extended phospholactate 4.36 as Michaelis (top) and Lineweaver-Burke (bottom) plots. Solutions of PEP (5-15 μM), A5P (50 μM), and extended phospholactate 4.36 (0-1670 μM) in 1 mL BTP buffer (50 mM, pH 7.2) were initiated by addition of *N. meningitidis* KDO8P synthase (2 μg) and the loss of PEP followed spectrophotometrically at 232 nm. Initial rates were obtained by linear least squares regression and subsequently converted to progress rates.

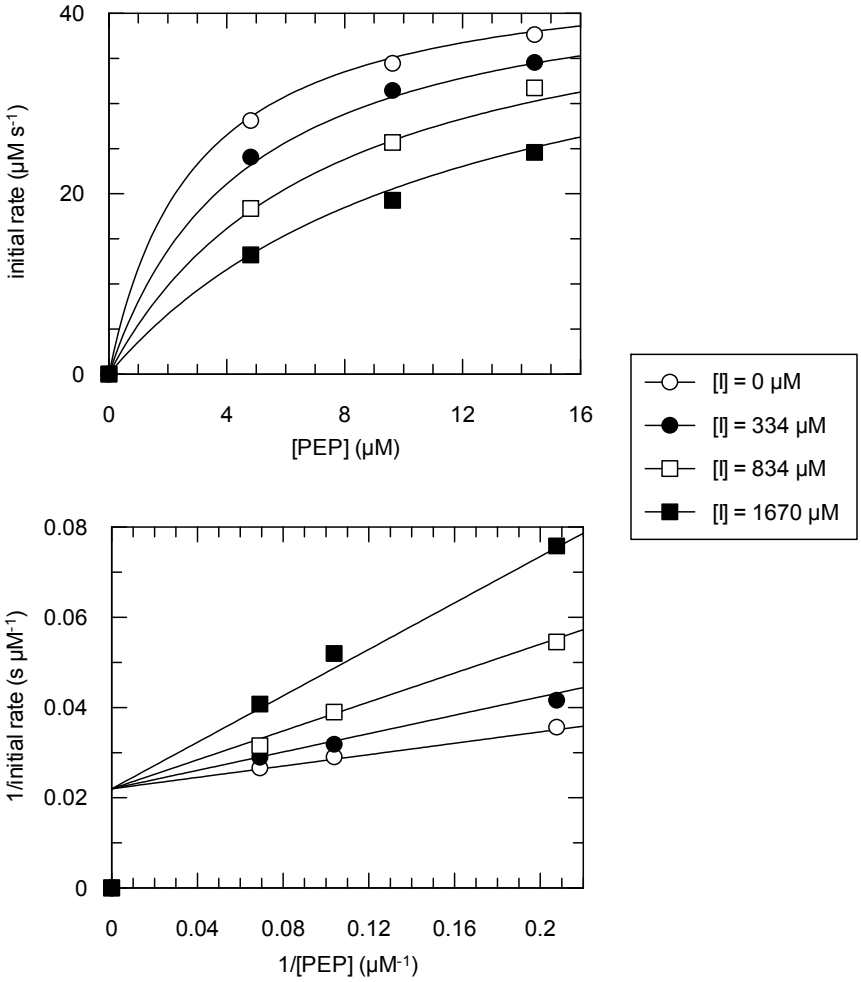

Figure 4.48: Inhibition of KDO8P synthase from *A. ferrooxidans* by monophosphorylated extended phospholactate 4.36 as Michaelis (top) and Lineweaver-Burke (bottom) plots. Solutions of PEP (5-15 μM), A5P (100 μM), manganese chloride (10 μM) and extended phospholactate 4.36 (0-1670 μM) in 1 mL BTP buffer (50 mM, pH 7.2) were initiated by addition of *A. ferrooxidans* KDO8P synthase (2 μg) and the loss of PEP followed spectrophotometrically at 232 nm. Initial rates were obtained by linear least squares regression and subsequently converted to progress rates.

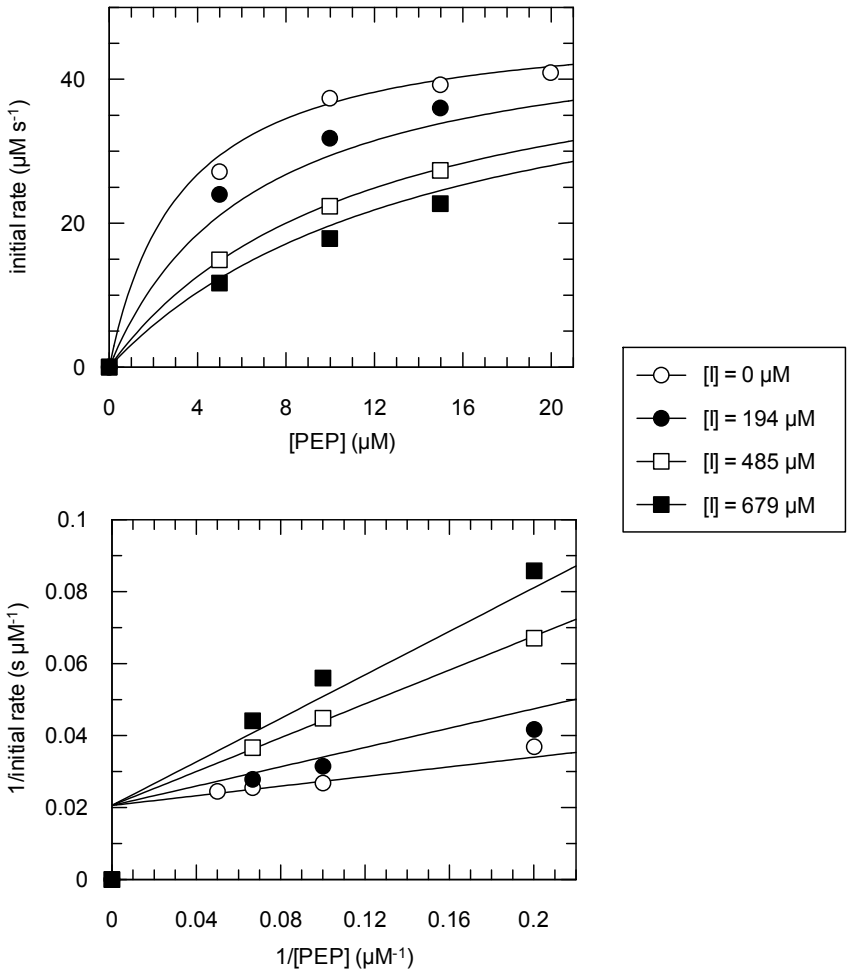

Figure 4.49: Inhibition of KDO8P synthase from *N. meningitidis* by monophosphorylated extended phospholactate 4.40 as Michaelis (top) and Lineweaver-Burke (bottom) plots. Solutions of PEP (5-20 μM), A5P (50 μM), and extended phospholactate 4.40 (0-679 μM) in 1 mL BTP buffer (50 mM, pH 7.2) were initiated by addition of *N. meningitidis* KDO8P synthase (2 μg) and the loss of PEP followed spectrophotometrically at 232 nm. Initial rates were obtained by linear least squares regression and converted to progress rates (μM s^{-1}).

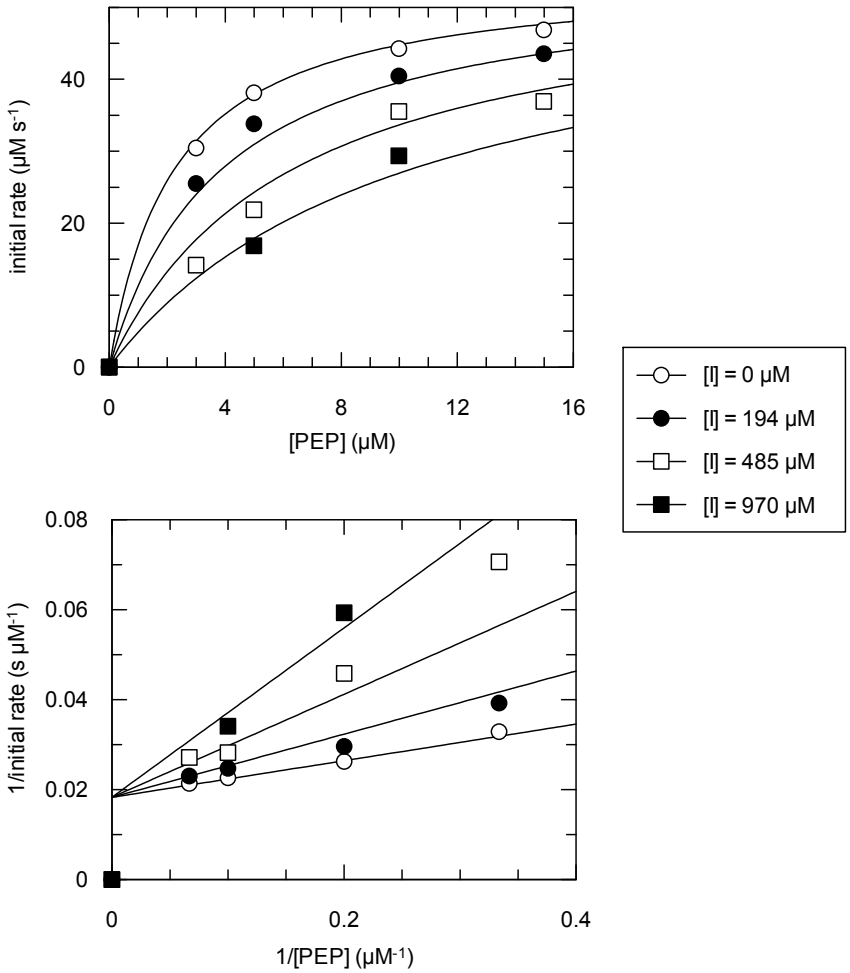

Figure 4.50: Inhibition of KDO8P synthase from *A. ferrooxidans* by monophosphorylated extended phospholactate 4.40 as Michaelis (top) and Lineweaver-Burke (bottom) plots. Solutions of PEP (3-15 μM), A5P (100 μM), manganese chloride (10 μM) and extended phospholactate 4.40 (0-970 μM) in 1 mL BTP buffer (50 mM, pH 7.2) were initiated by addition of *A. ferrooxidans* KDO8P synthase (2 μg) and the loss of PEP followed spectrophotometrically at 232 nm. Initial rates were obtained by linear least squares regression and converted to progress rates (μM s^{-1})

4.4. Discussion and summary

The research described in Chapter 4 was the synthesis of extended inhibitors containing features of the second KDO8P synthase substrate, A5P, from the PEP analogues tested as inhibitors in Chapter 3, in order to gain information for use in the design of future inhibitors. The synthesis of extended phospholactate 4.1 and aminophosphonate 4.19 were unsuccessful. The synthesis of extended phospholactate 4.33, and monophosphorylated analogues 4.36 and 4.40, were successful however, and these three compounds were tested as inhibitors of KDO8P synthase from *N. meningitidis* and *A. ferrooxidans*.

The extended phospholactate 4.33 had vastly improved inhibition over (2*R*)- and (2*S*)-phospholactate (3.5 and 3.6 respectively) with a K_i of 7.9 ± 1.6 μM against *Nme*KDO8PS and 20 ± 3 μM against *Afe*KDO8PS, improvements of 20-100 fold over the single site phospholactate inhibitors and only three fold higher than the K_m^{PEP} for each enzyme, reported in Chapter 2 (Figure 4.51). Extended phospholactate 4.33 can be reported as one of the most potent inhibitors of KDO8P synthase known.

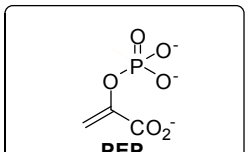

PEP
K_m (*Nme*): 2.5 ± 0.3 μM
K_m (*Afe*): 6.4 ± 0.7 μM

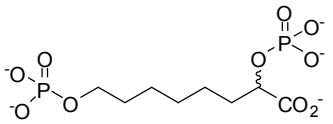

4.33
K_i (*Nme*): 7.9 ± 1.6 μM
K_i (*Afe*): 20 ± 3 μM

Figure 4.51: Inhibitory properties of extended phospholactate 4.33 compared with PEP for KDO8P synthase from *N. meningitidis* and *A. ferrooxidans*.

The two monophosphorylated analogues of extended phospholactate 4.33, 4.36 and 4.40, had K_i values that were much higher than this, indicating far poorer binding to the enzyme active site. For the inhibitor 4.36 that lacked the primary phosphate moiety, the K_i values increased to 1000 ± 180 μM against *Nme*KDO8PS and 540 ± 50 μM for *Afe*KDO8PS (Figure 4.52). This two fold difference between the two enzymes can be explained by the significant difference between the metal-dependent and metal-independent KDO8P synthase for the (2*R*)-phospholactate, 3.6. The extended phospholactates are all a 1:1 enantiomeric ratio between the (*R*) and (*S*) isomers and so increased binding of the (*R*) isomer could decrease the apparent inhibition constant for the metal-dependent KDO8P synthase from *A. ferrooxidans* down by two-fold. The K_i values for inhibitor 4.40, lacking the secondary phosphate group, were similar for both enzymes at 270 ± 40 μM for the metal-independent

KDO8P synthase from *N. meningitidis* and 190 ± 40 μM for the metal-dependent KDO8P synthase from *A. ferrooxidans* (Figure 4.52). They were however decreased from inhibitor 4.36, lacking the primary rather than secondary phosphate moiety. This is perhaps due to the ability of the inhibitor to bind at both ends of the KDO8P synthase binding pocket, and this greater stability should have an increased entropic effect, leading to increased affinity for the enzyme. The consequences of the inhibitor 4.40 containing an enzyme binding motif at either end of the pentamethyl chain, rather than both binding motifs contained in the PEP-like region in inhibitor 4.36 will be discussed further in Chapter 5 in regards to modelling studies with the three extended phospholactate inhibitors.

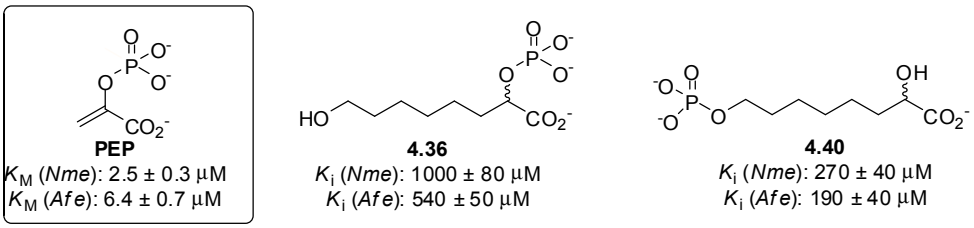

Figure 4.52: Inhibitory properties of monophosphorylated inhibitors 4.36 and 4.40 compared with PEP for KDO8P synthase from *N. meningitidis* and *A. ferrooxidans*.

Chapter 5: Discussion, conclusions and future directions

interpretations
has this research been in vain?
and where to from here?

The inhibition results of Chapters 3 and 4 could now be interpreted together in order to gain a greater understanding of the inhibition of KDO8P synthases from the metal-independent (*N. meningitidis*) and metal-dependent (*A. ferrooxidans*) class of enzyme.

A number of molecules were tested as potential inhibitors of the metal independent KDO8P synthase from *N. meningitidis* and the metal dependent KDO8P synthase from *A. ferrooxidans* (Figure 5.1). They were initially selected as mimics of either the oxocarbenium ion species (glyphosate, 1.6, and vinyl phosphonates 3.3 and 3.4) or the tetrahedral intermediate (phospholactates 3.5 and 3.6, extended phospholactate 4.33 and monophosphorylated analogues 4.36 and 4.40).

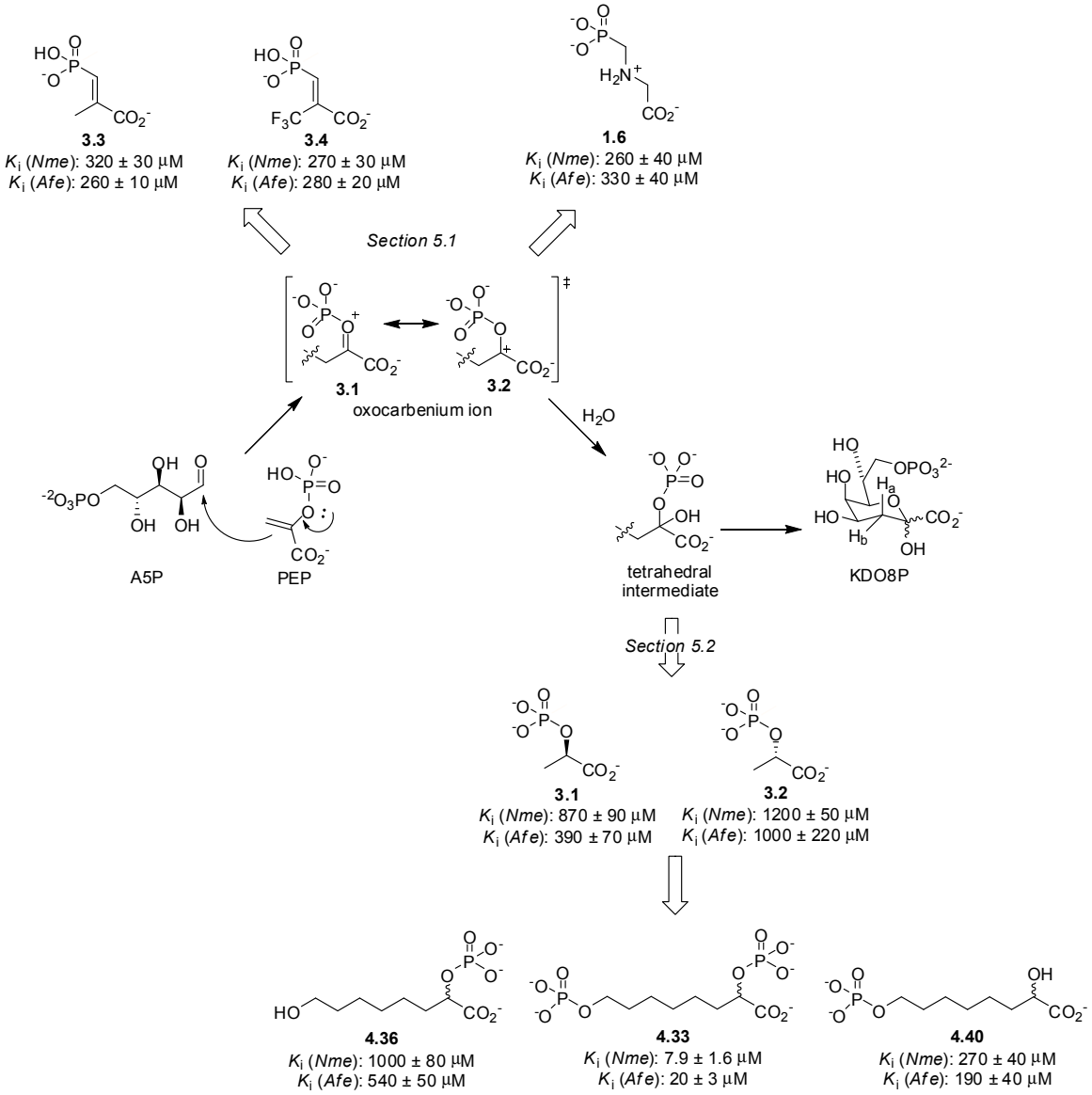

Figure 5.1: Molecules tested as potential inhibitors of KDO8P synthase from *N. meningitidis* and *A. ferrooxidans*, as mimics of the oxocarbenium ion species or tetrahedral intermediate of the KDO8P synthase reaction mechanism.

All of the molecules tested proved to be competitive inhibitors of KDO8P synthase, with respect to PEP, from *N. meningitidis* and *A. ferrooxidans*. This chapter will focus on interpretation of these results, as well as the direction this research can now take in order to both complete and advance the studies contained in this thesis.

5.1. Oxocarbenium ion mimics as inhibitors

Glyphosate, 1.6, was selected as an oxocarbenium ion mimic with a positively charged amine group, representative of the carbocation at the C2 trigonal centre arising from PEP. It was found to be a moderate inhibitor of KDO8P synthases from both *N. meningitidis* and *A. ferrooxidans* with K_i values of 260 ± 40 μM and 330 ± 40 μM respectively. (*E*)-Vinyl phosphonate 3.5 was selected as a geometric mimic of the oxocarbenium ion, containing the observed geometry of PEP as seen in a number of crystal structures of PEP bound KDO8P synthase.[31,34,105] It inhibited KDO8P synthases from *N. meningitidis* and *A. ferrooxidans* similarly, giving K_i values of 320 ± 30 and 260 ± 10 μM for the two enzymes respectively. Fluorinated vinyl phosphonate 3.6 also had similar K_i values to the non-fluorinated counterpart 3.5, and glyphosate, 1.6, of 270 ± 30 and 280 ± 20 μM for KDO8P synthase from *N. meningitidis* and *A. ferrooxidans* respectively.

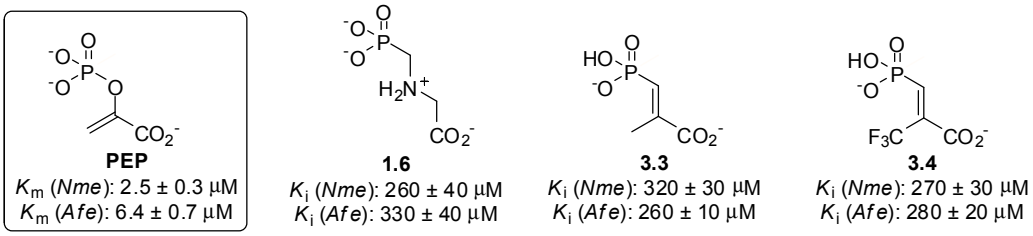

Figure 5.2: Inhibitors as oxocarbenium ion mimics tested against KDO8P synthase, compared with PEP.

The three oxocarbenium mimics used as inhibitors differ structurally, but were found to have remarkably similar K_i values. Although all three inhibitors contain both carboxyl and phosphonate motifs for binding, the linker portion between these two binding motifs is very different between glyphosate, 1.6, and the vinyl phosphonates. Glyphosate, 1.6, has far more flexibility within the molecule than the vinyl phosphonates, and this molecule also has an additional methylene group between the carboxyl group and nitrogen atom.

The (*E*)-isomer of the two vinyl phosphonates were selected due to their similarity with the bound PEP conformation shown in a number of crystal structures.[31,34,105] It was proposed

that the vinyl phosphonates with the (*E*) configuration may bind more strongly than a more flexible inhibitor compound due to entropic effects. Docking studies with the related aldolase DAH7P synthase have indicated that vinyl phosphonate 3.3 does have a similar mode of binding to PEP.[86] It is likely that vinyl phosphonate 3.3 would bind similarly to KDO8P synthase. Glyphosate, 1.6, has not been computationally docked in either the related aldolase DAH7P synthase's or KDO8P synthase's active site. However, the aminophosphonate 1.4 has been crystallised with *Aae*KDO8PS.[30] If we assume that glyphosate, 1.6, binds similarly to aminophosphonate 1.4, and (*E*)-vinyl phosphonate 3.3 binds similarly to PEP, we can compare the two modes of binding in the crystal structures of KDO8P synthase from *A. aeolicus* (Figure 5.3).

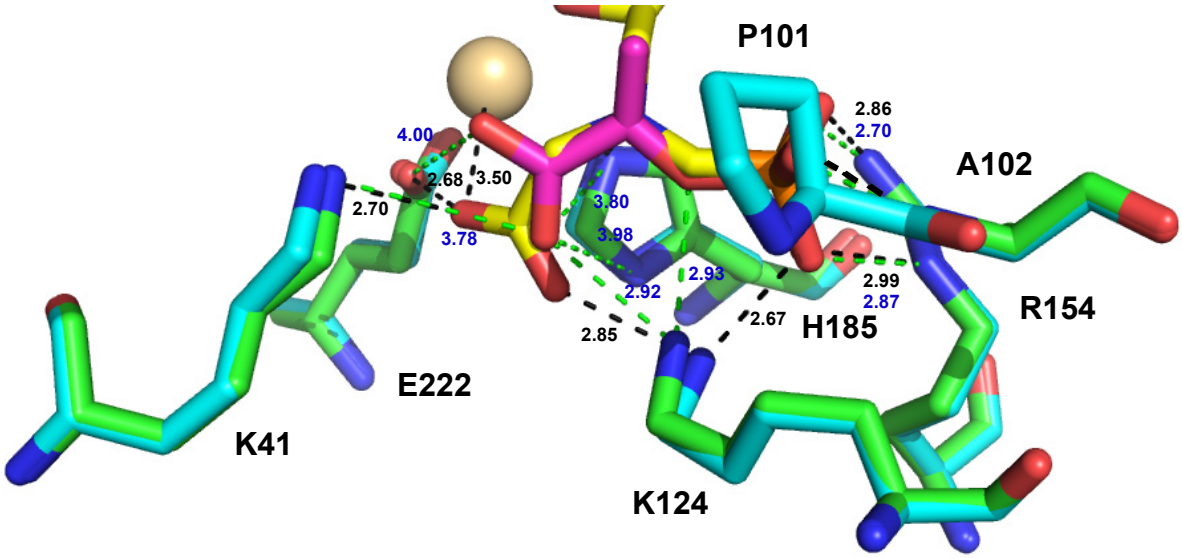

Figure 5.3: Comparison of PEP and aminophosphonate 1.4 binding in the active site of KDO8P synthase from *A. aeolicus* (drawn from 1FWW[34] (PEP) and 1JCX[30] (aminophosphonate 1.4)). For crystal structure 1FWW, PEP is coloured magenta, associated residues in green, potential bonds in green and bond distances in blue. For crystal structure 1JCX, aminophosphonate 1.4 is coloured yellow, associated residues in cyan, potential bonds in black and bond distances in black. Cadmium ion is shown in gold. All residues within 4 Å of PEP or the PEP portion of aminophosphonate 1.4 are shown, and bond distances are reported in angstroms. Some bond distances that are not significantly different between the two structures have been removed for clarity.

The nitrogen atom of aminophosphonate 1.4 binds in a similar position to the C2 atom of PEP, which it corresponds to. This causes the carboxyl group of aminophosphonate 1.4 to probe further into the active site of KDO8P synthase than that of PEP, due to an additional methylene group between the amine and carboxyl moieties. The change in binding that results from this alters a number of interactions with surrounding residues such as H185, however new interactions with the metal ion (cadmium) are seen. The phosphate moiety of both PEP and aminophosphonate 1.4 bind in the same location, emphasising the importance

of this region for inhibitor positioning. Overall a similar number of active site contacts are formed for both PEP and the PEP-like portion of aminophosphonate 1.4. The similar, moderate (50-100 times K_m^{PEP}) K_i values for the three inhibitors may be a result of this similar number of active site contacts, and not the ability of either molecule to mimic PEP or KDO8P synthase reaction intermediates.

The K_i values of the inhibitors against both classes of KDO8P synthase tested were very similar too, even though, as determined in the studies presented in Chapter 2, the K_m^{PEP} value for the metal dependent KDO8P synthase from *A. ferrooxidans* is more than twice that for the metal-independent KDO8P synthase from *N. meningitidis*. This may be a result of the inhibitor molecules interacting more strongly with the metal ion found in metal-dependent KDO8P synthases than the asparagine residue found in the metal-independent enzyme, as shown in Figure 5.3, where the carboxyl moiety of aminophosphonate 1.4 interacts with the cadmium ion in the KDO8P synthase crystal structure.

The final result from the testing of the oxocarbenium ion mimic inhibitors, was the comparison between the two vinyl phosphonates, 3.3 and 3.4. It has been proposed that the phosphate of PEP bound in the KDO8P active site is monoanionic,[30] and so monoanionic inhibitors may bind with greater affinity than the dianionic equivalent. Although phosphonates have higher pK_{a^2} values than their phosphate analogues (Section 3.3), previous investigations had shown that fluorine atoms adjacent to the phosphorous atom can decrease these values, through electron withdrawing effects on the phosphorous atom.[106] The fluorinated analogue 3.4 was originally designed in order to decrease the pK_{a^2} value for the phosphonate moiety. These effects are reported for adjacent fluorine atoms, and although not reported for vinylogous fluorine atoms, it was assumed that some of the same effect would be seen. This effect was not seen however, and vinyl phosphonate 3.3 and the fluorinated analogue 3.4 gave similar K_i values for both KDO8P synthases investigated here. These results indicate that inhibitors that bind with the phosphate or phosphonate moiety in the monoanionic state may not have greater binding affinities than the dianionic equivalent. There are two possible reasons for this, depending on whether the inhibitors are binding as PEP mimics, or mimics of the high energy intermediate or transition state. If the inhibitors bind as transition state mimics, this could be a result of the oxocarbenium ion binding with phosphate in the dianionic state, which is predicted to bind with greater affinity than the product or substrates of the KDO8P synthase reaction due to Transition State Theory,[98-100] as discussed in Chapter 3. If they bind as PEP mimics, recent computational studies have

suggested that PEP itself may bind as the dianion, and be involved in deprotonation of the water on the *si* face of PEP before attack of the hydroxide ion on the C2 of PEP as per the KDO8P synthase mechanism.[171]

5.2. Tetrahedral intermediate mimics as inhibitors

The (2*R*)- (3.5) and (2*S*)-phospholactate (3.6) molecules (Figure 5.4) were selected as mimics of the tetrahedral intermediate (Figure 5.1) to be used as inhibitors of these KDO8P synthases from *N. meningitidis* and *A. ferrooxidans*. They were found to be moderate to poor inhibitors of both enzymes. The addition of A5P phosphate functionality in bisphosphate 4.33 increased the inhibition dramatically giving K_i values of 7.9 ± 1.6 and 20 ± 3 μM for KDO8P synthase from *N. meningitidis* and *A. ferrooxidans* respectively. These values are approximately three-fold higher than the K_m^{PEP} value for both enzymes (Figure 5.4). The absence of either the secondary PEP-like phosphate, or the terminal A5P-like phosphate reduced inhibition significantly, returning K_i values similar to those found for the PEP analogues of Chapter 3 (Figure 5.4).

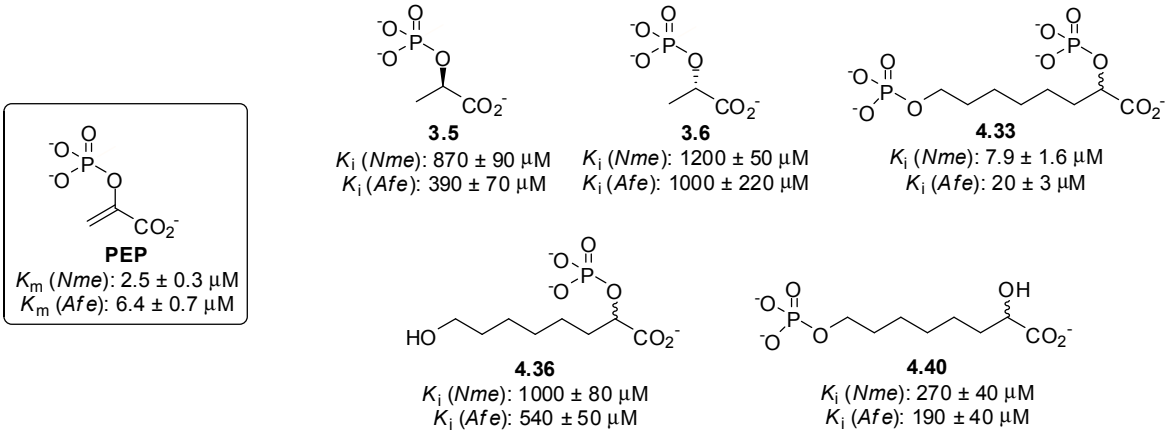

Figure 5.4: Phospholactate inhibitors as tetrahedral intermediate mimics (3.5, 3.6 and 4.33) and monophosphorylated inhibitors (4.36 and 4.40) as part of a structure-activity-relationship (SAR) study on bisphosphate inhibitor 4.33.

The dramatic increase in inhibition from the two phospholactate isomers to bisphosphate 4.33 is presumed to be due entirely to the increase in the number of polar contacts the inhibitor forms with the KDO8P synthase active site. Induced fit docking studies of both enantiomers of bisphosphate 4.33 helps to visualise this. The crystal structure of *Afe*KDO8PS is not available, and the *Nme*KDO8PS structure available is missing key residues as the structure

does not contain bound substrates, and so the L7 loop is disordered[30,34] as discussed in Chapter 1. Instead both enantiomers of extended phospholactate 4.33 were docked into crystal structure 1FWW of the KDO8P synthase from *A. aeolicus*,[34] and energy minimised using an induced fit method, by Wanting Jiao (Figure 5.5). The *Aae*KDO8PS enzyme shows sequence similarity with both enzymes (44 % for *Nme*KDO8PS and 51 % for *Afe*KDO8PS, calculated using ClustalW2) and so is appropriate as a model.

The resulting model shows that the (*R*)- and (*S*)-isomer of extended phospholactate 4.33 have similar IDF scores (a measure of the interactions of the docked molecule with the enzyme active site) (Figure 5.5) with the (*R*)-isomer being calculated as having slightly tighter binding, as indicated by the lower induced fit (IDF) score. The number, and nature of the active site contacts by both enantiomers of inhibitor 4.33 are very similar, except for the carboxyl moiety. The (*S*)-isomer binds as per PEP with the carboxyl moiety forming contacts with three lysine residues (K41, K46, K124) and R154 with a possible weak metal ion interaction. The (*R*)-isomer in comparison forms a strong interaction with the metal ion, with a loss of amino acid interactions with K41, K124 and R154, with a new interaction with N48 formed. Even though this difference in binding of the carboxyl moiety has caused the terminal phosphate moiety of the (*R*)-isomer of inhibitor 4.33 to protrude further from the active site, the number of contacts formed between the terminal phosphate moiety and active site is similar for the two enantiomers.

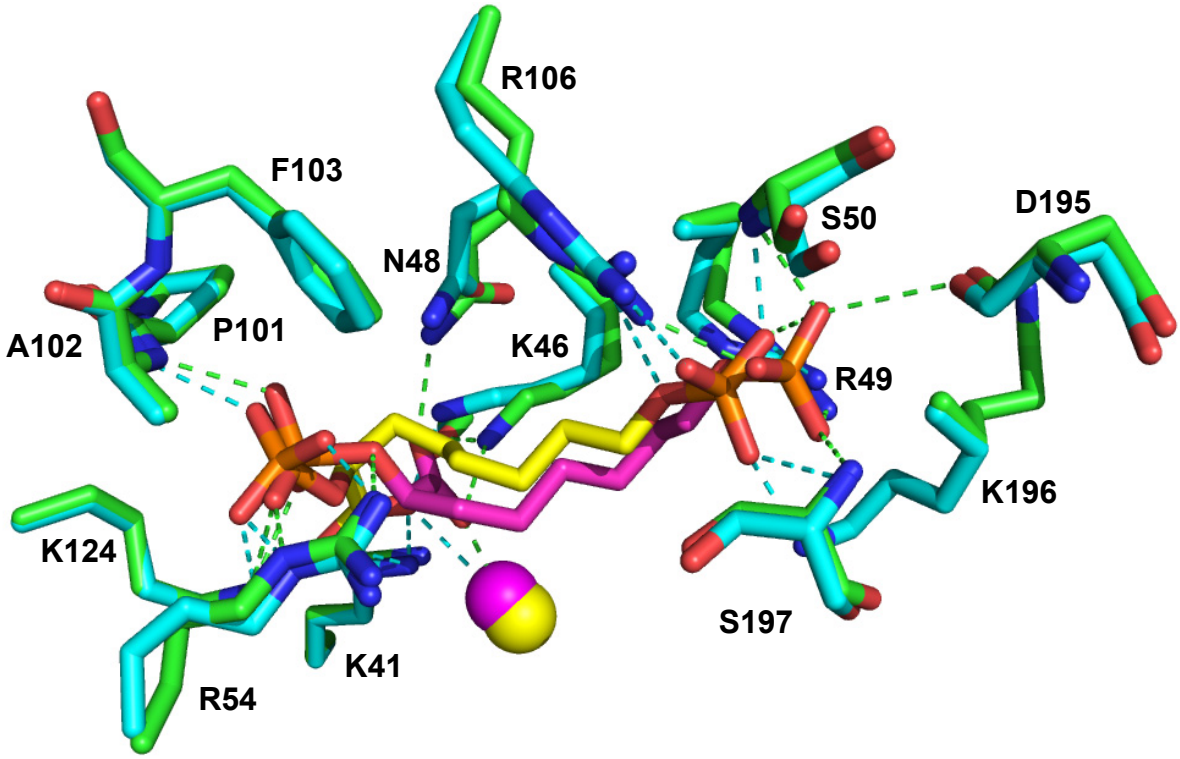

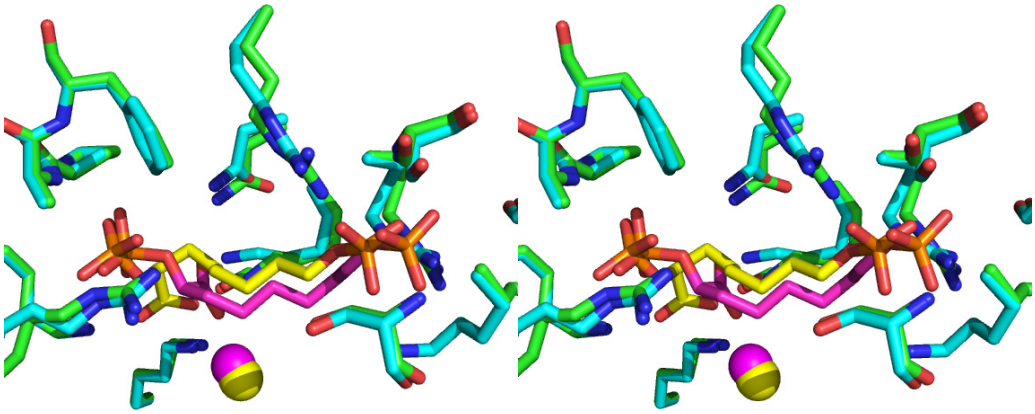

Stereoisomer	IDF score
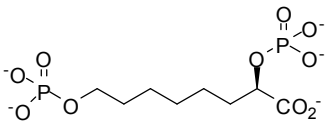 (*R*)	-1446.0
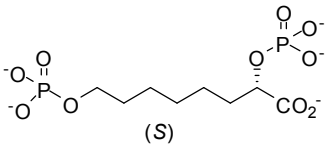 (*S*)	-1443.8

Figure 5.5: Comparison of the calculated positions of the (*R*)- (yellow) and (*S*)- (magenta) isomers of bisubstrate inhibitor 4.33 with bonding contacts (top), in stereo (middle) and scores for inhibitor docking studies (bottom). Metal ions (Mn^{2+}) are coloured as per inhibitor molecules. Bonding residues, within 4 Å of the phosphate or carboxyl moieties, are shown. Residues are labelled, and coloured green (calculated positions for (*R*) isomer) and cyan (calculated positions for (*S*) isomer). Polar contacts, within 4 Å of the phosphate or carboxyl moieties are coloured as per active site residues.

The enantioselectivity of the related aldolase DAH7P synthase for the phospholactates and extended phospholactates has been investigated crystallographically with the enzyme from *M. tuberculosis*.[114] This revealed that the selectivity of the (*R*)-isomer of the extended phospholactate (K_i = 360 ± 40 nM) over the (*S*)-isomer (K_i = 630 ± 110 nM) may be due to the ability for each to accommodate the water molecule responsible for attack of the C2 atom of PEP. In the case of the crystal structure of DAH7P synthase from *M. tuberculosis* the (*R*)-isomer is able to accommodate the water molecule on the *re* face of PEP where as the (*S*)-isomer cannot. The *re* face water is considered to be the most viable candidate for the attack on PEP for DAH7P synthase. An overlay of the docked bisphosphate 4.33 with the original 1FWW crystal structure[34] reveals similar attributes for KDO8P synthase (Figure 5.6). As shown, the (*R*)-isomer of inhibitor 4.33 does not allow for binding of the *si* face water molecule due to steric clashes with the carboxyl moiety which also is shown to bind the metal ion (Figure 5.5). The docking studies suggest that the enantioselectively is not reliant on the ability to accommodate the *si* face water molecule. The PEP-like phosphate moiety of both enantiomers is close to the *re* side water, and may form polar contacts. However, these contact distances are slightly longer for the (*R*)-isomer (3.22 Å, 3.53 Å) than the (*S*)-isomer (2.22 Å), perhaps causing less steric clash and resulting in better accommodation of this water molecule.

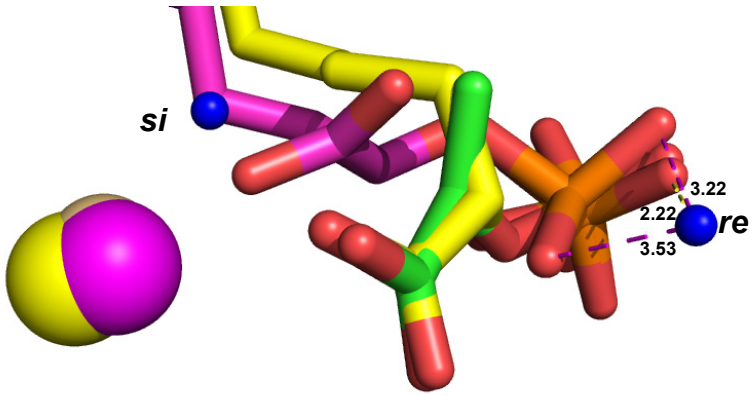

Figure 5.6: Overlay of the original 1FWW crystal structure[34] with PEP (green) and *re* and *si* face water molecules (blue) with that calculated from 1FWW for induced fit docking of (*R*)- (pink) and (*S*)-isomers (yellow) of inhibitor 4.33. Bond distances are coloured as per inhibitor enantiomer and distances are in angstroms.

The two monophosphate inhibitors, lacking either of the two phosphate moieties of inhibitor 4.33 had reduced inhibition compared to the bisphosphate inhibitor. Monophosphorylated inhibitor 4.36, lacking the A5P phosphate functionality, had much less potent inhibition

against KDO8P synthase from *N. meningitidis* and *A. ferrooxidans* with K_i values of 1000 ± 80 μM and 540 ± 50 μM respectively. These K_i values can be rationalised as being close to the average of the K_i values for the two enantiomers of phospholactate (3.5 and 3.6), being 1040 μM against *Nme*KDO8PS and 700 μM against *Afe*KDO8PS. This is likely due to the loss of active site contacts with the terminal (A5P-like) end of the inhibitor. When this molecule is docked into the *Aae*KDO8PS crystal structure 1FWW[34] by Wanting Jiao as per bisphosphate 4.33, this becomes more clear. The two enantiomers bind similarly, with the carboxyl moieties bound to the metal ion as per the (*R*)-isomer of inhibitor 4.33 rather than the PEP carboxyl binding pocket. This presumably indicates the increased flexibility of the inhibitor without the terminal phosphate interactions with the enzyme. The two phosphate moieties also bind similarly, in the PEP phosphate binding pocket and form a similar number of active site contacts, indicating the importance of this region for inhibitor placement. The hydroxyl moieties of both the respective inhibitor enantiomers are hydrogen bonded to a conserved arginine and serine (R49 and S50), part of the conserved KANRS(T) sequence in KDO8P synthase enzymes. This is the only interaction observed at this end of the inhibitor molecule with the enzyme active site, and a substantial decrease in contacts with the active site. This reinforces the hypothesis that the K_i values found for the monophosphorylated inhibitor 4.36 were similar to that found for the phospholactates 3.5 and 3.6 due to the small number, and relative weakness, of the contacts at the "A5P" terminal end of the inhibitor.

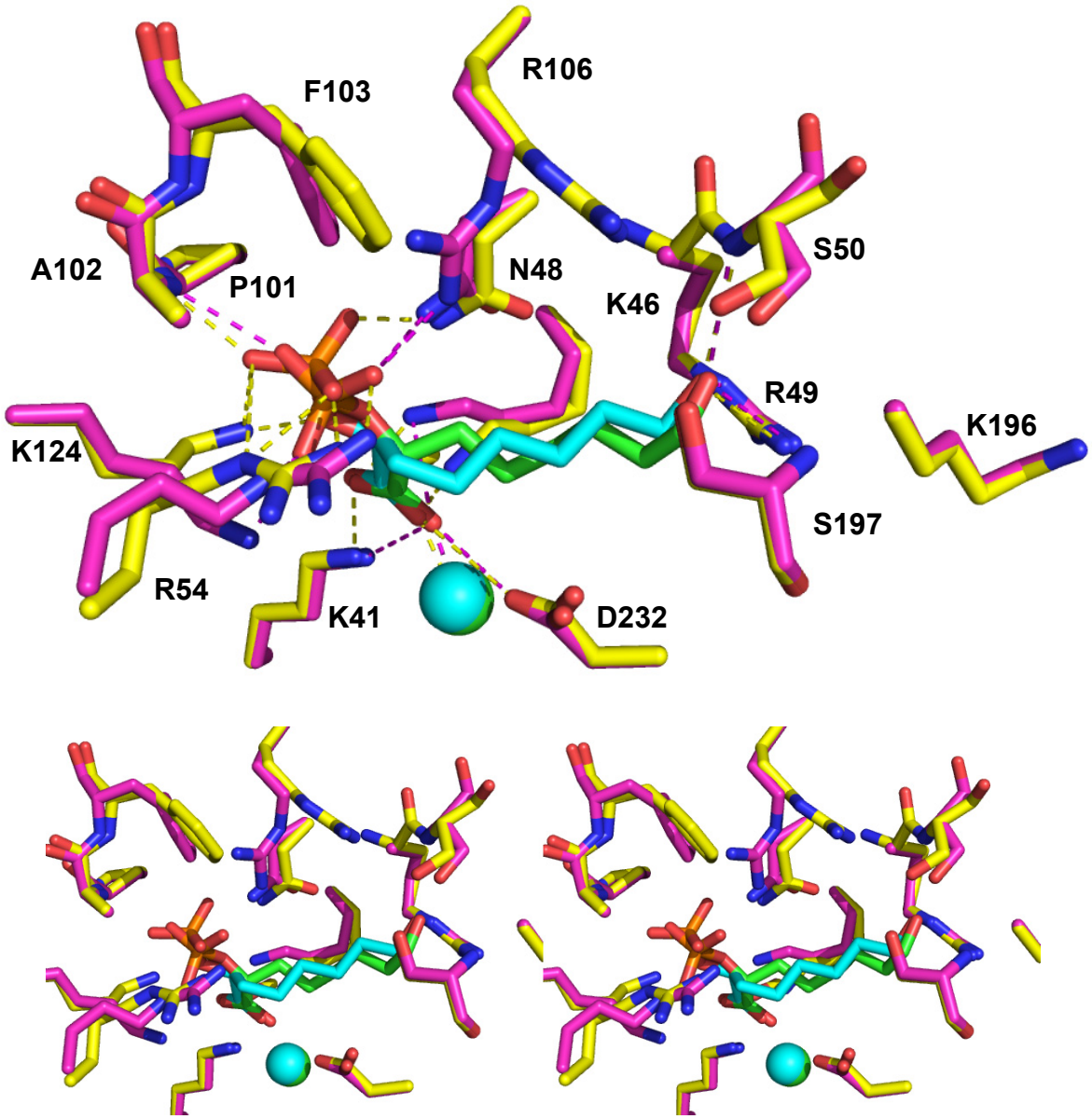

Stereoisomer	IDF score
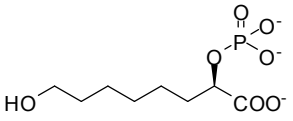 (*R*)	-1430.1
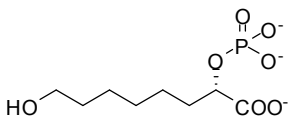 (*S*)	-1428.4

Figure 5.7: Comparison of the calculated positions of the (*R*)- (green) and (*S*)- (cyan) isomers of bisubstrate inhibitor 4.33 with bonding contacts (top), in stereo (middle) and scores for inhibitor docking studies (bottom). Metal ions (Mn^{2+}) are coloured as per inhibitor molecules. Bonding residues, within 4 Å of the phosphate or carboxyl moieties, are shown. Residues are labelled, and coloured magenta (calculated positions for (*R*) isomer) and yellow (calculated positions for (*S*) isomer). Polar contacts, within 4 Å of the phosphate, carboxyl or terminal hydroxyl moieties are coloured as per active site residues.

The monophosphate 4.40, missing the PEP phosphate functionality, gave better inhibition than monophosphate 4.36. This is maybe due to increased rigidity of the KDO8P synthase active site due to bonding in both the PEP and A5P binding pockets. Both isomers of inhibitor 4.40 were docked into the active site of *Aae*KDO8PS from the 1FWW structure[34] by Wanting Jiao (Figure 5.8). Interestingly the A5P-like phosphate moiety bound in the PEP binding pocket, so that the inhibitor was "flipped" from what is seen for inhibitors 4.33 and 4.36, so that the terminal phosphate, representative of A5P, bound in the PEP phosphate binding site. This adds weight to the hypothesis that the PEP phosphate binding site is responsible for positioning of the inhibitors. Compared with the docked structure of inhibitor 4.36, some of the active site contacts in the PEP binding pocket have been lost, such as those with residues R106 (still shown in Figure 5.8, but do not form contacts with the inhibitor) and K41. However, many of the contacts in the A5P phosphate binding site have been restored, forming contacts with the carboxyl moiety of inhibitor 4.40.

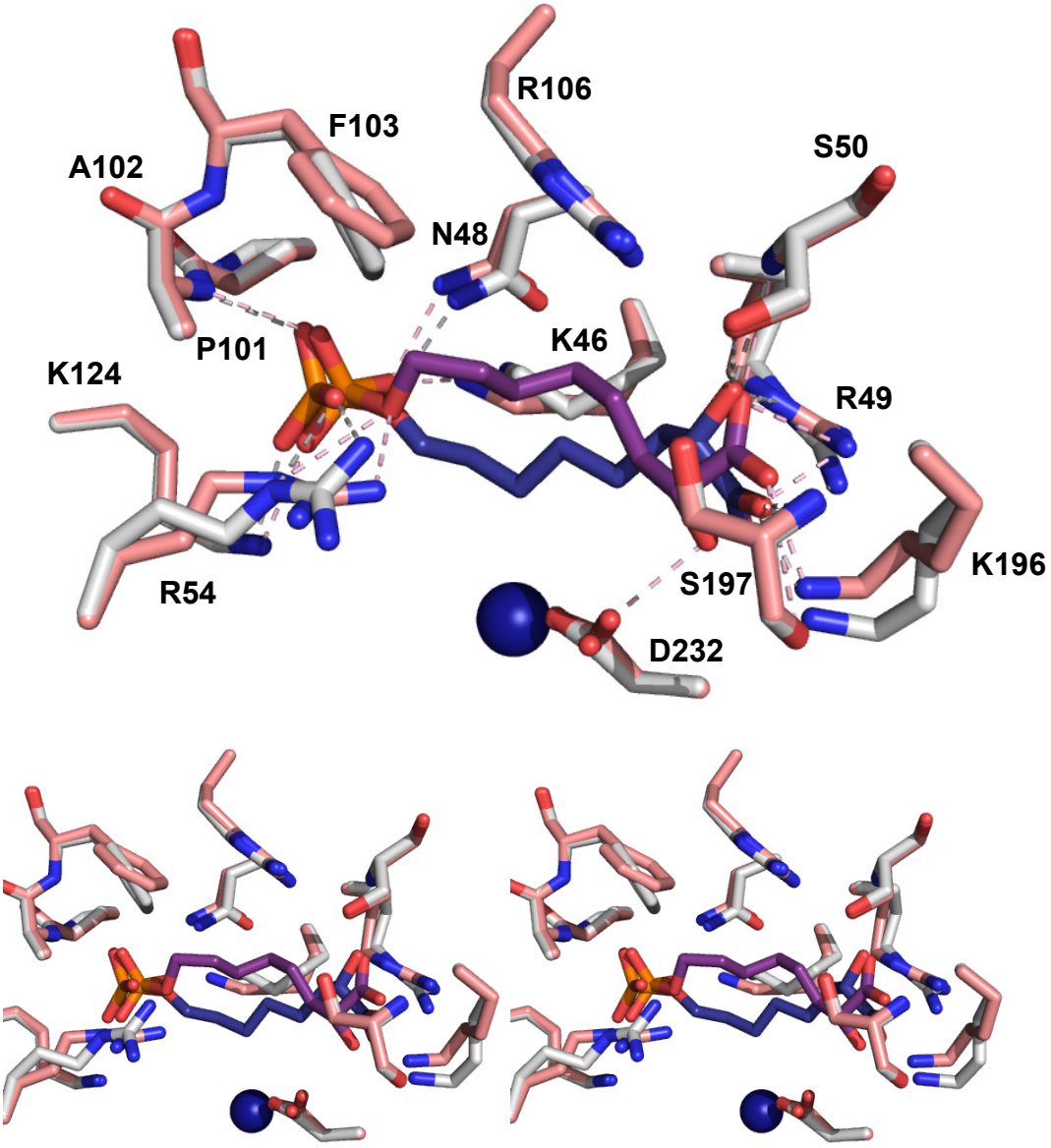

Stereoisomer	IDF score
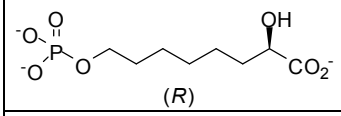 (*R*)	-1426.5
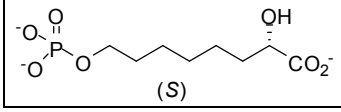 (*S*)	-1425.4

Figure 5.8: Comparison of the calculated positions of the (*R*)- (purple) and (*S*)- (dark blue) isomers of bisubstrate inhibitor 4.40 with bonding contacts (top), in stereo (middle) and scores for inhibitor docking studies (bottom). Metal ions (Mn^{2+}) ions are coloured as per inhibitor molecules. Bonding residues, within 4 Å of the phosphate or carboxyl moieties, are shown. Residues are labelled, and coloured pink (calculated positions for (*R*) isomer) and grey (calculated positions for (*S*) isomer). Polar contacts, within 4 Å of the phosphate, carboxyl or terminal hydroxyl moieties are coloured as per active site residues.

5.3. Conclusions on the inhibition of KDO8P synthase

The five PEP analogues selected as mimics of two reaction intermediates were all shown to be poor inhibitors of KDO8P synthase, competitive with respect to PEP, with K_i values ranging from 260 to 1200 μM. Those molecules chosen as mimics of the oxocarbenium ion (glyphosate, 1.6, and vinyl phosphonates 3.3 and 3.4) inhibited KDO8P synthase from both classes more effectively than those chosen as mimics of the tetrahedral intermediate (phospholactates 3.5 and 3.6). As discussed, the inhibition of each molecule may be due to the number of active site contacts with the carboxyl and phosphate moieties, and not the ability of each molecule to mimic the KDO8P synthase reaction intermediates. The increased inhibition of the oxocarbenium mimics over the phospholactates may be due to this, and not the tighter binding of the more unstable oxocarbenium ion over the tetrahedral intermediate, as per Transition State Theory.[98] Additionally all PEP analogue inhibitors tested gave smaller K_i/K_m^{PEP} ratios (more effective inhibition) for the metal-dependent KDO8P synthase from *A. ferrooxidans*. It is proposed that this may be a result of the inhibitors forming stronger contacts with the metal ion in *Afe*KDO8PS than the active site residues in this binding pocket in *Nme*KDO8PS. The metal ion is thought to be involved in ordering the active site residues and substrates, so increased interactions with the metal ion may cause rigidity in the active site that reduces the rate of dissociation of the inhibitor from the KDO8P synthase active site.

The docking studies of bisphosphate 4.33 with the active site of *Aae*KDO8P synthase reveal a possible source of the enantioselectivity of the enzyme, giving greater inhibition for phospholactate 3.5 than 3.6. This is due to the ability of each isomer to accommodate the water molecule (that found on the *re* face of PEP) involved in the KDO8P synthase reaction. This is in line with that found for the related aldolase DAH7P synthase, and agrees with the proposal that the *re* face water molecule attacks the C2 of PEP by anti addition as discussed in Chapter 1.

The addition of a terminal phosphate moiety in extended phospholactate 4.33 dramatically increased inhibition of KDO8P synthase 130-fold against the enzyme from *N. meningitidis* and 70-fold against that from *A. ferrooxidans* (averaging the K_i values for the two phospholactate isomers, 3.5 and 3.6 for each KDO8P synthase enzyme). This effect was lessened when either of the two phospholactate moieties were absent, as seen for the inhibition results for compounds 4.36 and 4.40, with the K_i values returning to those found

for the small molecule PEP analogues as shown in the studies presented in Chapter 3. These results confirm the initial hypothesis that extending a single-substrate mimic (PEP analogues) to include elements of the second substrate (A5P) can dramatically increase inhibitor binding to the enzyme active site, and therefore increase the inhibition of the KDO8P synthase enzyme.

5.4. Future directions

The investigations into inhibition of KDO8P synthase had revealed a number of interesting insights which could now be used in the proposal of future studies in order to complete and advance the research presented here.

5.4.1. Extended oxocarbenium ion mimics

The PEP analogues tested as inhibitors of KDO8P synthase in Chapter 3 that were selected as mimics of the oxocarbenium ion, glyphosate, 1.6, and vinyl phosphonates 3.3 and 3.4, were more effective inhibitors than the phospholactates, 3.5 and 3.6. In order to determine whether this effect is apparent for inhibitors incorporating structural aspects of A5P, extended aminophosphonate 4.19 was proposed in Chapter 4. The synthesis of aminophosphonate 4.19 failed due to the inability to generate the secondary amine 4.19, from reductive amination of the aldehyde or electrophilic substitution of the bromo ether, potentially due to the electron withdrawing ester substituent on the amine, reducing its nucleophilicity. An alternative to this, not trialled in the studies presented here, is the alkylation by electrophilic substitution of sulfonamides rather than amines, formed from the reaction of a primary amine (such as an amino acid) and 2- or 4-nitrophenylsulfonyl chloride. This sulfonamide anion, formed from the reaction between the sulfonamide and cesium carbonate as a base, can then be reacted with a bromo ether such as compound 4.26 (Chapter 4) to yield an alkylsulfonamide which can be purified, or treated with phenylthiolate to cleave the nitrophenylsulfonyl protecting group to give the secondary amine in high yield (Figure 5.9).[172]

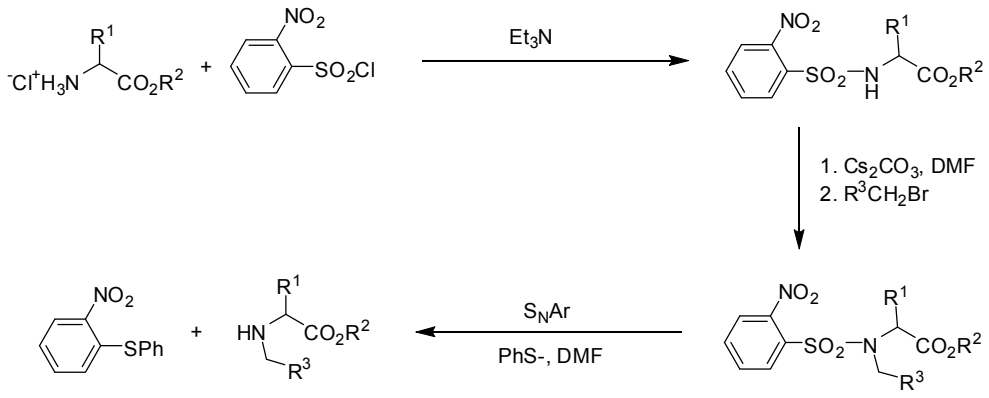

Figure 5.9: N-alkylation of amino acids *via* sulfonamide intermediate.[172]

Alternatively, and perhaps more readily, the extended vinyl phosphonate, based on the vinyl phosphonate 3.3, could be synthesised *via* the same α-chloroglycidic ester utilised in the synthesis of extended phospholactates 4.33, 4.36 and 4.40. The α-chloroglycidic esters are versatile synthetic intermediates. As well as being reduced to the corresponding α-hydroxy ester, they can undergo rearrangements to the β-halo-α-keto ester, which can be reduced to give the α-keto ester.[173] This α-keto ester can then undergo a Horner-Wadsworth-Emmons reaction to form the vinyl phosphonate moiety (Figure 5.10). The advantage of this route is that it incorporates chemistry previously proven to be successful in this thesis. Additionally, it provides a small number of synthetic steps to what can be considered a complicated motif (the vinyl phosphonate ester), an advantage discussed in Chapter 4 for the synthesis of the extended phospholactates.

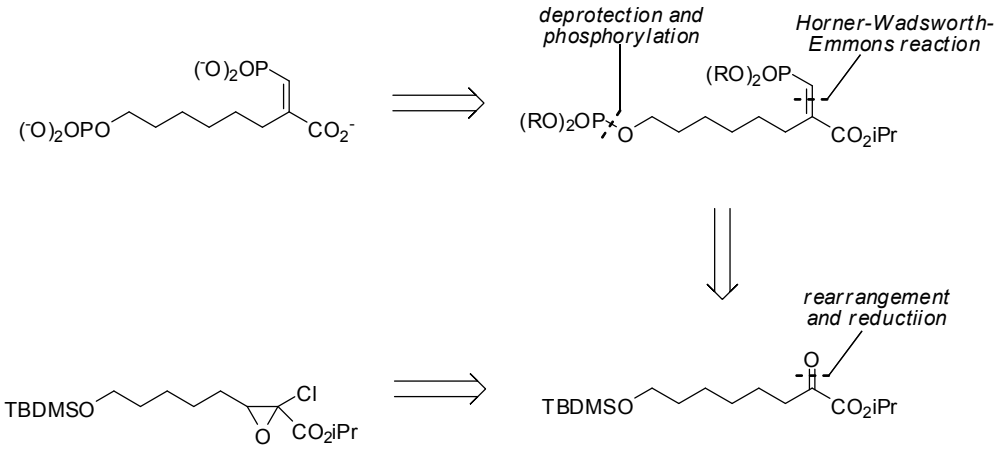

Figure 5.10: Retrosynthetic analysis of extended vinyl phosphonate 5.2.

5.4.2. Extended inhibitors with A5P-like hydroxyl functionality associated stereochemistry

The addition of an A5P-like terminal phosphate moiety was shown to increase inhibition by around 100-fold for the phospholactates 3.5 and 3.6. It was originally proposed that this principle of including structural elements of the second substrate, A5P, to known PEP analogues, would include the A5P-like hydroxyl functionality associated stereochemistry as presented in extended phospholactate 4.1. Additionally, an extended (*E*)-vinyl phosphonate inhibitor containing this same hydroxyl stereochemistry could be synthesised *via* the same Darzens chemistry as presented in Section 5.4.1. Both these compounds require the appropriately protected aldehyde. The synthesis of this aldehyde was unsuccessful due to the inability to perform a vital deprotection step in both routes investigated in Chapter 4. In order to synthesise this aldehyde other protecting groups for the aldehyde moiety are proposed, which may offer a viable synthetic route to phospholactate 4.1 and an extended (*E*)-vinyl phosphonate.

Oxathianes have been considered as potential replacements for the dithianes because they can be deprotected under mild conditions,[174] and have been shown to undergo hydrolysis more readily than the dithianes, but are more stable than the *O*,*O*-acetals which are readily cleaved under acidic conditions.[175] The drawbacks to the oxathiane protecting group is that their formation often require harsh conditions, long reaction times or expensive reagents such as TMSOTf.[174] In the context of the synthesis of the appropriately protected aldehyde for synthesis of extended phospholactate 4.1 or the extended (*E*)-vinyl phosphonate, this oxathiane protection may have to be performed before the protection of the hydroxyl groups of D-mannose. Acetonide protection of the hydroxyl groups may not be as straight forward as it was for the dithiane 4.12, and an extensive study into the acetonides formed under various protection conditions would have to be undertaken in order to synthesise the appropriately protected compound.

Recently 5-methoxysalicylic alcohol, 5.1, has been proposed as a photo labile *O*,*O*-acetal protecting group that shows stability under acidic conditions, but is able to be removed by exposure to light from a 450 W medium pressure mercury lamp (Figure 5.11).[176] The conditions for formation of the *O*,*O*-acetal require catalytic $TsOH.H_2O$ in benzene at room temperature, with the requirement of copper(II) sulfate in some cases. These conditions may result in cleavage of acetonide moieties, so would have to be investigated, but it may be possible to directly protect the aldehyde functionality of lactol 4.6. Because of the stability of

the 5-methoxysalicylic alcohol *O*,*O*-acetal to mildly acidic conditions, the selective deprotection of the primary acetonide could be reinvestigated.

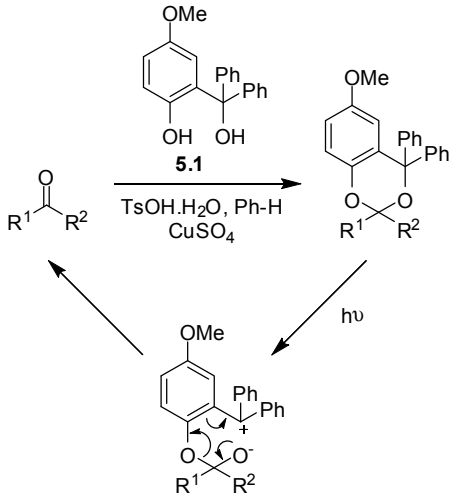

Figure 5.11: Protection of carbonyls with 5-methoxysalicylic alcohol, 5.1.

5.4.3. New scaffolds as potential inhibitors of KDO8P synthase

The synthesis of the appropriately protected aldehyde necessary for the synthesis of extended phospholactate 4.1 was shown to be problematic, and although new routes have been proposed in Section 5.4.2, these are not without their own problems. Alternatively it may be possible to synthesise inhibitors that incorporate some of the hydroxyl functionality associated stereochemistry *via* a much simpler route incorporating chemistry, previously established in this thesis.

A promising target for this are inhibitors that incorporate a hydroxyl group representative of that formed from the A5P aldehyde moiety upon attack by the C3 carbon of PEP. The crystal structure of aminophosphonate inhibitor 1.4 bound in the active site of *Aae*KDO8PS shows this hydroxyl moiety within bonding distance of the metal ion (Figure 5.12), and so this group may provide a potentially useful way of of increasing inhibition of the metal-dependent KDO8P synthases *via* metal coordination.

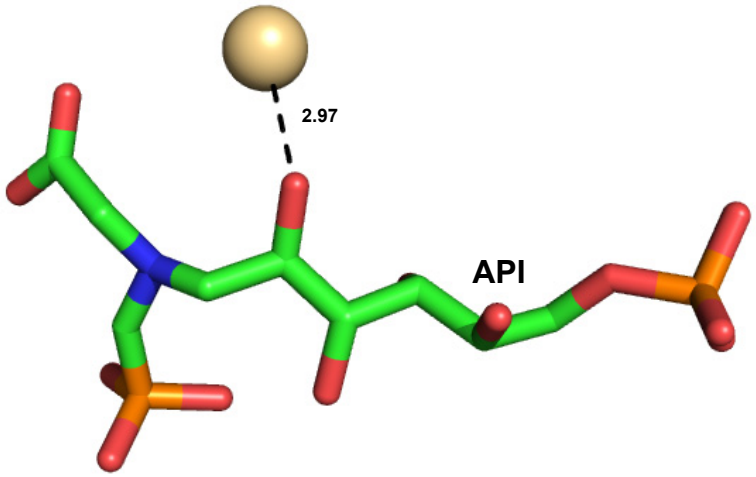

Figure 5.12: Aminophosphonate 1.4 (API) bound in the active site of KDO8P synthase from A. ferrooxidans (1JCX)[30] showing potential bonding between the hydroxyl representative of that formed from the aldehyde of A5P and the metal ion (Cd^{2+}). Distances are measured in angstroms.

This hydroxyl can be incorporated into the previously designed inhibitors *via* the Sharpless asymmetric dihydroxylation combined with the previously utilised Darzens chemistry. The Sharpless asymmetric dihydroxylation involves stereospecific dihydroxylation of an alkene moiety by osmium tetroxide in the presence of a chiral quinine ligand to produce a vicinal diol.[177] The secondary hydroxyl moiety can be selectively protected by protection of the 1,2-diol as the methoxymethyl ether (MOM) and selective deprotection of the primary hydroxyl.[178] The primary hydroxyl, oxidised to the aldehyde, can then be reacted in the Darzens condensation reaction as previously described to give the α-glycidic ester (Figure 5.13). As previously discussed, the α-chloroglycidic ester is a versatile intermediate able to be used in the synthesis of extended vinyl phosphonates and phospholactates. The additional advantage of these compounds for the synthesis of the extended phospholactates is that the diastereoisomers formed from the racemic reduction of the α-chloroglycidic ester may be separable by flash chromatography, where as the enantiomers formed in the synthesis of extended phospholactate 4.33 were not. This can be used to determine the difference the two phospholactate isomers have on inhibition of KDO8P synthase.

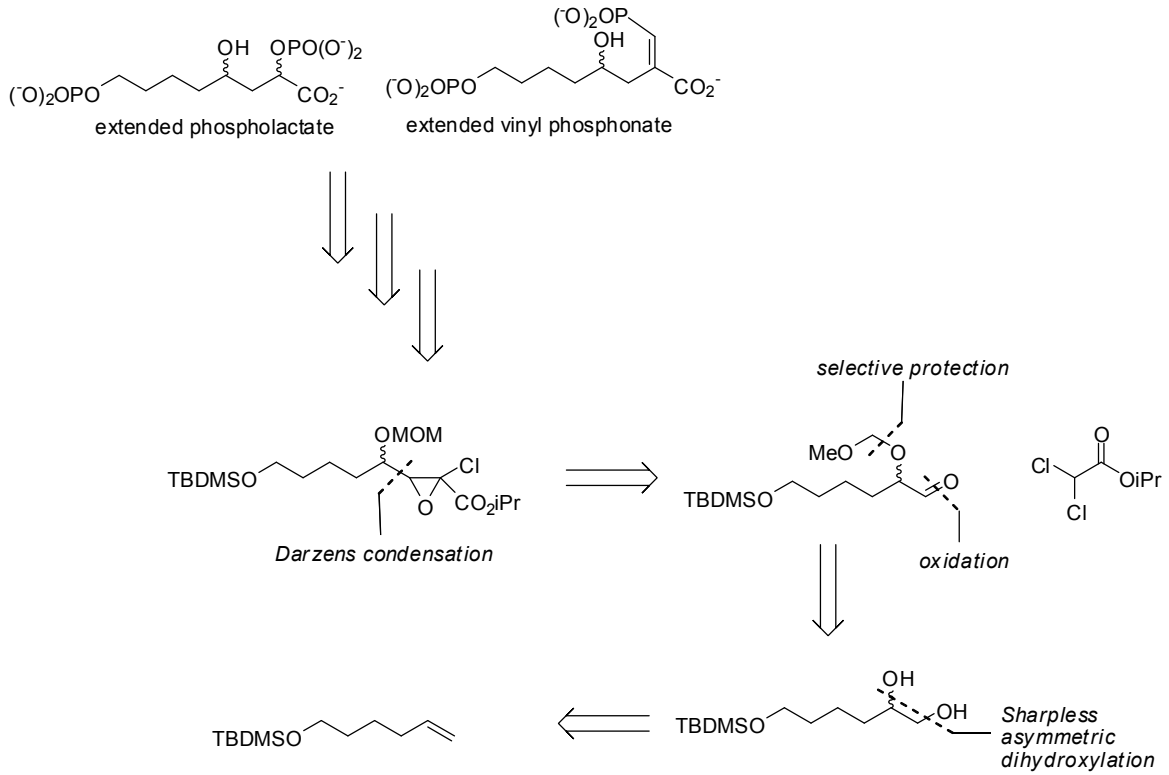

Figure 5.13: Retrosynthetic analysis of α-chloroglycidic ester containing additional hydroxyl moiety for synthesis of extended phospholactates and vinyl phosphonates containing additional metal coordinating hydroxyl moiety.

5.5. Summary

This project describes investigations into the inhibition of the metal-independent KDO8P synthase from *N. meningitidis* and the metal-dependent KDO8P synthase from *A. ferrooxidans*. A number of small molecules were selected as mimics of reaction intermediates and tested as inhibitors. The information gathered from these studies was then used in the design of new inhibitors of KDO8P synthase incorporating aspects of both substrates. Based on the results of this investigation, new directions have been proposed for the inhibition of KDO8P synthase, and it is hoped that this will lead to the development of more potent KDO8P synthase inhibitors.

Chapter 6: Experimental

proof of synthesis
relevant data to show
experimental

6.1. General experimental

6.1.1. Chromatography

All buffers and solvents used during FPLC chromatography were filtered using a 0.45 μM filter (Millipore) before use.

Anion exchange chromatography was carried out on a SOURCE™ 15Q (Amersham) column, using a Biorad Biologic® FPLC pump, quad wavelength detector and automated fraction collection system at 4 °C.

Hydrophobic interaction chromatography was carried out on a SOURCE™ 15Phe (Amersham) column using a Biorad Biologic® FPLC pump, quad wavelength detector and automated fraction collection system at 4 °C.

Size exclusion chromatography was carried out on a HiLoad 26/60 Superdex™ S200 pg (*N. meningitidis*) and Superdex™ S200 10/300 GL (*A. ferrooxidans*) (GE Healthcare) using a Biorad Biologic® FPLC pump, quad wavelength detector and automated fraction collection system at 4 °C.

TLC was carried out on Merck Silica Gel 60 F254 aluminium-backed sheets and visualised under UV light (254 nm), followed by staining with basic aqueous potassium permanganate (general stain) or ethanolic ninhydrin (amines) and developed using a stream of hot air. Flash chromatography was carried out on silica gel (230-400 mesh). Chromatographic hexane, petroleum ether and ethyl acetate were distilled prior to use from calcium hydride if necessary; analytical grade diethyl ether, petroleum ether and ethyl acetate were used as supplied.

6.1.2. Polyacrylamide gel electrophoresis

SDS-PAGE was performed using the method of Laemmli[179] with a NuPAGE® Novex® 10% bis-tris gel, using a Mini Protean III cell (Biorad). A current of 200 V was applied for 50 minutes so that the dye front reached the bottom of the resolving gel. Novex® Sharp pre-stained protein weight standards were used. Protein in the gels were detected by staining the gels for at least 30 mnutes in a solution of 1 g L^{-1} Coomassie Brilliant Blue R 250 (Park Scientific) in 50 % (v/v) methanol and 10 % (v/v) acetic acid in water. Excess dye was removed by soaking gels overnight in 40 % (v/v) methanol and 10 % (v/v) acetic acid in water.

6.1.3. Determination of protein concentration

Protein concentration was determined by the method of Bradford,[180] using bovine serum albumin (BSA) as a standard. BSA protein standards were made to concentrations of 0, 0.1, 0.2, 0.4, 0.6, 0.8 and 1 mg mL^{-1}. 1 mL of Bradford reagent (Biorad) was added to 20 μL of each standard and the samples left for 10 minutes to develop colour. A standard curve was constructed from absorbance readings of each sample at 595 nm. Protein samples of unknown concentration were diluted to 20 μL and treated as previously described for the BSA standards. The absorbance readings of these unknown protein samples at 595 nm were used to determine the concentrations of the original samples.

6.1.4. Enzyme assays

Enzyme assays were performed by following the change in absorbance at 232 nm due to the consumption of PEP. Assays were either performed in duplicate so that there was a difference of less than 10 % between the two values obtained, or globally fitted over the whole data set in order to obtain error of less than 10 % in the final value. Enzyme assays were conducted with recombinant *N. meningitidis* and *A. ferrooxidans* KDO8P synthase, prepared as previously described and stored at -80 °C until required. Enzyme solutions were thawed and vortexed before use and stored at 0 °C during use.

Bis-tris-propane (BTP) buffer used for activity measurements was prepared by dissolving sufficient BTP free base in MilliQ water to give a 50 mM solution, then adjusting the pH to 7.2 with hydrochloric acid. Stock solutions of PEP, A5P and inhibitor were prepared from

monopotassium-PEP (Sigma) and sodium-A5P (Sigma) respectively, in MilliQ water. Inhibitor solutions and 10 mM stock solutions of manganese(II) chloride were similarly prepared in MilliQ water. BTP buffer, PEP, A5P and inhibitor solutions were treated with Chelex® resin for one hour, filtered through a 0.45 μM membrane and stored at 4 °C until use. Stock solutions of manganese(II) chloride were filtered through a 0.45 μM membrane and stored at 4 °C until use. Substrate solution concentrations were determined prior to use by the loss of PEP as determined by UV spectrophotometric measures of the absorbance at 232 nm.

Enzyme activity data and inhibition constants were measured by enzyme assay. Curvettes (1 mL) containing PEP, A5P, manganese(II) chloride (for assays with *Afe*KDO8PS) and inhibitor in BTP buffer were incubated at 30 °C (*Nme*KDO8PS) or 37 °C (*Afe*KDO8PS) for 10-15 minutes, initiated by the addition of ~2 μg enzyme, and the initial rate of reaction determined by linear least-squares fitting of the change in absorbance with time. To determine KDO8P synthase kinetic data for each substrate, initial rate data for was collected at a range of concentrations of each substrate, converted to positive values and globally fitted by multivariable non-linear least squares regression using Grafit® to the Michealis-Menten equation:

$$v = \frac{V_{\max}[S]}{K_{\mathrm{m}} + [S]}$$

Where v = intial rate
$V_{\max}$ = maximum rate
$[S]$ = competitive substrate concentration
K_{m} = Michealis constant in the absence of inhibitor

To determine inhibition constants, initial rate data for specified substrate and inhibitor concentrations was collected and fitted by multivariable non-linear least squares regression using Grafit® to the Michealis-Menten equation modified for competitive inhibition:

$$v = \frac{V_{\max}[S]}{K_{\mathrm{m}}\left(1 + \frac{[I]}{K_{\mathrm{i}}}\right) + [S]}$$

Where the variables are as stated above and,
$[I]$ = inhibitor concentration
K_{i} = inhibition constant

6.1.5. Reactions and work-ups

All reactions were carried out under an inert atmosphere of nitrogen unless otherwise stated. Crude organic extractions were dried with magnesium sulfate followed by filtration, unless otherwise stated. Evaporations were carried out on a rotary evaporator under reduced pressure, preferably utilising a water bath of less than 50 °C.

6.1.6. Solvents and reagents

Solvents and reagents were dried by standard methods[181] where required before use. Diethyl ether and tetrahydrofuran were freshly distilled from sodium/benzophenone. Dichloromethane, ethyl acetate and pyridine were freshly distilled from calcium hydride. Methanol and isopropyl alcohol were distilled from calcium hydride and stored over dried 4 Å molecular sieves until needed. Sodium borohydride, *tert*-butyldiphenylsilyl chloride and *tert*-butyldimethylsilyl chloride were obtained from commercial sources, and once opened stored in a desiccator over silica. Benzoyl chloride was purified by dilution with benzene, washing with aqueous sodium bicarbonate and distillation over calcium hydride. Acetyl chloride was dried by refluxing with PCl_5 and distillation. Sodium hydride was obtained from an oil dispersion by washing with hexane or petroleum ether and drying under vacuum. Dimethylsulfoxide (DMSO) was dried azeotropically by distilling out ~25 % of the volume and discarding. The remaining DMSO was distilled and storing over dried 4 Å molecular sieves until use. Oxalyl chloride was stored frozen at -20 °C. Dess-Martin periodinane (DMP) was prepared from the oxidation of 2-iodobenzoic acid with Oxone® to give iodoxybenzoic acid (IBX),[182] which was acetylated with hot acetic anhydride and p-toluenesulfonic acid to give DMP,[143] which was filtered under nitrogen and stored at -20 °C under nitrogen until use. Methanesulfonyl chloride was distilled from P_2O_5 under vacuum. Triphenylphosphine dibromide was synthesised by bromination of triphenylphosphine in dichloromethane.[154] The solid formed was filtered, washed with hexane and dried under vacuum. Isopropyl dichloroacetate was obtained from Scott Walker[183] or synthesised from the esterification of dichloroacetic acid using isopropyl alcohol and concentrated sulfuric acid. The reagent was stored at 4 °C until use. TBAF was obtained from commercial sources as a 1 M solution in tetrahydrofuran and stored under nitrogen at all times. Meta-chloroperbenzoic acid was recrystallised from dichloromethane and stored at 4 °C until needed. Silver(I) oxide was prepared fresh from 1 M sodium hydroxide solution and aqueous

silver nitrate at 80 °C; filtered and washed with boiling ethanol and water, dried under vacuum at 50 °C and stored under nitrogen before use. Commercial DOWEX resin was washed well with 1.2 M hydrochloric acid until the filtrate ran colourless; washed with water until the filtrate ran neutral as detected by pH paper, and air dried before use. All other reagents were obtained from commercial sources, and used as received.

6.1.7. NMR spectroscopy

NMR spectroscopy was carried out at the Institute of Fundamental Sciences at Massey University, Palmerston North on a Bruker Avance® 400 MHz NMR spectrometer utilising a quad-nuclei $^{1}H/^{13}C/^{19}F/^{31}P$ detection probe; or at the Department of Chemistry, University of Canterbury, Christchurch on a Varian UNITY 300 MHz or Varian INOVA 500 MHz NMR spectrometer, utilising a variable temperature direct broadband or inverse $^{1}H/^{13}C$ probe respectively. ^{1}H and ^{13}C spectra are referenced to $CHCl_3$, TMS or another solvent standard; ^{31}P spectra are referenced to external 85% phosphoric acid.

6.1.8. Mass spectrometry

High-resolution mass spectroscopy was carried by the Department of Chemistry, University of Canterbury on either a Micromass LCT spectrometer or Bruker maXis™ 3G Ultra High Resolution Time of Flight tandem mass spectrometer (positive and negative ion electrospray techniques). High resolution mass spectroscopic data (HRMS) refers to positive electrospray data unless otherwise stated.

6.1.9. UV-visible spectrometry

UV-visible spectrophotometry was carried out on a Varian Cary® One UV-visible spectrophotometer in stoppered quartz cells (UV) or plastic cells (visible). The temperature was continuously controlled at 298 K unless otherwise stated by the use of a jacketed multicell holder and external Varian Peltier temperature controller filled with either water or ethylene glycol.

6.1.10. Lanzetta phosphate assay for detection of products

The Lanzetta reagent was prepared fresh prior to use by the following preparation:

3 parts 0.045 % w/v malachite green chloride in water (freshly prepared),
1 part 4.2 % w/v ammonium molybdate in 4M HCl,
0.1 parts 1.5 % v/v Triton X-100

The reactions were mixed in the dark and stirred for 30 minutes before filtering through a 0.45 μM filter before use. For qualitative detection of anion exchange products, 25 μL of Lanzetta reagent was added to 150 μL of sample and incubated for 30 minutes. The change in absorbance due to organic phosphate cleavage in an acidic environment was detected visually over a white surface. For quantitative analysis of inhibitor solutions, 300 μL of sample is mixed with 10 μL of calf alkaline phosphatase solution (10 units/mL, in 4 mM $MgCl_2$) and incubated for three hours. A 100 μL digest sample was then mixed with 700 μL of Lanzetta reagent and incubated for 30 minutes. The absorbance was determined at 630 nm and compared to the absorbance values from a series of known standards (0-100 μM) in order to determine the inorganic phosphate concentration in the digested inhibitor samples.

6.1.11. Computational methods

All protein structures were drawn from files downloaded from the Protein Data Bank and drawn using the PyMol Molecular Graphics System.

Computational docking studies were undertaken by Wanting Jiao.

Inhibitor molecules were built in Maestro and minimized with MacroModel. A conformational search was undertaken and the low energy conformers selected with Xcluster, based on the atomic RMSD of heavy atoms in the molecule, for modelling into the KDO8P synthase active site.

The KDO8P synthase receptor was prepared from chain A of the *A. aeolicus* KDO8P synthase structure 1FWW. The receptor was prepared *via* the following procedure;

1. Import crystal structure of KDO8PS (PDB 1FWW)
2. Delete all water molecules except water coordinated to the metal ion, HOH 3194 and HOH 3211.

3. Correct bond order of PEP in both chains, add -1 charges to the carboxylic acid group and the phosphate group on PEP. The residue PEP is left in the active site at this stage, so that the residues interacting with PEP are oriented correctly during minimization and refinement of the receptor. The substrate A5P in both chains in the crystal structure is deleted. Covalent bonds to the metal ion are deleted. MacroModel is unable to model Cd^{2+} ion, which is the active site metal ion present in the crystal structure, therefore, this ion is changed to a Mn^{2+} ion for modelling purposes.
4. Add hydrogen atoms to all appropriate positions.
5. Atom type of the P atom in PEP phosphate is changed to P5 for pentavalent phosphorus as in the Macromodel atom typing system.
6. Minimization of the corrected KDO8PS receptor structure. The residues within 5 Å of the active site Mn^{2+} ion in chain A, and all residues in chain B except Arg2106, Gln2107, Asn2136 and Lys2140 are frozen during the minimization.
7. Refine minimized structure.
8. Delete PEP and water molecules in the active site in both chains.

The centre of the grid is defined as the centroid of residues within 5 Å of the PEP and A5P molecule in the original crystal structure (residues 1101, 1041, 1043, 1046, 1048, 1049, 1050, 1051, 1054, 1081, 1099, 1100, 1101, 1102, 1103, 1124, 1127, 1154, 1182, 1185, 1188, 1191, 1195, 1196, 1197, 1220, 1222, 1233, 1270 and 2106 from chain B). The vad der Waals radii of the active site atoms are not scaled, while a scale factor of 0.80 is applied to the van der Waals radii of the inhibitor atoms. The side chains of residues within 5 Å of the docked ligand are optimized, with an additional optimization for side chain of Arg2106 from chain B.

Induced Docking Fit (IDF) scores are relative numbers associated with the overall stability of the docked molecule in the enzyme active site. They are used to find the most stable conformer of the molecule in the enzyme active site from the number of confirmations produced during computational docking.

6.2. Experimental procedures

6.2.1. Experimental for Chapter 2

Purification of KDO8P synthase from *N. meningitidis*

Overnight precultures of *E. coli* BL21(DE3) cells containing pT7-7-Nme*kdsA* were grown in 50 mL Luria Bertani (LB) broth supplemented with ampicillin (0.1 mg mL^{-1}) and used the following day to inoculate a 1 L LB broth supplemented with ampicillin (0.1 mg mL^{-1}). The culture was grown at 37 °C to an OD_{600} of 0.734 whereupon IPTG was added (final concentration 1 mM). The culture was grown for a further four hours then harvested by centrifugation (14000 G, 30 minutes, 4 °C). Cell pellet was resuspended in 10 mL MilliQ water and centrifuged (12000 G, 5 minutes, 4 °C) before being stored at -80 °C overnight. Cell pellet was resuspended in 10 mL cold lysis buffer (10 mM BTP, 1mM EDTA, 0.2 M potassium chloride, pH 7.5) and lysed by sonication on ice (3 x 4 minutes at 80 % pulse, 1 x 2 minutes at 40 % pulse). Cell debris was removed by centrifugation (24000 G, 30 minutes, 4 °C) and the supernatant diluted five-fold with Buffer A (10 mM BTP, 1 mM EDTA, pH 7.5). The dilute protein sample was loaded onto an AEC column in two separate runs (20 mL and 30 mL, 4 °C) pre-equilibrated with Buffer A. After washing the column with two column volumes (CV) of Buffer A, a linear sodium chloride gradient (0.1 to 0.2 M, 7 CV, 2 mL fractions) was used to elute the *N. meningitidis* KDO8P synthase protein. Fractions were analysed by SDS-PAGE using Laemmli's[179] buffer system under denaturing and reducing conditions. Fractions determined to contain *Nme*KDO8PS were pooled (49 mL) and solid ammonium sulfate was added (final concentration 1 mM). The protein was loaded onto an HIC column pre-equilibrated with Buffer B (10 mM BTP, 1 mM EDTA, 1 M $(NH_4)_2SO_4$, pH 7.5). The column was washed with three and a half CV of Buffer B, and a linear gradient of 0.7 to 0 M $(NH_4)_2SO_4$ (13 CV) was applied to the column. The KDO8P synthase protein was eluted from 0.61 to 0.42 M $(NH_4)_2SO_4$ (1 mL fractions, 3.5 CV). The fractions were analysed by SDS-PAGE and those determined to contain KDO8P synthase were pooled (26 mL) and loaded onto SEC column pre-equilibrated with Buffer C (50 mM BTP, 50 mM sodium chloride, pH 7.5) in two separate runs (13 mL each). The protein was eluted in 340 mL Buffer C in 2 mL fractions, and those fractions analysed by SDS-PAGE. Those fractions determined to contain KDO8P synthase were pooled and concentrated using a 20 mL Vivaspin 10 kDa MWCO concentrator (Sartorius Stedim). The protein was divided into 50

μL aliquots and flash frozen in liquid nitrogen before storage at -80 °C. Protein concentration was determined by the Bradford method[180] using bovine serum albumin as a standard.

Purification of KDO8P synthase from *A. ferrooxidans*

Overnight precultures of *E. coli* BL21(DE3) cells containing pT7-7-Afe*kdsA* were grown in 50 mL LB broth supplemented with ampicillin (0.1 mg mL^{-1}) and used the following day to inoculate a 1 L LB broth supplemented with ampicillin (0.1 mg mL^{-1}). The culture was grown at 37 °C to an OD_{600} of 0.652 whereupon IPTG was added to give a final concentration of 1 mM. The large culture was grown for four hours and harvested by centrifugation (14000 G, 30 minutes, 4 °C). The cell pellet was resuspended in MilliQ water (10 mL) and centrifuged again (12000 G, 5 minutes, 4 °C) before storage of the cell pellet at -80 °C overnight. The cell pellet was responded in 10 mL cold lysis buffer (10 mM BTP, 1mM EDTA, 0.2 M potassium chloride, pH 7.5) and lysed by sonication on ice (3 x 4 minutes at 80 % pulse, 1 x 2 minutes at 40 % pulse). Cell debris was removed by centrifugation (24000 G, 30 minutes, 4 °C) and the supernatant was diluted four-fold with Buffer A (10 mM BTP, 1 mM EDTA, pH 7.5) before being loaded onto the AEC column in two separate runs (20 mL and 20 mL, 4 °C). After washing the column with two column volumes (CV) of Buffer A, a linear sodium chloride gradient (0.14 to 0.38 M, 7 CV, 2 mL fractions) was used to elute the *A. ferrooxidans* KDO8P synthase protein. The fractions were analysed by SDS-PAGE and those fractions containing the KDO8P synthase protein had ammonium sulfate added to give a final concentration of 1 M and were loaded onto an HIC column pre-equilibrated with Buffer B (10 mM BTP, 1 mM EDTA, 1 M $(NH_4)_2SO_4$, pH 7.5). The column was washed with 2 CV of Buffer B, and a linear gradient of 0.5 to 0 M $(NH_4)_2SO_4$ (8.5 CV) was applied to the column. The KDO8P synthase protein was eluted from 0.3 to 0.15 M $(NH_4)_2SO_4$ (1 mL fractions, 3 CV). The fractions were analysed by SDS-PAGE and those determined to contain KDO8P synthase were pooled (26 mL), concentrated using a 20 mL Vivaspin 10 kDa MWCO concentrator (Sartorius Stedim) and exchanged into a low salt buffer (10 mM BTP, 1 mM EDTA, pH 7.5) to give 1.25 mL of concentrated protein. This sample was loaded onto a SEC column pre-equilibrated with Buffer C (50 mM BTP, 50 mM sodium chloride, pH 7.5). The protein was eluted in 48 mL Buffer C in 1 mL fractions, and those fractions analysed by SDS-PAGE. Those fractions determined to contain KDO8P synthase were pooled, and concentrated using a 20 mL Vivaspin 10 kDa MWCO

concentrator (Sartorius Stedim). The protein was divided into 50 µL aliquots and flash frozen in liquid nitrogen before storage at -80 °C. Protein concentration was determined by the Bradford method[180] using bovine serum albumin as a standard.

6.2.2. Experimental for Chapter 4

(4S)-6-(2,2-Dimethyl-1,3-dioxolan-4-yl)-2,2-dimethyltetrahydrofuro[3,4-d][1,3]dioxol-4-ol *via* boron-trifluoride diethyl etherate catalysis

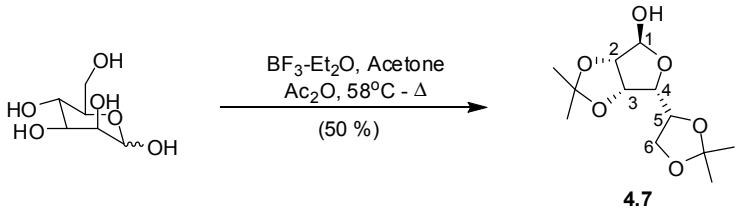

4.7

Boron trifluoride diethyl etherate (10 µL, 0.079 mmol) was added to D-mannose (1.0859 g, 6.03 mmol) stirring in acetone (15 mL). The solution was warmed to 58 °C and acetic anhydride (850 µL, 9.01 mmol) was added dropwise over 5 minutes. The solution was heated to reflux and stirred for five hours before being quenched with 25 % w/w aqueous sodium hydroxide (20 mL). The volatile components were evaporated and the aqueous phase extracted with chloroform (2 x 100 mL). The combined organic phase was washed with water (50 mL), brine (50 mL), dried over magnesium sulfate and evaporated to give an oil which was subjected to flash chromatography (20 % ethyl acetate in hexane) to give furanose 4.7 as a white solid (0.7807 g, 50 %). R_f (75 % ethyl acetate/petroleum ether): 0.74; ^{1}H NMR (500 MHz, $CDCl_3$): δ ppm 5.37 (s, 1H, H1), 4.80 (dd, J = 5.9, 3.7 Hz, 1H, H3), 4.60 (d, J = 5.9 Hz, 1H, H2), 4.42-4.28 (m, 1H, H5), 4.17 (dd, J = 7.1, 3.7 Hz, 1H, H4), 4.09-4.03 (m, 2H, H6), 3.40 (br, 1H, OH), 1.46 (s, 3H, C(C$\underline{H}_3$)$_2$), 1.45 (s, 3H, C(C$\underline{H}_3$)$_2$), 1.37 (s, 3H, C(C$\underline{H}_3$)$_2$), 1.32 (s, 3H, C(C$\underline{H}_3$)$_2$); ^{13}C NMR (126 MHz, $CDCl_3$) δ ppm 112.8 ($\underline{C}$(CH$_3$)$_2$), 109.3 ($\underline{C}$(CH$_3$)$_2$), 101.4 (C1), 80.3 (C4), 85.7 (C2), 79.8 (C3), 73.5 (C5), 66.7 (C6), 27.0 (C($\underline{C}$H$_3$)$_2$), 26.0 (C($\underline{C}$H$_3$)$_2$), 25.4 (C($\underline{C}$H$_3$)$_2$), 24.7 (C($\underline{C}$H$_3$)$_2$); HRMS required for $C_{12}H_{20}NaO_6$: 283.1158, Found: 283.1146.

(4S)-6-(2,2-Dimethyl-1,3-dioxolan-4-yl)-2,2-dimethyltetrahydrofuro[3,4-d][1,3]dioxol-4-ol *via* toluenesulfonic acid mono hydrate catalysis

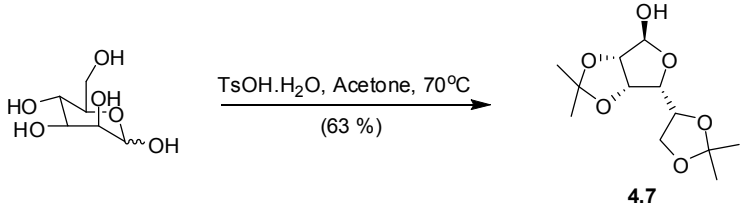

4.7

Toluenesulfonic acid mono hydrate (31.8 mg, 0.167 mmol) was added to D-mannose (1.4735 g, 8.18 mmol) stirring in acetone (50 mL). After 23 hours at 70 °C the pH of the solution was adjusted to 7 with saturated sodium bicarbonate solution, and then filtered. The filtrate was washed with acetone (200 mL) and the organic solvents evaporated to give an off-white solid that was dissolved in diethyl ether and filtered before the volatile solvents were evaporated to give a white solid, that was recrystallised from petroleum ether to give furanose 4.7 as a white solid (1.3368 g, 63 %).

Spectral data as above for (4S)-6-(2,2-Dimethyl-1,3-dioxolan-4-yl)-2,2-dimethyltetrahydrofuro[3,4-d][1,3]dioxol-4-ol *via* boron-trifluoride diethyl etherate catalysis.

(*R*)-((*R*)-2,2-Dimethyl-1,3-dioxolan-4-yl)((4*S*,5*R*)-5-(hydroxymethyl)-2,2-dimethyl-1,3-dioxolan-4-yl)methanol

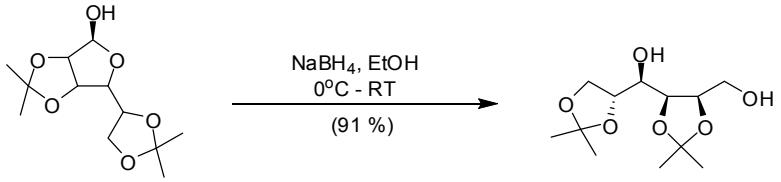

4.7 **4.9**

Sodium borohydride (0.1390 g, 3.67 mmol) was added portion wise to furanose 4.7 (0.4786 g, 1.84 mmol) in ethanol (5 mL) cooled to 0 °C. The reaction mixture was allowed to warm to room temperature and stirred for 21 hours before it was neutralised with acetic acid and the volatile components evaporated under reduced pressure. The resin was redissolved in ethyl acetate (50 mL), washed with brine (15 mL) and the aqueous phase extracted with ethyl acetate (2 x 50 mL). The combined organic phase was dried over anhydrous magnesium sulfate and evaporated to give an oil that was subjected to flash chromatography to give diacetonide 4.9 as a white solid (0.4395 g, 91 %). R_f (75 % ethyl acetate/petroleum ether):

0.41; ^{1}H NMR (500 MHz, $CDCl_3$) δ ppm 4.35 (dd, *J* = 7.3, 1.4 Hz, 1H, H4), 4.27 (td, *J* = 7.3, 4.4 Hz, 1H, H5), 4.08 (dd, *J* = 7.9, 6.0 Hz, 1H, H3), 4.06-4.02 (m, 1H, H1), 3.98 (dd, *J* = 7.9, 4.9 Hz, 1H, H1'), 3.87 (dd, *J* = 12.2, 4.4 Hz, 1H, H6), 3.79 (dd, *J* = 12.2, 4.4 Hz, 1H, H6'), 3.55 (dd, *J* = 7.9, 1.4 Hz, 1H, H2), 3.17 (s, 2H, OH), 1.48 (s, 3H, $C(C\underline{H}_3)_2$), 1.37 (s, 3H, $C(C\underline{H}_3)_2$), 1.36 (s, 3H, $C(C\underline{H}_3)_2$), 1.32 (s, 3H, $C(C\underline{H}_3)_2$); ^{13}C NMR (126 MHz, $CDCl_3$) δ ppm 109.2 ($\underline{C}(CH_3)_2$), 108.1 ($\underline{C}(CH_3)_2$), 76.9 (C4), 75.8 (C5), 75.6 (C3), 70.1 (C2), 67.1 (C1), 60.5 (C6), 26.6 ($C(\underline{C}H_3)_2$), 26.5 ($C(\underline{C}H_3)_2$), 25.1 ($C(\underline{C}H_3)_2$), 24.7 ($C(\underline{C}H_3)_2$); HRMS required for $C_{12}H_{22}NaO_6$: 285.1309, Found: 285.1313.

((4*R*,5*S*)-5-((*R*)-((*R*)-2,2-Dimethyl-1,3-dioxolan-4-yl)(hydroxy)methyl)-2,2-dimethyl-1,3-dioxolan-4-yl)methyl benzoate

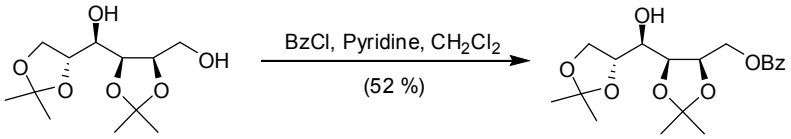

4.9 **4.10**

Benzoyl chloride (700 µL, 6.03 mmol) was added to diacetonide 4.9 (1.501 g, 5.43 mmol) in pyridine (10 mL) and dichloromethane (10 mL) at 0 °C and left to warm to room temperature. The reaction was stirred for 17 hours and quenched with ethyl acetate (200 mL). The organic phase was washed with saturated aqueous copper sulphate (2 x 100 mL) and water (100 mL) before being dried over anhydrous magnesium sulfate and evaporated to give an oil. This crude product was subjected to flash chromatography (25 % ethyl acetate/ petroleum ether) to give a clear oil (1.0748 g, 52 %). R_f (80 % ethyl acetate/petroleum ether): 0.62; ^{1}H NMR (500 MHz, $CDCl_3$) δ ppm 8.08-8.03 (m, 2H, $OCOPh_b$), 7.58-7.52 (m, 1H, $OCOPh_d$), 7.45-7.40 (m, 1H, $OCOPh_c$), 4.68-4.55 (m, 3H, H6 and H4), 4.50-4.46 (m, 1H, H5), 4.15-4.09 (m, 1H, H1'), 4.07-4.01 (m, 2H, H1 and H2), 3.66 (dd, *J* = 7.8, 1.6 Hz, 1H, H3), 1.53 (s, 3H, $C(C\underline{H}_3)_2$), 1.41 (s, 3H, $C(C\underline{H}_3)_2$), 1.40 (s, 3H, $C(C\underline{H}_3)_2$), 1.35 (s, 3H, $C(C\underline{H}_3)_2$); ^{13}C NMR (126 MHz, $CDCl_3$) δ ppm 166.2 ($O\underline{C}OPh$), 133.1 ($OCO\underline{Ph}_a$), 130.1 ($OCO\underline{Ph}_d$), 129.7 ($OCO\underline{Ph}_b$), 128.3 ($OCO\underline{Ph}_c$), 109.5 ($\underline{C}(CH_3)_2$), 108.8 ($\underline{C}(CH_3)_2$), 76.1 (C2), 75.4 (C5), 75.0 (C4), 70.2 (C3), 67.1 (C1), 64.2 (C6), 26.8 ($C(\underline{C}H_3)_2$), 26.7 ($C(\underline{C}H_3)_2$), 25.2 ($C(\underline{C}H_3)_2$), 24.6 ($C(\underline{C}H_3)_2$); HRMS required for $C_{19}H_{26}NaO_7$: 389.1571, Found: 389.1567.

(*S*)-(1,3-Dithian-2-yl)((4*R*,4'*R*,5*R*)-2,2,2',2'-tetramethyl-4,4'-bi(1,3-dioxolan)-5-yl)methanol

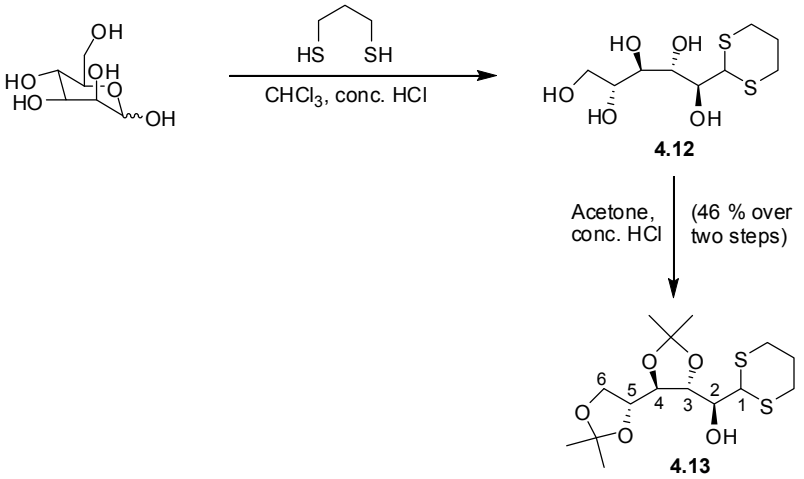

Propandithiol (2 mL, 19.9 mmol) was added to D-mannose (3.0921 g, 17.2 mmol) in chloroform (3 mL). Concentrated hydrochloric acid (1.5 mL) was added and the mixture stirred vigorously for 18 hours. The solid formed was transferred to another flask with water (75 mL) and adjusted to pH 8 with aqueous ammonia. The liquids were evaporated under reduced pressure, and co-distilled with n-butanol (180 mL) and toluene (100 mL) to give a brown solid (4.98 g). Hydrochloric acid (6.0 M, 10 mL) was added to this crude product dissolved in acetone (500 mL). The solution was stirred for 24 hours and neutralised with aqueous ammonia. The liquids were evaporated and co-distilled with toluene (800 mL) and the solid redissolved in chloroform (500 mL) and filtered before the chloroform was evaporated to give a white solid (7.117 g). The crude product was subjected to flash chromatography (50 % ethyl acetate in petroleum ether) to give diacetonide 4.13 as a white solid (2.741 g, 46 % over two steps from D-mannose). R_f (33 % ethyl acetate/hexane): 0.66; ^{1}H NMR (500 MHz, $CDCl_3$): δ ppm 4.28 (d, *J* = 2.8 Hz, 1H, H1), 4.14 (dd, *J* = 8.7, 5.7 Hz, 1H, H6'), 4.05 (dd, J = 8.3 Hz, 7.3 Hz, 1H, H3), 4.02 (dd, J = 5.7, 2.8 Hz, 1H, H5), 3.94 (dd, J = 8.7, 5.7 Hz, 1H, H6), 3.89 (dd, J = 8.3, 2.8 Hz, 1H, H2), 3.73 (dd, *J* = 8.3, 7.3 Hz, 1H, H4), 2.98 (ddd, *J* = 13.9, 6.5, 2.9 Hz, 2H, (SC$\underline{H}_2$)$_2$CH$_2$), 2.86 (ddd, *J* = 13.9, 10.1, 2.9 Hz, 1H, (SC$\underline{H}_2$)$_2$CH$_2$), 2.79 (ddd, *J* = 13.9, 10.1, 2.9 Hz, 1H, (SC$\underline{H}_2$)$_2$CH$_2$), 2.11-2.02 (m, 1H, (SCH$_2$)$_2$C$\underline{H}_2$), 2.01-1.91 (m, 1H, (SCH$_2$)$_2$C$\underline{H}_2$), 1.39 (s, 3H, C(C$\underline{H}_3$)$_2$), 1.33 (s, 6H, C(C$\underline{H}_3$)$_2$), 1.31 (s, 3H, C(C$\underline{H}_2$)$_2$); ^{13}C NMR (126 MHz, $CDCl_3$): δ ppm 110.4 (C(CH$_3$)$_2$), 109.8 (C(CH$_3$)$_2$), 80.8 (C2), 79.8 (C5), 76.6 (C4), 76.2 (C2), 67.2 (C1), 49.2 (C6), 29.9 ((S$\underline{C}$H$_2$)$_2$CH$_2$), 29.1 ((S$\underline{C}$H$_2$)$_2$CH$_2$), 26.8 (C($\underline{C}$H$_3$)$_2$), 26.8 (C($\underline{C}$H$_3$)$_2$), 26.3 (C($\underline{C}$H$_3$)$_2$), 26.1

($S(CH_2)_2\underline{C}H_2$), 25.1 ($C(\underline{C}H_3)_2$); HRMS required for $C_{15}H_{26}NaO_5S_2$: 373.1114, Found: 373.1120.

(*S*)-(1,3-Dithian-2-yl)((4R,4'*R*,5*R*)-2,2,2',2'-tetramethyl-4,4'-bi(1,3-dioxolan)-5-yl)methanol

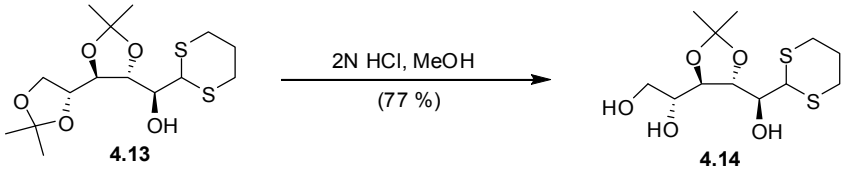

Hydrochloric acid (2.0 M, 5 mL) was added to diacetonide 4.13 (5.335 g, 15.2 mmol) dissolved in methanol (800 mL), and the reaction stirred for 23 hours before the pH of the solution was adjusted to 7 with aqueous ammonia and the liquids evaporated under reduced pressure. The solid formed was dissolved in chloroform (400 mL), filtered, and the chloroform evaporated under reduced pressure to give a white solid (4.6928 g) that was subjected to flash chromatography (20 % petroleum ether/ethyl acetate) to give monoacetonide 4.14 as a white solid (3.6523 g, 77 %). R_f (20 % ethyl acetate/hexane): 0.39; ^{1}H NMR (500 MHz, $CDCl_3$) δ ppm 4.38 (d, *J* = 1.8 Hz, H1), 4.36 (s, 1H, OH), 4.10 (dd, *J* = 8.8, 7.3 Hz, 1H, H3), 3.87 (dd, *J* = 7.3, 7.3 Hz, 1H, H4), 3.86 (dd, *J* = 8.8, 1.8 Hz, 1H, H2), 3.82 (dd, *J* = 11.2, 2.6 Hz, 1H, H6), 3.71 (dd, J = 5.2, 2.6 Hz, 1H, H5), 3.66 (dd, J = 11.2, 5.2 Hz, 1H, H6), 2.99-2.86 (m, 3H, $(SC\underline{H}_2)_2CH_2$), 2.82 (dd, J = 13.8, 10.1, 2.3 Hz, 1H, $(SC\underline{H}_2)_2CH_2$), 2.10-2.02 (m, 1H, $(SCH_2)_2C\underline{H}_2$), 1.96-1.85 (m, 1H, $(SCH_2)_2C\underline{H}_2$), 1.35 (s, 3H, $C(C\underline{H}_3)_2$), 1.34 (s, 3H, $C(C\underline{H}_3)_2$); ^{13}C NMR (126 MHz, $CDCl_3$) δ ppm 109.66 ($\underline{C}(CH_3)_2$), 79.61 (C5), 78.89 (C3), 76.63 (C2), 72.68 (C4), 63.73 (C6), 50.29 (C1), 30.19 ($(S\underline{C}H_2)_2CH_2$), 29.33 ($(S\underline{C}H_2)_2CH_2$), 26.84 ($(SCH_2)_2\underline{C}H_2$), 26.78 ($C(\underline{C}H_3)_2$), 25.90 ($C(\underline{C}H_3)_2$); HRMS required for $C_{15}H_{27}O_5S_2$: 311.0981, Found: 311.0995.

(*R*)-1-((4*R*,5*R*)-5-((*S*)-(1,3-Dithian-2-yl)(hydroxy)methyl)-2,2-dimethyl-1,3-dioxolan-4-yl)-2-(tert-butyldiphenylsilyloxy)ethanol

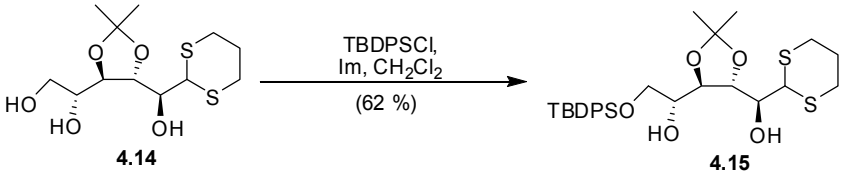

4.14 4.15

Tert-butyldiphenylsilyl chloride (3.97 mL, 15.3 mmol) was added drop-wise to imidazole (2.4134 g, 35.4 mmol) and monoacetonide 4.14 (4.4073. 14.2 mmol) dissolved in dichloromethane (140 mL) at 0 °C. The mixture was allowed to warm to room temperature and stirred for 19 hours before being quenched with chloroform (600 mL) and the organic phase washed with water (600 mL). The aqueous phase was extracted with chloroform (2 x 300 mL) and the combined organic fractions washed with brine (400 mL) and dried over magnesium sulfate and evaporated under reduced pressure to give an oil that was subjected to flash chromatography (20 % ethyl acetate/ petroleum ether) to give silyl ether 4.15 as a clear oil (4.8423 g, 62 %). R_f (20 % ethyl acetate/hexane): 0.36; ^{1}H NMR (500 MHz, $CDCl_3$) δ ppm: 7.65 (d, J = 6.9 Hz, 4H, OSi($\underline{Ph}_b$)$_2$C(CH_3)$_3$), 7.43 (dd, J = 7.1, 7.1 Hz, 4H, OSi($\underline{Ph}_c$)$_2$C(CH_3)$_3$), 7.38 (t, J = 7.1 Hz, 2H, OSi($\underline{Ph}_d$)$_2$C(CH_3)$_3$), 4.33 (d, J = 2.0 Hz, 1H, H1), 4.15-4.08 (m, 1H, H3), 3.96-3.89 (m, 2H, H6' and H2), 3.82 (dd, J = 7.3, 7.3 Hz, 1H, H4), 3.77 (dd, J = 10.3, 6.3 Hz, 1H, H6), 3.71 (dd, J = 7.3, 2.7 Hz, 1H, H5), 3.09-2.99 (m, 2H, (SC$\underline{H}_2$)$_2$CH$_2$), 3.31 (s, 1H, OH), 2.92-2.85 (m, 1H, (SC$\underline{H}_2$)$_2$CH$_2$), 2.83-2.76 (m, 1H, (SC$\underline{H}_2$)$_2$CH$_2$), 2.12-1.94 (m, 2H, (SCH2)$_2$C$\underline{H}_2$), 1.33 (s, 3H, C(C$\underline{H}_3$)$_2$), 1.30 (s, 3H, C(C$\underline{H}_3$)$_2$), 1.06 (s, 9H, OSi(Ph)$_2$C(C$\underline{H}_3$)$_3$); ^{13}C NMR (126 MHz, $CDCl_3$) δ ppm 135.5, 135.5 (OSi($\underline{Ph}_b$)$_2$C(CH_3)$_3$), 132.7, 132.7 (OSi($\underline{Ph}_a$)$_2$C(CH_3)$_3$), 129.8 (OSi($\underline{Ph}_c$)$_2$C(CH_3)$_3$), 127.7, 127.7 (OSi($\underline{Ph}_d$)$_2$C(CH_3)$_3$), 80.1 (s, C2), 79.1 (s, C4), 77.3 (s, C3), 72.9 (s, C5), 65.2 (s,C6), 49.0 (s, C1), 29.7 (s, (S$\underline{C}H_2$)$_2$CH$_2$), 29.0 (s, (S$\underline{C}H_2$)$_2$CH$_2$), 26.8 (s, OSi(Ph)$_2$C($\underline{C}H_3$)$_3$), 26.7 (s, C($\underline{C}H_3$)$_2$), 26.7 (s, $\underline{C}$(CH_3)$_2$), 25.9 (s, (SCH$_2$)$_2$C$\underline{H}_2$), 19.2 (s, OSi(Ph)$_2\underline{C}$(CH_3)$_3$); HRMS required for $C_{28}H_{40}NaO_5S_2Si$: 571.1984, Found: 571.1979.

(*R*)-1-((4*R*,5*S*)-5-((S)-Acetoxy(1,3-dithian-2-yl)methyl)-2,2-dimethyl-1,3-dioxolan-4-yl)-2-(tert-butyldiphenylsilyloxy)ethyl acetate

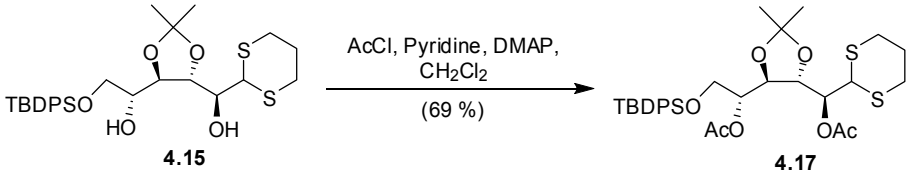

Acetyl chloride (1.7 mL, 23.9 mmol) was added drop-wise to silyl ether 4.15 (3.3033 g, 6.03 mmol), pyridine (1.95 mL, 24.2 mmol) and DMAP (0.2947 g, 2.41 mmol) stirring in dichloromethane (40 mL) at 0 °C. The reaction was refluxed for 20 hours before being quenched with dichloromethane (350 mL). The organic phase was washed with water (200 mL) and the aqueous phase extracted with dichloromethane (2 x 250 mL). The organic phase was dried over magnesium sulfate and the organic solvents evaporated under reduced pressure to give an oil that was subjected to flash chromatography (33 % ethyl acetate/ petroleum ether) to give protected sugar 4.17 as a clear oil (2.615 g, 69 %). R_f (25 % ethyl acetate/petroleum ether): 0.60; ^{1}H NMR (500 MHz, $CDCl_3$) δ ppm 7.66 (td, J = 8.1, 1.6 Hz, 2H, OSi(Ph$_d$)$_2$C(CH$_3$)$_3$), 7.45-7.35 (m, 10H, OSi(Ph$_{b-d}$)$_2$C(CH$_3$)$_3$), 5.43 (dd, J = 6.2, 6.2 Hz, 1H, H2), 5.09 (dt, J = 6.2, 3.4 Hz, 1H, H5), 4.45 (dd, J = 6.2, 6.2 Hz, 1H, H3), 4.29 (dd, J = 6.2, 6.2 Hz, 1H, H4), 4.18 (d, J = 6.2 Hz, 1H, H1), 3.91 (dd, J = 11.3, 3.4 Hz, 1H, H6), 3.85 (dd, J = 11.3, 6.2 Hz, 1H, H6'), 2.93 (ddt, J = 13.9, 7.5, 2.9 Hz, 2H, SCH$_2$)$_2$CH$_2$), 2.80 (ddd, J = 13.9, 8.9, 2.9 Hz, 1H, SCH$_2$)$_2$CH$_2$), 2.73 (ddd, J = 13.9, 8.9, 2.9 Hz, 1H, SCH$_2$)$_2$CH$_2$), 2.13 (s, 3H, OCOCH$_3$), 2.09 (s, 3H, OCOCH$_3$), 2.09-1.92 (m, 2H, (SCH$_2$)$_2$CH$_2$), 1.38 (s, 3H, C(CH$_3$)$_2$), 1.33 (s, 3H, C(CH$_3$)$_2$), 1.04 (s, 9H, OSi(Ph)$_2$C(CH$_3$)$_3$); ^{13}C NMR (126 MHz, $CDCl_3$) δ ppm 170.2 (OCOCH$_3$), 170.0 (OCOCH$_3$), 135.5 (OSi(Ph$_d$)$_2$C(CH$_3$)$_3$), 133.1 (OSi(Ph$_a$)$_2$C(CH$_3$)$_3$), 129.7, 129.7 (OSi(Ph$_{b,c}$)$_2$C(CH$_3$)$_3$), 127.6, 127.6 (OSi(Ph$_{b,c}$)$_2$C(CH$_3$)$_3$), 77.2 (C3), 76.6 (C4), 74.4 (C5), 73.2 (C2), 62.3 (C6), 46.1 (C1), 28.4 ((SCH$_2$)$_2$CH$_2$), 28.3 ((SCH$_2$)$_2$CH$_2$), 27.2 (C(CH$_3$)$_2$), 27.1 (C(CH$_3$)$_2$), 26.6 (OSi(Ph)$_2$C(CH$_3$)$_3$), 25.5 ((SCH$_2$)$_2$CH$_2$), 21.1 (OCOCH$_3$), 20.8 (OCOCH$_3$), 19.2 (OSi(Ph)$_2$C(CH$_3$)$_3$); HRMS required for $C_{32}H_{44}NaO_7S_2Si$: 655.2199, Found: 655.2190.

6-(Benzyloxy)hexan-1-ol[140]

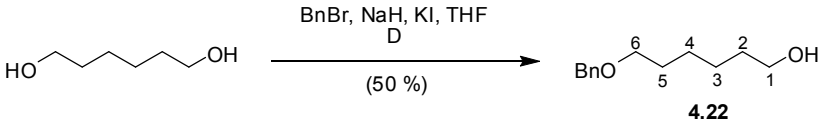

4.22

To a stirred solution of sodium hydride (0.5700g, 23.8 mmol) in dry tetrahydrofuran (30 mL) was added 1,6-hexandiol (4.011 g, 33.9 mmol) in dry tetrahydrofuran (20 mL), potassium iodide (0.560 g, 3.37 mmol) and benzyl bromide (2.8 mL, 23.6 mmol). After 24 hours at reflux the solution was quenched with ethyl acetate (125 mL) and water (120 mL). The organic phase was washed with saturated sodium bicarbonate (3 x 100 mL) and the combined aqueous phase extracted with ethyl acetate (3 x 100 mL). The combined organic phase was washed with brine (150 mL), dried over anhydrous magnesium sulfate and evaporated to give an oil which was subjected to flash chromatography (33 % ethyl acetate/hexane) to give a clear oil (2.446 g, 50 %). R_f (50 % ethyl acetate/hexane): 0.66; ^{1}H NMR (400 MHz, $CDCl_3$) δ ppm 7.37-7.24 (m, 5H), 4.50 (s, 2H), 3.58 (t, J = 6.6 Hz, 2H), 3.47 (t, J = 6.6 Hz, 2H), 1.63 (quin, J = 6.6 Hz, 2H), 1.55 (quin., J = 7.0 Hz, 2H), 1.45-1.30 (m, 4H); ^{13}C NMR (101 MHz, $CDCl_3$) δ ppm 138.4, 128.2, 127.5, 127.3, 72.7, 70.2, 62.4, 32.5, 29.5, 25.8, 25.4.

6-(Benzyloxy)hexanal *via* Swerns oxidation[140]

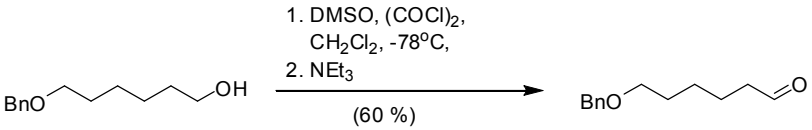

4.22 **4.23**

Dimethylsulfoxide (1.75 mL, 25.7 mmol) was dissolved in dry dichloromethane (56 mL) and cooled to -78 °C before oxalyl chloride (1.05 mL, 12.0 mmol) was added over ten minutes. The reaction was stirred for a further ten minutes before benzyl ester 4.22 (2.172 g, 10.4 mmol) dissolved in dichloromethane (9 mL) was added drop-wise over eight minutes. The reaction was stirred for one hour before triethylamine (7.2 mL, 51.7 mmol) was added and the reaction allowed to warm to room temperature. After one hour the reaction was quenched with diethyl ether (130 mL) and the organic phase washed with saturated aqueous ammonium chloride solution (130 mL). The organic phase was diluted with hexane (300 mL) and washed with saturated aqueous potassium carbonate solution (130 mL), water (130 mL), brine (2 x 130 mL), dried over magnesium sulfate and the organic solvents evaporated to give an oil that was subjected to flash chromatography (15% ethyl acetate/hexane) to give

aldehyde 4.23 (1.293 g, 60 %) as a clear oil. R_f (20 % ethyl acetate/hexane): 0.21; ^{1}H NMR (400 MHz, $CDCl_3$) δ ppm 9.75 (t, *J* = 1.7 Hz, 1H), 7.36-7.24 (m, 1H), 4.49 (s, 2H), 3.47 (t, *J* = 6.5 Hz, 2H), 2.42 (dt, *J* = 7.4, 1.7 Hz, 2H), 1.69-1.59 (m, 4H), 1.47-1.37 (m, 2H); ^{13}C NMR (101 MHz, $CDCl_3$) δ ppm 202.6, 138.5, 128.3, 127.6, 127.5, 72.9, 70.0, 43.8, 29.4, 25.8, 21.8.

6-(Benzyloxy)hexanal *via* Dess-Martin oxidation[140]

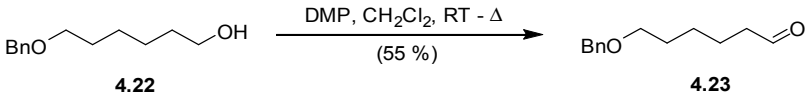

4.22 **4.23**

Benzyl ester 4.22 (1.230 g, 5.90 mmol) was dissolved in dichloromethane (45 mL) and Dess-Martin periodinane (3.633, 8.57 mmol) was added in portions over ten minutes. The reaction was stirred for three hours before a second amount of Dess-Martin periodinane (3.684, 8.69 mmol) was added. The reaction was stirred for 24 hours at room temperature and refluxed a further 20 hours before being quenched with ethyl acetate (250 mL) and saturated aqueous sodium bicarbonate solution (120 mL). The organic phase was washed with saturated aqueous sodium thiosulfate (80 mL), water (250 mL), brine (250 mL), dried over anhydrous magnesium sulfate and the organic solvents evaporated to give an oil that was subjected to flash chromatography to give aldehyde 4.23 (0.670 g, 55 %) as a clear oil.

Spectral data as above for 6-(Benzyloxy)hexanal *via* Swern oxidation.

6-(Benzyloxy)hexylmethanesulfonate[150]

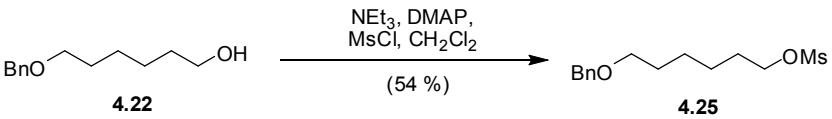

4.22 **4.25**

Methanesulfonyl chloride (80 µL, 1.03 mmol) was added drop-wise over five minutes to a solution of alcohol 4.22 (0.1055 g, 0.51 mmol), 4-dimethylaminopyridine (6.5 mg, 53 µmol) and triethylamine (210 µL, 1.51 mmol) in dichloromethane (1 mL), cooled to 0 °C. The reaction was stirred at 0 °C for 90 minutes before it was quenched with water (15 mL) and the aqueous phase extracted with ethyl acetate (3 x 10 mL). The combined organic phase was washed with brine (15 mL), dried over magnesium sulfate and the organic phase evaporated under reduced pressure to afford an oil. This crude oil was subjected to flash

chromatography to give mesylate 4.25 (72.8 mg, 54 %) as a clear oil. R_f (50 % ethyl acetate/hexane): 0.63; ^{1}H NMR (400 MHz, $CDCl_3$) δ ppm 7.36-7.31 (m, 5H), 4.50 (s, 2H), 4.21 (t, J = 6.5 Hz, 2H), 3.47 (t, J = 6.4 Hz, 2H), 2.98 (s, 3H), 1.48-1.38 (m, 2H), 1.81-1.69 (m, 2H), 1.69-1.56 (m, 2H); ^{13}C NMR (101 MHz, $CDCl_3$) δ ppm 138.5, 128.2, 127.5, 127.4, 72.8, 70.2, 69.8, 37.2, 29.4, 29.0, 25.6, 25.2.

((6-Bromohexyloxy)methyl)benzene *via* phosphorous tribromide bromination[155]

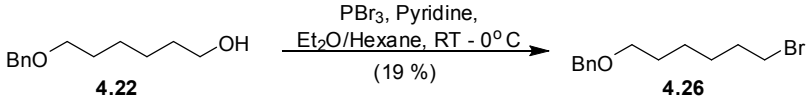

Pyridine (6.5 µL, 0.08 mmol) was added to benzyl ester 4.22 (0.2111 g, 1.01 mmol) stirring in diethyl ether (1.25 mL) and the solution cooled to 0 °C before the addition of phosphorous tribromide (40 µL, 0.41 mmol) dissolved in hexane (0.4 mL) drop-wise over eight minutes. Upon addition of phosphorous tribromide a white precipitate formed. After 150 minutes the reaction was decanted into a 1:1 mixture of water and ice (30 mL) and the precipitate washed with hexane (20 mL). The aqueous phase was extracted with diethyl ether (3 x 10 mL) and the combined organic extracts washed with brine (2 x 20 mL), dried over magnesium sulfate and evaporated under reduced pressure to give an oil that was subjected to flash chromatography (50 % ethyl acetate/hexane) to give bromo ether 4.26 (51.9 mg, 19 %) as a clear oil. R_f (50 % ethyl acetate/hexane): 0.89; ^{1}H NMR (400 MHz, $CDCl_3$) δ ppm 7.37-7.27 (m, 5H), 4.50 (s, 1H), 3.47 (t, J = 6.5 Hz, 2H), 3.39 (t, J = 6.8 Hz, 2H), 1.90-1.80 (m, 2H), 1.65-1.59 (m, 2H), 1.49-1.35 (m, 4H); ^{13}C NMR (101 MHz, $CDCl_3$) δ ppm 138.5, 128.3, 127.6, 127.4, 72.8, 70.1, 33.8, 32.7, 29.5, 27.9, 25.4.

((6-Bromohexyloxy)methyl)benzene *via* triphenylphosphine dibromide bromination[155]

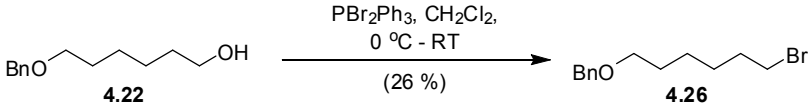

Alcohol 4.22 (0.2545 g, 1.20 mmol in dichloromethane (1 mL) was added to triphenylphosphine dibromide (0.6044 g, 1.43 mmol) dissolved in dichloromethane (2 mL) at 0 °C drop-wise, over five minutes. The reaction was stirred for twenty minutes at 0 °C and then left to warm to room temperature. After five hours, an additional portion of

triphenylphosphine dibromide (0.5044 g, 1.20 mmol) was added and the reaction stirred for 20 hours before being quenched with ethyl acetate (20 mL). The organic phase was washed with saturated aqueous sodium thiosulfate (2 x 10 mL), water (3 x 10 mL), brine (2 x 10 mL), dried over magnesium sulfate and the organic solvents evaporated under reduced pressure to give an oil that was subjected to flash chromatography (50 % ethyl acetate/hexane) to give bromide 4.25 (82.3 mg, 25 % yield) as a clear oil.

Spectral data as above for ((6-Bromohexyloxy)methyl)benzene *via* phosphorous tribromide bromination.

6-(*Tert*-butyldimethylsilyloxy)hexan-1-ol

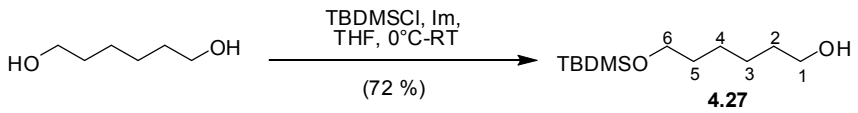

4.27

Tert-butyldimethylsilyl chloride (2.9031 g, 19.3 mmol) dissolved in tetrahydrofuran (50 mL) was added over 30 minutes to a stirred solution of 1,6-hexandiol (6.7580 g, 57.2 mmol) and imidazole (2.5912 g, 37.0 mmol) in dichloromethane (200 mL) at 0 °C. The reaction was stirred at room temperature for 26 hours, filtered and the volatile components evaporated to give a resin that was purified by flash chromatography (50 % diethyl ether/petroleum ether) to give silyl ether 4.27 as a clear oil (3.228 g, 72 %). R_f (20 % ethyl acetate/petroleum ether): 0.25; ^{1}H NMR (500 MHz, $CDCl_3$) δ ppm 3.57 (t, J = 6.7 Hz, 2H, H1 or H6), 3.57 (t, J = 6.5 Hz, 2H, H1 or H6), 2.42 (s, 1H, OH), 1.55-1.46 (m, 4H, H2 and H5), 1.35-1.28 (m, 4H, H3 and H4), 0.85 (s, 9H, $Si(CH_3)_2C(C\underline{H}_3)_3$), 0.01 (s, 6H, $Si(C\underline{H}_3)_2C(CH_3)_3$); ^{13}C NMR (126 MHz, $CDCl_3$) δ ppm 63.12 (C1 or C6), 62.60 (C1 or C6), 32.70 (C2 or C5), 32.62 (C2 or C5), 25.88 ($Si(CH_3)_2C(\underline{C}H_3)_3$), 25.54 (C3 or C4), 25.48 (C3 or C4), 18.27 ($Si(CH_3)_2\underline{C}(CH_3)_3$), -5.36 ($Si(\underline{C}H_3)_2C(CH_3)_3$); HRMS required for $C_{12}H_{29}O_2Si$: 233.1937, Found: 233.1938.

Isopropyl 8-(tert-butyldimethylsilyloxy)-2-hydroxyoctanoate

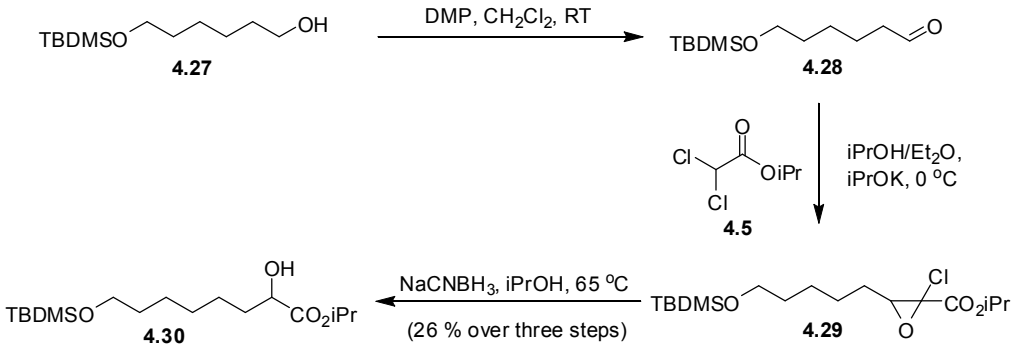

To a stirred solution of Dess-Martin periodinane (8.772 g, 20.7 mmol) in dichloromethane (60 mL) was added silyl ether 4.27 (3.228 g, 13.8 mmol) in dichloromethane (40 mL) over fifteen minutes. The reaction was stirred for three hours and quenched with aqueous sodium hydroxide (1.0 M, 70 mL). The organic phase was separated and the aqueous phase extracted with dichloromethane (3 x 100 mL). The combined organic phases were washed with aqueous sodium hydroxide (1.0 M, 50 mL), brine (50 mL), dried over anhydrous magnesium sulfate and evaporated to give a crude oil containing aldehyde 4.28 (2.6709 g). Potassium isoproponate (25.5 mL, 25.5 mmol) was added to a solution of isopropyl dichloroacetate 4.5 (3.947 g, 23.1 mmol) in dry isopropyl alcohol (25.5 mL) and dry diethyl ether (25.5 mL), cooled to 0 °C, over ten minutes. After ten minutes of stirring, a solution of crude aldehyde 4.28 (2.6709 g, 11.5 mmol crude) in dry isopropyl alcohol (13 mL) was added over five minutes and the reaction stirred at 0 °C for 95 minutes. The reaction was quenched with diethyl ether (150 mL) and water (100 mL) and the aqueous layer extracted with diethyl ether (2 x 200 mL). The combined organic phases were washed with brine (100 mL), dried and evaporated to give a crude oil containing α-chloroglycidic ester 4.29 (3.685 g). To a solution of this crude mixture in dry isopropyl alcohol (70 mL) was added sodium cyanoborohydride (1.2818 g, 20.4 mmol) and the reaction heated to 70 °C under a calcium hydride drying tube. After 24 hours, sodium cyanoborohydride (0.6012 g, 9.56 mmol) was added and the reaction stirred at 70 °C for a further 19 hours before quenched with saturated ammonium chloride solution (70 mL) and the isopropyl alcohol evaporated. Water (25 mL) was added to dissolve solids in the remaining solution and the aqueous phase extracted with diethyl ether (3 x 200 mL). The combined organic phases were washed with brine, dried over anhydrous magnesium sulfate and evaporated to give an oil that was subjected to flash chromatography (20% diethyl ether/petroleum ether) to give the α-hydroxy ester 4.30 as a clear oil (1.309 g,

28 % over three steps from silyl ether 4.27). R_f (20 % ethyl acetate/petroleum ether): 0.69; ^{1}H NMR (500 MHz, $CDCl_3$) δ ppm 5.07 (sept., J = 6.3 Hz, 1H, CHCOOC<u>H</u>$(CH_3)_2$), 4.10 (dd, J = 7.3, 4.2 Hz, 1H, C<u>H</u>COOCH$(CH_3)_2$), 3.57 (t, J = 6.7 Hz, 2H, H6), 2.73 (s, 1H, OH), 1.78-1.69 (m, 1H, H1'), 1.64-1.55 (m, 1H, H1), 1.52-1.45 (m, 2H, H5), 1.46-1.37 (m, 2H, H2), 1.41-1.26 (m, 4H, H3 and H4), 1.25 (d, J = 6.3 Hz, 3H, CHCOOCH(C<u>H</u>$_3)_2$), 1.25 (d, J = 6.3 Hz, 3H, CHCOOCH(C<u>H</u>$_3)_2$), 0.86 (s, 9H, Si(C<u>H</u>$_3)_2$C$(CH_3)_3$), 0.02 (s, 6H, Si$(CH_3)_2$C$(CH_3)_3$); ^{13}C NMR (126 MHz, $CDCl_3$) δ ppm 174.8 (CH<u>C</u>OOCH$(CH_3)_2$), 70.4 (<u>C</u>HCOOCH$(CH_3)_2$), 69.2 (CHCOO<u>C</u>H$(CH_3)_2$), 63.1 (C6), 34.3 (C1), 32.7 (C5), 29.1 (C3), 25.9 (Si$(CH_3)_2$C(<u>C</u>H$_3)_3$), 24.6 (C2), 25.6 (C4), 21.7, 21.7 (CHCOOCH(<u>C</u>H$_3)_2$), 18.3 (Si$(CH_3)_2$<u>C</u>$(CH_3)_3$), -5.34 (Si(<u>C</u>H$_3)_2$C$(CH_3)_3$); HRMS required for $C_{17}H_{37}O_4Si$: 333.2461, Found 333.2468.

Isopropyl 2,8-dihydroxyoctanoate

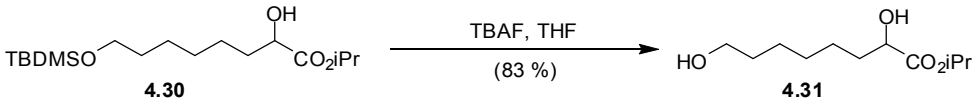

4.30 **4.31**

Tetrabutylammonium fluoride dissolved in tetrahydrofuran (6.70 mL, 6.70 mmol) was added to α-hydroxy ester 4.30 (0.637 g, 1.92 mol) stirring in dry tetrahydrofuran (25 mL). The reaction was stirred for four hours and the organic solvents evaporated to give a crude oil that was subjected to flash chromatography (75 % ethyl acetate/petroleum ether) to give ester 4.31 as a clear oil (0.3483 g, 83 %). R_f (75 % ethyl acetate/petroleum ether): 0.31; ^{1}H NMR (500 MHz, $CDCl_3$) δ ppm 5.07 (sept., J = 6.3 Hz, 1H, CHCOOC<u>H</u>$(CH_3)_2$), 4.10 (dd, J = 7.3, 4.1 Hz, 1H, C<u>H</u>COOCH$(CH_3)_2$), 3.61 (t, J = 6.6 Hz, 2H, H6), 2.42 (s, 2H, OH), 1.79-1.70 (m, H1'), 1.65-1.56 (m, 1H, H1), 1.59-1.51 (m, 2H, H5), 1.50-1.39 (m, 2H, H4), 1.40-1.29 (m, 4H, H2 and H3), 1.25 (d, J = 6.3 Hz, 3H, CHCOOCH(C<u>H</u>$_3)_2$), 1.25 (d, J = 6.3 Hz, 3H, CHCOOCH(C<u>H</u>$_3)_2$); ^{13}C NMR (126 MHz, $CDCl_3$) δ ppm 174.9 (CH<u>C</u>OOCH$(CH_3)_2$), 70.4 (<u>C</u>HCOOCH$(CH_3)_2$), 69.4 (CHCOO<u>C</u>H$(CH_3)_2$), 62.8 (C6), 34.2 (C1), 32.5 (C5), 29.0 (C3), 25.5 (C2), 24.6 (s, C4), 21.7, 21.7 (CHCOOCH(<u>C</u>H$_3)_2$); HRMS required for $C_{11}H_{23}O_4$: 219.1596, Found 219.1592.

Isopropyl 2,8-bis(bis(benzyloxy)phosphoryloxy)octanoate

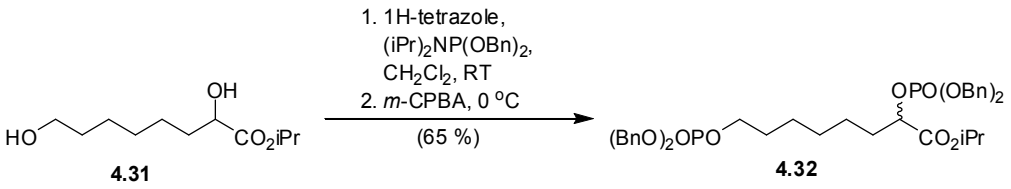

Dibenzyl *N,N*-diisopropylphosphoramidite (1.45 mL, 4.41 mmol) was added to diol 4.31 (0.2359 g, 10.8 mmol) dissolved in dry dichloromethane (20 mL). After twenty minutes 1H-tetrazole (0.5314 g, 7.59 mmol) was added and the reaction stirred at room temperature for a further three hours before being cooled to 0°C and *meta*-chloroperbenzoic acid, 75% by weight (1.1279 g, 4.90 mol) was added in one portion and the reaction stirred for two hours. The reaction was then quenched with saturated sodium thiosulfate solution (10 mL) and the organic phase washed twice with saturated sodium bicarbonate solution (10 mL), brine (10 mL), dried over anhydrous sodium sulfate and evaporated to give a white solid (1.1696 g) that was subjected to column chromatography (50 % ethyl acetate/petroleum ether) to give diphosphate 4.32 as a clear oil (0.4895 g, 65 %). R_f (50 % ethyl acetate/petroleum ether): 0.27; ^{1}H NMR (500 MHz, $CDCl_3$) δ ppm 7.37-7.29 (m, 20H, $\underline{Ph}_{b\text{-}d}$), **5**.13 (m, 4H, OPO(OC$\underline{H}_2$Ph)$_2$), 5.07-4.99 (m, 5H, CHCOOC$\underline{H}$(CH$_3$)$_2$ and OPO(OC$\underline{H}_2$Ph)$_2$), 4.76 (ddd, *J* = 7.8, 6.0, 6.0 Hz, 1H, C$\underline{H}$COOCH(CH$_3$)$_2$), 3.95 (dt, *J* = 7.2, 6.7 Hz, 2H, H6), 1.76 (dt, *J* = 7.3, 7.3 Hz, 2H, H1), 1.59-1.50 (m, 2H, H5), 1.37-1.28 (m, 2H, H2), 1.29-1.21 (m, 4H, H3 and H4), 1.21 (d, *J* = 6.3 Hz, 1H, CHCOOCH(C$\underline{H}_3$)$_2$); ^{13}C NMR (126 MHz, $CDCl_3$) δ ppm 169.42 (d, *J* = 3.2 Hz, CH$\underline{C}$OOCH(CH$_3$)$_2$), 135.7, 135.7 (OPO(OCH$_2\underline{Ph}_a$)$_2$), 128.4, 128.4, 128.3, 127.8, 127.8, 127.7 (OPO(OCH$_2\underline{Ph}_{b\text{-}d}$)$_2$), 75.5 (d, *J* = 5.8 Hz, $\underline{C}$HCOOCH(CH$_3$)$_2$), 69.3 (d, *J* = 5.8 Hz, OPO(O$\underline{C}$H$_2$Ph), 69.3 (d, *J* = 5.8 Hz, OPO(O$\underline{C}$H$_2$Ph), 69.1 (t, *J* = 5.5 Hz, CHCOO$\underline{C}$H(CH$_3$)$_2$), 67.7 (d, *J* = 6.1 Hz, C1), 32.7 (d, *J* = 6.7 Hz, C6), 29.8 (d, *J* = 7.0 Hz, C2), 28.4 (C3), 25.0 (C4), 24.2 (C5), 21.5 (CHCOOCH($\underline{C}$H$_3$)$_2$). ^{31}P NMR (121 MHz, *CDCl$_3$*) δ ppm -0.38 (sext., *J* = 7.8 Hz, CHOPO(OBn)$_2$), -1.24 (sept., J = 7.2 Hz, CH$_2$OPO(OBn)$_2$); HRMS required for $C_{39}H_{49}NaO_{10}P_2$: 761.2620, Found: 761.2601.

2,8-Bis(phosphonatooxy)octanoate

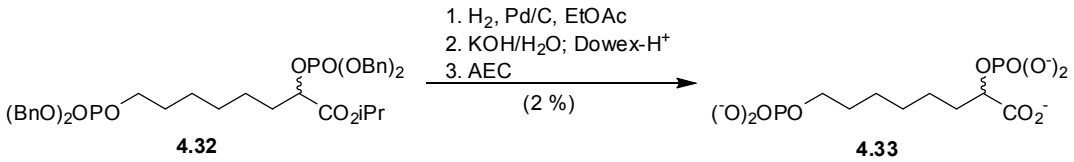

10 % palladium over carbon (0.3398 g) was added to phosphorylated ester 4.32 (0.7033 g, 952 mmol) dissolved in ethyl acetate (40 mL). The reaction vessel was purged with hydrogen gas and stirred for 26 hours before being washed through a celite plug with ethyl acetate (250 mL) and methanol (250 mL). The organic solvents were evaporated to give an oil that was stirred in 10 % w/v aqueous potassium hydroxide (5 mL) for two hours before being passed down a column (20 x 100 mm) of Dowex-50X8 H^+ resin. This solution was lypholised to give a pink solid (0.3162 g). 0.1624 g of this solid was further purified by anion exchange chromatography (0-1 M ammonium bicarbonate). The fractions containing product were lypholised to give the synthetic target 4.33 (28.7 mg, 2 %).

^{1}H NMR (500 MHz, D_2O) δ ppm 4.38 (td, *J* = 8.7, 5.3 Hz, 1H, C<u>H</u>COO$^-$), 3.77 (dt, *J* = 6.8, 6.7 Hz, 2H, H6), 1.78-1.67 (m, 2H, H1), 1.62-1.54 (m, 2H, H5), 1.44-1.34 (m, 2H, H2), 1.37-1.25 (m, 4H, H3 and H4); ^{13}C NMR (75 MHz, D_2O) δ ppm 182.6 (CH<u>C</u>OO$^-$), 78.6 (d, *J* = 5.3 Hz, <u>C</u>HCOO$^-$), 67.7 (d, *J* = 5.2 Hz, C6), 36.0 (d, *J* = 5.3 Hz, C1), 32.5 (d, *J* = 6.8 Hz, C5), 30.9 (C4), 27.3 (C3), 26.5 (C2); ^{31}P NMR (121 MHz, D_2O) δ ppm 1.1 (d, *J* = 8.7 Hz, CHO<u>P</u>(O$^-$)$_2$), 2.5 (t, *J* = 6.7 Hz, CH$_2$O<u>P</u>(O$^-$)$_2$); HRMS (electrospray, negative ion) required for $C_8H_{17}O_{10}P_2$: 335.0297, Found 335.0310.

Isopropyl 2-(bis(benzyloxy)phosphoryloxy)-8-(tert-butyldimethylsilyloxy)octanoate

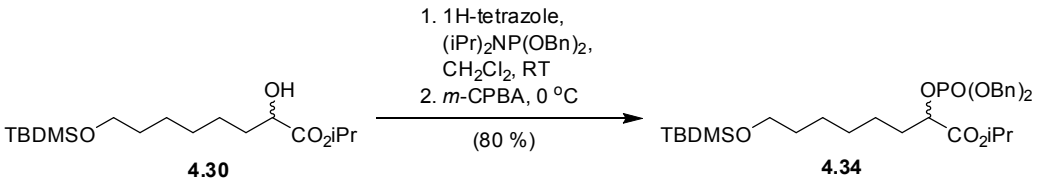

Dibenzyl *N,N*-diisopropylphosphoramidite (1.40 mL, 4.17 mmol) was added to α-hydroxy ester 4.30 (0.3566 g, 1.07 mmol) and 1-H tetrazole (0.5257 g, 7.51 mmol) in dry dichloromethane (20 mL). The reaction was stirred for two hours and cooled to 0 °C before the addition of *meta*-chloroperbenzoic acid (1.1216 g, 6.50 mmol). The solution was stirred

for two hours before being quenched with diethyl ether (100 mL). The organic phase was washed with saturated sodium thiosulfate solution (2 x 20 mL), saturated sodium bicarbonate solution (2 x 20 mL), brine (20 mL), dried over anhydrous magnesium sulphate and evaporated to give an oil which was subjected to column chromatography to give phosphorylated ester 4.34 (0.5061 g, 80 %). R_f (25 % ethyl acetate/petroleum ether): 0.39; ^{1}H NMR (500 MHz, $CDCl_3$) δ ppm: 7.37-7.32 (m, 10H, $OPO(OCH_2\underline{Ph}_{b\text{-}d})_2$), 5.13 (m, 4H, $OPO(OC\underline{H}_2Ph)_2$), 5.06 (hept., J = 6.6 Hz, 1H, $CHCOOC\underline{H}(CH_3)_2$), 4.76 (ddd, J = 7.6, 6.1, 6.1 Hz, 1H, $C\underline{H}COOCH(CH_3)_2$), 3.57 (t, J = 6.5 Hz, 1H, H6), 1.79 (dt, J = 7.6, 7.4 Hz, 2H, H1), 1.51-1.43 (m, 2H, H5), 1.43-1.32 (m, 2H, H2), 1.33-1.23 (m, 4H, H3 and H4), 1.22 (d, J = 6.6 Hz, 6H, $COOCH(C\underline{H}_3)_2$), 0.89 (s, 9H, $Si(CH_3)_2C(C\underline{H}_3)_3$), 0.04 (s, 6H, $Si(C\underline{H}_3)_2C(CH_3)_3$); ^{13}C NMR (126 MHz, $CDCl_3$): δ ppm: 169.6 (d, J = 3.2 Hz, $CH\underline{C}OOCH(CH_3)_2$), 128.5, 128.4, 128.4, 128.4, 127.9, 127.7 ($OPO(OCH_2\underline{Ph}_{b\text{-}d})_2$), 75.7 (d, J = 5.7 Hz, $\underline{C}HCOOCH(CH_3)_2$), 69.3, 69.3 (d, J = 5.7 Hz, $OP(O\underline{C}H_2Ph)_2$), 69.1 ($CHCOO\underline{C}H(CH_3)_2$), 63.1 (C6), 32.9 (d, J = 6.4 Hz, C1), 32.6 (C5), 28.9 (C3), 25.9 ($Si(CH_3)_2C(\underline{C}H_3)_3$), 25.5 (C4), 24.4 (C2), 21.6, 21.6 ($CHCOOCH(\underline{C}H_3)_2$), 18.3 ($Si(CH_3)_2\underline{C}(CH_3)_2$), -5.3 ($Si(\underline{C}H_3)_2C(CH_3)_3$); ^{31}P NMR (121 MHz, $CDCl_3$) δ ppm -1.39 (sext, J = 7.6 Hz, $CHO\underline{P}O(OBn)_2$); HRMS required for $C_{39}H_{42}O_7PSi$: 593.3063, Found: 593.3055.

Isopropyl 2-(bis(benzyloxy)phosphoryloxy)-8-hydroxyoctanoate

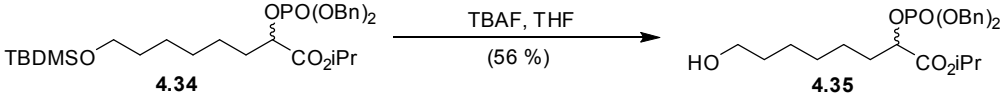

A 1M solution of tetrabutylammonium fluoride in tetrahydrofuran (3.0 mL, 3.0 mmol) was added to phosphorylated silyl ether 4.34 (0.5061 g, 0.854 mmol) in dry tetrahydrofuran (6 mL) and stirred for 28 hours. The tetrahydrofuran was evaporated to give a brown oil which was purified by flash chromatography (75 % ethyl acetate/petroleum ether) to give alcohol 4.35 as a clear oil (0.2288 g, 56 %). R_f (50 % ethyl acetate/petroleum ether): 0.13; ^{1}H NMR ($CDCl_3$): δ ppm 7.37-7.32 (m, 10H, $PO(OCH_2\underline{Ph}_{b\text{-}d})_2$, 5.11 (dq, J = 11.7, 7.4 Hz, 2H, $CHOPO(OC\underline{H}_2Bn)_2$), 5.08-5.00 (m, 3H, $CHOPO(OC\underline{H}_2Bn)_2$ and $CHCOOC\underline{H}(CH_3)_2$), 4.75 (ddd, J = 7.6, 6.1, 6.1 Hz, 1H, $C\underline{H}COOCH(CH_3)_2$), 3.59 (t, J = 6.6 Hz, 1H, H6), 2.13 (s, 1H, OH), 1.79 (dt, J = 7.6, 7.1 Hz, 2H, H1), 1.54-1.47 (m, 2H, H5), 1.42-1.31 (m, 2H, H2), 1.34-1.24 (m, 4H, H3 and H4), 1.21 (d, J = 6.3 Hz, 6H, $CHCOOCH(C\underline{H}_3)_2$); ^{13}C NMR (126 MHz, $CDCl_3$): δ ppm: 169.6 (d, J = 3.1 Hz, $CH\underline{C}OOCH(CH_3)_2$), 135.7, 135.7 (d, J = 7.6 Hz,

CHOPO(OCH$_2$<u>Ph</u>$_a$)$_2$), 128.4, 127.9, 127.7, (br, CHOPO(OCH$_2$<u>Ph</u>$_{b-d}$), 75.6 (d, *J* = 5.7 Hz, <u>C</u>HCOOCH(CH$_3$)$_2$), 69.3, 69.3 (d, *J* = 5.6 Hz, CHOPO(O<u>C</u>H$_2$Ph)$_2$), 69.2 (CHCOO<u>C</u>H(CH$_3$)$_2$), 62.6 (C6), 32.8 (d, *J* = 6.4 Hz, C1), 32.4 (C5), 28.6 (C3), 25.4 (C4), 24.3 (C2), 21.6, 21.6 (CHCOOCH(<u>C</u>H$_3$)$_2$); ^{31}P NMR (121 MHz, CDCl$_3$) δ ppm -1.62 (sext., *J* = 7.6 Hz, CHO<u>P</u>O(OPh)$_2$); HRMS required for $C_{25}H_{36}O_7P$: 479.2199, Found: 479.2191.

8-hydroxy-2-(phosphonatooxy)octanoate

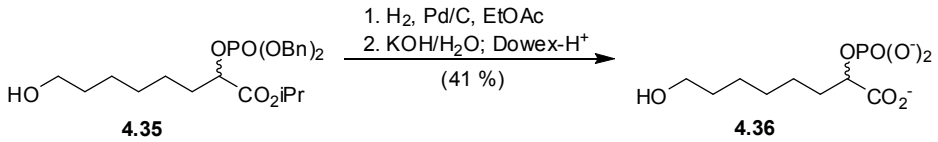

Ethyl acetate (15 mL) was added to 10 % palladium over carbon (162.4 mg) and the reaction mixture stirred under hydrogen for 10 minutes before protected phosphate 4.35 (272.0 mg, 0.568 mmol) in ethyl acetate (5 mL) was added by syringe. The reaction vessel was repurged with hydrogen and stirred for 18 hours before being filtered through a celite plug with ethyl acetate (100 mL) and methanol (100 mL). The filtrate was evaporated and the residue was resuspended in aqueous potassium hydroxide (1 M, 3 mL) and stirred at room temperature for one hour. The solution was diluted with 5 mL water and extracted twice with dichloromethane (5 mL each) and the organic phase discarded. The aqueous phase was passed down a column of Dowex-50X8-H$^+$ resin (20 x 100 mm) and eluted with water (50 mL). The solution was lypholised to give the product 4.36 (0.2053 g, 41 %). ^{1}H NMR (500 MHz, D$_2$O) δ ppm 4.40 (td, *J* = 8.7, 5.5 Hz, 1H, C<u>H</u>COO$^-$), 3.62 (t, *J* = 6.6 Hz, 2H, H6), 2.26 (s, 1H, OH), 1.80-1.72 (m, 2H, H1), 1.63-1.52 (m, 2H, H5), 1.50-1.26 (m, 6H, H2, H3 and H4); ^{13}C NMR (126 MHz, D$_2$O) δ ppm 181.2 (d, *J* = 4.7 Hz, CH<u>C</u>OO$^-$), 76.2 (d, *J* = 5.5 Hz, <u>C</u>HCOO$^-$), 62.4 (C6), 34.17 (d, *J* = 3.9 Hz, C1), 31.7 (C2), 29.0 (C3), 25.4 (C4), 24.5 (C2); ^{31}P NMR (121 MHz, D$_2$O) δ ppm 2.5 (d, *J* = 5.5 Hz, CHO<u>P</u>O(O$^-$)$_2$); HRMS (electrospray, negative ion) required for $C_8H_{16}O_7P$: 255.0634, Found 255.0645.

Isopropyl 2-(benzyloxy)-8-(tert-butyldimethylsilyloxy)octanoate

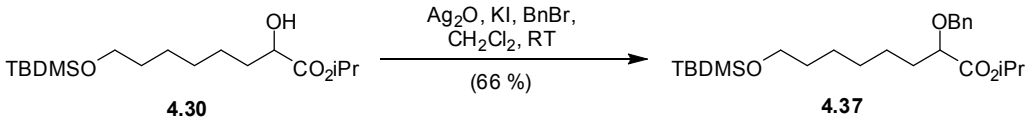

To a stirred solution of silver oxide (0.2402 g, 1.04 mmol), potassium iodide (11.8 mg, 0.00711 mmol) and α-hydroxy ester 4.30 (0.2304 g, 0.693 mmol) in dry dichloromethane (1.5 mL) was added benzyl bromide (205 μL, 1.72 mmol) and the solution stirred for nine hours before being washed through a celite plug with diethyl ether (140 mL). The organic phase was washed with water (25 mL), brine (25 mL), dried and evaporated to give an oil that was subjected to flash chromatography (5 % diethyl ether/petroleum ether) to give benzylated ester 4.37 as an oil (0.1924 g, 66 %). R_f (20 % ethyl acetate/petroleum ether): 0.66; ^{1}H NMR (500 MHz, $CDCl_3$) δ ppm 7.40-7.25 (m, 5H, $CHOCH_2\underline{Ph}_{b\text{-}d}$), 5.11 (sept., J = 6.3 Hz, 1H, $CHCOOC\underline{H}(CH_3)_2$), 4.70 (d, J = 11.6 Hz, 1H, $OC\underline{H}_2Ph$), 4.40 (d, J = 11.6 Hz, 1H, $OC\underline{H}_2Ph$), 3.89 (t, J = 5.8 Hz, 1H, $C\underline{H}COOCH(CH_3)_2$), 3.59 (t, J = 6.6 Hz, 2H, H6), 1.80-1.70 (m, 2H, H1), 1.55-1.23 (m, 8H, H2, H3, H4 and H5), 1.30-1.25 (m, 6H, $CHCOOCH(C\underline{H}_3)_2$), 0.90 (s, 9H, $Si(CH_3)_2C(C\underline{H}_3)_3$), 0.05 (s, 6H, $Si(C\underline{H}_3)_2C(CH_3)_3$); ^{13}C NMR ($CDCl_3$): δ 172.4 ($\underline{C}OOCH(CH_2)_2$), 137.6 ($CH_2\underline{Ph}_a$), 127.950 ($CH_2\underline{Ph}_{b\text{-}c}$), 128.3 ($CH_2\underline{Ph}_{b\text{-}c}$), 127.7 ($CH_2\underline{Ph}_d$), 78.1 ($\underline{C}HCOOCH(CH_2)_2$), 72.1 ($\underline{C}H_2C_6H_6$), 63.1 (C1), 68.1 ($CHCOO\underline{C}H(CH_2)_2$), 32.8 (C2), 32.7 (C6), 29.0 (C4), 25.9 ($OSi(CH_3)_2C(\underline{C}H_3)_3$), 25.6 (C3), 25.2 (C5), 21.8, 21.8 ($CHCOOCH(\underline{C}H_3)_2$), 18.3 ($OSi(CH_3)_2\underline{C}(CH_3)_3$), -5.3 ($Si(\underline{C}H_3)_2C(CH_3)_3$); HRMS required for $C_{24}H_{43}O_4Si$: 423.2931, Found: 423.2930.

Isopropyl 2-(benzyloxy)-8-hydroxyoctanoate

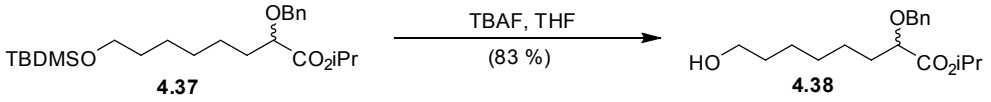

A 1M solution of tetrabutylammonium fluoride in dry tetrahydrofuran (2.8 mL, 2.8 mmol) was added to silyl ether 4.37 (0.3429 g, 0.811 mmol) in dry tetrahydrofuran (10 mL) and stirred for four hours. The volatile components were evaporated to give a viscous oil that was subjected to flash chromatography (40 % ethyl acetate/petroleum ether) to give alcohol 4.38 as a clear oil (0.2073 g, 83 % yield). R_f (50 % ethyl acetate/petroleum ether): 0.49; ^{1}H NMR (500 MHz, $CDCl_3$) δ ppm 7.35-7.23 (m, 5H, $CHOCH_2\underline{Ph}_{b\text{-}d}$), 5.07 (sept., J = 6.3 Hz, 1H, $CHCOOC\underline{H}(CH_3)_2$), 4.66 (d, J = 11.6 Hz, 1H, $CHOC\underline{H}_2Ph$), 4.37 (d, J = 11.6 Hz, 1H,

C$\underline{H}_2$Ph), 3.85 (dd, *J* = 7.2, 5.6 Hz, 1H, C$\underline{H}$COOCH(CH_3)$_2$), 3.56 (t, *J* = 6.7 Hz, 2H, H6), 2.01 (br, 1H, OH), 1.75-1.68 (m, 2H, H1), 1.53-1.46 (m, 2H, H5), 1.47-1.35 (m, 2H, H2), 1.38-1.25 (m, 2H, H3 and H4), 1.25, 1.25 (d, *J* = 6.3 Hz, 6H, CHCOOCH(C$\underline{H}_3$)$_2$); ^{13}C NMR (126 MHz, *CDCl$_3$*) δ ppm: 172.4 (CH$\underline{C}$OOCH(CH_3)$_2$), 137.5 (OCH$_2\underline{Ph}_a$), 128.2, 127.9 (OCH$_2\underline{Ph}_{b-c}$), 127.7 (OCH$_2\underline{Ph}_d$), 78.0 ($\underline{C}$HCOOCH(CH_3)$_2$), 72.0 (O$\underline{C}$H$_2$Ph), 68.2 (CHCOO$\underline{C}$H(CH_3)$_2$) 62.6 (C6), 32.7 (C1) 32.4 (C5), 28.9 (C3), 25.4 (C2), 25.1 (C4), 21.7, 21.7 (CHCOOCH(C$\underline{H}_3$)$_2$); HRMS required for $C_{18}H_{29}O_4$: 309.2066, Found: 309.2066.

Isopropyl 2-(benzyloxy)-8-(bis(benzyloxy)phosphoryloxy)octanoate

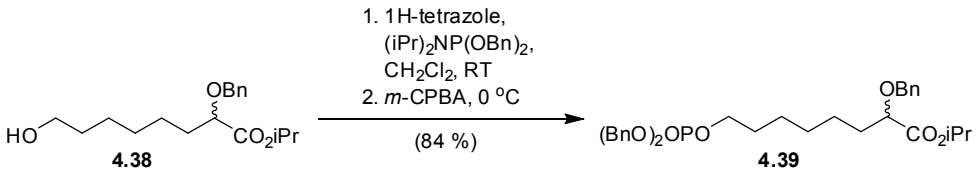

Dibenzyl N,N-Diisopropylphosphoramidite (200 µL, 0.596 mmol) was added to a solution of alcohol 4.38 (0.1438 g, 0.301 mmol) and 1H-tetrazole (74.6 mg, 1.06 mmol) dissolved in dichloromethane (10 mL) and the reaction stirred for four hours before being cooled to 0 °C and *meta*-chloroperbenzoic acid (0.1564 g, 0.906 mmol) was added. The mixture was stirred for a further two hours before quenching with diethyl ether (40 mL) and the organic phase washed with aqueous 10 % solution of sodium thiosulfate (2 x 5 mL), saturated aqueous sodium bicarbonate (2 x 5 mL), brine (5 mL), dried over anhydrous magnesium sulfate and the organic solvents evaporated to give an oil which was subjected to flash chromatography (25% ethyl acetate/petroleum ether) to give a clear oil (0.1579 g) that contained monophosphate 4.39 (0.1446 g, 84 %) and dibenzyl phosphite (14.4 mg, 8.9 % w/w) and was used in the next reaction step without any further purification. R_f (50 % ethyl acetate/petroleum ether): 0.41; ^{1}H NMR (500 MHz, $CDCl_3$) δ ppm 7.42-7.27 (m, 15H, OPO(OCH$_2\underline{Ph}_{b-d}$)$_2$ and CHOCH$_2\underline{Ph}_{b-d}$), 5.12 (sept., *J* = 6.2 Hz, 1H, CHCOOC$\underline{H}$(CH_3)$_2$), 5.05 (dd, *J* = 8.3, 6.5 Hz, 4H, OPO(OC$\underline{H}_2$Ph)$_2$), 4.71 (d, *J* = 11.6 Hz, 1H, CHOC$\underline{H}_2$Ph), 4.41 (d, *J* = 11.6 Hz, 1H, CHOC$\underline{H}_2$Ph), 3.98 (dt, *J* = 6.7, 6.7 Hz, 2H, H6), 3.89 (dd, *J* = 7.2, 5.5 Hz, 1H, C$\underline{H}$COOCH(CH_3)$_2$), 1.79-1.70 (m, 2H, H1), 1.63-1.56 (m, 2H, H5), 1.50-1.21 (m, 6H, H2, H3 and H4), 1.29 (dd, *J* = 6.2 Hz, 6H, CHCOOCH(C$\underline{H}_3$)$_2$); ^{13}C NMR (126 MHz, $CDCl_3$) δ ppm 172.3 (CH$\underline{C}$OOCH(CH_3)$_2$), 137.5 (CHOCH$_2\underline{Ph}_a$), 135.8, 135.8 (OPO(OCH$_2\underline{Ph}_a$)$_2$), 128.6, 128.4, 128.4, 128.2, 127.9, 127.9, 127.8, 127.7 (OCH$_2\underline{Ph}_{b-d}$ and OPO(CH$_2\underline{Ph}_{b-d}$)$_2$), 77.9 ($\underline{C}$HOOCH(CH_3)$_2$), 72.05 (CHO$\underline{C}$H$_2$Ph), 69.0, 69.0 (dd, *J* = 4.1 Hz, OPO(O$\underline{C}$H$_2$Ph)$_2$),

68.1 (CHOO<u>C</u>H(CH$_3$)$_2$), 67.8 (d, *J* = 6.2 Hz, C6), 32.7 (C1), 29.9 (d, *J* = 7.1 Hz, C5), 28.6 (s,C3), 25.1 (C4), 25.0 (C2), 21.8, 21.7 (CHCOOCH(<u>C</u>H$_3$)$_2$); ^{31}P NMR (121 MHz, CDCl$_3$): δ ppm -0.8 (sept., *J* = 7.7 Hz, CH$_2$O<u>P</u>O(OBn)$_2$), 7.8 (dp, *J* = 707.4, 9.5 Hz, HPO(OBn)$_2$); HRMS required for $C_{32}H_{41}NaO_7P$: 591.2482, Found: 591.2484.

2-Hydroxy-8-(phosphonatooxy)octanoate

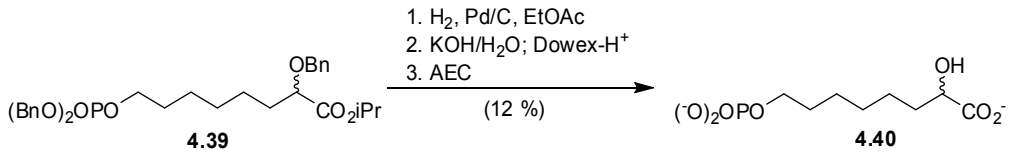

10 % palladium over carbon (83.7 mg) was added to phosphorylated ester 4.39 (0.149 g, 952 mmol) in ethyl acetate (15 mL). The reaction vessel was purged with hydrogen gas and stirred for 18 hours before being washed through a celite plug with ethyl acetate (100 mL) and methanol (100 mL). The volatile components were evaporated. The resin was resuspended in 10% w/v aqueous potassium hydroxide (5 mL) and stirred for one hour before being passed down a column (20 x 100 mm) of Dowex-50X8 H^+ type resin and eluted with water (50 mL). This solution was lypholised to give a white powder which was dissolved in MilliQ water (20 mL), filtered using a 0.45 μM membrane and further purified by anion exchange chromatography (0-1 M ammonium bicarbonate). The fractions containing product were lypholised to give the synthetic target 4.40 (35.4 mg, 12 %). ^{1}H NMR (500 MHz, D$_2$O): δ ppm 3.93 (dd, *J* = 7.3, 4.3 Hz, C<u>H</u>COOH), 3.64 (dt, *J* = 6.9, 6.9 Hz, 2H, H6), 1.67-1.57 (m, 1H, H1), 1.53-1.46 (m, 3H, H5 and H1'), 1.34-1.19 (m, 6H, H2, H3 and H4); ^{13}C NMR (126 MHz, *Solvent*) δ ppm 182.5 (CH<u>C</u>OO$^-$), 72.9 (<u>C</u>HCOO$^-$), 65.3 (d, *J* = 4.3 Hz, C6), 34.5 (C1), 30.8 (d, *J* = 7.0 Hz, C5), 29.0, 25.5, 24.92 (C2, C3 and C4); ^{31}P NMR (121 MHz, D$_2$O) δ ppm 3.6 (t, *J* = 5.0 Hz, CH$_2$OPO(O$^-$)$_2$); HRMS (electrospray, negative ion) required for $C_8H_{16}O_7P$: 255.0634, Found 255.0642.

References

The findings of one,
impossible without the
knowledge of many

1. Raetz, C. R. H.; Whitfield, C., Lipopolysaccharide endotoxins, *Annu. Rev. Biochem.* **2002**, *71*, 635-700.

2. Holst, O., Chemical structure of the core region of lipopolysaccharides - an update, *Trends Glycosci. Glycotechnol.* **2002**, *14*, 87-103.

3. Doong, R. L., *Isolation and characterization of KDOP synthase and two isozymes of DAHP synthase in Spinacia oleracea L. and Solanum tuberosum L.*; MSc, University of Florida, 1990.

4. Cipolla, L.; Polissi, A.; Airoldi, C.; Galliani, P.; Sperandeo, P.; Nicotra, F., The KDO biosynthetic pathway toward OM biogenesis as target in antibacterial drug design and development, *Curr. Drug Discovery Technol.* **2009**, *6*, 19-33.

5. Meredith T., C.; Woodard R., W., Escherichia coli YrbH is a D-arabinose 5-phosphate isomerase, *J. Biol. Chem.* **2003**, *278*, 32771-7.

6. Bateman, A., The SIS domain: a phosphosugar-binding domain, *Trends Biochem. Sci.* **1999**, *24*, 94-95.

7. Jeffery, C. J.; Hardre, R.; Salmon, L., Crystal structure of rabbit phosphoglucose isomerase complexed with 5-phospho-D-arabinonate identifies the role of Glu357 in catalysis, *Biochemistry* **2001**, *40*, 1560-1566.

8. Straus, D.; Raines, R.; Kawashima, E.; Knowles, J. R.; Gilbert, W., Active site of triosephosphate isomerase: in vitro mutagenesis and characterization of an altered enzyme, *Proc. Natl. Acad. Sci. U. S. A.* **1985**, *82*, 2272-6.

9. Lolis, E.; Petsko, G. A., Crystallographic analysis of the complex between triosephosphate isomerase and 2-phosphoglycolate at 2.5 Å resolution: implications for catalysis, *Biochemistry* **1990**, *29*, 6619-25.

10. Bigham, E. C.; Gragg, C. E.; Hall, W. R.; Kelsey, J. E.; Mallory, W. R.; Richardson, D. C.; Benedict, C.; Ray, P. H., Inhibition of arabinose 5-phosphate isomerase. An approach to the inhibition of bacterial lipopolysaccharide biosynthesis, *J. Med. Chem.* **1984**, *27*, 717-26.

11. Goldman, R. C.; Devine, E. M., Isolation of *Salmonella typhimurium* strains that utilize exogenous 3-deoxy-D-*manno*-octulosonate for synthesis of lipopolysaccharide, *J. Bacteriol.* **1987**, *169*, 5060-5.

12. Goldman, R.; Kohlbrenner, W.; Lartey, P.; Pernet, A., Antibacterial agents specifically inhibiting lipopolysaccharide synthesis, *Nature* **1987**, *329*, 162-4.

13. Goldman, R. C.; Doran, C. C.; Capobianco, J. O., Analysis of lipopolysaccharide biosynthesis in *Salmonella typhimurium* and *Escherichia coli* by using agents which specifically block incorporation of 3-deoxy-D-*manno*-octulosonate, *J. Bacteriol.* **1988**, *170*, 2185-91.

14. Tadanier, J.; Lee, C. M.; Whittern, D.; Wideburg, N., Synthesis of some C-8-modified 3-deoxy-β-D-*manno*-2-octulosonic acid analogs as inhibitors of CMP-KDO synthetase, *Carbohydr. Res.* **1990**, *201*, 185-207.

15. Adachi, H.; Kondo, K.-I.; Kojima, F.; Umezawa, Y.; Ishino, K.; Hotta, K.; Nishimura, Y., Synthesis and inhibitory activity of 8-substituted 2-deoxy-β -KDO against CMP-KDO synthetase, *Nat. Prod. Res., Part B* **2006**, *20*, 361-370.

16. Levin, D. H.; Racker, E., Condensation of arabinose 5-phosphate and phosphoryl enol pyruvate by 2-keto-3-deoxy-8-phosphooctonic acid synthetase, *J. Biol. Chem.* **1959**, *234*, 2532-9.

17. Ray, P. H.; Benedict, C. D., Purification and characterization of specific 3-deoxy-D-*manno*-octulosonate 8-phosphate phosphatase from *Escherichia coli* B, *J. Bacteriol.* **1980**, *142*, 60-8.

18. Rick, P. D.; Fung, L. W. M.; Ho, C.; Osborn, M. J., Lipid A mutants of *Salmonella typhimurium*. Purification and characterization of a lipid A precursor produced by a mutant in 3-deoxy-D-*manno*-octulosonate-8-phosphate synthetase, *J. Biol. Chem.* **1977**, *252*, 4904-12.

19. Meredith, T. C.; Aggarwal, P.; Mamat, U.; Lindner, B.; Woodard, R. W., Redefining the requisite lipopolysaccharide structure in *Escherichia coli.*, *ACS Chem. Biol.* **2006**, *1*, 33-42.

20. Stryer, L.; Editor, *Biochemistry, 4th Revised Edition*, 1996.

21. Hedstrom, L.; Abeles, R., 3-Deoxy-D-*manno*-octulosonate-8-phosphate synthase catalyzes the carbon-oxygen bond cleavage of phosphoenolpyruvate, *Biochem. Biophys. Res. Commun.* **1988**, *157*, 816-20.

22. Dotson, G. D.; Nanjappan, P.; Reily, M. D.; Woodard, R. W., Stereochemistry of 3-deoxyoctulosonate 8-phosphate synthase, *Biochemistry* **1993**, *32*, 12392-7.

23. Baasov, T.; Sheffer-Dee-Noor, S.; Kohen, A.; Jakob, A.; Belakhov, V., Catalytic mechanism of 3-deoxy-D-*manno*-2-octulosonate-8-phosphate synthase. The use of synthetic

analogs to probe the structure of the putative reaction intermediate, *Eur. J. Biochem.* **1993**, *217*, 991-9.

24. D'Souza, F. W.; Benenson, Y.; Baasoy, T., Catalytic mechanism of KDO8P synthase: synthesis and evaluation of a putative reaction intermediate, *Bioorg. Med. Chem. Lett.* **1997**, *7*, 2457-2462.

25. Liang, P.-H.; Lewis, J.; Anderson, K. S.; Kohen, A.; D'Souza, F. W.; Benenson, Y.; Baasov, T., Catalytic mechanism of KDO8P synthase: transient kinetic studies and evaluation of a putative reaction intermediate, *Biochemistry* **1998**, *37*, 16390-16399.

26. Du, S.; Tsipori, H.; Baasov, T., Synthesis and evaluation of putative oxocarbenium intermediate mimic in the KDO8P synthase-catalyzed reaction as a tool for the design of potent inhibitors for lipopolysaccharide biosynthesis, *Bioorg. Med. Chem. Lett.* **1997**, *7*, 2469-2472.

27. Du, S.; Faiger, H.; Belakhov, V.; Baasov, T., Towards the development of novel antibiotics: synthesis and evaluation of a mechanism-based inhibitor of Kdo8P synthase, *Bioorg. Med. Chem.* **1999**, *7*, 2671-2682.

28. Li, Z.; Sau, A. K.; Shen, S.; Whitehouse, C.; Baasov, T.; Anderson, K. S., A snapshot of enzyme catalysis using electrospray ionization mass spectrometry, *J. Am. Chem. Soc.* **2003**, *125*, 9938-9939.

29. Li, Z.; Sau, A. K.; Furdui, C. M.; Anderson, K. S., Probing the role of tightly bound phosphoenolpyruvate in *Escherichia coli* 3-deoxy-D-*manno*-octulosonate 8-phosphate synthase catalysis using quantitative time-resolved electrospray ionization mass spectrometry in the millisecond time range, *Anal. Biochem.* **2005**, *343*, 35-47.

30. Wang, J.; Duewel, H. S.; Woodard, R. W.; Gatti, D. L., Structures of *Aquifex aeolicus* KDO8P synthase in complex with R5P and PEP, and with a bsubstrate Inhibitor: role of active site water in catalysis, *Biochemistry* **2001**, *40*, 15676-15683.

31. Asojo, O.; Friedman, J.; Adir, N.; Belakhov, V.; Shoham, Y.; Baasov, T., Crystal structures of KDO8P synthase in its binary complexes with the substrate phosphoenolpyruvate and with a mechanism-based inhibitor, *Biochemistry* **2001**, *40*, 6326-6334.

32. Alberg, D. G.; Lauhon, C. T.; Nyfeler, R.; Faessler, A.; Bartlett, P. A., Inhibition of 5-enolpyruvoylshikimate 3-phosphate (EPSP) synthase by analogs of the tetrahedral intermediate and of EPSP, *J. Am. Chem. Soc.* **1992**, *114*, 3535-46.

33. Kim, D. H.; Lees, W. J.; Haley, T. M.; Walsh, C. T., Kinetic characterization of the inactivation of UDP-GlcNAc enolpyruvyl transferase by (Z)-3-fluorophosphoenolpyruvate:

evidence for two oxocarbenium ion intermediates in enolpyruvyl transfer catalysis, *J. Am. Chem. Soc.* **1995**, *117*, 1494-502.

34. Duewel, H. S.; Radaev, S.; Wang, J.; Woodard, R. W.; Gatti, D. L., Substrate and metal complexes of 3-deoxy-D-*manno*-octulosonate-8-phosphate synthase from *Aquifex aeolicus* at 1.9 Å. resolution. Implications for the condensation mechanism, *J. Biol. Chem.* **2001**, *276*, 8393-8402.

35. Kona, F.; Xu, X.; Martin, P.; Kuzmic, P.; Gatti, D. L., Structural and mechanistic changes along an engineered path from metallo to nonmetallo 3-Deoxy-D-*manno*-octulosonate 8-phosphate synthases, *Biochemistry* **2007**, *46*, 4532-4544.

36. Tao, P.; Gatti, D. L.; Schlegel, H. B., The energy landscape of 3-deoxy-D-*manno*-octulosonate 8-phosphate synthase, *Biochemistry* **2009**, *48*, 11706-11714.

37. Duewel, H. S.; Woodard, R. W., A metal bridge between two enzyme families. 3-Deoxy-D-*manno*-octulosonate-8-phosphate synthase from *Aquifex aeolicus* requires a divalent metal for activity, *J. Biol. Chem.* **2000**, *275*, 22824-22831.

38. Shulami, S.; Yaniv, O.; Rabkin, E.; Shoham, Y.; Baasov, T., Cloning, expression, and biochemical characterization of 3-deoxy-D-*manno*-2-octulosonate-8-phosphate (KDO8P) synthase from the hyperthermophilic bacterium *Aquifex pyrophilus*, *Extremophiles* **2003**, *7*, 471-481.

39. Birck, M. R.; Woodard, R. W., *Aquifex aeolicus* 3-Deoxy-D-*manno*-2-octulosonic acid 8-phosphate synthase: a new class of KDO 8-P synthase?, *J. Mol. Evol.* **2001**, *52*, 205-214.

40. Ahn, M.; Cochrane, F. C.; Patchett, M. L.; Parker, E. J., Arabinose 5-phosphate analogues as mechanistic probes for *Neisseria meningitidis* 3-deoxy-D-*manno*-octulosonate 8-phosphate synthase, *Bioorg. Med. Chem.* **2008**, *16*, 9830-9836.

41. Walker, G. E.; Dunbar, B.; Hunter, I. S.; Nimmo, H. G.; Coggins, J. R., Evidence for a novel class of microbial 3-deoxy-D-*arabino*-heptulosonate-7-phosphate synthase in *Streptomyces coelicolor* A3(2), *Streptomyces rimosus* and *Neurospora crassa*, *Microbiology (Reading, U. K.)* **1996**, *142*, 1973-1982.

42. Jensen, R. A.; Xie, G.; Calhoun, D. H.; Bonner, C. A., The correct phylogenetic relationship of KdsA (3-deoxy-D-*manno*-octalosonate 8-phosphate synthase) with one of two independently evolved classes of AroA (3-deoxy-D-*arabino*-heptulosonate 7-phosphate synthase), *J. Mol. Evol.* **2002**, *54*, 416-423.

43. Webby C., J.; Baker H., M.; Lott, J. S.; Baker E., N.; Parker E., J., The structure of 3-deoxy-D-*arabino*-heptulosonate 7-phosphate synthase from *Mycobacterium tuberculosis*

reveals a common catalytic scaffold and ancestry for type I and type II enzymes, *J. Mol. Biol.* **2005**, *354*, 927-39.

44. Webby C., J.; Patchett M., L.; Parker E., J., Characterization of a recombinant type II 3-deoxy-D-*arabino*-heptulosonate-7-phosphate synthase from *Helicobacter pylori*, *Biochem. J.* **2005**, *390*, 223-30.

45. Stephens, C. M.; Bauerle, R., Analysis of the metal requirement of 3-deoxy-D-*arabino*-heptulosonate-7-phosphate synthase from *Escherichia coli*, *J. Biol. Chem.* **1991**, *266*, 20810-17.

46. Schofield, L. R.; Patchett, M. L.; Parker, E. J., Expression, purification, and characterization of 3-deoxy-D-*arabino*-heptulosonate 7-phosphate synthase from *Pyrococcus furiosus*, *Protein Expression Purif.* **2004**, *34*, 17-27.

47. Wu, J.; Howe, D. L.; Woodard, R. W., *Thermotoga maritima* 3-deoxy-D-*arabino*-heptulosonate 7-phosphate (DAHP) synthase: The ancestral eubacterial DAH7P synthase?, *J. Biol. Chem.* **2003**, *278*, 27525-27531.

48. Wu, J.; Sheflyan, G. Y.; Woodard, R. W., *Bacillus subtilis* 3-deoxy-D-*arabino*-heptulosonate 7-phosphate synthase revisited: resolution of two long-standing enigmas, *Biochem. J.* **2005**, *390*, 583-590.

49. Wagner, T.; Kretsinger, R. H.; Bauerle, R.; Tolbert, W. D., 3-Deoxy-D-*manno*-octulosonate-8-phosphate Synthase from *Escherichia coli*. Model of binding of phosphoenolpyruvate and D-arabinose-5-phosphate, *J. Mol. Biol.* **2000**, *301*, 233-238.

50. Furdui, C. M.; Sau, A. K.; Yaniv, O.; Belakhov, V.; Woodard, R. W.; Baasov, T.; Anderson, K. S., The use of (*E*)- and (*Z*)-phosphoenol-3-fluoropyruvate as mechanistic probes reveals significant differences between the active sites of KDO8P and DAHP synthases, *Biochemistry* **2005**, *44*, 7326-7335.

51. Li, J.; Wu, J.; Fleischhacker, A. S.; Woodard, R. W., Conversion of *Aquifex aeolicus* 3-deoxy-D-*manno*-octulosonate 8-Phosphate Synthase, a metalloenzyme, into a nonmetalloenzyme, *J. Am. Chem. Soc.* **2004**, *126*, 7448-7449.

52. Shulami, S.; Furdui, C.; Adir, N.; Shoham, Y.; Anderson, K. S.; Baasov, T., A reciprocal single mutation affects the metal requirement of 3-Deoxy-D-*manno*-2-octulosonate-8-phosphate (KDO8P) synthases from *Aquifex pyrophilus* and *Escherichia coli*, *J. Biol. Chem.* **2004**, *279*, 45110-45120.

53. Oliynyk, Z.; Briseno-Roa, L.; Janowitz, T.; Sondergeld, P.; Fersht, A. R., Designing a metal-binding site in the scaffold of *Escherichia coli* KDO8PS, *Protein Eng., Des. Sel.* **2004**, *17*, 383-390.

54. Radaev, S.; Dastidar, P.; Patel, M.; Woodard, R. W.; Gatti, D. L., Structure and mechanism of 3-deoxy-D-*manno*-octulosonate 8-phosphate synthase, *J. Biol. Chem.* **2000**, *275*, 9476-9484.

55. Cochrane, F. C.; Cookson, T. V. M.; Jameson, G. B.; Parker, E. J., Reversing evolution: re-establishing obligate metal ion dependence in a metal-independent KDO8P synthase., *J. Mol. Biol.* **2009**, *390*, 646-661.

56. Kelly, D. P.; McDonald, I. R.; Wood, A. P., Proposal for the reclassification of *Thiobacillus novellus* as *Starkeya novella* gen. nov., comb. nov., in the α-subclass of the Proteobacteria, *Int J Syst Evol Microbiol* **2000**, *50 Pt 5*, 1797-802.

57. Shumilin I., A.; Bauerle, R.; Kretsinger R., H., The high-resolution structure of 3-deoxy-D-*arabino*-heptulosonate-7-phosphate synthase reveals a twist in the plane of bound phosphoenolpyruvate, *Biochemistry* **2003**, *42*, 3766-76.

58. Shumilin I., A.; Bauerle, R.; Wu, J.; Woodard R., W.; Kretsinger R., H., Crystal structure of the reaction complex of 3-deoxy-D-*arabino*-heptulosonate-7-phosphate synthase from *Thermotoga maritima* refines the catalytic mechanism and indicates a new mechanism of allosteric regulation, *J. Mol. Biol.* **2004**, *341*, 455-66.

59. Konig, V.; Pfeil, A.; Braus, G. H.; Schneider, T. R., Substrate and metal complexes of 3-deoxy-D-*arabino*-heptulosonate-7-phosphate synthase from *Saccharomyces cerevisiae* provide new insights into the catalytic mechanism, *J. Mol. Biol.* **2004**, *337*, 675-690.

60. Wierenga, R. K., The TIM-barrel fold: a versatile framework for efficient enzymes, *FEBS Lett.* **2001**, *492*, 193-198.

61. Li, Z.; Sau, A. K., Structural studies on *Helicobacter pylori* 3-deoxy-D-*manno*-2-octulosonate-8-phosphate synthase using electrospray ionization mass spectrometry: a tetrameric complex composed of dimeric dimers, *Rapid Commun. Mass Spectrom.* **2009**, *23*, 1573-1578.

62. Allison, T. M.; Yeoman, J. A.; Hutton, R. D.; Cochrane, F. C.; Jameson, G. B.; Parker, E. J., Specificity and mutational analysis of the metal-dependent 3-deoxy-D-manno-octulosonate 8-phosphate synthase from *Acidithiobacillus ferrooxidans*, *Biochim. Biophys. Acta, Proteins Proteomics* **2010**, *1804*, 1526-1536.

63. Xu, X.; Kona, F.; Wang, J.; Lu, J.; Stemmler, T.; Gatti, D. L., The catalytic and conformational cycle of *Aquifex aeolicus* KDO8P synthase: role of the L7 loop, *Biochemistry* **2005**, *44*, 12434-12444.

64. Li, Y.; Evans, J. N. S., The hard-soft acid-base principle in enzymic catalysis: dual reactivity of phosphoenolpyruvate, *Proc. Natl. Acad. Sci. U. S. A.* **1996**, *93*, 4612-4616.

65. Wang, J.; Duewel, H. S.; Stuckey, J. A.; Woodard, R. W.; Gatti, D. L., Function of His185 in *Aquifex aeolicus* 3-deoxy-D-*manno*-octulosonate 8-phosphate synthase, *J. Mol. Biol.* **2002**, *324*, 205-214.

66. Vainer, R.; Belakhov, V.; Rabkin, E.; Baasov, T.; Adir, N., Crystal Structures of *Escherichia coli* KDO8P Synthase Complexes Reveal the Source of Catalytic Irreversibility, *J. Mol. Biol.* **2005**, *351*, 641-652.

67. Ahn, M.; Pietersma, A. L.; Schofield, L. R.; Parker, E. J., Mechanistic divergence of two closely related aldol-like enzyme-catalysed reactions, *Org. Biomol. Chem.* **2005**, *3*, 4046-4049.

68. Howe, D. L.; Sundaram, A. K.; Wu, J.; Gatti, D. L.; Woodard, R. W., Mechanistic insight into 3-Deoxy-D-*manno*-octulosonate-8-phosphate synthase and 3-deoxy-D-*arabino*-heptulosonate-7-phosphate synthase utilizing phosphorylated monosaccharide analogues, *Biochemistry* **2003**, *42*, 4843-4854.

69. Williamson, R. M.; Pietersma, A. L.; Jameson, G. B.; Parker, E. J., Stereospecific deuteration of 2-deoxyerythrose 4-phosphate using 3-deoxy-D-arabino-heptulosonate 7-phosphate synthase, *Bioorg. Med. Chem. Lett.* **2005**, *15*, 2339-2342.

70. Ahn, M., *Substrate analogues as mechanistic probes for 3-deoxy-D-arabino-heptulosonate 7-phosphate synthase and 3-deoxy-D-manno-octulosonate 8-phosphate synthase.*; PhD, Massey University, 2007.

71. DeLeo, A. B.; Sprinson, D. B., Mechanism of 3-deoxy-D-arabinoheptulosonate-7-phosphate (DAHP) synthetase, *Biochem. Biophys. Res. Commun.* **1968**, *32*, 873-7.

72. Gunawan, J.; Simard, D.; Gilbert, M.; Lovering, A. L.; Wakarchuk, W. W.; Tanner, M. E.; Strynadka, N. C. J., Structural and mechanistic analysis of sialic acid synthase NeuB from *Neisseria meningitidis* in complex with Mn^{2+}, phosphoenolpyruvate, and *N*-acetylmannosaminitol, *J. Biol. Chem.* **2005**, *280*, 3555-3563.

73. Bondinell, W. E.; Vnek, J.; Knowles, P. F.; Sprecher, M.; Sprinson, D. B., Mechanism of 5-enolpyruvylshikimate 3-phosphate synthetase, *J. Biol. Chem.* **1971**, *246*, 6191-6.

74. Eschenburg, S.; Kabsch, W.; Healy, M. L.; Schoenbrunn, E., A New View of the Mechanisms of UDP-N-Acetylglucosamine Enolpyruvyl Transferase (MurA) and 5-Enolpyruvylshikimate-3-phosphate Synthase (AroA) Derived from X-ray Structures of Their Tetrahedral Reaction Intermediate States, *J. Biol. Chem.* **2003**, *278*, 49215-49222.

75. Bravo, I. G.; Garcia-Vallve, S.; Romeu, A.; Reglero, A., Prokaryotic origin of cytidylyltransferases and α-ketoacid synthases, *Trends Microbiol.* **2004**, *12*, 120-128.

76. Traving, C.; Schauer, R., Structure, function, and metabolism of sialic acids, *Cell. Mol. Life Sci.* **1998**, *54*, 1330-1349.

77. Varki, A., Sialic acids as ligands in recognition phenomena, *FASEB J.* **1997**, *11*, 248-255.

78. Preston, A.; Mandrell, R. E.; Gibson, B. W.; Apicella, M. A., The lipooligosaccharides of pathogenic Gram-negative bacteria, *Crit. Rev. Microbiol.* **1996**, *22*, 139-180.

79. Angata, T.; Varki, A., Chemical Diversity in the Sialic Acids and Related alpha -Keto Acids: An Evolutionary Perspective, *Chem. Rev. (Washington, D. C.)* **2002**, *102*, 439-469.

80. Jia, Z.; DeLuca, C. I.; Chao, H.; Davies, P. L., Structural basis for the binding of a globular antifreeze protein to ice, *Nature* **1996**, *384*, 285-8.

81. Sundaram, A. K.; Pitts, L.; Muhammad, K.; Wu, J.; Betenbaugh, M.; Woodard, R. W.; Vann, W. F., Characterization of N-acetylneuraminic acid synthase isoenzyme 1 from *Campylobacter jejuni*, *Biochem. J.* **2004**, *383*, 83-89.

82. Onderka, D. K.; Floss, H. G., Steric course of the chorismate synthetase reaction and the 3-deoxy-D-*arabino*-heptulosonate 7-phosphate (DAHP) synthetase reaction, *J. Am. Chem. Soc.* **1969**, *91*, 5894-6.

83. Sheffer-Dee-Noor, S.; Belakhov, V.; Baasov, T., Insight into the catalytic mechanism of KDO8P synthase. Synthesis and evaluation of the isosteric phosphonate mimic of the putative cyclic intermediate, *Bioorg. Med. Chem. Lett.* **1993**, *3*, 1583-8.

84. Xu, X.; Wang, J.; Grison, C.; Petek, S.; Coutrot, P.; Birck, M. R.; Woodard, R. W.; Gatti, D. L., Structure-based design of novel inhibitors of 3-deoxy-D-*manno*-octulosonate 8-phosphate synthase, *Drug Design and Discovery* **2003**, *18*, 91-99.

85. Belakhov, V.; Dovgolevsky, E.; Rabkin, E.; Shulami, S.; Shoham, Y.; Baasov, T., Synthesis and evaluation of a mechanism-based inhibitor of KDO8P synthase, *Carbohydr. Res.* **2004**, *339*, 385-392.

86. Walker, S. R., *Design, Synthesis and Characterisation of Inhibitors of 3-Deoxy-D-arabino-Heptulosonate 7-Phosphate Synthase*; PhD, University of Canterbury, 2007.

87. Weichselbaum, A., Ueber die Aetiologie der akuten Meningitis cerebro-spinalis., *Fortschr Med* **1887**, *5*, 573-83.

88. Noekleby, H.; Aavitsland, P.; O'Hallahan, J.; Feiring, B.; Tilman, S.; Oster, P., Safety review: Two outer membrane vesicle (OMV) vaccines against systemic *Neisseria meningitidis* serogroup B disease, *Vaccine* **2007**, *25*, 3080-3084.

89. Rosenstein, N. E.; Perkins, B. A.; Stephens, D. S.; Popovic, T.; Hughes, J. M., Meningococcal disease, *N. Engl. J. Med.* **2001**, *344*, 1378-1388.

90. Nikulin, J.; Panzner, U.; Frosch, M.; Schubert-Unkmeir, A., Intracellular survival and replication of *Neisseria meningitidis* in human brain microvascular endothelial cells, *Int. J. Med. Microbiol.* **2006**, *296*, 553-558.

91. Colmer, A. R.; Hinkle, M. E., The role of microorganisms in acid mine drainage: a preliminary report, *Science (Washington, DC, U. S.)* **1947**, *106*, 253-6.

92. Leduc, L. G.; Ferroni, G. D., The chemolithotropic bacterium *Thiobacillus ferrooxidans*, *FEMS Microbiol. Rev.* **1994**, *14*, 103-20.

93. Gasteiger, E.; Hoogland, C.; Gattiker, A.; Duvaud, S.; Wilkins, M. R.; Appel, R. D.; Bairoch, A., Protein identification and analysis tools on the ExPASy server, *Proteomics Protoc. Handb.* **2005**, 571-607.

94. Allison, T. M., *Investigations into the role of a lysine residue of 3-deoxy-D-manno-octulosonate 8-phosphate synthase*; BSc(Hons), University of Canterbury, 2007.

95. Taylor, W. P.; Sheflyan, G. Y.; Woodard, R. W., A single point mutation in 3-deoxy-D-*manno*-octulosonate-8-phosphate synthase is responsible for temperature sensitivity in a mutant strain of *Salmonella typhimurium*, *J. Biol. Chem.* **2000**, *275*, 32141-6.

96. Sheflyan, G. Y.; Sundaram, A. K.; Taylor, W. P.; Woodard, R. W., Substrate ambiguity of 3-deoxy-D-*manno*-octulosonate 8-phosphate synthase from *Neisseria gonorrhoeae* revisited, *J. Bacteriol.* **2000**, *182*, 5005-5008.

97. Krosky, D. J.; Alm, R.; Berg, M.; Carmel, G.; Tummino, P. J.; Xu, B.; Yang, W., *Helicobacter pylor*i 3-deoxy-D-*manno*-octulosonate-8-phosphate (KDO-8-P) synthase is a zinc-metalloenzyme, *Biochim. Biophys. Acta, Protein Struct. Mol. Enzymol.* **2002**, *1594*, 297-306.

98. Pauling, L., Nature of forces between large molecules of biological interest, *Nature* **1948**, *161*, 707-9.

99. Wolfenden, R. V., Transition state analogues for enzyme catalysis, *Nature (London)* **1969**, *223*, 704-5.

100. Wolfenden, R.; Snider, M. J., The depth of chemical time and the power of enzymes as catalysts, *Acc. Chem. Res.* **2001**, *34*, 938-945.

101. Singh, V.; Evans, G. B.; Lenz, D. H.; Mason, J. M.; Clinch, K.; Mee, S.; Painter, G. F.; Tyler, P. C.; Furneaux, R. H.; Lee, J. E.; Howell, P. L.; Schramm, V. L., Femtomolar Transition State Analogue Inhibitors of 5'-Methylthioadenosine/S-Adenosylhomocysteine Nucleosidase from Escherichia coli, *J. Biol. Chem.* **2005**, *280*, 18265-18273.

102. Walker, S. R.; Cumming, H.; Parker, E. J., Substrate and reaction intermediate mimics as inhibitors of 3-deoxy-D-*arabino*-heptulosonate 7-phosphate synthase, *Org. Biomol. Chem.* **2009**, *7*, 3031-3035.

103. Duncan, K.; Lewendon, A.; Coggins, J. R., The purification of 5-enolpyruvylshikimate 3-phosphate synthase from an overproducing strain of *Escherichia coli*, *FEBS Lett.* **1984**, *165*, 121-7.

104. Anderson, K. S.; Johnson, K. A., Kinetic and structural analysis of enzyme intermediates: lessons from EPSP synthase, *Chem. Rev. (Washington, D. C.)* **1990**, *90*, 1131-49.

105. Kona, F.; Tao, P.; Martin, P.; Xu, X.; Gatti, D. L., Electronic structure of the metal center in the Cd2+, Zn2+, and Cu2+ substituted forms of KDO8P synthase: implications for catalysis, *Biochemistry* **2009**, *48*, 3610-3630.

106. Romanenko, V. D.; Kukhar, V. P., Fluorinated Phosphonates: Synthesis and Biomedical Application, *Chem. Rev. (Washington, D. C.)* **2006**, *106*, 3868-3935.

107. Caplan, N. A.; Pogson, C. I.; Hayes, D. J.; Blackburn, G. M., Novel bisphosphonate inhibitors of phosphoglycerate kinase, *Bioorg. Med. Chem. Lett.* **1998**, *8*, 515-520.

108. Jakeman, D. L.; Ivory, A. J.; Williamson, M. P.; Blackburn, G. M., Highly potent bisphosphonate ligands for phosphoglycerate kinase, *J. Med. Chem.* **1998**, *41*, 4439-4452.

109. Halazy, S.; Ehrhard, A.; Danzin, C., 9-(Difluorophosphonoalkyl)guanines as a new class of multisubstrate analog inhibitors of purine nucleoside phosphorylase, *J. Am. Chem. Soc.* **1991**, *113*, 315-17.

110. Nowak, T.; Mildvan, A. S., Stereoselective interactions of phosphoenolpyruvate analogs with phosphoenolpyruvate-utilizing enzymes, *J. Biol. Chem.* **1970**, *245*, 6057-64.

111. Rose, I. A., Stereochemistry of pyruvate kinase, pyruvate carboxylase, and malate enzyme reactions, *J. Biol. Chem.* **1970**, *245*, 6052-6.

112. Cohn, M.; Pearson, J. E.; O'Connell, E. L.; Rose, I. A., Nuclear magnetic resonance assignment of the vinyl hydrogens of phosphoenolpyruvate. Stereochemistry of the enolase reaction, *J. Am. Chem. Soc.* **1970**, *92*, 4095-8.

113. Cumming, H., *Probing the Substrate Specificity of 3-Deoxy-D-arabino-Heptulosonate 7-Phosphate Synthase and 3-Deoxy-D-manno-Octulosonate 8-Phosphate Synthase using Analogues of Phosphoenolpyruvate*; MSc, University of Canterbury, 2007.

114. Reichau, S., Crystallographic studies of DAH7P synthase from *Mycobacterium tuberculosis* with a tetrahedral intermediate analogue inhibitor., *Personal communication*.

115. Mammen, M.; Chio, S.-K.; Whitesides, G. M., Polyvalent interactions in biological systems: implications for design and use of multivalent ligands and inhibitors, *Angew. Chem., Int. Ed.* **1998**, *37*, 2755-2794.

116. Coutrot, P.; Grison, C.; Tabyaoui, M.; Czernecki, S.; Valery, J. M., Novel application of alkyl dihaloacetates; chain extension with an alpha -keto ester unit of carbohydrates, *J. Chem. Soc., Chem. Commun.* **1988**, 1515-16.

117. Grison, C.; Coutrot, F.; Comoy, C.; Lemilbeau, C.; Coutrot, P., New efficient synthesis of α-hydroxy esters from carbonyl compounds via α-chloroglycidic esters, *Tetrahedron Lett.* **2000**, *41*, 6571-6574.

118. Sobotta, R.; Klingler, F. D.; Schneider, H.; (Boehringer Ingelheim KG, Germany; Boehringer Ingelheim International GmbH). Application: EP
EP, 1995, p 9 pp.

119. Buchanan, J. G.; Chacón-Fuertes, M. E.; Edgar, A. R.; Moorhouse, S. J.; Rawson, D. I.; Wightman, R. H., Assignment of ring size in isopropylidene acetals by ^{13}C N.M.R, *Tetrahedron Lett.* **1980**, *21*, 1793-1796.

120. Einhorn, C.; Luche, J. L., Ultrasound in organic synthesis. Part 8. Ready preparation of sugar acetals under ultrasonic irradiation, *Carbohydr. Res.* **1986**, *155*, 258-61.

121. Sato, K.-I.; Akai, S.; Hiroshima, T.; Aoki, H.; Sakuma, M.; Suzuki, K.-j., Chemoenzymatic synthesis of [3,9-13C]-labeled NeuAc and KDN, *Tetrahedron Lett.* **2003**, *44*, 3513-3516.

122. Webb, T. H.; Thomasco, L. M.; Schlachter, S. T.; Gaudino, J. J.; Wilcox, C. S., Insight into the unusual reactions of stabilized phosphorus ylides with lactols. A specific intramolecular hyroxyl group effect leads to high *Z*-selectivity, *Tetrahedron Lett.* **1988**, *29*, 6823-6.

123. Yoda, H.; Nakaseko, Y.; Takabe, K., Studies toward a synthesis of trilobatin B, a lignan from the liverwort Bazzania trilobata: asymmetric construction of the tetrahydrofuran segment, *Tetrahedron Lett.* **2004**, *45*, 4217-4220.

124. Austin Kerrie, A. B.; Banwell Martin, G.; Loong David, T. J.; Rae, A. D.; Willis Anthony, C., A chemoenzymatic total synthesis of the undecenolide (-)-cladospolide B via a mid-stage ring-closing metathesis and a late-stage photo-rearrangement of the E-isomer, *Org. Biomol. Chem.* **2005**, *3*, 1081-8.

125. Grison, C.; Petek, S.; Finance, C.; Coutrot, P., Synthesis and antibacterial activity of mechanism-based inhibitors of KDO8P synthase and DAH7P synthase, *Carbohydr. Res.* **2005**, *340*, 529-537.

126. Shen, X.; Wu, Y.-L.; Wu, Y., Enantioselective synthesis of ethyl 4,5,7,8,9-penta-*O*-acetyl-2,6-anhydro- 3-deoxy-D-*erythro*-L-*gluca*-nononate: a 2-monodeoxygenated derivative of `2-keto-3-deoxy-D-*glycero*-D-*galacto*-nononic acid', *Helv. Chim. Acta* **2000**, *83*, 943-953.

127. Setoi, H.; Takeno, H.; Hashimoto, M., Total synthesis of (+)-castanospermine from D-mannose, *Tetrahedron Lett.* **1985**, *26*, 4617-20.

128. Mashimo, K.; Sato, Y., Synthesis of isoajmaline, *Tetrahedron* **1970**, *26*, 803-12.

129. Cunico, R. F.; Bedell, L., The triisopropylsilyl group as a hydroxyl-protecting function, *J. Org. Chem.* **1980**, *45*, 4797-8.

130. Davies, J. S.; Higginbotham, C. L.; Tremeer, E. J.; Brown, C.; Treadgold, R. C., Protection of hydroxy groups by silylation: use in peptide synthesis and as lipophilicity modifiers for peptides, *J. Chem. Soc., Perkin Trans. 1* **1992**, 3043-8.

131. Schlessinger, R. H.; Lopes, A., A total synthesis of racemic senepoxide: formal syntheses of crotepoxide and pipoxide, *J. Org. Chem.* **1981**, *46*, 5252-3.

132. Jarowicki, K.; Kocienski, P., *Protecting groups*, 2000.

133. Xiao, X.; Bai, D., An efficient and selective method for hydrolysis of acetonides, *Synlett* **2001**, 535-537.

134. Koelln, O.; Redlich, H.; Frank, H., Trimethylenedithioacetals of carbohydrates; Part 2. D-Arabinose, D-glucose, and D-mannose propane-1,3-diyldithioacetals and their isopropylidene derivatives, *Synthesis* **1995**, 1383-8.

135. Pedrocchi-Fantoni, G.; Servi, S., Simple synthesis of the two enantiomeric forms of erythro-octane-2,3-diol and 2-hydroxyoctan-3-one, proposed pheromones of Xylotrechus pyrrhoderus, *J. Chem. Res., Synop.* **1986**, 199.

136. Anwer, M. K.; Spatola, A. F., An advantageous method for the rapid removal of hydrogenolyzable protecting groups under ambient conditions; synthesis of leucine-enkephalin, *Synthesis* **1980**, 929-32.

137. Coleman, R. S.; Carpenter, A. J., Synthesis of the aziridino[1,2-α]pyrrolidine substructure of the antitumor agents azinomycin A and B, *J. Org. Chem.* **1992**, *57*, 5813-15.

138. Greene, T. W.; Wuts, P. G. M., *Protective Groups in Organic Synthesis. 3rd Ed*, 1999.

139. Hoefle, G.; Steglich, W.; Vorbrueggen, H., New synthetic methods. 25. 4-Dialkylaminopyridines as acylation catalysts. 4. Puridine syntheses. 1. 4-Dialkylaminopuridines as highly active acylation catalysts, *Angew. Chem.* **1978**, *90*, 602-15.

140. Narayan, R. S.; Borhan, B., Synthesis of the Proposed Structure of Mucoxin via Regio- and Stereoselective Tetrahydrofuran Ring-Forming Strategies, *J. Org. Chem.* **2006**, *71*, 1416-1429.

141. Willson, T. M.; Kocienski, P.; Jarowicki, K.; Isaac, K.; Hitchcock, P. M.; Faller, A.; Campbell, S. F., Studies related to the synthesis of pederin. Part 2. Synthesis of pederol dibenzoate and benzoylpedamide, *Tetrahedron* **1990**, *46*, 1767-82.

142. Bolitt, V.; Mioskowski, C.; Kollah, R. O.; Manna, S.; Rajapaksa, D.; Falck, J. R., Total synthesis of vineomycinone B2 methyl ester via double Bradsher cyclization, *J. Am. Chem. Soc.* **1991**, *113*, 6320-1.

143. Dess, P. B.; Martin, J. C., A Useful 12-I-4 Triacetoxyperiodinane (the Dess-Martin Periodinane) for the Selective Oxidation of Primary of Secondary Alcohols for a Variety of Related 12-I-5 Species, *J. Am. Chem. Soc.* **1991**, *113*, 7277-7287.

144. Omura, K.; Swern, D., Oxidation of alcohols by "activated" dimethyl sulfoxide. A preparative steric and mechanistic study, *Tetrahedron* **1978**, *34*, 1651-60.

145. Emerson, W. S., Preparation of amines by reductive alkylation, *Org. React. (N.Y.)* **1948**, *4*, 174-255.

146. Abdel-Magid, A. F.; Carson, K. G.; Harris, B. D.; Maryanoff, C. A.; Shah, R. D., Reductive amination of aldehydes and ketones with sodium triacetoxyborohydride. Studies on direct and indirect reductive amination procedures, *J. Org. Chem.* **1996**, *61*, 3849-3862.

147. Sato, S.; Sakamoto, T.; Miyazawa, E.; Kikugawa, Y., One-pot reductive amination of aldehydes and ketones with α-picoline-borane in methanol, in water, and in neat conditions, *Tetrahedron* **2004**, *60*, 7899-7906.

148. Uenishi, J.; Hamada, M.; Aburatani, S.; Matsui, K.; Yonemitsu, O.; Tsukube, H., Synthesis of chiral nonracemic 1-(2-pyridinyl)ethylamines: stereospecific introduction of amino function onto the 2-pyridinylmethyl carbon center, *J. Org. Chem.* **2004**, *69*, 6781-6789.

149. Hong, Y.-R.; Gorman, C. B., Synthetic approaches to an isostructural series of redox-active, metal tris(bipyridine) core dendrimers, *J. Org. Chem.* **2003**, *68*, 9019-9025.

150. Micali, E.; Chehade, K. A. H.; Isaacs, R. J.; Andres, D. A.; Spielmann, H. P., Protein farnesyltransferase isoprenoid substrate discrimination is dependent on isoprene double bonds and branched methyl groups, *Biochemistry* **2001**, *40*, 12254-12265.

151. Rybczynski, P., J.; Zeck, R., E.; Dudash, J., Jr.; Combs, D., W.; Burris, T., P.; Yang, M.; Osborne, M., C.; Chen, X.; Demarest, K., T., Benzoxazinones as PPAR-γ agonists. 2. SAR of the amide substituent and *in vivo* results in a type 2 diabetes model, *J. Med. Chem.* **2004**, *47*, 196-209.

152. Van der Klei, A.; De Jong, R. L. P.; Lugtenburg, J.; Tielens, A. G. M., Synthesis and spectroscopic characterization of [1'-14C]ubiquinone-2, [1'-14C]-5-demethoxy-5-hydroxyubiquinone-2, and [1'-14C]-5-demethoxyubiquinone-2, *Eur. J. Org. Chem.* **2002**, 3015-3023.

153. Wiley, G. A.; Hershkowitz, R. L.; Rein, B. M.; Chung, B. C., Organophosphorus chemistry. I. Conversion of alcohol and phenols to halides by tertiary phosphine dihalides, *J. Am. Chem. Soc.* **1964**, *86*, 964-5.

154. Cossio, F. P.; Ganboa, I.; Palomo, C., Reagents and synthetic methods. 48. Triphenylphosphine dibromide and dimethylsulfide dibromide as versatile reagents for β-lactam synthesis, *Tetrahedron Lett.* **1985**, *26*, 3041-4.

155. Jew, S.-S.; Kim, H.-O.; Jeong, B.-S.; Park, H.-G., Asymmetric synthesis of (*R*)-(+)-etomoxir, *Tetrahedron: Asymmetry* **1997**, *8*, 1187-1192.

156. Szardenings, A. K.; Burkoth, T. S.; Look, G. C.; Campbell, D. A., A reductive alkylation procedure applicable to both solution- and solid-phase syntheses of secondary amines, *J. Org. Chem.* **1996**, *61*, 6720-6722.

157. Salvatore, R. N.; Nagle, A. S.; Schmidt, S. E.; Jung, K. W., Cesium hydroxide promoted chemoselective *N*-alkylation for the generally efficient synthesis of secondary amines, *Org. Lett.* **1999**, *1*, 1893-1896.

158. Corey, E. J.; Venkateswarlu, A., Protection of hydroxyl groups as *tert*-butyldimethylsilyl derivatives, *J. Am. Chem. Soc.* **1972**, *94*, 6190-1.

159. Nurminen, E. J.; Mattinen, J. K.; Lonnberg, H., Kinetics and mechanism of tetrazole-catalyzed phosphoramidite alcoholysis, *J. Chem. Soc. Perkin Trans. 2* **1998**, 1621-1628.

160. Perich, J. W.; Johns, R. B., Di-*tert*-butyl *N*,*N*-diethylphosphoramidite. A new phosphitylating agent for the efficient phosphorylation of alcohols, *Synthesis* **1988**, 142-4.

161. Lindberg, J.; Ekeroth, J.; Konradsson, P., Efficient synthesis of phospholipids from glycidyl phosphates, *J. Org. Chem.* **2002**, *67*, 194-199.

162. Hartung, W. H.; Simonoff, R., Hydrogenolysis of benzyl groups attached to oxygen, nitrogen or sulfur, *Org. React. (N.Y.)* **1953**, *VII*, 263-326.

163. Castro, B.; Villieras, J.; Ferracutti, N., Aliphatic aldehydes in the Darzens reaction of mono- and dichloroacetic [acid] esters. Specific solvation by hydrogen bonding, *C. R. Acad. Sci., Paris, Ser. C* **1969**, *268*, 1403-6.

164. Reichau, S., Two-step conversion of aldehyde functionality to α-hydroxy ester., *Personal communication*.

165. Gottlieb, H. E.; Kotlyar, V.; Nudelman, A., NMR chemical shifts of common laboratory solvents as trace impurities, *J. Org. Chem.* **1997**, *62*, 7512-7515.

166. Lanzetta, P. A.; Alvarez, L. J.; Reinach, P. S.; Candia, O. A., An improved assay for nanomole amounts of inorganic phosphate, *Anal. Biochem.* **1979**, *100*, 95-7.

167. Heathcock, C. H.; Ratcliffe, R., Stereoselective total synthesis of the guaiazulenic sesquiterpenoids α-bulnesene and bulnesol, *J. Am. Chem. Soc.* **1971**, *93*, 1746-57.

168. Czernecki, S.; Georgoulis, C.; Provelenghiou, C.; Fusey, G., New method of benzylation of hindered glucosidic hydroxyl groups, *Tetrahedron Lett.* **1976**, 3535-6.

169. Kanai, K.; Sakamoto, I.; Ogawa, S.; Suami, T., Synthesis on 1,4-diaminocyclitol antibiotics. III. Synthesis of 4-hydroxypurpurosamine B derivatives, *Bull. Chem. Soc. Jpn.* **1987**, *60*, 1529-31.

170. Kuhn, R.; Low, I.; Trischmann, H., The constitution of lycotetraose, *Chem. Ber.* **1957**, *90*, 203-18.

171. Tao, P.; Schlegel, H. B.; Gatti, D. L., Common basis for the mechanism of metallo and non-metallo KDO8P synthases, *J. Inorg. Biochem.* **2010**, *104*, 1267-1275.

172. Bowman, W. R.; Coghlan, D. R., A facile method for the N-alkylation of alpha -amino esters, *Tetrahedron* **1997**, *53*, 15787-15798.

173. Coutrot, P.; Legris, C., Convenient synthesis of α-keto-esters and unsymmetrical 1,2-diketones from carbonyl compounds, *Synthesis* **1975**, 118-20.

174. Hajipour, A. R.; Khoee, S.; Ruoho, A. E., Regeneration of carbonyl compounds from oximes, hydrazones, semicarbazones, acetals, 1,1-diacetates, 1,3-dithiolanes, 1,3-dithianes and 1,3-oxathiolanes, *Org. Prep. Proced. Int.* **2003**, *35*, 527-581.

175. Satchell, D. P. N.; Satchell, R. S., Mechanisms of hydrolysis of thioacetals, *Chem. Soc. Rev.* **1990**, *19*, 55-81.

176. Wang, P.; Hu, H.; Wang, Y., Novel Photolabile Protecting Group for Carbonyl Compounds, *Org. Lett.* **2007**, *9*, 1533-1535.

177. Crispino, G. A.; Jeong, K. S.; Kolb, H. C.; Wang, Z. M.; Xu, D.; Sharpless, K. B., Improved enantioselectivity in asymmetric dihydroxylations of terminal olefins using pyrimidine ligands, *J. Org. Chem.* **1993**, *58*, 3785-6.

178. Takasu, M.; Naruse, Y.; Yamamoto, H., A convenient procedure for the regioselective monoprotection of 1,n-diols, *Tetrahedron Lett.* **1988**, *29*, 1947-50.

179. Laemmli, U. K., Cleavage of structural proteins during the assembly of the head of bacteriophage T4, *Nature (London, U. K.)* **1970**, *227*, 680-685.

180. Bradford, M. M., A rapid and sensitive method for the quantitation of microgram quantities of protein utilizing the principle of protein-dye binding, *Anal. Biochem.* **1976**, *72*, 248-54.

181. Armarego, W. L. F.; Chai, C., *Purification of Laboratory Chemicals, 5th Edition*, 2003.

182. Frigerio, M.; Santagostino, M.; Sputore, S., A user-friendly entry to 2-iodoxybenzoic acid (IBX), *J. Org. Chem.* **1999**, *64*, 4537-4538.

183. Walker, S. R.; Parker, E. J., Synthesis and evaluation of a mechanism-based inhibitor of a 3-deoxy-D-*arabino* heptulosonate 7-phosphate synthase, *Bioorg. Med. Chem. Lett.* **2006**, *16*, 2951-2954.